LANSCE Activity Report
2007-2009

LOUIS ROSEN
The Father of LANSCE
June 10, 1918 - August 20, 2009

LANSCE ACTIVITY REPORT 2007-2009

LA-UR-2010-07025

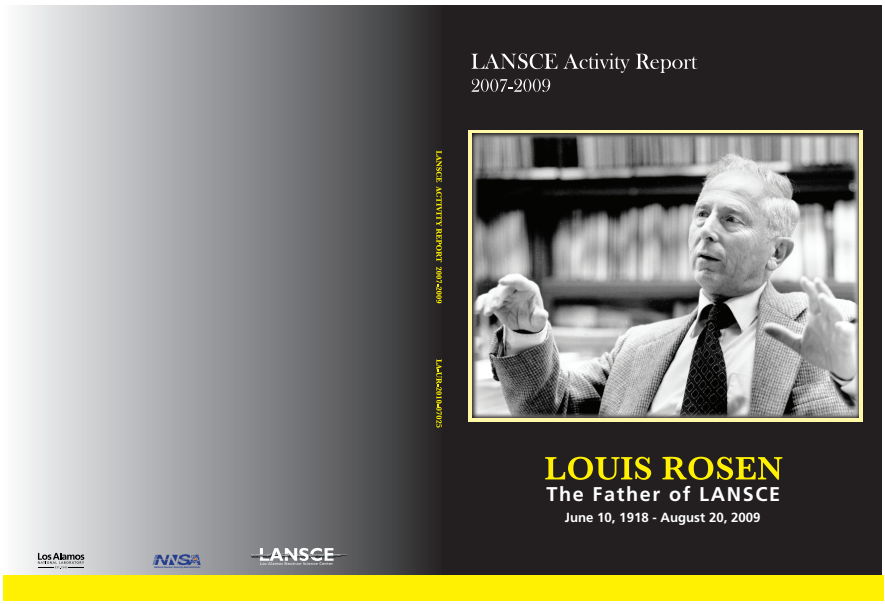

About the cover

Laboratory Senior Fellow Emeritus, Louis Rosen, was the driving force behind the conception and the development of the Los Alamos Neutron Science Center (LANSCE). Louis directed LANSCE from its inception in 1972 until 1985. Louis continued to work at LANSCE until two days before his death in August of 2009. He was 91. Known as the Father of LANSCE, Louis is remembered for his tireless efforts, scientific achievements, humor, and compassion. Louis lives on in the hearts all who had the privilege to know him.

Editor: Clay Dillingham
Design Direction: Barbara Maes
Composition: Barbara Maes
Illustration: Barbara Maes

The editor acknowledges the valuable contributions of all the Laboratory subject-matter experts who provided technical information and guidance.

This is the eighth report in this series.

LA-UR-2010-07025
Approved for public release; distribution is unlimited.

Issued: December 2010

LANSCE Activity Report 2007-2009

Compiled by:
Clay Dillingham and Barbara Maes

LANSCE Activity Report 2007-2009

LANSCE: supporting basic and applied research for national defense and civilian applications.

Abstract

The Los Alamos Neutron Science Center (LANSCE) Activity Report describes scientific and technological progress and achievements at LANSCE during calendar years 2007, 2008, and 2009. This report includes a dedication from the LANSCE Division Director, a message from the LANSCE Deputy Division Director, a homage to Louis Rosen, the Father of LANSCE, LANSCE research highlights, accelerator operations highlights, and user program accomplishments. This report is available on a compact disc.

Los Alamos National Laboratory, an affirmative action/ equal opportunity employer, is operated by Los Alamos National Security, LLC, for the National Nuclear Security Administration of the U.S. Department of Energy under contract DE-AC52-06NA25396.

Table of contents

Louis Rosen
June 10, 1918 - August 20, 2009

The Linear Accelerator

The particle accelerator Louis envisioned—a linear accelerator—would be as efficient and multi-functional as possible. It was to be the first dual-beam machine ever built. It would use both halves of the radio-frequency cycle to simultaneously accelerate both negative and positive hydrogen ions. Thus, twice as many experimental ports—without a significant increase in cost—would be possible.

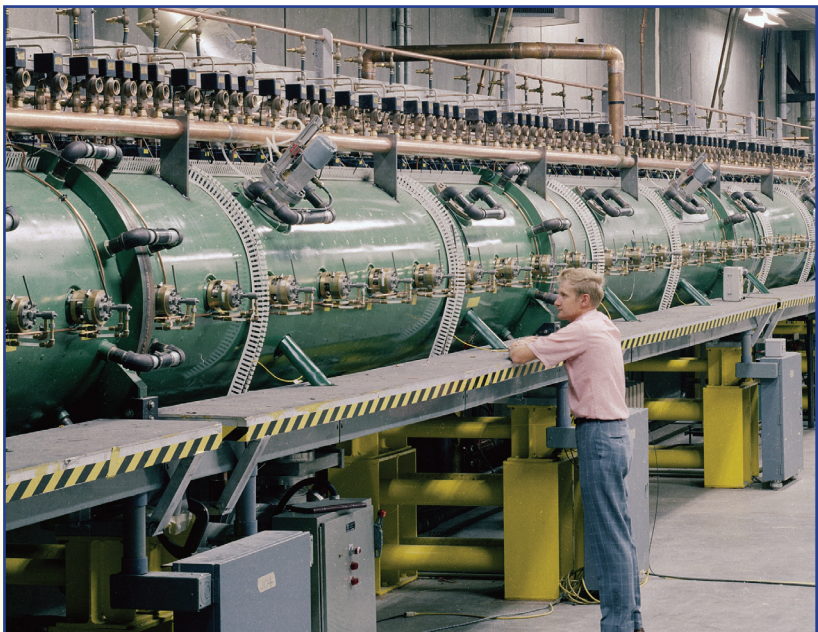

Dedication

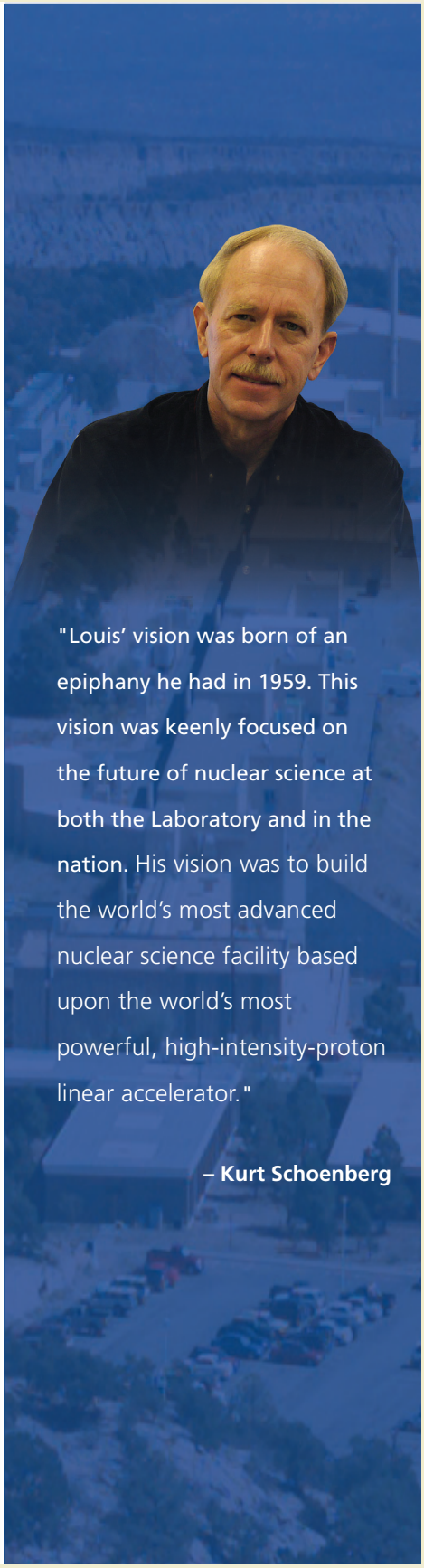

"Louis' vision was born of an epiphany he had in 1959. This vision was keenly focused on the future of nuclear science at both the Laboratory and in the nation. His vision was to build the world's most advanced nuclear science facility based upon the world's most powerful, high-intensity-proton linear accelerator."

– Kurt Schoenberg

Laboratory Senior Fellow Emeritus, Louis Rosen, may have been small in stature, but he was a giant among nuclear physics researchers. Louis was the driving force behind the conception, funding, design, and development of the Los Alamos Meson Physics Facility (LAMPF); for decades the largest and most powerful linear accelerator in the world. Louis headed LAMPF, today known as the Los Alamos Neutron Science Center (LANSCE), from its dedication in 1972 until 1985. Louis had plenty of incredibly talented, devoted, and similarly driven confederates to help him realize his vision, including Laboratory Director Norris Bradbury and fellow scientists Edward Knapp, Donald Hagerman, and Darragh Nagel. But everyone involved then and now in the life of LANSCE will agree that Louis Rosen was the Father of LANSCE.

Louis' vision was born of an epiphany he had in 1959, while on a Laboratory- and Guggenheim Memorial Foundation-sponsored sabbatical in Paris. This vision was keenly focused on the future of nuclear science at both the Laboratory and in the nation. Louis believed that the Laboratory could not remain the cornerstone of national security without achieving international scientific excellence: the so-called "deterrence through competence" argument. In addition, meeting the broad challenges of national security required solving problems in, for example, energy security, medicine, environmental stewardship, and nuclear non-proliferation.

Louis understood that nuclear science played a key role in solving each of these challenges. His vision was to build the world's most advanced nuclear science facility based upon the world's most powerful, high-intensity-proton linear accelerator. This accelerator would be capable of producing Pi-mesons at intensities up to 10,000 times over anything then in use, making LAMPF a kind of Pi-meson factory. These mesons would be used to probe the structure and function of the nucleus and would keep Los Alamos at the forefront of nuclear physics for decades.

LANSCE continues to honor Louis' vision. Today, LANSCE strives to maintain a balance between the fundamental and applied nuclear, materials, biological, and defense sciences to help meet the complex challenges of national security.

Even after retirement, Louis continued to work at LANSCE where he served as an inspiration and mentor to students, scientists, and Laboratory management. Louis worked in his office until just two days before his death. On August 20, 2009, he died in his sleep. He was 91. Louis left behind family members, coworkers, students, political leaders, and the world's nuclear scientific community in mourning.

Louis is remembered for his tireless efforts, scientific achievements, humor, and compassion. Louis lives on in the hearts of all who had the privilege to know him.

This Activity Report is dedicated to Louis.

Kurt Schoenberg
LANSCE User Facility Director

Introduction

Colleagues,

On behalf of the User Program at the Los Alamos Neutron Science Center (LANSCE), I am pleased to present the *LANSCE Activity Report 2007-2009*.

The first chapter is dedicated to recounting Louis' tenure at LANL and his approach to creating our state-of-the-art facility. His ingenuity and leadership were paramount to creating an experimental facility with the capabilities and flexibilities that, three decades later, remain powerful and relevant to our international user-community and to our national security.

In addition, this report provides our key scientific and technical accomplishments during calendar years 2007, 2008, and 2009. A short introduction is presented to each facility fed by the LANSCE linear accelerator: Ultracold Neutrons, Isotope Production, Weapons Neutron Research (WNR), Proton Radiography, and the Lujan Center.

Over the last three years several important events should be noted. The Department of Energy's (DOE's) Office of Science reviewed very favorably the Lujan Center and its user program in February 2009. Also, there was a change in the sponsorship for the Isotope Production Facility in 2009, from DOE's Office of Nuclear Energy to their Office of Science. This transition emphasizes DOE's renewed commitment to commercial isotope production and their interest in supporting the expansion of isotope research.

LANSCE continued to work in collaboration with the Spallation Neutron Source (SNS) at Oak Ridge National Laboratory. For example, a team of scientists and engineers from SNS used our pulsed-proton beam at LANSCE's WNR facility to test the performance of the SNS spallation target. LANSCE's proton beam offers the same energy density as what the SNS target is experiencing.

Over the years 2007–2009, LANSCE's Materials Test Station (MTS) project worked toward completing a fundamental milestone: cleaning out the Area A Experimental Hall in preparation for construction of the MTS. A total of 1,205 tons of activated steel shielding will soon be removed, packed and shipped to LANL's Waste Disposal facility. An additional 10,488 tons will be removed and stored on-site. This monumental task will be completed in 2010.

We conclude our report by highlighting the accomplishments and awards of our very talented staff.

I plan reactivating LANSCE's Annual Activity Report, so stay tuned for the 2010 report, and beyond.

I hope you enjoy reading this report and find the information useful. In addition to thanking all who contributed materials for this report, a special thank-you goes to Barb Maes and Clay Dillingham; without their great help completing it would not have been possible.

Alex Lacerda
LANSCE Deputy Division Director


L.A.M.P.F.

Louis Rosen

The Father of LANSCE

Louis Rosen
The Father of LANSCE

Manhattan project

Louis was born in New York City on June 10, 1918. After receiving his doctorate in classical physics from Pennsylvania State University, he came to Los Alamos in April of 1944 where he worked on the Manhattan Engineering District's Project Y, aka the Manhattan Project. His recruitment was simple and direct.

"I was called to the dean's office. Here was this prominent scientist introducing himself and telling me, 'I want you to join a project that can bring an end to the war.' That was a very powerful statement. People were dying by the hundreds of thousands. Along with many others, I was trying to get into the Navy, but I was two pounds underweight. So when he said that he wanted me to join such a project, I immediately said okay. He wouldn't tell me where it was, what it was about, what I would be doing, or who I would be working for—just to come to 109 East Palace Avenue in Santa Fe, NM, for further instructions."

That was the address used by the Manhattan Project in New Mexico. The Project was actually located at Los Alamos, over 30 miles away to the northwest, on a series of mesas overlooking the Rio Grande River Valley on land that had been, in part, a private boys school.

Louis was married by the time he arrived at Los Alamos and had a two-month-old baby. "It was rough in Los Alamos during the Manhattan Project, especially for families. Housing was primitive. Everything was rationed. There were no grocery or clothing stores. There wasn't even a cemetery. Even so, people were never happier than during those challenging years. We were all one big family. We all pitched in and helped one another," he said.

Life within the Laboratory was in sharp contrast to life outside: at the Laboratory, money was no object and everything needed was, when possible, quickly made available. When it wasn't available, the staff needed to be self-sufficient and self-reliant. Louis recalled, "When a scientist needed a device and the machine shops could not produce it immediately, he made it himself. No task was too menial. Time was of the essence."

Louis and his staff discussing their plans for the world's most powerful linear accelerator (1967). A model of a section of the half-mile long accelerator is in a case behind them. Construction of the accelerator began in 1968.

There was a war to win. The staff believed they were in a race with the Nazis to build the first Atomic bomb. Scientists in Nazi Germany had already split the uranium atom in 1938. It was inevitable that nuclear energy would be violently released—and very soon. But by whom? Louis would often point out, "That (the atomic bomb) was first revealed to a democratic society rather than to a Hitler or Stalin or Saddam Hussein may be one of the most fortuitous events in history."

When the situation is urgent, the level of acceptable risk is higher. At the Laboratory, as soon as material became available, criticality assemblies were begun, by hand, not remotely. Of course, many experimental programs involved the frequent use of high explosives. High explosives were machined, hands-on, and transported the same way. "I recall riding in a jeep over rough terrain, with 40 pounds of high explosive cradled in my lap on the way to the firing site. That was standard procedure."

In the Manhattan Project, safety and security, tempered by the "the rule of reason," was everybody's job. Supervisors provided training and oversight. There was also a high-level safety committee empowered to shut down any operation for reasons of safety.

Louis liked to point out that during the project people worked as many hours as they could, and didn't complain about it. The wartime atmosphere was informal and collegial. On one occasion, Louis remembered Robert Oppenheimer felt it necessary to request that all conversations be in English, so that everyone would be aware of what was happening. (Many of the scientific staff were refugees from Nazi-controlled countries.) "There was no compartmentalization, which I believe was crucial to early success. There were, of course, technical debates on how to proceed. However, once a course of action was adopted, everybody pitched in to make it work, or quickly ascertain that it doesn't work. This, in itself, was remarkable. Many key players were prima donnas at home institutions. They were accustomed to questioning authority rather than doing what was decided by consensus or edict." While the day-to-day environment was often tense, it was not without humor. "I recall a classic incident involving Enrico Fermi and Emilio Segré, who had been Fermi's student in Italy. Segré, also a future Nobel Laureate, was in Fermi's group. Fermi noticed that sometimes Segré didn't come to work on Sunday and he was curious as to why this was, so he asked him. Segré said that he 'sometimes goes fishing on Sunday,' to which Fermi responded,

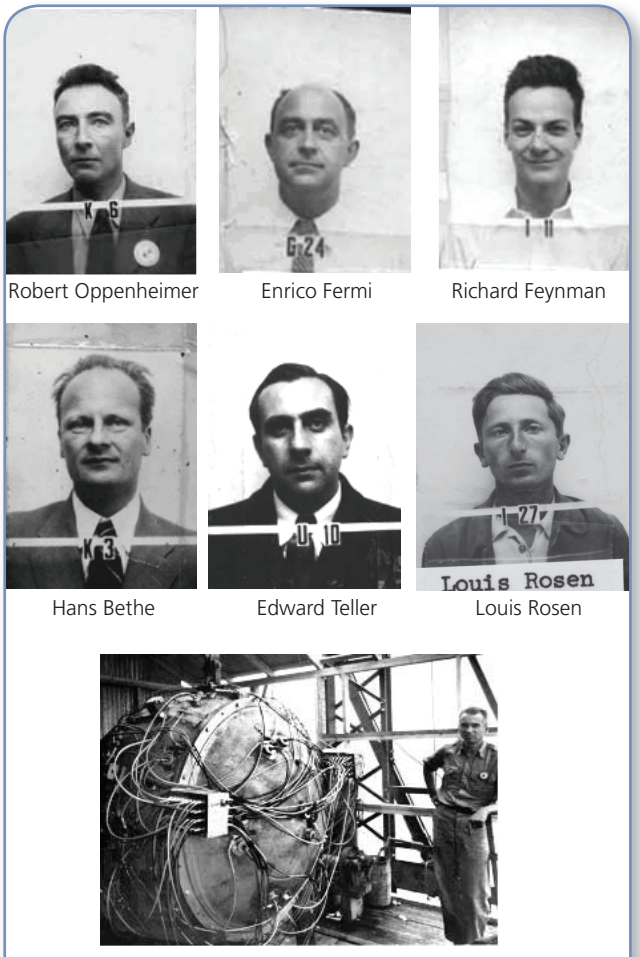

Robert Oppenheimer | Enrico Fermi | Richard Feynman

Hans Bethe | Edward Teller | Louis Rosen

The Gadget. The first atomic bomb was nicknamed "The Gadget." The Gadget was detonated on July 16, 1945 at White Sands Proving Ground, New Mexico, giving birth to the Atomic Age.

'What is so satisfying about fishing that it takes precedence over the extremely important problems we must solve?' Segré replied with a detailed explanation of the technology required for fly-fishing—in order to outsmart the fish. Fermi concluded: 'Finally I understand, it is a battle of wits!'"

One of Louis' favorite stories concerned the Laboratory's cyclotron, which had been "liberated" from Harvard for use by the Project. It was a very temperamental machine, but they had a sergeant who was an expert with it. As Louis told the story, this sergeant "could get a beam out when nobody else could. One day, he was working at the control desk, and he was having a beer, which was okay at that time. In comes a general on inspection, his eye catches this beer-drinking sergeant, and he says to him, 'Soldier, is that necessary?' and Stan replies, 'Sir, it won't run without it.' The general graciously retreated."

Louis' early work in neutron cross-section measurements and nuclear-test diagnostics were key to the success of the first atomic bomb and to the development of the thermonuclear bomb that followed. Louis would often tell people that, ironically, he'd never taken a course in nuclear physics. Indeed, the science was too new and no such course existed at Penn State (or most large universities) in those pre-war days.

From 1943–1945, Los Alamos was the focus of arguably the greatest assemblage of scientific brainpower that had ever occurred. Louis worked at Los Alamos amongst the giants who opened the door to the atomic era—men like

The mesa before (in 1964, looking west) and after the construction of LANSCE (looking east, photo taken in 2005).

Robert Oppenheimer, Hans Bethe, Enrico Fermi, Edward Teller, and Richard Feynman—but it was scientists, like Louis, who stepped through that door and advanced the atomic era beyond weaponization.

The war and the Manhattan Project ended, but the world's problems did not. The Soviet Union, with the world's largest army, did not demilitarize and Stalin was now threatening Europe, just as Hitler had. The world's supply of carbon-based fuels would eventually run out. The world's population and its need of abundant, cheap, clean energy would continue to grow. Louis recognized very early on that nuclear energy would play a dominant role in the solution to securing the nation's future. He knew, for example, that nuclear energy was an essential component for meeting the world's energy needs, cheaply, while protecting the environment. Thus, whereas the scientific luminaries and most senior scientists returned to their universities, Louis chose to stay on in the "Atomic City."

In February 1968, New Mexico Senator Clinton P. Anderson (LANL), Glenn T. Seaberg, Chairman of the Atomic Energy Commission (center), and Louis Rosen broke ground for the construction of LAMPF.

The linear accelerator

Los Alamos began as a national defense laboratory, building the world's first fission and fusion bombs, and then miniaturizing them. Fortunately, the U.S. had taken the lead in developing nuclear weaponry. Unfortunately, Joseph Stalin's Soviet Union was not far behind, it had the largest army in the world, and it was overtly threatening Europe and the U.S. The early 1960s was a time of great uncertainty. The Cold War was at its peak. The fear and stress this generated was palpable, leading to air raid shelters and evacuation exercises becoming a way of life. To avoid technological or military surprise, the U.S. must remain at the forefront of national security research and discovery. Allowing a hostile nation to gain technological or military superiority was simply not an option. There was an urgent need to maintain a credibly safe and reliable nuclear weapons stockpile. Yet, because of the dangers of radiation, there was also the realization that atmospheric tests–and eventually all nuclear tests–could eventually be prohibited. In that event, to ensure confidence that the nuclear stockpile was safe and reliable, the U.S. would have to maintain the scientific and technological competence to interrogate and maintain the stockpile. If the stockpile's safety and reliability were ever in question, the U.S. must also maintain that competence to resume manufacturing and testing. In addition, national security, in its broadest sense, requires more than military might. Louis wrote:

> *"There is now recognition that military capability, by itself, is no longer sufficient. Technological superiority is now critical… it is essential for reducing the causes that give rise to, and feed, violence. For example, the availability of affordable, clean, energy is, today, arguably, the most crucial component of international stability, as well as quality of life everywhere. Nuclear energy is increasingly recognized as an essential source."*

National security also requires energy security, food security, economic security, and environmental security. Nuclear science plays a key role in all of these. As a national defense laboratory, LANL was acutely aware of these facts. To help meet the broadest needs of national security, the Laboratory needed to diversify its scientific and technological expertise.

Louis' and Norris Bradbury's (the Laboratory's director after Oppenheimer) vision was to bring more fundamental nuclear science into the Laboratory; nuclear weapons research and fundamental nuclear physics research would collocate, collaborate, and energize one another. Science is the mother to technology; technology provides the tools to resolve human problems. Thus, basic nuclear science would spawn practical applications of nuclear energy to be applied to multiple issues in national security. The drive to constantly improve these practical applications would in turn, drive the need for more nuclear science.

Louis was convinced that no category of nuclear science and technology was more important than probing the atomic nucleus and unlocking the secrets of nuclear structure and function. It was with this in mind that Louis came up with the idea for the accelerator.

The particle accelerator Louis envisioned—a linear accelerator—would be as efficient and multi-functional as possible. "We're going to use the whole hog, including the squeal"! as Louis would say. It was to be the first dual-beam machine ever built. It would use both halves of the radio-frequency cycle to accelerate both negative and positive hydrogen ions, simultaneously. Thus, twice as many experimental ports—without a significant increase in cost—were possible.

The accelerator achieved its designed beam-energy of 800 MeV on Louis' birthday, June 10, 1972. Happy Birthday, Louis!

For example, the positive hydrogen ions, protons, are used to make neutrons. Neutrons are a critical tool for doing nuclear science. The collision of free-flying neutrons into other atoms is what catalyzes reactions in nuclear reactors and in nuclear weapons. These same neutron-induced nuclear reactions are what cause the stars to burn, create the elements, and heat and light the universe. Thus, to understand and safely use nuclear energy, and to recombine atoms to create new elements for space-age materials, vast numbers of neutrons are needed.

Neutrons are powerful tools for interrogating the structure and function of materials. For example, because neutrons have no change, they can see deep inside materials, map magnetic structures, or identify hydrogen and helium effectively. Ultracold neutrons are ideal for studying soft matter such as biological structures and processes. Thus, the generation of neutrons and the pursuit of neutron science can contribute mightily to both fundamental nuclear science and to national security.

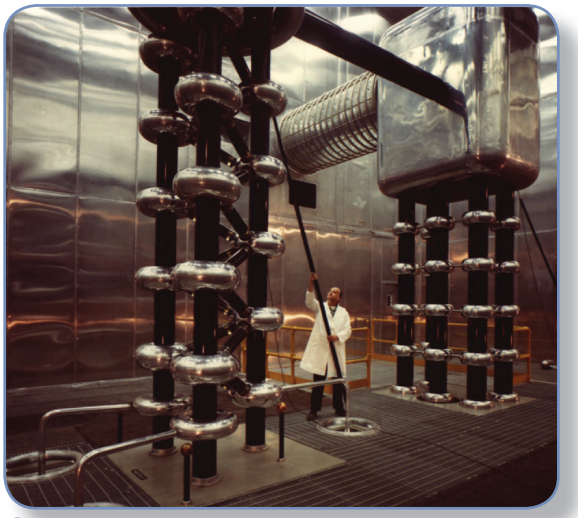

The LAMPF linear accelerator's Crockcroft-Walton generator's H^+ injector is made ready for beam operation testing (1970).

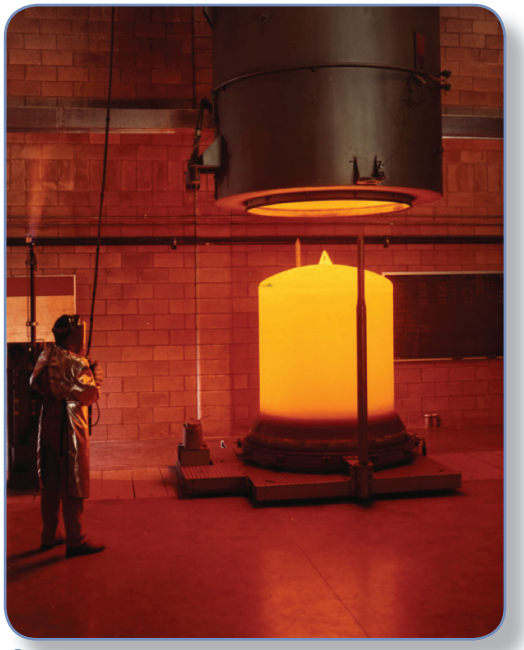

Because of the revolutionary design of the accelerator, the vast majority of its components were manufactured on site. Here, one of the Laboratory's hydrogen brazing furnaces is used to fabricate a unique component.

Louis' accelerator would create copious free neutrons for use in neutron and nuclear science. It would be the world's highest-power-linear-proton accelerator, capable of generating 800-million-electron-volt protons, with a current of 1 milliampere, at 120-pulses every second, and then accelerate a beam of these protons to 84% the speed of light. These accelerated protons would smash into a plate of tungsten steel. The protons' intense impact shatters the nuclei of the tungsten atoms, releasing millions of free neutrons.

But his accelerator would require brand new technology—the side-coupled cavity structure, which would permit phase stability, high intensity and high efficiency, and reduce neutron beam loss. Because it was so advanced and unique, the side-coupled cavity structure would have to be designed, built, and tested at LANL. (Today, every multi-hundred-million-electron-volt proton linear accelerator built uses the LANSCE design. It has

made efficient and stable mega-voltage x-ray machines possible.)

If successful, his accelerator would produce proton beams 10,000 times greater in intensity than any accelerator available at the time, making it the most capable—and most expensive (by a factor of ten)—nuclear physics facility ever contemplated. It would provide the means to reinvigorate and advance nuclear science while also research nuclear weapons development and stockpile stewardship. It would provide powerful new capabilities to research biological systems, condensed matter, produce radioisotopes for medicine and science, do radiography, research nuclear energy for civilian use and an eventual nuclear-hydrogen-based economy, and open the door to new materials science, offering the possibility of building unique "designer materials" for industry, space exploration, and everyday applications.

Such a wondrous machine would attract top-level scientists and students, and help retain them. The accelerator and its research infrastructure would become a National User Facility open to researchers from around the world. By inviting scientists from counties embroiled in the Cold War, it could reduce international tensions. Louis was acutely aware of scientific rivalries and political realities. He deftly lobbied the nuclear science community, federal agencies, and members of Congress for support.

Won over by Louis vision of a facility that would create a synergy between nuclear science and national security research, be a nuclear science center open to the world's scientific community, and improve international relationships, in 1965 Congress authorized funding for LAMPF. The total construction cost would be $57 million. Today, it would take over $1.5 billion to build a facility with the capabilities of LANSCE.

In 1972, just four years after breaking ground, LAMPF became a reality, on schedule and on budget.

The linear accelerator achieved its designed beam-energy of 800 MeV on Louis' birthday, June 10, 1972.

Ambassador of peace through science

The need to de-escalate and end the decades-old Cold War convinced Louis, and a few other politicians and scientists, that sharing some nuclear science and technology with the Soviet Union and Chinese should be encouraged rather than discouraged. Sharing knowledge and working together on common scientific challenges might build mutual trust, encourage camaraderie, and help shift national antagonisms to alliances.

At the height of the Cold War, even while under construction, Louis worked to convince the Laboratory, members of Congress, and the DOE that LAMPF should give limited access to Soviet scientists. Louis' efforts eventually met with success, and the Laboratory was permitted to share LAMPF's designs with Soviet scientists.

In 1968, during the early construction of LAMPF, the first in a series of Russian scientific delegations came to witness the development of LAMPF's novel and massive accelerator. The Russians wanted to discuss its scientific goals. Many also questioned its feasibility.

Many scientists in the Russian Academy of Sciences thought it was impossible for Louis to build his linear accelerator. It was, they believed, beyond current technology, and if not technologically impossible, than far too expensive. And even if it was technologically and economically feasible, it was still far too dangerous to attempt. The intensity of the neutrons, they believed, would certainly be uncontrollable, escape, and the neutron particle-beam loss would destroy the Los Alamos scientists. In short, it was an expensive gamble: too dangerous and with little hope of success. However, other Academy scientists believed the neutrons could be safely harnessed and used for research. These supporters hoped to

convince their nay-saying colleagues, and the Soviet government, that a similar project should be initiated behind the Iron Curtin. It could revolutionize Soviet nuclear physics research. In the end, the Russian scientists were enthralled by Louis' revolutionary project. After careful study, the majority became convinced that it could succeed. The delegation returned, advocating that a similar high-intensity meson physics facility be built for Soviet Bloc scientists.

Soon after their return, a Russian scientist, perhaps cynical but certainly jovial, sent Louis a hand-carved wooden ladle with the following inscription:

Dr. Louis Rosen! I am pleased to present you a Russian magic instrument which may help liquidate the remains of the beam losses in the accelerator.
–A. P. Fedolov, March 2, 1973.

Getting Chinese scientists access to LAMPF was even more difficult. But Louis was determined. Later he would say that, "One of the most important things I ever did was to make it possible for scientists from the People's Republic of China to come to this Laboratory, work at LAMPF, and stay much longer than the canonical eight to ten days that were allowed at the time."

Louis told the story like this:

"Sometime in the 1980s, I received an invitation from the Chinese Academy of Science to come to China with my wife, Mary, under the following arrangement: If I provided three lectures, one of which had to be on energy, they would take us anywhere we wanted to go in China. I got permission from the Laboratory and Washington to go to China, and off we went.

When we got to there they treated us like royalty. They told me where I would lecture, and

Louis' "Russian magic instrument," a hand-carved wooden ladle, presented to him by a Russian scientist to protect Louis and his staff from the dangerous "remains of the beam losses" that might escape the world's most powerful linear accelerator.

I provided the lectures, but they also permitted me to visit any laboratory. I chose the major science laboratories. When our visit was almost at an end, a messenger from Fong Yi, the deputy premier in China at that time, told me that Fong Yi would like to talk to me in the Emperor's Palace in the Forbidden City and asked whether I would be willing to meet with him.

Of course I agreed, and the next morning Mary and I were taken to the Forbidden City in a black limousine. There, at the Emperor's Palace, we were confronted by a huge number of stairs leading up to the palace proper. Fong Yi and his entourage had come down halfway to meet us, and it was up to us to mount the stairs. But Mary already was having trouble walking, as she had had polio, and I wondered how in the world we were going to get her up those stairs. But I needn't have worried. Fong Yi had arranged for two very stout Chinese officers who carried her up the stairs as easy as if she were a butterfly, while I tagged along behind. We then introduced ourselves, went up the rest of the stairs to his office, Mary with her accomplices, and had an hour-and-a-half conversation.

He took half the time to tell me about the advances China had made during the Great March. The other half I talked about what I had found out about his laboratories—the good and the bad. Then he said, 'Now Professor Rosen, I do not have even a high school education, but I am in charge of all the science, technology, and education in all of China. If you were in my place, what would you do to catch up with the West in science and technology?'

I had not anticipated the question (although I should have suspected something like this), but after thinking for a minute or two, I said, 'Well, the first thing I would do is identify, every year, some hundreds of your brightest young scientists and engineers and send them to centers of excellence, not for a week or a month, but for a year or even two years. That way they can become engaged not only with the frontiers of science and technology but also with the

Chinese scientists and Louis exchange information during a guided tour of the Institute for Modern Physics in Lanchow, China. Louis' visit resulted in an ongoing exchange of scientists between the two adversarial superpowers, helping relieve political tentions, encouraging a broader dialogue, and improving relations.

environment that permits science and technology to flourish.' He replied, 'Yes, Professor Rosen, that's a very, very good idea. Now, would you accept some of them at your facility?'

Now I understood the reason for our invitation and the reason for all the things that had happened before. My answer was, 'Mr. Vice Premier, the rules of my government are that we can accept Chinese citizens at Los Alamos for only a few days. But if you will nominate scientists whom we know by their reputation, I will do what I can to get that rule changed."

About three months later, a letter came from his Deputy for Science nominating three renowned scientists. One was director of their main nuclear physics laboratory, another was a group leader of their chemistry group, and a third was an expert on radioactive nuclei. Now, the monkey was on my back.

Fortunately, if you're lucky, you don't have to be smart, and I have been lucky many times. Congress had already been persuaded that LAMPF must be an open facility if world-class science and technology was to continue at the Laboratory. I'm not sure that everyone in the Congress understood that. But, as luck would have it, it turned out that a former neighbor of mine, Herman Roser, who had been the Atomic Energy Commission representative at the Laboratory, was now head of the Division of Military Applications in the Atomic Energy Program. It was up to him to decide what the security rules were. I went to see Herman and told him, 'Look, if we could make friends with these people, one quarter of the people on Earth, it would be worth more than any number of aircraft carriers or bombers that we could possibly build.' Herman understood this. In a few months word came that, yes, we could invite the Chinese scientists for an extended stay.

Soon after his visit to China, Louis brought a delegation of Chinese scientists to LANSCE.

They were marvelous visitors and worked all hours of the day and night. I suspect that our initiative was a factor in improving our relations with China at a critical time."

The Legacy of Louis Rosen

Under Louis' leadership, LAMPF became a science magnet; it attracted students and scientists with exceptional talent and ideas to the Laboratory from all over the world. This cross-cultural interaction fostered an environment that encouraged a symbiotic relationship among national laboratories, academia, and industries, and promoted not only a cross-fertilization of scientific ideas but promoted and contributed to reducing international tensions.

Louis' legacy continues at LANSCE. Today, LANSCE is a DOE-designated National User Facility. LANSCE's User Program plays a key role in training the next generation of top scientists, attracting the best graduate students, postdoctoral researchers, and early-career scientists from around the world. In addition, each summer the LANSCE Neutron Scattering School invites approximately 30 of the world's brightest future neutron scattering users for an intensive nine-day program of lectures and hands-on experiments in neutron scattering. Together, these programs provide the cutting-edge in science and training in nuclear and materials science for the benefit of the nation and world.

LANSCE honors the vision that Louis had more than forty years ago—collocating basic nuclear research with programmatic work to nurture engagement between fundamental nuclear science and nuclear science for our national security.

Finis

Louis received many awards and honors throughout his career. In 1963, the DOE awarded Louis the E. O. Lawrence Award. The E. O. Lawrence Award, first awarded in 1960, was established in 1959 and honors U.S. scientists and engineers, at mid-career, "for exceptional contributions in research and development supporting the Department of Energy and its mission to advance the national, economic and energy security of the United States." In 2002, he received the Los Alamos National Laboratory Medal—the highest award the Laboratory bestows upon an individual.

The citation for the Medal reads:

"For vision, leadership, and sustained contributions to nuclear science and its applications. For his inspired and dedicated efforts to successfully bring the Los Alamos Meson Physics Facility, a premier international research capability, to fruition. For his untiring efforts during the Cold War period as a spokesman for maintaining relationships with scientists from the former Soviet Union and China as a means of improving understanding."

Selected Highlights of Louis' Career

- B.A. and M.S., University of Alabama.
- Ph.D., Pennsylvania State University.
- Scientific Staff, Manhattan Project, Los Alamos, 1944.
- Measured 14-MeV neutrons in thermonuclear deuterium-tritium processes.
- E. O. Lawrence Award, 1963.
- Group Leader and Alternate Division Leader in the LANL Experimental Physics Division until 1965.
- Proposed, obtained support for, and directed the development of the Los Alamos Meson Physics Facility, the world's largest linear accelerator, providing nuclear science research facilities for scientists in the national and international communities.
- Contributed significantly to understanding the fission process, the fusion process, the interactions of light nuclei, the interactions of neutrons with nuclei, and the role of spin-dependent forces.

- Leader of the LANL Medium-Energy Physics Division and Director of the Los Alamos Meson Physics Facility, 1964–1985.
- Vice-Chairman and Chairman, Division of Nuclear Physics, American Physical Society, 1984–1985.
- LANL Senior Fellow and member of the Center for National Security Studies, 1985–1990. Authored more than 100 scientific publications.
- Los Alamos National Laboratory Medal, 2002.

LANSCE Division Office Building today. Louis's wife, Mary, designed and supervised the layout of the gardens, patios, parks, and other landscaping.

LANSCE Research Highlights

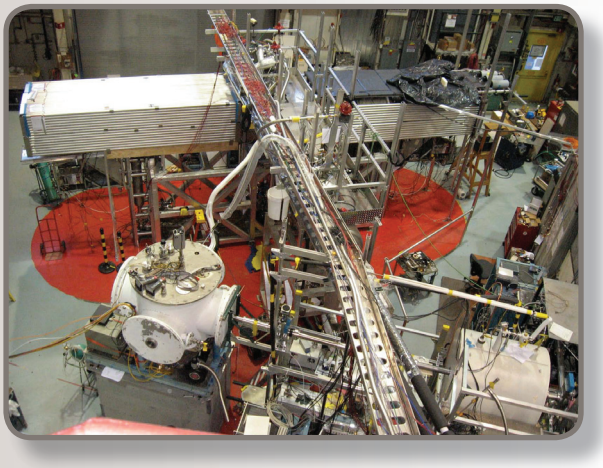

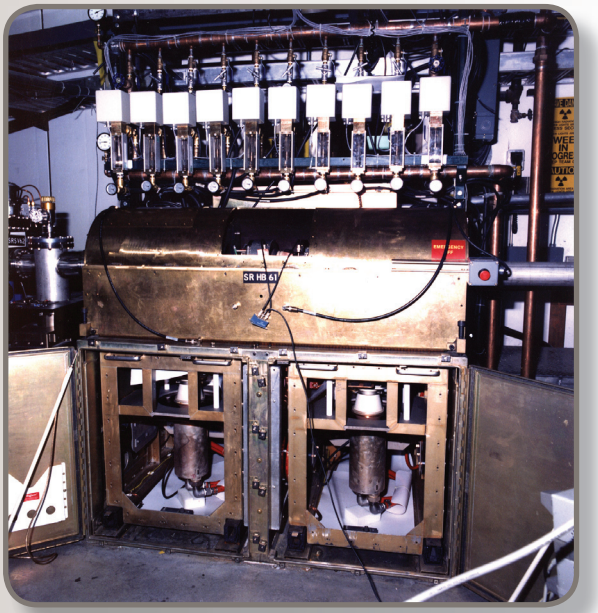

Lujan Center

Introduction

Research Highlights

Lujan Neutron Scattering Center

A unique research environment exists at the Lujan Neutron Scattering Center (Lujan Center) at LANSCE academic researchers work side-by-side with national security researchers. Perched on a mesa between steep canyons laden with archeological sites, the Lujan Center provides state-of-the-art instrumentation and world-class scientific staff for user-driven research in materials and nuclear physics. With an average of over 600 user-visits per year from all over the world, the Lujan Center fosters a broad research agenda—from bridge-cable failure to the Standard Model. Unlike any other user facility, the Lujan Center specializes in melding academic science and national security science: because the fundamental science is the same, the interaction of these two communities strengthens the science in both camps.

Neutron scattering is indispensable in today's condensed matter and materials sciences. Neutrons are created at LANSCE by a spallation nuclear reaction of tungsten nuclei after being hit by the speed-of-light protons from the LANSCE accelerator. Once liberated from the nucleus and cooled down by moderation with hydrogen, neutrons are directed toward samples inside. These neutrons are then scattered from interacting with nuclei and internal magnetic fields in solid and liquid matter. The scattered neutrons provide useful information about atomic spacing, vibrational motion, and magnetism. When combined with their high penetration ability through materials containing heavy metal atoms, unmatched sensitivity to hydrogen and other light atoms, and their ability to distinguish isotopes of the same element, neutrons probe materials in special, powerful ways.

Lujan researchers measure the scattered neutrons' time-of-flight and scattering angle to determine the neutrons' momentum and their energy (i.e., wavelength) accurately even after losing or gaining small quanta of thermal energy by interacting with a sample. Tracking the neutrons' energy and momentum allows one to determine where atoms are and how they move. This information is fundamental to the properties of materials.

Neutrons are scarce even at a powerful spallation source like LANSCE. While the Lujan Center currently has highly competitive power—running at 100 kW—the Lujan Center's distinction is in having the world's lowest repetition rate, 20 Hz, between neutron pulses and efficient, liquid-hydrogen moderators that cool the neutrons to long wavelengths. The low repetition rate provides very high peak flux and a relatively long time frame between the fastest and the slowest scattered neutrons in a pulse. This large "bandwidth" allows full utilization of the long neutron wavelengths that probe biological and soft matter so well.

Among recent scientific results, Lujan Center instruments have been used to: determine the fundamental chemical function of xylose isomerase, the enzyme used by industry to convert fructose to higher sugars; to test the hypothesis that the Egyptian pyramids were cast of an ancient form of concrete; to explore the packing characteristics of amyloid proteins implicated in Alzheimer's Disease; to observe "spin capacitance" in materials whose magnetization changes with applied electric field; and to observe shape memory in metals under both thermal and magnetic fields.

Even more distinctive than its bandwidth is the Lujan Center's ability to stage sensitive, and even classified, experiments in support of national security. Recent advances include studies of challenging materials, such as cholera toxin, high explosives, and fundamental studies of excitations in plutonium relating to how it compresses in a nuclear weapon to reach

critical mass. A major breakthrough is the new Safety Basis that makes it easier to perform high pressure and heated experiments on plutonium and other transuranics.

Designed over the years 2005–2009, the new Mark III spallation target incorporates several innovations over Mark II. The Mark III doubles the production of cold neutron flux yet again. Flux-trap targets with coupled moderators invented at Lujan Center have established a widely copied, world-wide standard of flux. It is worth noting that the LANSCE accelerator has been a megawatt-class proton accelerator since 1986 and has delivered over 4000 hrs of beam as recently as 2005 with good reliability.

A special treat for both staff and users is the annual LANSCE Neutron Scattering School Serving 30 graduate students and postdocs per class, the school is one of the few topical scattering schools in the world, rotating between concentrated subjects like magnetism, materials engineering, soft matter, and hydrogen materials. Students learn from world-leading faculty followed by hands-on experience with actual neutron scattering experiments. Begun in 2004, alumni of the school are a growing part of the worldwide neutron community. The school fortifies the early career demographic slice (under the age of 40), representing over 60% of Lujan Center users, and the academic cadre, representing half of Lujan users.

While the years 2007–2009 have been extremely productive for the Lujan Center by averaging 640 annual user visits for 3000 hrs of beam, the halcyon years 2004–2006 indicated even greater potential for the user program. By running 4100 hrs, user visits peaked in 2005 at over 750. This measure and others indicate that the Lujan Center runs at approximately 50% of maximum utilization. Major areas of improvement for the next phase of Lujan Center development are beam hours and reliability, user support, and instrument capability.

The Enhanced Lujan Program (ELP) will more than double the utilization of existing beamlines and will emphasize materials in extreme environments. Nine of Lujan Center's 17 flightpaths were equipped in 2007–2009 with new or upgraded instruments from an instrumentation campaign that ended in 2002. Twelve instruments do materials research, three are devoted to fundamental nuclear physics, and two beamlines are open and available for new instruments.

Six of the 12 materials research instruments and two of the three nuclear physics beamlines are internationally competitive. Because of the urgency in the national innovation agenda, particularly for energy materials research, we can ill-afford the underutilization of this national resource. Although the Lujan Center's core strength in diffraction will continue, much of the planned new instrumentation will be for inelastic scattering.

From 2004 through 2009, the Lujan Center has led DOE neutron scattering programs in user base, drawing heavily from New Mexico, California, and Tennessee. Until the Spallation Neutron Source at Oak Ridge National Laboratory (ORNL) achieves full power and instrumental strength, and ORNL's High Flux Isotope Reactor opens all of its beams, the Lujan Center could remain second in the U.S. only to National Institute of Standards and Technology's Center for Neutron Research in user program size.

The Lujan Center serves the nation in a way unique to all user facilities by providing a place to perform national security research in a safe and secure manner without disrupting access to academic and industrial users. With modest investment to reach full utilization, the Lujan Center's future is bright.

Magnetic exchange energies in changed order $La_1/3Sr_2/3FeO_3$-δ

Using the Pharos inelastic scattering spectrometer at the Lujan Center, researchers M. Hehlen and F. Touw and their collaborators from Iowa State University and the Ames Laboratory have determined the magnetic exchange energies in charge ordered $La_1/3Sr_2/3FeO_3$-δ (LSFO) and its parent compound $LaFeO_3$ (LFO). In LSFO, the measured ratio of ferromagnetic exchange between Fe_3+ - Fe_5+ pairs (JF) and anti-ferromagnetic exchange between Fe_3+ - Fe_5+ pairs (JAF) fulfills the criterion for charge ordering driven by magnetic interactions (|JF/JAF|>1) (Figure 1).

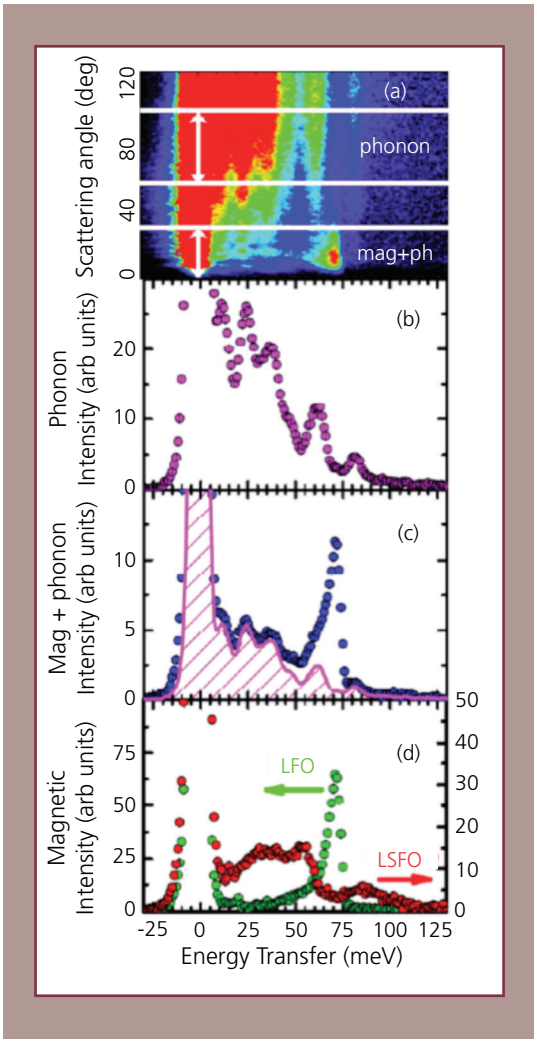

Figure 1. (a) Inelastic neutron-scattering intensity of $LaFeO_3$ (color scale) versus scattering angle and energy transfer at T = 10 K and Ei = 160 meV. Horizontal white lines delineate regions where phonon and magnetic scattering are isolated. (b) Neutron intensity summed over the angle range from 55 to 95° originating from phonons. (c) Neutron intensity summed over the low-angle range from 1–30° (dots) and phonon background scaled from high-angle sum (hatched region). (d) Isolated magnetic scattering from LFO and LSFO at T = 10 K.

The 30% reduction of JAF as compared to LFO indicates that doped holes are delocalized, and charge ordering occurs without dominant influence from Coulomb interactions. These findings are of significance because charge ordered, or nearly charge ordered, ground states are thought to play an important role in colossal magneto-resistive manganites and high-temperature cuprate superconductors. (*Physical Review Letters* **98**:126402 (2007).)

Researchers examine elusive technetium oxides

Technetium (Tc) is an artificial element and is the only transition metal without a stable isotope. It is a byproduct of nuclear weapons and the production of fission power; it constitutes about 8% of the fission yield of uranium-234. Surprisingly little is known about the oxides of Tc, and TcO_2 is the only simple transition metal oxide for which the structure had not been determined.

The Lujan Center formed a team, E. Rodriguez (graduate student, University of California, Santa Barbara) and A. Llobet, in collaboration with A. Sattelberger (Argonne National Laboratory), A. K. Cheetham (University of California, Santa Barbara), and F. Poineau and K. Czerwinski (University of Nevada, Las Vegas), that success-fully synthesized and characterized new Tc-based compounds. The researchers published the synthesis and characterization of two of the three expected Tc binary oxides (Tc_2O_7 and TcO_2).

Their publication is the first report of the crystal structure determination by neutron powder diffraction. The results show metal-metal bonding between Tc pairs along the edge-sharing chains of TcO_6 octahedra (Figure 1). The researchers performed electronic structure calculations to further elucidate the bonding mechanisms in TcO_2. (*Journal of the American Chemical Society* **129(33)**:10244-10248 (2007).)

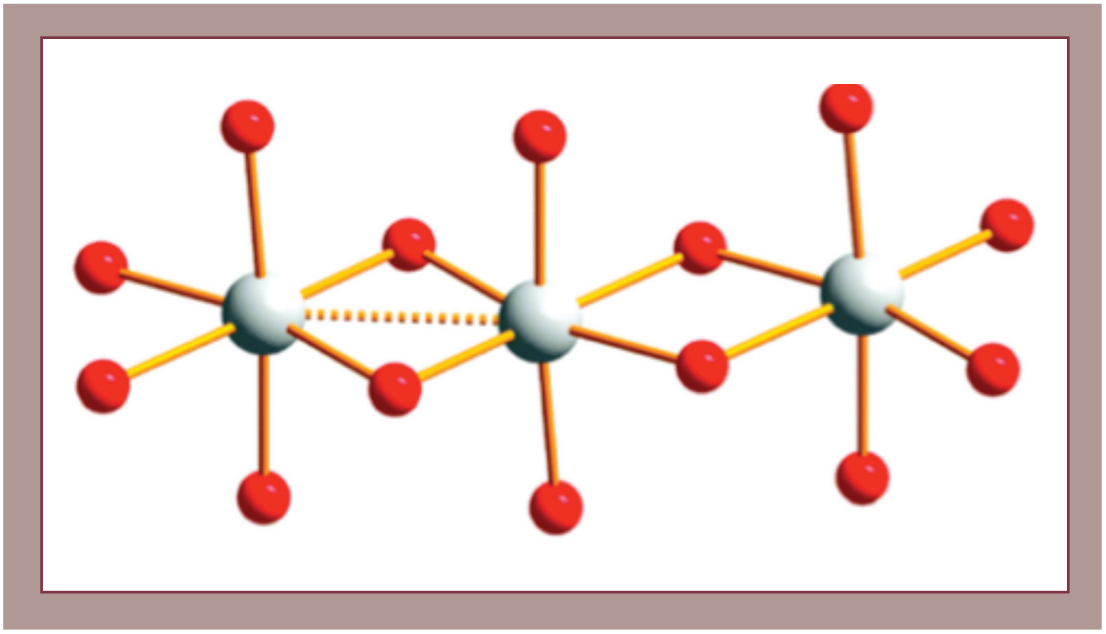

Figure 1. A structural unit of TcO_2 consisting of three edge-sharing TcO_6 octahedra. The metal-metal bond is labeled by the dashed line.

The researchers have synthesized the new compounds Bi_3TcO_8, $Bi_2Tc_2O_7$, $Bi_3Tc_3O_{11}$, and others from the Sr-Tc-O, such as Sr_2TcO_4. The scientists used neutron scattering and x-ray absorption spectroscopy to characterize the crystalline structures of these new materials. Analogous rhenium and ruthenium-based oxides, like Sr_2RuO_4 or $Cd_2Re_2O_7$, exhibit superconductivity or show metallic ferromagnetism ($SrRuO_3$), thus the new Tc materials are very promising candidates for displaying superconductivity or other emergent phenomena.

Neutron scattering studies reveal high-density hydrogen storage

Alternative energy sources, such as hydrogen and methane gases, are under investigation for the future energy economy. Developing suitable materials to store hydrogen under a variety of conditions is a major challenge. Addressing this challenge requires systematic studies of the structures, stability, and kinetics of proposed hydrogen-storing compounds.

Inclusion and cage-like compounds, called clathrates, in which a gas molecule guest is physically incorporated into the host framework, are possible means to store hydrogen. Neutron scattering is a particularly useful analytical tool in conjunction with variable temperature and pressure capabilities to monitor the gas uptake/release processes in these inclusion compounds,

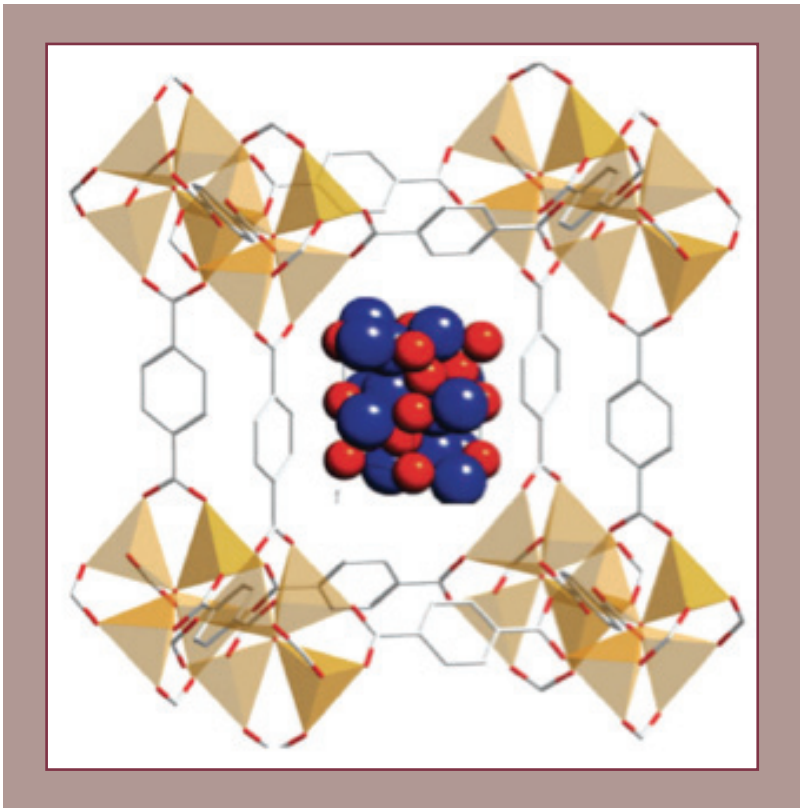

Figure 1. Structure diagram of a potential hybrid material of the MOF with the $CH_4(H_2)_4$ molecular compound encapsulated into its cage. MOF consists of metaloxygen clusters (tetrahedra) on the vertices of the lattice and organic linker molecules (hexagons) along its edges, which largely define the size and shape of the cage. Blue balls in $CH_4(H_2)_4$ represent CH_4, and red balls represent H_2.

especially for locating the incorporated gas molecules and characterizing their interactions with the host frameworks. Researchers have used the Lujan Center's High-Pressure Preferred Orientation (HIPPO) spectrometer to make advances in high-pressure instrumentation that enable detailed studies of uptake and release, structure, and dynamics of hydrogen in so-called "framework" compounds, such as clathrates and metal organic frameworks (MOFs) (Figure 1). The new instruments allow in situ and real-time examination of reaction kinetics with methane and hydrogen clathrates, a group of inclusion compounds consisting of frameworks of hydrogen-bonded water molecules with gas molecules trapped inside the cages. Their results reveal that cage-like compounds can compress and hold hydrogen at states over twice the density of solid or even metallic hydrogen. A clathrate can store up to four hydrogen molecules in each of its large cages. The framework-pressurizing effect is striking and may exist in other inclusion compounds, such as MOFs. (*Proceedings of the National Academy of Sciences* **104**:5727-5723 (2007).)

"Training" shape-memory alloys

A China-U.S. research team at the Lujan Center has direct evidence how microscopic stress influences the choice of crystal structure in magnetic alloys that remember their shape while undergoing a phase transition. This insight suggests ways to "train" materials for selected response in applications requiring adaptive response to environmental conditions.

In ferromagnetic shape-memory-alloys, the distribution of crystallographic variants should be equally partitioned after a phase transition without applied external fields; but often some variants are favored, while others are suppressed. Although residual stress inside the materials was suspected, no direct experimental evidence was seen because of the lack of effective experimental tools. Using the Spectrometer for Materials Research at Temperature and Stress (SMARTS) instrument at the Lujan Center, D. W. Brown (LANSCE) and Y. D. Wang (Northeastern University, China and the University of Tennessee) characterized the structure of Ni_2MnGa ferromagnetic shape-memory-alloy under a uniaxial stress field by neutron scattering.

The ratios of intensity for the two texture components (the two variants belonging to the same orientation of parent phase) are taken as the simple indicators to evaluate the influence of external stress on the selections of variants. The experimental values are shown in Figure 1.

The experimental values at zero MPa obviously deviates from the linear relationship and are not equal to one. This indicates that the present alloy does not obey the equivalent

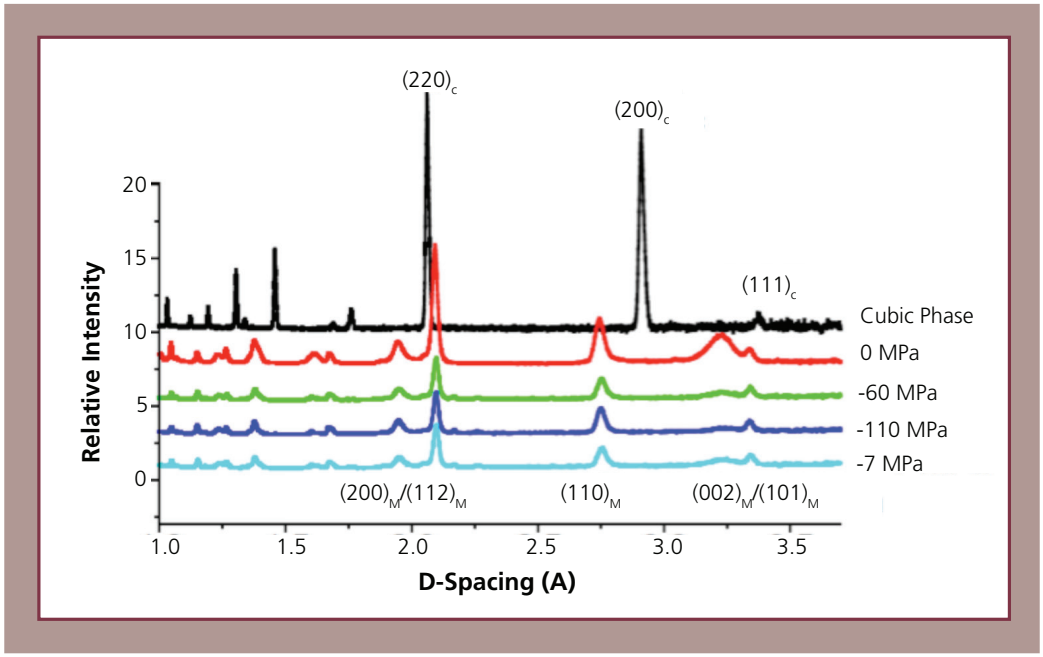

Figure 1. SMARTS data for the shape-memory alloy.

partition of variants at the initial state. The result can be attributed to the existence of intergranular stress or the influence of amellar microstructures in the cast alloy. However, a stress of -60 and -110 MPa obviously disturbed the distributions of variants. When the stress was released to -7 MPa, the initial partition of variants was not recovered. Thus, a small stress applied during phase transformation may cause obvious redistribution of variants.

The neutron experiments further verified that the texture in the specimen was not changed by just a simple cyclic heat-treatment, that is, repeatedly heating (up to 973 K) and cooling under no external stress field. Thus, the present observation on the "broken" memory or reselections of variants during the phase transformation under the external stress provides direct and unique experimental evidence on the "training" mechanisms by changing the internal stress field that lead to the redistribution of the variants.

Competing magnetic interactions and electrical conduction research in mixed valent $YBaFe_2O_5$

Mixed-valent oxides are the basis for many important modern materials with desirable electrical properties, such as high-temperature superconductors and colossal magneto-resistive-manganites. $YBaFe_2O_5$ is an example of a mixed valent oxide where low temperature charge ordering results in an electrical insulator. Melting of the charge order increases the electrical conductivity.

The magnetic interactions between iron (Fe) ions in both the charge ordered and mixed valent (metallic) phases are predominantly antiferromagnetic. However, conduction can only proceed through ferromagnetic Fe-Fe bonds. Electronic exchange processes cause magnetic interactions between Fe ions, and measurement of the magnetic excitation spectrum with inelastic neutron scattering

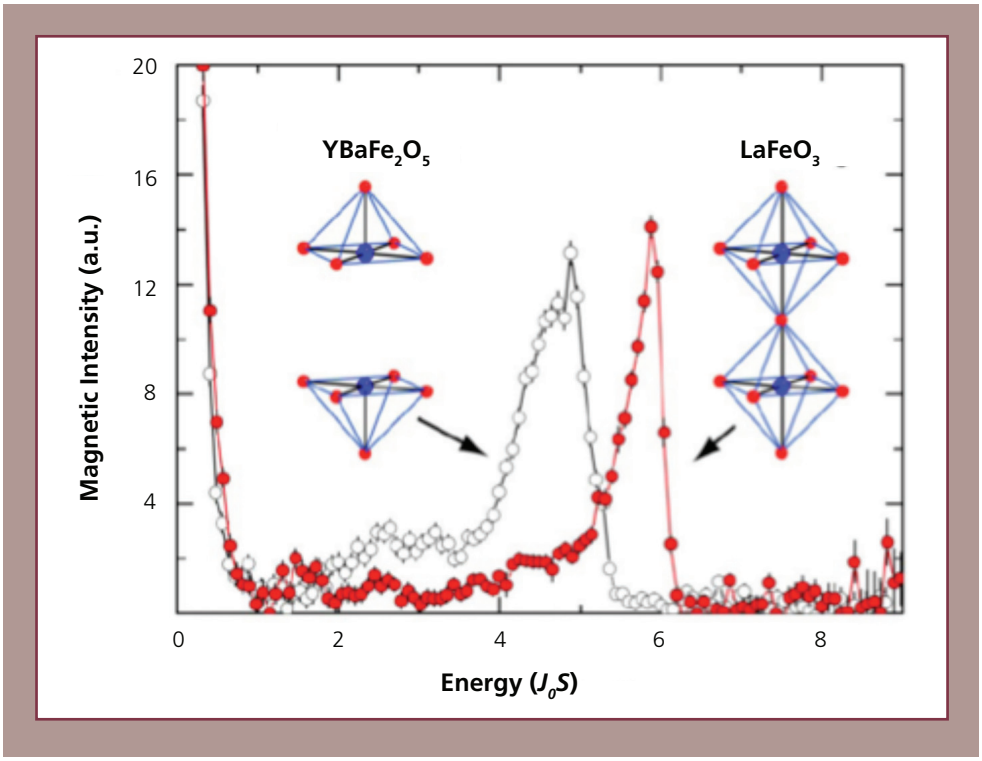

Figure 1. Magnetic scattering intensity for $YBaFe_2O_5$ at 6 K and $LaFeO_3$ at 10 K. Insets show idealized oxygen square pyramids in $YBaFe_2O_5$ and octahedra in $LaFeO_3$, illustrating the broken magnetic bond in $YBaFe_2O_5$ in comparison to $LaFeO_3$.

provides a window to view the underlying charge dynamics. Researchers F. Trouw, M. Hehlen, and collaborators from the Ames Laboratory, University of Oslo, and Iowa State University have used the Pharos spectrometer (at the Lujan Center), which can accommodate the full range of inelastic scattering experiments on liquid, polycrystalline, and single-crystal samples; to determine the strength of the exchange interactions in both phases.

Measurements of polycrystalline-averaged spin excitation spectra of long-range magnetically ordered material result in neutron scattering intensities related to the spin-wave density of states (SWDOS). The SWDOS in $YBaFe_2O_5$ is comparable to $LaFeO_3$, after accounting for the one broken antiferromagnetic exchange bond (five nearest neighbors) present in the square-pyramidal coordination (Figure 1). From these measurements the scientists conclude that electrical conduction proceeds within the antiferromagnetic Fe sublattice by an electron hopping process that requires a Fe spin-flip, thereby temporarily creating a ferromagnetic channel. The hopping process disrupts near-neighbor spin correlations, leading to massive damping of magnetic excitations. (*Physical Review Letters* **99**:037202 (2007).)

Neutron reflectometry helps iron out origin of wrinkles

On a supporting substrate, the propensity of a membrane-like skin to wrinkle when it overfills an assigned area is universal, and the transition from a gentle, reversible washboard to a single deep arroyo is viewed as a competition between the potential energy for making deep displacements in the substrate and the bending energy of the overlying membrane.

Understanding the mechanical stability of thin elastic membranes resting on softer substrates has biomedical (inside wall of arteries and lung lining) and technical (polymers) applications.

Lujan Center neutron users from the University of Chicago and J. Majewski (LANL) have used reflectometry at the Surface Profile Analysis

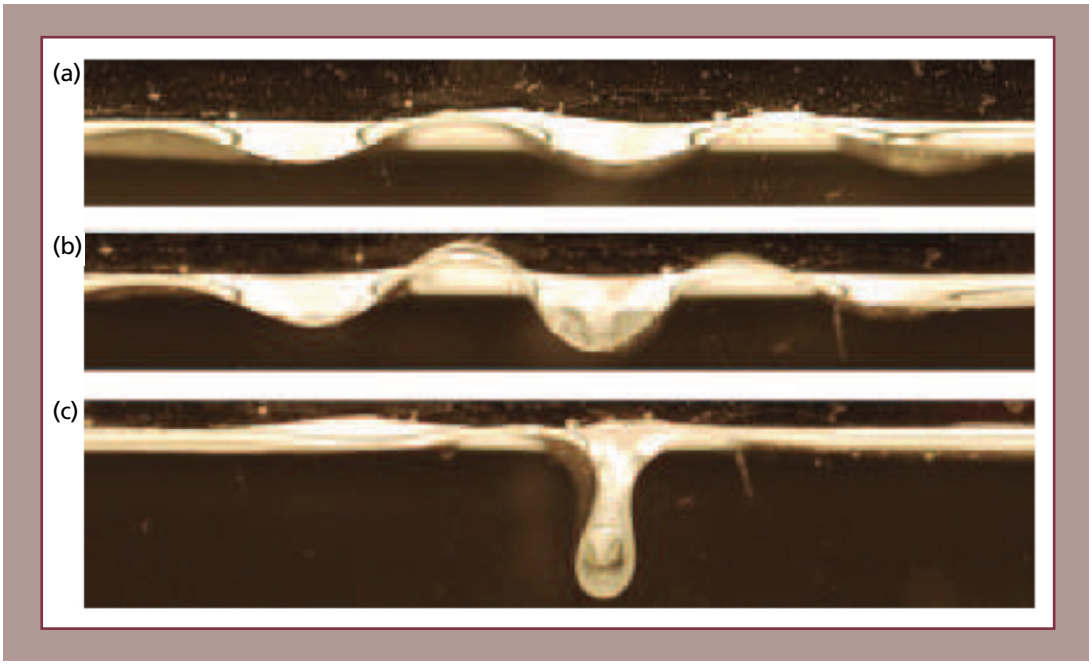

Figure 1. Wrinkles in time. Left panels: Ten-micron polyester film on water at three different compression states (imaged from the side). Right panels: Tri-layer of colloidal gold nanoparticles on water (top view) transitioning from an extended wrinkled state (A) to a localized folded state upon further compression (C). Nanoparticle layer is 15 nm. The nanoparticles, compressed in a Langmuir trough, are microscopically imaged from above. (A) Shows a uniform wrinkled surface; the wrinkle troughs appearing brighter due to scattering. As one wrinkle grows in amplitude it becomes brighter still (B). Upon fold completion (C), the fold extending underneath the surface is several microns long and far below the focal plane of the surface, so scattering is not seen. Thus, the fold appears dark due to its thickness suppressing transmission. The membranes span three orders-of-magnitude in thickness and initial wrinkle wavelength.

Reflectometer (SPEAR) to establish physico-chemical changes in a glycerol-water substrate that govern wrinkles formed in a single-molecular layer riding at the liquid-air interface. By compressing the layer, comprised of soap-like lipid molecules that orient with their greasy hydrocarbon tails pointing skyward, and using teflon barriers, the layer first condenses into a two-dimensional solid from a dispersed gaseous state and then begins to wrinkle upon further compression.

The bending of the membrane to form wrinkles costs energy. At that point, the gravitational potential energy for the glycerol-water substrate to form a wavy surface accommodating the compressed layer also becomes important, even though the up-down displacements are tiny (order of nanometers) and the wavelengths are small (micrometers). Minimizing the total energy, bending-plus-potential, gives a successful description of wrinkling to a point—at a certain confining surface pressure, one wrinkle becomes unstable and dives into the liquid substrate allowing adjoining wrinkles to flatten out. Though this single deep-invagination comes at great energy cost, the savings from flattening dozens or hundreds of neighboring wrinkles more than buys back the debt. This trade-off can be seen in photos of a polyester-film and a gold-nanoparticles-film on water in Figure 1. Varying in the glycerol-water substrate composition tests this theory by changing the effective bending modulus of the membrane and, to a lesser extent, the potential energy via the density. Neutron reflectometry results show that the water-glycerol ratio varies near the free surface in a way consistent with the wrinkling results. The experimental data and theoretical calculations are in good agreement. One of the Lujan Center users, L. Pocivavsek of the University of Chicago, was honored with an invited talk on this topic at the 2008 March Meeting of the American Physical Society.

Soft- and biological-matter communities are growing at the Lujan Center

Several Lujan Center instruments cater to the needs of a growing user community interested in soft and biological matter. Therefore, the Lujan Center attracts soft matter experiments relevant to national security. For example, a major paper in *Macromolecules* by R. Hjelm (LANL) et al. elucidates the structure of Estane, a linear polymer with hard and soft segments that create unusual strength and thermodynamics.

Based on small-angle neutron scattering results from the low-Q diffractometer (LQD), the authors showed how Estane's hard segments unlink then agglomerate in situ in the aging of high explosives.

Biomembrane physics has become a major focus of the Surface Profile Analysis Reflectometer (SPEAR), a neutron reflectometer. In national security science research, results were published on membrane attack mechanisms by biotoxins from botulinum, diphtheria, cholera, and anthrax in *Biophysical Journal* by J. Majewski (LANL) et al. Most other scattering centers do not embrace these complicated experiments. The SPEAR team published toxicity mechanisms of an amyloid-beta peptide associated with Alzheimer's disease in *Proteins*.

The Lujan Center's Protein Crystallography Station (PCS), funded by DOE Basic Energy

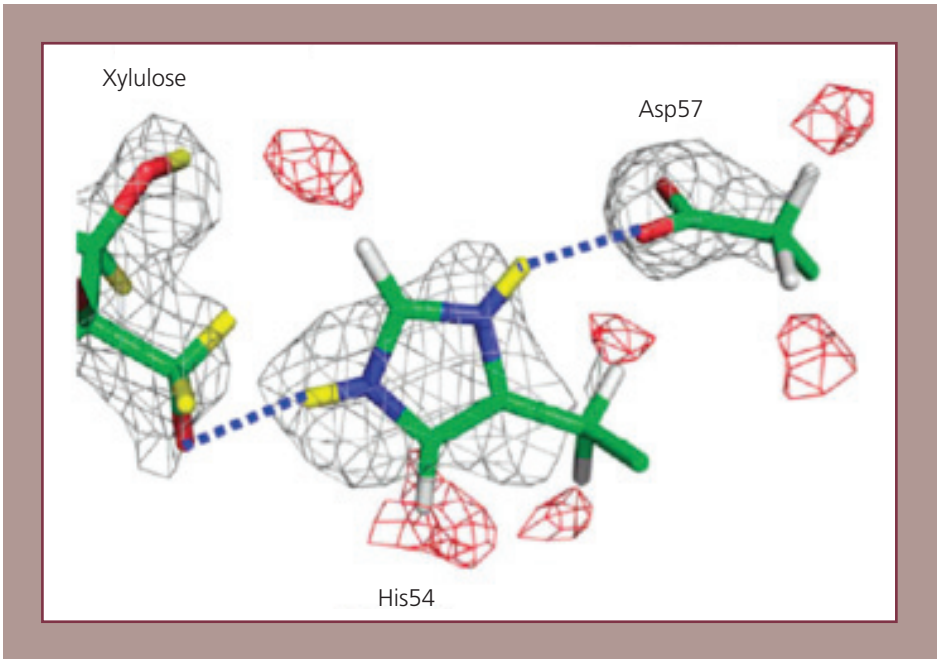

Figure 1. Active sites in xylose isomerase illustrated by nuclear density map from PCS. Carbon, oxygen, nitrogen, and deuterium atoms are green, red, blue, and yellow.

Sciences, has international impact by establishing the catalytic pathways of hydrogen in important enzymes. Aspartic proteinases, a class of enzymes that cleave peptides, is involved in numerous disease conditions, including hypertension, amyloid disease, malaria, and AIDS. In the HIV virus, for example, aspartic proteinase is essential for the maturation of the virus, which makes it an important target of pharmaceuticals. Similarly, xylose isomerase (Figure 1) is relevant to the origins of cancer but is also a crucial enzyme in sugar metabolism. This enzyme has substantial commercial application in the production of high-fructose corn syrup and biofuels. In high-profile publications in *Biochemistry* and *Journal of the American Chemical Society*, PCS users show how hydrogen atoms are transferred during enzyme-catalyzed reactions, significantly improving our understanding of the reaction mechanisms.

Neutron scattering pressure studies lead to new insights in hydrogen storage compounds

Cage-like compounds and metals can compress and hold hydrogen at states more than twice the density of solid or even metallic hydrogen, according to Lujan Center researchers. Since alternative energy carriers, such as hydrogen, are becoming increasingly important for the future economy, solving the major challenge for hydrogen storage is urgent. This work has profound impact on National Nuclear Security Administration's (NNSA's) production schedules as well.

In two reports, one published in *Proceedings of the National Academy of Sciences*, researchers studied hydrogen uptake, release, siting, and dynamics in materials, particularly in "framework" compounds such as clathrates (Figure 1) and metal organic frameworks. Neutron scattering in situ kinetics experiments are very powerful because deuterium can be used to enhance signal. With clathrates, H_2 capacity is up to four molecules per cage with an intermolecular spacing 30% closer than metallic hydrogen (3.78 Å). This striking framework-pressurizing effect exists in other inclusion compounds such as nanotubes.

Hydrogen materials are important in neutron tubes for NNSA systems. A separate Lujan-based team monitored deuterium site occupancy in erbium (Er) metal during target loading (Figure 2). In a neutron tube, the target film contains tritium, which is bombarded with deuterium ions from

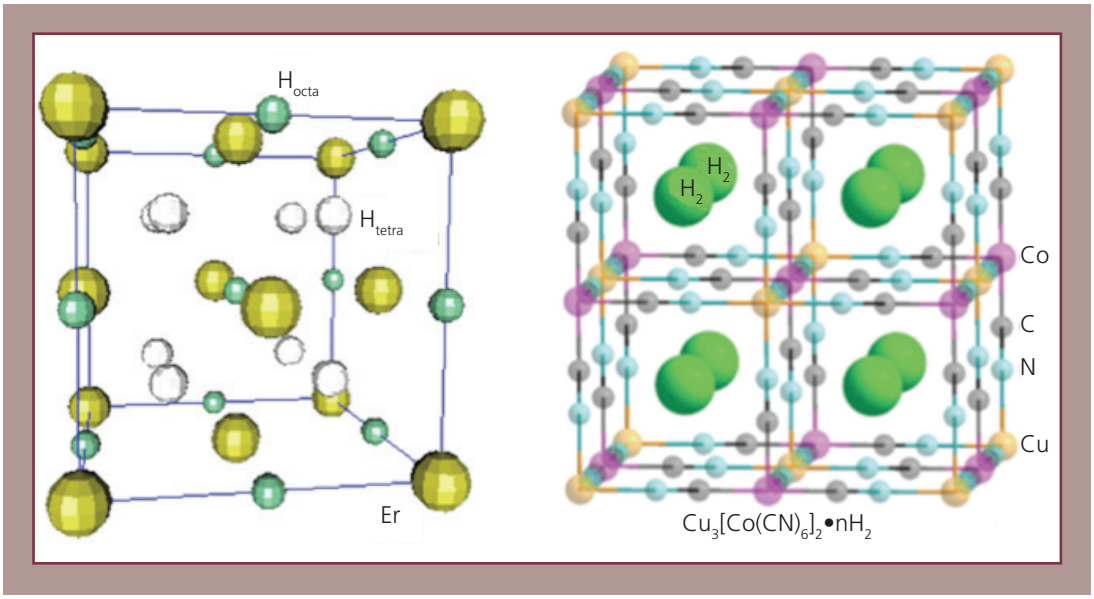

Figure 1. Hydrogen inclusion compounds. Er hydride (left) is used in tritide form to produce neutrons in neutron tubes. It takes up hydrogen first in tetrahedral positions, followed by octahedral positions, with increasing hydrogen pressure. For energy storage applications, complex cage molecules formed at high pressure, such as the semiclathrate (right), capture freely rotating hydrogen molecules.

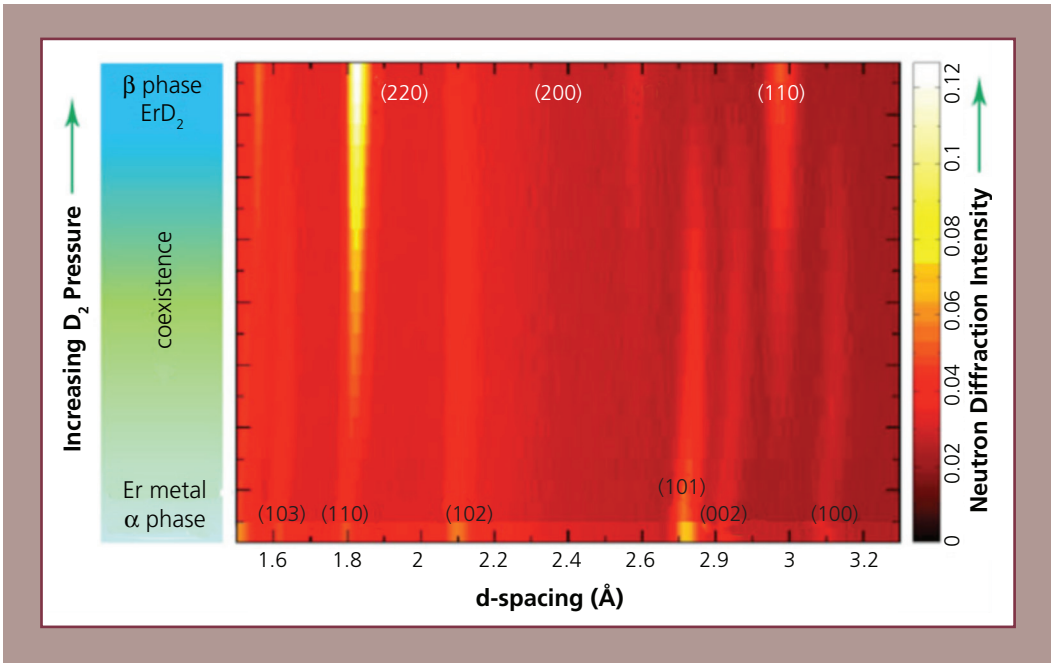

Figure 2. Neutron diffraction intensity as function of deuterium gas pressure (vertical) for Er deuteride. Orange/yellow peaks at the bottom of graphic indicate diffraction lines from Er metal (hexagonal) without D_2 exposure. Upon addition of D_2 gas, the hexagonal peaks shift as the deuterium incorporates into the hexagonal Er lattice. This results in a shifting of the peaks to larger d-spacing. Upon further addition of deuterium, the Er develops a second phase of ErD_2 (FCC). The FCC phase continues to grow in phase fraction at the expense of the hexagonal Er lattice.

a high-voltage source. The resulting deuterium-tritium fusion reaction produces copious on-demand neutrons used in military, homeland security, industrial, defense, and medical applications. Vagabond radiogenic helium atoms released from Er-tritide target films decrease tube lifetime, already limited by natural tritium decay.

Sandia, Los Alamos, and Oak Ridge National Laboratories' staff used neutron diffraction to measure hydrogen-site occupancies within the Er lattice and found that octahedral site occupancy causes lattice expansion-induced stress. At various temperatures and hydrogen pressures, the site occupancy changes, as does the phase of hydride from ErD_2 (fluorite structure) to ErD_3 (hexagonal). Knowledge of gas temperature and pressure provides a science-based rationale for processing variables in loading tritium into Er.

Protein Crystallography Station makes impacts in understanding enzyme catalysis

The Protein Crystallography Station at the Lujan Center made major scientific impacts in understanding the role of hydrogen in the enzyme aspartic proteinase. Aspartic proteinase cleaves peptides and is involved in numerous disease conditions including hypertension, amyloid disease, malaria, and AIDS. In HIV, the proteinase is essential for the maturation of the virus particle, and inhibitors have a proven therapeutic effect in the treatment of AIDS. Thus, inhibitors to this class of enzyme with improved characteristics are potential therapeutic agents.

Aspartic proteinase consists of two structurally similar domains, each contributing an aspartic acid residue to form a catalytic dyad that cleaves the substrate peptide bond. Most aspartic proteinases are inhibited by pepstatin, a microbial peptide that contains the unusual amino acid statine. The statine-based inhibitors contain one hydroxyl that occupies the same position as the water molecule in the native

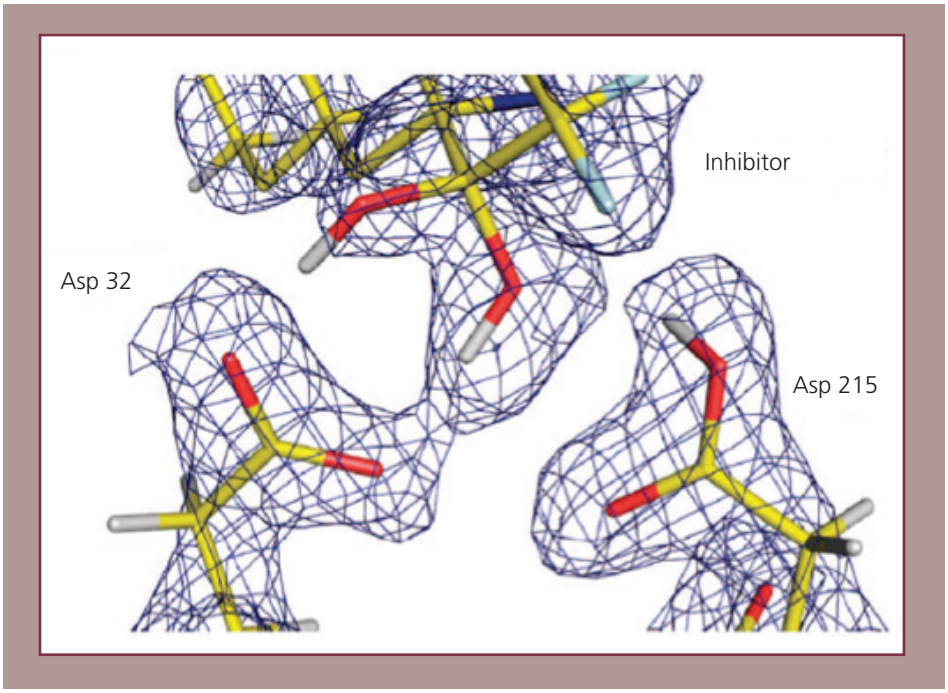

Figure 1. Nuclear density map at the active site of aspartic proteinase co-crystallized with an inhibitor (1.5-rms contour level).

enzyme and binds via hydrogen bonds to both catalytic aspartates (Asp) in the enzyme.

A. Kovalevsky and M. Mustyakimov (LANL) and their collaborators employed a combination of neutron and x-ray crystallography to examine the structure of the transition state of aspartic proteinase catalysis. They used an enzyme-inhibitor complex as a transition state mimic. This structural research shows how protons transfer within the enzyme's active site during catalyzed reactions, significantly increasing the understanding of reaction mechanisms and providing information for rational pharmaceutical design.

The scientists conclude that the transition state is stabilized by a negative charge on Asp 32, one of the two catalytic aspartate residues, while Asp 215 is protonated (Figure 1). (*Journal of the American Chemical Society* **130**:7235-7237 (2008).)

First production of ultracold neutrons from solid oxygen at the Lujan Center

Principal Investigator C. -Yu Liu (LANL) and her team from Indiana University have performed the first successful production of ultracold neutrons (UCNs) via inelastic magnetic scattering on a solid oxygen crystal. LANL researchers include A. Couture, A. Saunders, and M. Makela.

The researchers took advantage of the cold-neutron flux available at a LANSCE. Most facilities studying UCNs use solid deuterium to produce ultra-cold neutrons. However, the ultimate yield of UCNs is limited by the intrinsic absorption in the UCN production source. Oxygen-16 has a neutron absorption cross-section that is a factor-of-five smaller than that of deuterium and a zero incoherent cross-section, offering the opportunity to develop significantly larger UCN sources and larger fluxes of UCNs.

The preliminary UCN production is shown in Figure 1 as a function of the temperature and

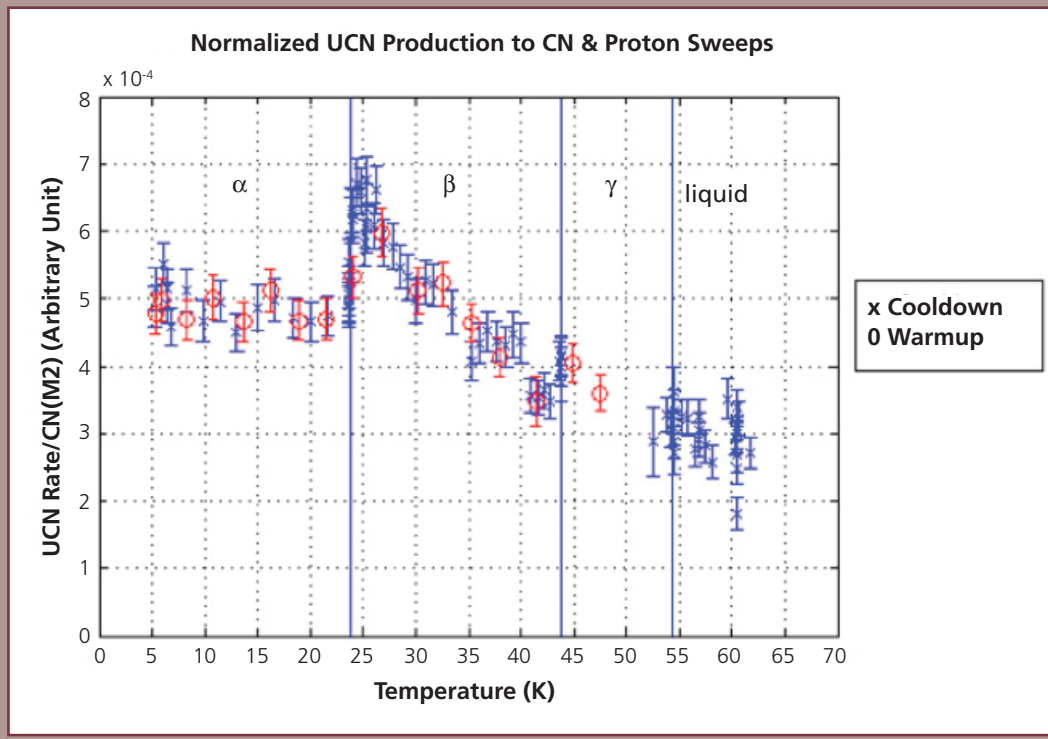

Figure 1. Nuclear density map at the active site of aspartic proteinase co-crystallized with an inhibitor (1.5-rms contour level).

solid oxygen phase. While the present results are qualitative, ongoing measurements will quantify the UCN production rate on the present solid oxygen crystal in several low temperature phases. In addition, the crystal has been grown inside of a 5.5-T superconducting solenoid. This will enable a detailed study of the magnetic interactions, and may lead to the possibility of fine-tuning the production of UCNs through the application of an external magnetic field.

Superhydrophobic films stop corrosion

Corrosion is a significant materials issue, that is estimated to cost the U.S. economy nearly $300 B per year. For example, aluminum in dry, non-salty environments develops a thick aluminum-oxide layer (on the order of 20 Å), which inhibits further corrosion. However, in wet, salty environments, the oxide layer is penetrated, enabling further corrosion and producing more oxide. Therefore, research efforts are devoted to prevent corrosion through the use of a coating to protect surfaces exposed to corrosive environments. Unusually high-porosity silica films can be made so hydrophobic that they prevent the corrosion of an underlying metal by preventing liquid contact, even under demanding brine conditions (Figure 1.)

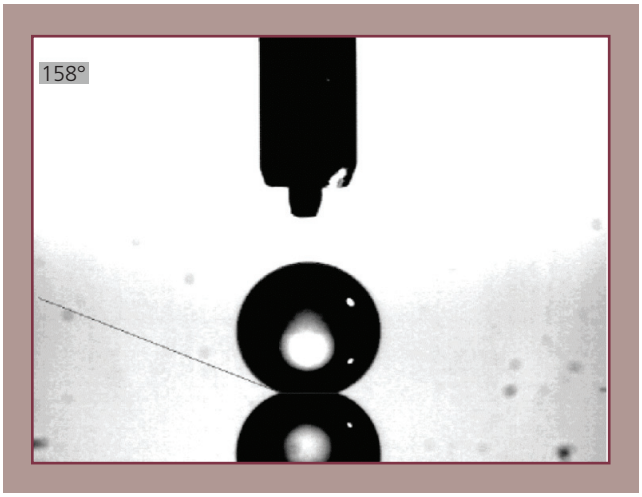

Figure 1. Representative image of a sessile drop measurement of the water contact angle on a superhydrophobic aerogel film showing a contact angle of 158 ± 2°.

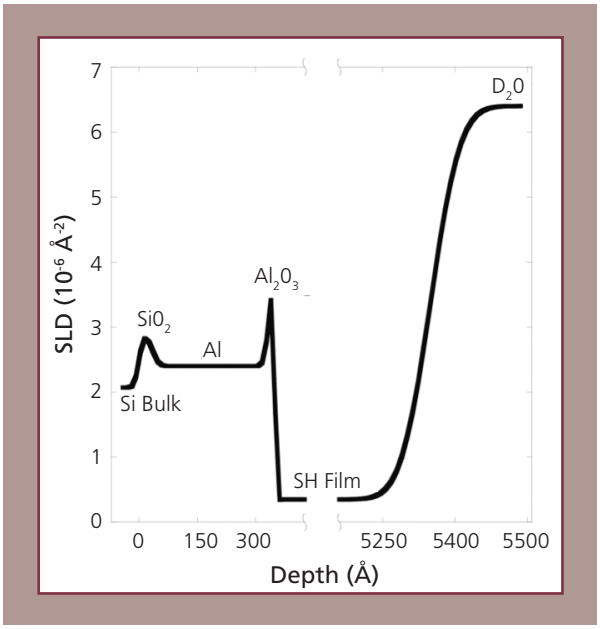

Figure 2. An example of a scattering length density (SLD) profile, consisting of an aluminum layer covered by a superhydrophobic (> 160° contact angle) film at time zero in contact with saline D_2O.

This mechanism of corrosion inhibition was studied using neutron reflectivity at LANSCE by P. Barkadarov,an undergraduate physics major at the University of Utrecht, Netherlands, and his collaborators.

The team, led by Barkadarov's mentor J. Majewski (LANL) and J. Brinker (Sandia National Laboratories), used low-temperature, low-pressure to prepare a rough, highly porous, aerogel-like film. UV-ozone treatments controlled the surface coverage of hydrophobic organic ligands bonded to the silica frame-work, allowing the contact angle with water to be continuously varied over the range of 160° (superhydrophobic) to <10° (hydrophilic).

Thin (~500 nm) nanoporous films were layered onto aluminum surfaces and submerged in 5 w% NaCl in D_2O (Figure 2). The heavy water was needed to enhance neutron reflectivity measurements, which were taken over time to observe interfacial changes in thickness, density, and roughness, and therefore to monitor the corrosion of the metal. The reflectivity showed that the superhydrophobic nature of the surface prevents infiltration of water into the porous superhydrophobic film, and thus limits the exposure of corrosive elements to the metal surface.

The research, "Corrosion Inhibition Using Superhydrophobic Films," has been accepted for publication in the journal *Corrosion Science*.

Pressure-induced structural changes in potential hydrogen storage compound ammonia borane

Onboard hydrogen fuel cells require safe, efficient and environmental friendly materials for storing and releasing hydrogen. In recent years metal hydrides have been studied extensively due to their high relative weight percentage of hydrogen. Ammonia borane (NH_3BH_3) is one of the most promising candidates which contains 19.6 wt% of hydrogen and is stable at ambient conditions. Because theoretical calculations predict high-pressure phases of hydrogen-storage-materials may exhibit superior hydrogen-storage-properties, it is important to investigate pressure-induced phase transformation and the corresponding structural behaviors in NH_3BH_3.

High-pressure neutron scattering provides a powerful analytical tool for these types of studies because neutrons are sensitive to light elements, particularly the hydrogen bonding in crystal structures. Researchers R. S. Kumar, A. L. Cornelius, and C. Chen (University of Nevada at Las Vegas); J. Zhang, Z. Lin, S. C. Vogel, M. Hartl, L. Daemen, and Y. Zhao (LANL); and S. Sinogeikin (HPCAT and Carnegie Institution of Washington) carried out a high-pressure experiment using TAP-98 on deuterated NH_3BH_3 at the Lujan Center's High Pressure Preferred Orientation (HIPPO) spectrometer.

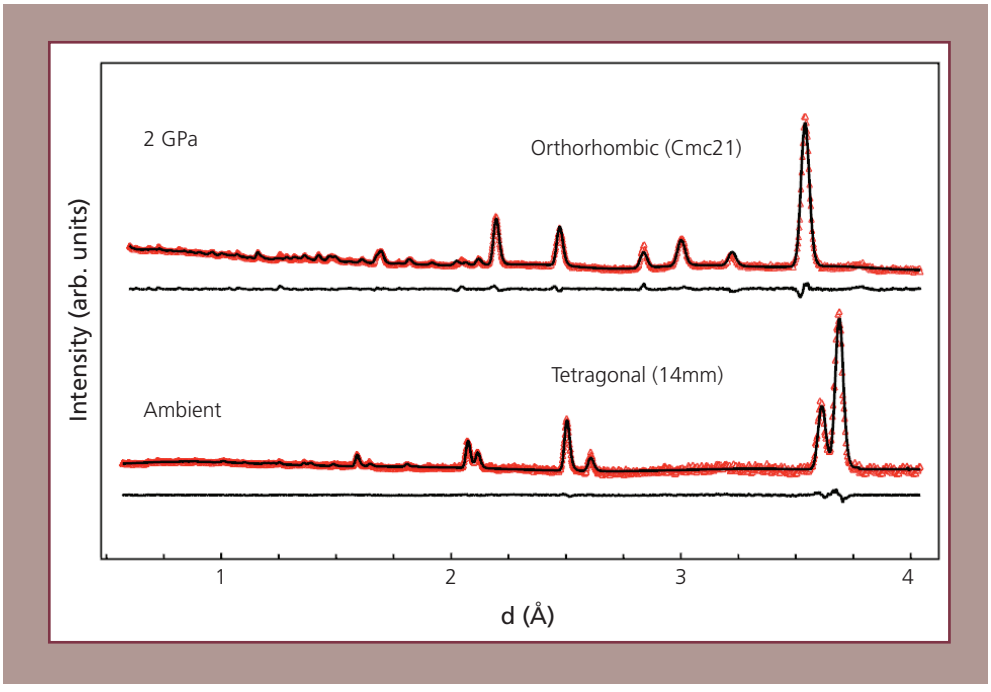

Figure 2. An example of a scattering length density (SLD) profile, consisting of an aluminum layer covered by a superhydro-phobic (>160° contact angle) film at time zero in contact with saline D_2O.

A combination of neutron scattering, synchrotron x-ray diffraction, and density functional theoretical calculations confirms a pressure-induced phase transition from the tetragonal I4mm phase to an orthorhombic Cmc21 phase at pressures above 1.2 GPa (Figure 1). The combined studies allow the first and accurate determination of atomic positions and hence hydrogen bonding in the high-pressure phase of NH_3BH_3. The results are of significant importance for understanding the release and uptake properties of this novel high-pressure phase. (Accepted for publication in *Chemical Physics Letters*.)

Erbium material studies for neutron tubes

Erbium (Er) tritide is the target material in neutron tubes produced by Sandia National Laboratories (SNL). A neutron tube is a miniature linear accelerator inside a neutron generator designed to provide deuterium-tritium (D-T) reaction neutrons on demand. Because of tritium decay, tubes are a limited-life component in Department of Energy systems. Neutron scattering and reflectometry are useful probes to study the kinetics of radiogenic helium release; now the researchers have used neutrons to study the thermodynamics of hydrogen loading.

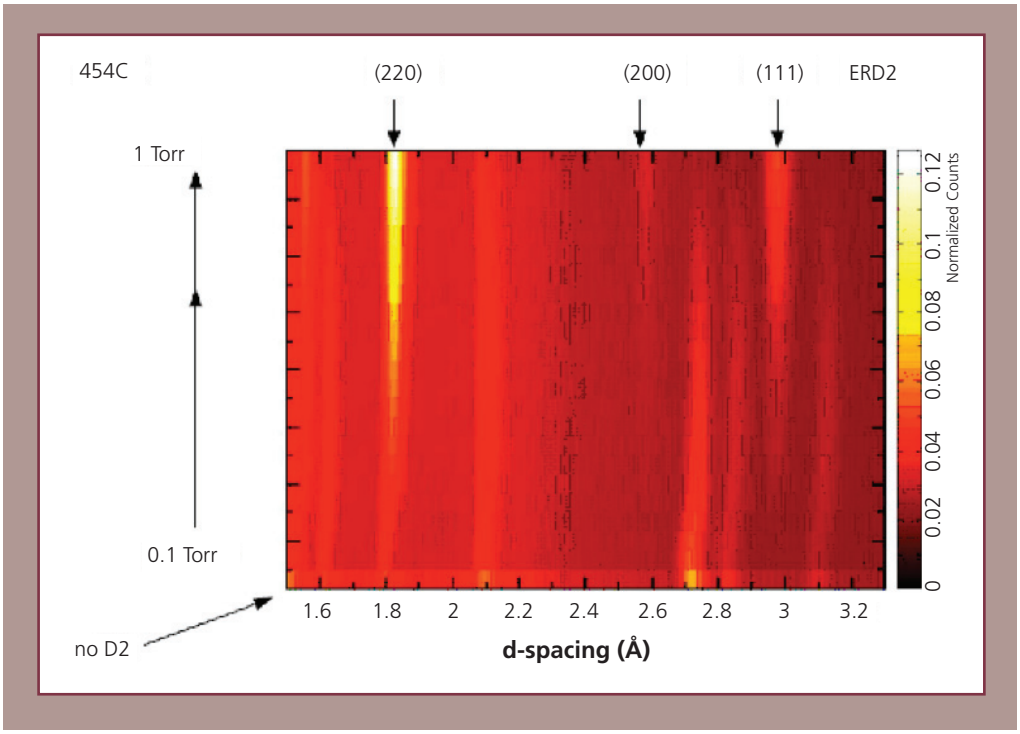

Figure 1. Contour plot of a series of neutron spectra at constant temperature (450 °C). Orange/yellow peaks at the bottom of graphic indicate diffraction lines from Er metal (hexagonal) at 450 °C without D_2 exposure. Upon addition of D_2 gas at 0.1 Torr, the hexagonal peaks shift as the D incorporates into the hexagonal Er lattice. This results in a shifting of the peaks to larger d-spacing. Further addition of D into the Er begins to develop a second phase of ErD_2 (FCC). The FCC phase continues to grow in phase fraction at the expense of the hexagonal Er lattice. The system eventually stabilized as a two-phase system at 0.1 Torr. Conversion of Er to ErD_2 was finalized by increasing the pressure to 1-Torr pressure, as illustrated by the break in the arrow along the side of the contour plot.

This neutron diffraction study of a deuteriding reaction—forward and backward—informs SNL's production process for neutron generators. Researchers have been able to convert Er metal to ErD_2 (FCC) in situ using the High-Intensity Powder Diffractometer at the Lujan Center (Figure 1). These experiments have ramifications regarding process control for neutron generators.

Role of water in the ion selectivity of niobate-based octahedral molecular sieves

Confinement in microporous materials is an attractive subject for a variety of both experimental and theoretical studies. The case of nanoconfined water is of importance because understanding how the various confining matrices modify the water properties (compared to those in the bulk state) is of significance to the control and optimization of a broad spectrum of industrial processes.

Researchers T. M. Nenoff, N. W. Ockwig, R. T. Cygan, T. M. Alam, K. Leung, J. D. Pless, H. Xu, M. A. Hartl, and L. L. Daemen at the Lujan Center are particularly focused on the ability to understand and, therefore, tune and predict ion-exchange selectivity for water purification with zeolitic materials, especially for environmental remediation applications. Their research is focused on a systematic study of the role of occluded water molecules in the small-pored, highly-selective Sandia Octahedral Molecular Sieves (SOMS): $Na_2Nb_{2-x}M_xO_{6x}(OH)_x,H_2O$ (i. e., M) Ti; ($0 < x < 0.4$), a new class of molecular sieves that show exceptionally high selectivity for divalent cations, in particular Sr^{2+} (Figure 1).

Evidence from inelastic neutron scattering (INS) and Fourier transform infrared spectroscopy (FTIR) data indicate the ability of the occluded water molecules to form structures (such as hexamers and distorted tetrahedral networks) through hydrogen bonding inside the zeolite pore. The data also indicate that the occluded water is structurally similar to bulk water.

INS on Lujan Center's Filter Difference Spectrometer (FDS) is ideally suited to investigate the librational and rotational modes (wagging, rocking, and twisting) of water molecules in confined environments and is extremely sensitive to localized hydrogen bonding. Conceptually, the behavior of nanoconfined water molecules is the direct result of complex equilibria among four distinct types of interactions: (1) H_2O-H_2O, (2) H_2O-ion, (3) H_2O-framework, and (4) ion-framework. The collective effect of these interactions (hydrogen bonds, ion-dipole, and electrostatics) produces localized restrictions that alter the behavior of the nanoconfined water. Spectroscopically, these behavioral modifications are manifested by changes in the librational and rotational (300-1100 cm^{-1}) modes and to a lesser extent the intra-molecular bending (~1600 cm^{-1}) and stretching (3300-3700 cm^{-1}) modes. Water has a librational band in the 450-900 cm^{-1} region. Typical FDS INS results are shown in Figure 2.

INS enables probing the nature of hydrogen bonding of water molecules in the SOMS materials. INS shows that, in the low-selectivity-as-synthesized end member, the water exhibits an ice-like extended hydrogen-bonding nature. Data from *^{1}H MAS NMR Studies of Alumina-Supported Metal Oxide Catalysts (J. Phys. Chem.* **98**:51, pp. 13621–13624, 1994) confirm the INS data; there is a great difference in the mobility between the Na2Nb2O6,H2O end member (low selectivity) and the $Na_2Nb_{1.6}Ti_{0.4}O_{5.6}(OH)_{0.4},H_2O$ material (high selectivity). The occluded water molecules in the end member are very rigid, almost immobile. This is in contrast to the water molecules of the 20% Ti SOMS where they have very high mobility. In molecular sieves in which the water is mobile, there is a cation solvation effect associated with the water, thereby allowing greater mobility of the cation. Contrary to this, when there is little water mobility, the cation is locked into its crystallographic site, while the water is forming relatively rigid hydrogen bonding with itself throughout the channels. In both the 20% Ti-SOMS and the Sr-exchanged samples, the effective free volumes of the pores are

decreased. This is due to cation size and charge balancing framework -O_fH molecules present in the pore. The result is a disruption of the extended H-bonding network, further resulting in the disruption of possibly "ice-like" structural formations. (*J. Phys. Chem. C* **111**, 13212 (2007).)

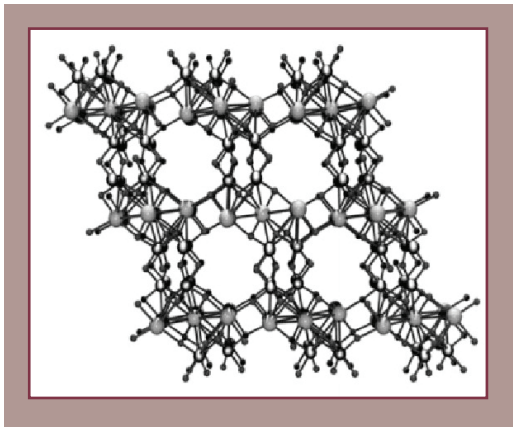

Figure 1. SOMS framework, $Na_2Nb_{2-x}MIV_xO_{6-x}(OH)_x$, where H_2O: small balls; O: medium balls; and Nb/Ti: large balls. Na occluded waters and Na(1) are not shown, for clarity, but are located in the pores.

Figure 1. SOMS framework, $Na_2Nb_{2-x}MIV_xO_{6-x}(OH)_x$, where H_2O: small balls; O: medium balls; and Nb/Ti: large balls. Na occluded waters and Na(1) are not shown, for clarity, but are located in the pores.

Vibrational property study of $SrGa_2H_2$ and $BaGa_2H_2$ by inelastic neutron scattering and first principles calculations

Many metals and intermetallic compounds exhibit the ability to absorb and react with hydrogen. Metal hydride compounds can be polymeric, salt-like, or metallic materials, depending on the kind of metal involved and the preparation method applied. The many shapes of metal-hydrogen compounds have been puzzling for a very long time, and today there is still no conclusive understanding of the nature of the various metal/semimetal-hydrogen interactions and its consequences for chemical structures and physical properties

.

Additional variation is provided by recently discovered polyanionic hydrides, which are obtained from the hydrogenation of Zintl phase precursors. The peculiar feature of these hydrides is the incorporation of hydrogen (H) in polymeric anions composed of p-block metal or semimetal atoms where it acts as a terminating ligand. This creates chemically new coordination environments for both metal and H atoms. the compound should be a metallic conductor. The bonding properties and lattice dynamics of polyanionic hydrides are virtually unexplored; however, their knowledge would provide valuable insight into the fundamental question of how hydrogen interacts with metals and semimetals.

Using inelastic neutron scattering (INS), researchers M. H. Lee, M. J. Evans, L. L. Daemen, O. F. Sankey, and U. Häussermann at the Lujan Center found that $SrGa_2H_2$ and $BaGa_2H_2$ crystallize with the trigonal $SrAl_2H_2$ structure (Figure 1). The INS spectra of $SrGa_2H_2$ and $BaGa_2H_2$ are shown, in Figure 2, for the ranges between 500 and 2900 cm-1 and 70 and 250 cm^{-1} (insets). Both spectra are characterized by high-intensity bands centered around 800 and 1350 cm^{-1} and associated overtones above 1500 cm^{-1}. The band around 800 cm^{-1} appears split. High-intensity bands imply H motion and correspond to [Ga-H] bending and stretching modes. The dispersion implies that H atoms from neighboring unit cells, which is primarily between polyanionic layers, interact.

Pivotal for the interpretation of the INS spectra is the correct assignment of modes. For this, results from first principles calculations are invaluable, and usually analysis of the situation at the Γ point in the Brillouin zone is sufficient. Calculated spectra appear in Figure 2.

The INS spectra of the two alkaline earth gallium hydrides $SrGa_2H_2$ and $BaGa_2H_2$ are very similar and also resemble closely that for $SrAl_2H_2$. Comparing $SrGa_2H_2$ with $SrAl_2H_2$ allows discussion of the differences of vibrational properties between the polyanions $[Al_2H2]^{2-}$and $[Ga_2H_2]^{2-}$, while a comparison of $SrGa_2H_2$ with $BaGa_2H_2$ allows discussion of the influence of the countercation on the vibrational properties of $[Ga_2H_2]^{2-}$.

The vibrational properties of $SrGa_2H_2$ and $BaGa_2H_2$ were characterized by a combined INS and computational study and compared with those of $SrAl_2H_2$. The exchange of Sr for heavier and larger Ba in $AeGa_2H_2$ leads structurally to a larger separation of polyanionic $[Ga_2H_2]^2$ layers and elongated Ga-Ga distances. The larger separation of layers has virtually no consequences to vibrations involving H; however, the covalent Ga-Ga bond is weaker in $BaGa_2H_2$ as expressed by a lower in-plane stretching frequency. Compared to molecular entities (EH_n (n) 1, 2, 3), the bond strength of

E-H in $[E_2H_2]^{2-}$ is clearly weaker as indicated in the low frequencies of the stretching mode. This phenomenon is attributed to the effective coordination of H by Ae in the solidstate polyanionic hydrides and demonstrates the complex interplay of different metal-H interactions in multinary metal hydride systems. (*Inorg. Chem.* **47**, 1496 (2008).)

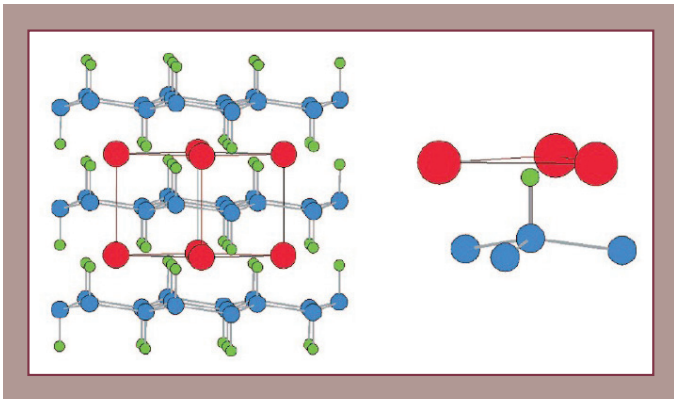

Figure 1. Crystal structure of $SrAl_2H_2$. Red, blue, and green circles denote Sr, Al, and H atoms, respectively. On the right, the local environment of an H atom is highlighted.

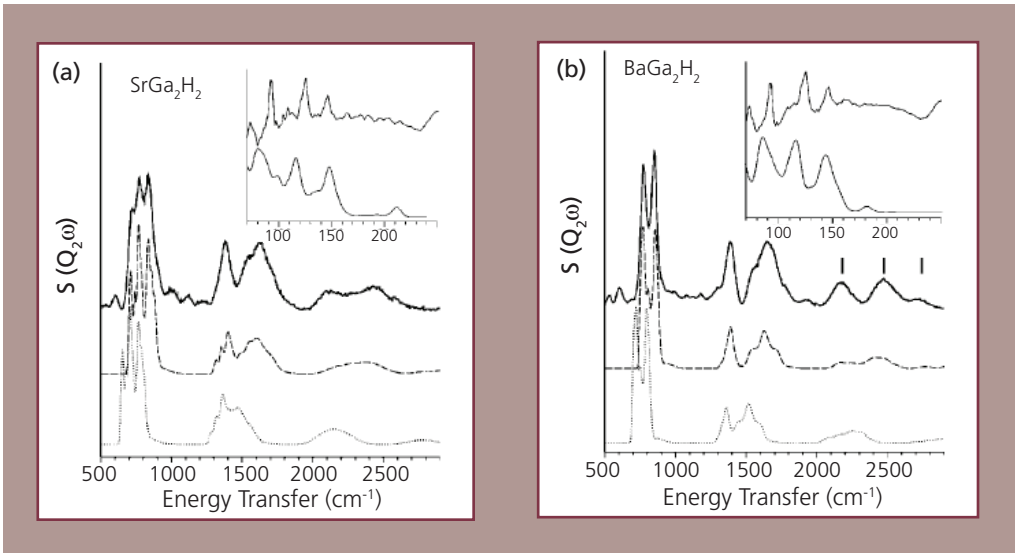

Figure 2. Measured (solid line) and calculated (broken and dotted lines) INS spectrum of $SrGa_2H_2$ (a) and $BaGa_2H_2$ (b). The calculated spectra are based on frequencies and displacements obtained from first principles phonon calculations. For spectra represented with broken lines, frequencies of external fundamentals have been scaled to match the experimental ones, while those represented with dotted lines were obtained with the original frequencies. In the spectra calculations, overtones and combinations up to three quanta are included. Vertical markers in (b) indicate the locations of maxima from the combination, 0–3 bending, and 0–2 stretching modes. The insets show the internal modes at low frequency (solid line: experimental spectrum, dotted line: calculated spectrum).

Nanomechanics of polycrystalline nickel at elevated temperatures

Nanoscale materials have been the focus of extensive research because they exhibit rich fundamental physics phenomena and have tremendous potentials for industrial applications. Because of its technological importance, nanocrystalline nickel (Ni) has been the subject of considerable experimental and theoretical work in recent years.

Researchers Y. Zhao, J. Zhang, S. C. Vogel, and T.D. Shen (LANL) conducted experiments on severely deformed nanocrystalline Ni (nm-Ni) and coarse-grain Ni (cg-Ni) using the Lujan Center's ILL furnace at High Pressure Preferred Orientation (HIPPO) spectrometer. Analysis of neutron diffraction patterns provides the lattice parameter, dislocation density, surface or grain boundary strain, and grain size of nm-Ni (Figure 1).

The results show that 80% of the excess volume in nm-Ni (relative to cg-Ni) is due to the statistically stored dislocations whereas the grain boundary contributes only 20% to the total volume expansion. A low-temperature (T < 260 °C) anneal of nm-Ni annihilates the statistically stored dislocations, and a further

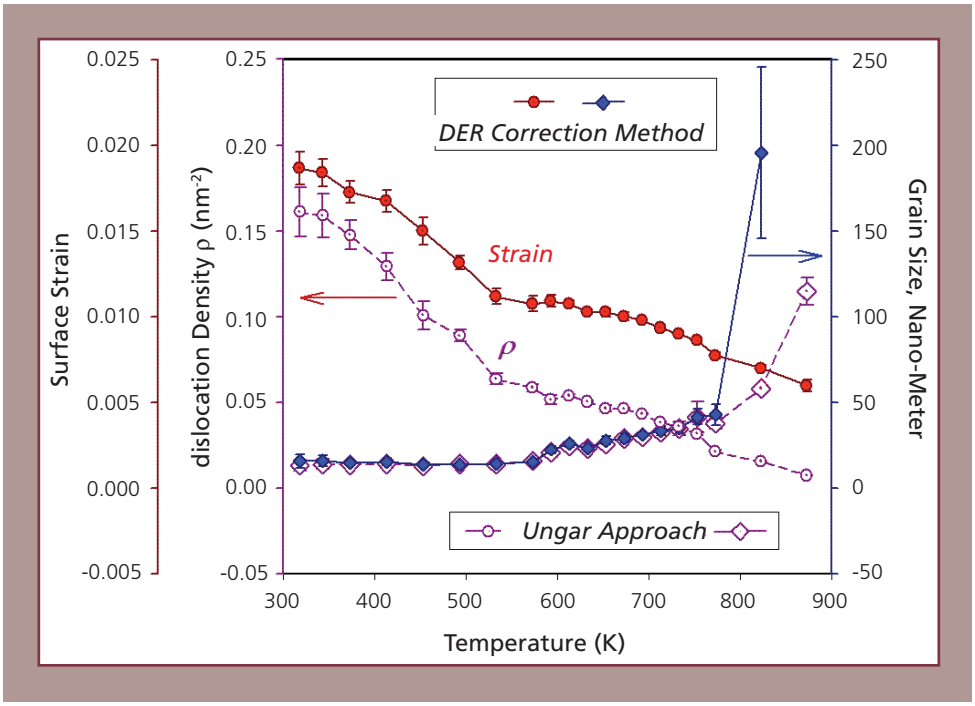

Figure 1. High-temperature annealing and grain growth of nm-Ni. DER method corrects the strain differences on individual lattice planes by multiplying the square of the diffraction elasticity ratio (DER²). Ungar approaches assumes that dislocations are the main contributors to the residual strain.

heating from 260 to 600 °C leads to growth of the nanograins. For T < 260 °C, where nm-Ni has a constant grain size, the excess volume is proportional to the density of statistically stored dislocations. For T > 260 °C, where the statistically stored dislocations are completely annealed out, the excess volume is inversely proportional to the grain size. The findings are important for better understanding of nano-mechanics and theoretical density of nanocrystalline materials. (The research resulted in three publications: *Acta Materialia* **55**, 5007-5013, 2007; *Journal of Applied Crystallography* **41**, 1095-1108, 2008; *Acta Materialia* **56**, 3663-3671, 2008.)

In situ observation of texture evolution during $\alpha \leftrightarrow \beta$ phase transformations in titanium alloys investigated by neutron diffraction

Titanium and its alloys are widely used in aerospace, electronics, biomedical, and energy applications due to their low density–strength ratio, high-biocompatibility and high-corrosion resistance. In all these fields, the crystallographic texture developed during thermomechanical treatments plays a crucial role on the physical properties of the material. For this reason, texture changes in titanium alloys during cold work, primary re-crystallization, grain growth and the $\alpha \leftrightarrow \beta$ phase transformation are of longstanding interest.

Concerning the phase transformation, a texture memory effect is often reported when the hexagonal α metal is heated, transforms into the cubic β-phase and returns to the hexagonal α-phase after cooling. In situ neutron diffraction texture measurements of the textures, extracting the orientation distributions in both phases from

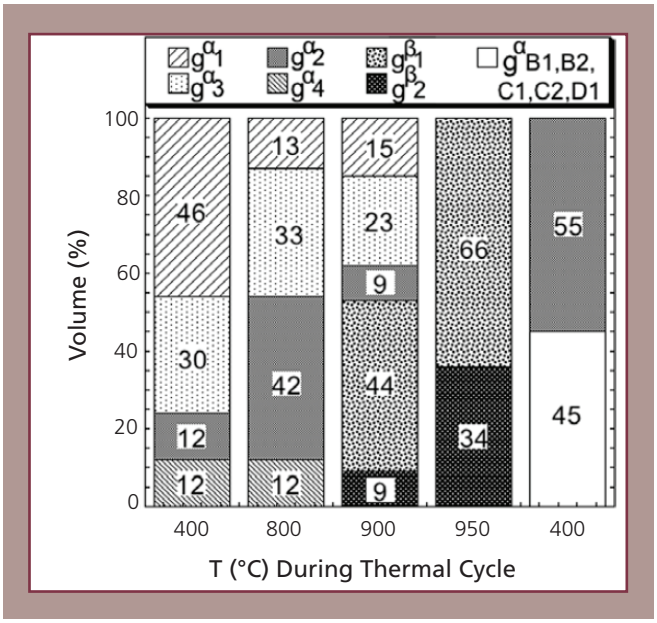

Figure 1. The texture components of the initial material at 400 °C. At 800 °C, re-crystallization and grain growth occur. The HIPPO data uniquely identifies that grains with orientations around the g^{α}_2 orientation grow at the cost of grains in the orientation labeled g^{α}_1. The two other orientations observed in the initial texture are unaffected. At 900 °C, more than half the volume of the sample has transformed from α to β.

thousands of grains, have proven to be extremely valuable to study the phase transformation in the bulk material. Alternative methods have may suffer from poor sampling statistics from a small number of observed grains, surface versus bulk differences, or rely on back calculation of the high-temperature texture from the room-temperature α texture.

The orientation relationship between low-temperature α high-temperature β-phase is described by the so-called Burgers orientation relationship: $\{0001\}<1120>_{hcp} \rightarrow \{110\}<111>_{bcc}$. This means that for a given hexagonal closed packed α grain the (0001) plane normal (c-axis) becomes a (110) plane normal in the cubic β-phase with the [11-20] direction of the α grain becoming a [111] direction in the β-grain. From the crystal symmetry, this results in six possible symmetry equivalent transformations between a α- and β-grain, or so-called variants. Conversely, during the β→α back transformation during cooling, there are 12 potential α-variants for a given β-grain. A variant selection can occur during the heating and/or cooling phase transformations. The proportion of variants from this process of variant selection determines the final texture. Obviously, an understanding of the physics of variant selection is necessary to develop predictive capabilities for thermo-mechanical treatments of titanium and its alloys.

Researchers I. Lonardelli (University of California, Berkeley, and Universita` di Trento, It.), N. Gey and M. Humbert (University of Metz, Fr.), H.-R. Wenk (LANL and University of California, Berkeley), S.C. Vogel (LANL), and L. Lutterotti (Universita` di Trento, It.) used the Lujan Center's HIPPO instrument, because with it bulk textures can be measured uniquely at temperatures between 10 and 1300 K, allowing the study of phase transformation textures in materials from pure metals, such as, in this example, state-of-the art steels to shape memory alloys. The texture information, the so-called orientation distribution function (ODF), is extracted from ~100 diffraction histograms measured for typically four sample orientations by performing multi-histogram Rietveld refinements. Special crystal orientations within the bulk material (with a given spread around the orientation) are called texture components. Figure 1 shows the texture components of the initial material (400 °C). At 800 °C, re-crystallization and grain growth occur and the HIPPO data uniquely identifies that grains with orientations around the g^{α}_{2} orientation grow at the cost of grains in the orientation labeled g^{α}_{1} with the two other orientations observed in the initial texture unaffected. At 900 °C, more than half the volume of the sample has transformed from α to β.

While this kind of information could be gathered by other methods, the additional value provided by the HIPPO in situ texture measurement is that grains with orientations g^{α}_{2} and g^{α}_{4} are the ones that transform first, while the grains in the orientations g^{α}_{1}, which survived the grain growth in the first step, and the grains in the orientations g^{α}_{3}, which did not exhibit grain growth, are the ones that predominantly remain in the low-temperature α-phase. At 950 °C, the transformation is complete and only β grains are observed in the diffraction data.

Note that the population of β-grains in the g^{β}_{2} orientations grows much faster in this step of the transformation than the other β-orientation observed. During subsequent cooling, the initial texture is mostly lost, resulting in a much weaker overall preferred orientations of grains in the final material. (*Acta Mater.* **55**, 5718-5727 (2007).)

Single-crystal diffraction studies of natural gold crystal growth under extreme conditions

Because large single-crystals bring a much higher collectors' price, crystal formats and growth habits are used to distinguished authentic natural crystals from forgeries. It is, therefore, important to understand the characteristic growth habits that arise in nature, such as the "hopper growth" that enhances crystal edges and depresses faces as shown in the 18 g Venezuelan specimen (Figure 1 top). X-ray diffraction studies generally fail to establish whether extreme crystals such as this one are crystalline throughout. Even high-energy x-rays cannot both penetrate the sample and diffract from the interior, owing to the strong absorption of a high-Z material such as gold.

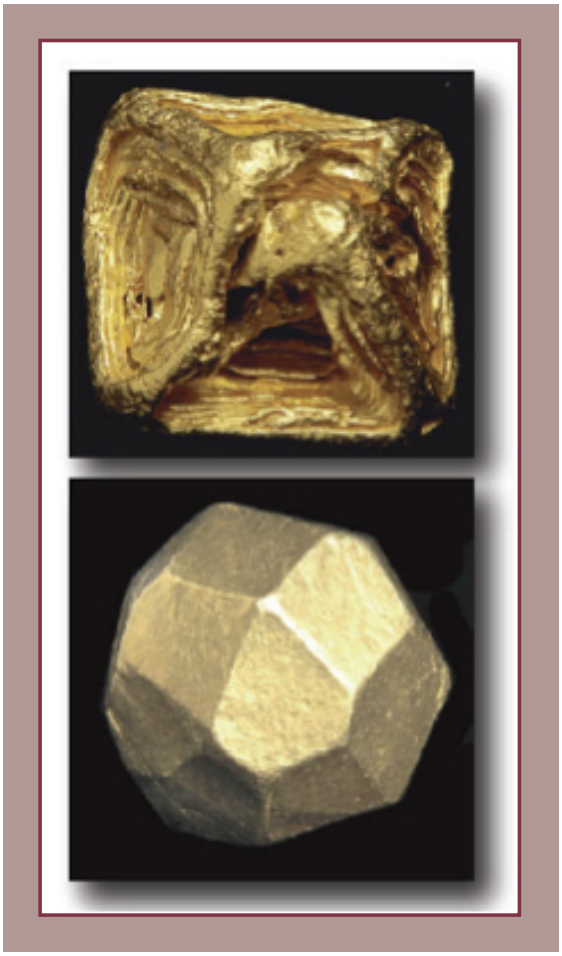

Figure 1. Examples of gold specimens. Top: Venezuelan specimen. Bottom: Alleged single crystal.

Neutrons are not limited in this way. Within minutes, on the Lujan Center's Single-Crystal Diffractometer, the specimen was shown to be a single, large octahedral crystal and therefore natural. By contrast, two samples with bizarre cross-shaped crystal faces were shown to be forgeries, deftly cast with quartz chunks that naturally occur with free gold.

S. Vogel (LANL) conducted complementary texture measurements on the High-Pressure Preferred Orientation Diffractometer spectrometer, which verified the powder pattern of these crystals.

Having demonstrated that neutron diffraction is the best non-destructive method to establish gold crystallinity in extreme samples, the team is considering studying the largest example of an alleged single-crystal of unusual 24-sided format (Figure 1 bottom). X-rays have determined that this 78-g behemoth has disrupted surfaces, which might be alluvial damage from rolling in a stream bed.

Single-crystal neutron diffraction studies on a small crystal of $BaNi_2As_2$

Pnictides superconductors have received much recent attention in the effort to understand the relation between structure, superconductivity, and magnetism. Using the flux growth method, it is possible to grow single crystals of such materials, but those are typically very limited in size, smaller than crystals typically needed for single-crystal neutron studies.

H. Nakotte (LANL and New Mexico State University), in collaboration with F. Ronning and E. Bauer (LANL), performed neutron-diffraction studies on a very small plate-like single crystal of $BaNi_2As_2$ with approximate dimensions of 1.3 x 2.0 x 0.1 mm^3 (volume ~1/4 mm^3) and a total weight of only ~0.8 mg.

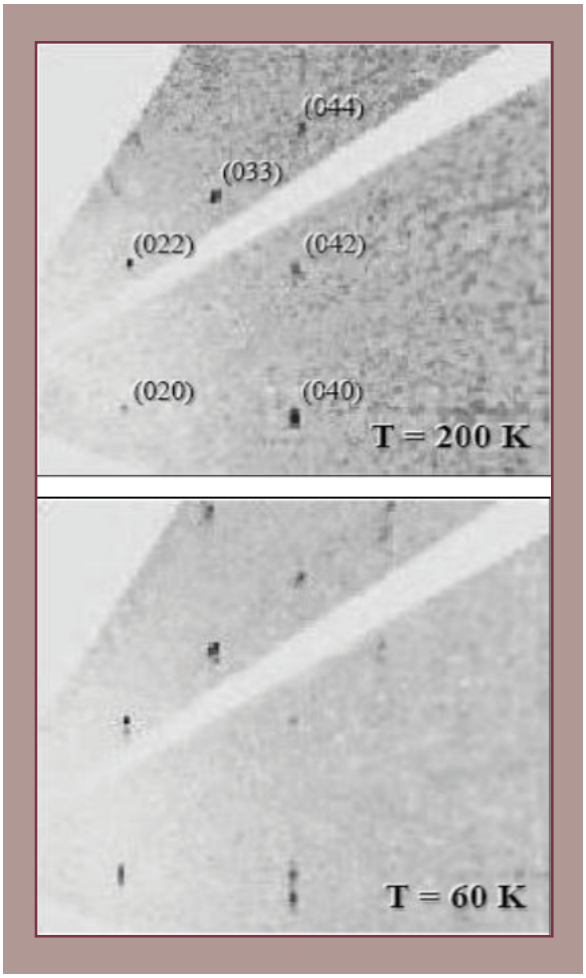

Figure 1. Exemplary (0kl) slice of the data at 200 K and 60 K. Tetragonal indices for the peaks at 200 K are provided. Note that the reflections seen at 200 K are found to be broadened or split at 60 K.

The experiments were performed on the Lujan Center's Single-Crystal Diffractometer (SCD). SCD had been in operation at the Intense Pulsed Neutron Source (IPNS), Argonne National Laboratory. It was reinstalled at the Lujan Center following the recent closure of the IPNS. SCD benefits from a significantly higher neutron-beam currents (compared to IPNS) and it is therefore possible to obtain sufficient statistics at reasonable measuring times (3-4 hrs per histogram) on samples that are much smaller (~0.1 mm3) than samples typically used for neutron diffraction experiments. Only 3 hrs of neutron-beam time per histogram were sufficient to obtain sufficient statistics.

In Figure 1, exemplary results at 60 and 200 K for $BaNi_2As_2$ are shown. Splitting or broadening of the 'high-temperature' tetragonal (*hkl*) peaks provide clear evidence for a structural phase transition in $BaNi_2As_2$. Data were collected at various temperatures and the results are consistent with a structural distortion within the tetragonal basal plane, while atom displacements are most prominent along the c-axis.

Thermal expansion and decomposition of jarosite: a high-T neutron diffraction study

Jarosite, a hydrous sulfate mineral ($KFe_3(SO4)_2(OH)_6$), is of considerable interest for its geological and industrial applications. Jarosite occurs in acid mine drainage environments as a weathering product of sulfide ore deposits and precipitates in epithermal environments and hot springs associated with volcanic activity. Jarosite is used as an iron-impurity extractor from zinc sulfide ores in the zinc industry and has been also proposed as a potential host for immobilization of radioactive fission products and toxic heavy metals. In 2004, jarosite was detected by the Mars Exploration Rover's Mössbauer spectrometer, which has been interpreted as a strong evidence for the existence of water (and possibly life) on ancient Mars. This discovery has spurred considerable interests in stability and structural behavior of jarosite and related phases at various temperature, pressure, and aqueous conditions.

H. Xu, Y. Zhao, S. C. Vogel, D. D. Hickmott, L. L. Daemen, and M.A. Hartl (LANL) have performed neutron diffraction experiments at Lujan Center's HIPPO to investigate the structure and stability of a deuterated jarosite at temperatures up to 650 K. Since the scattering power of neutrons does not vary with the number of electrons in an element (as for x-rays), neutron diffraction is much more sensitive to the positions of light elements (especially hydrogen and its isotopes) and is thus a powerful technique for studying hydrogen-bearing minerals/materials.

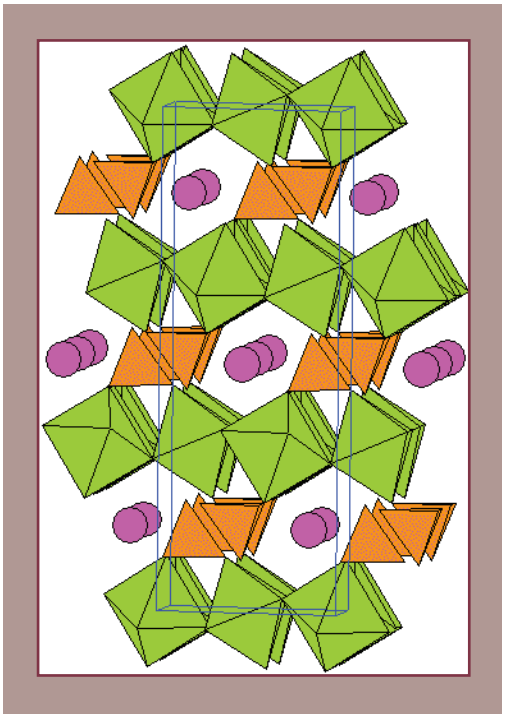

Figure 1. Crystal structure of jarosite. Tetrahedra represent [SO_4] units, octahedra represent [$Fe(O,OH)_6$] units, pink balls represent K. Blue lines outline the unit cell where the c-axis is vertical.

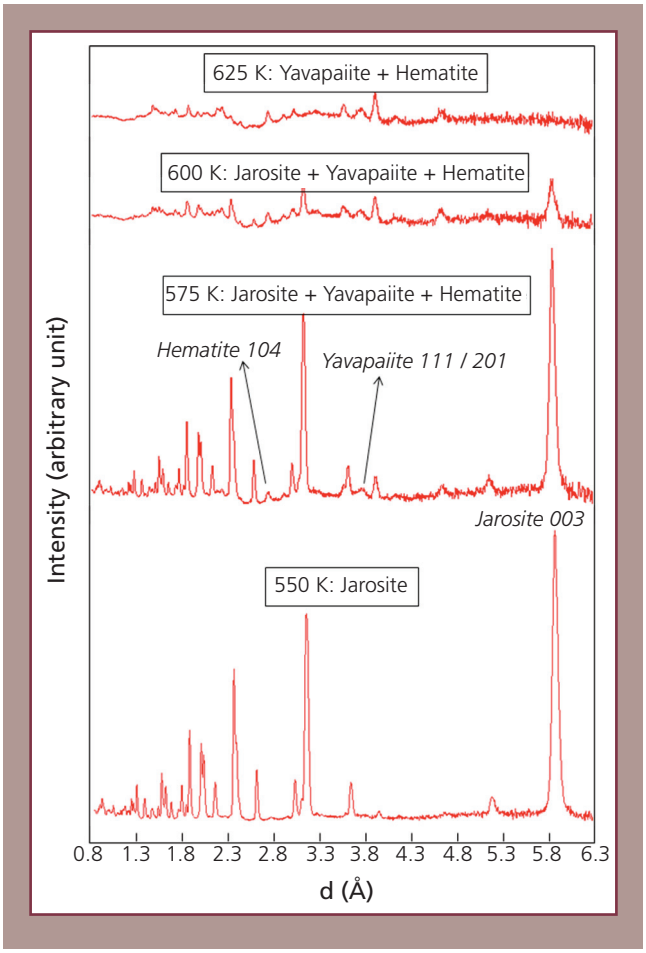

Figure 2. Neutron diffraction patterns ($2\theta = 90^{\circ}$) of jarosite collected at 550, 575, 600, and 625 K. At 575 K, jarosite started to decompose into yavapaiite and hematite, as evidenced by the appearance of their diffraction peaks (e.g., hematite 104 and yavapaiite 111/-201). The decomposition was completed at 625 K, as indicated by the disappearance of jarosite peaks such as 003.

Structural analysis of jarosite reveals that with increasing temperature, its c dimension expands at a rate ~10 times greater than that for a. This anisotropy of thermal expansion is due to rapid increase in the thickness of the (001) sheet of $[Fe(O,OH)_6]$ octahedra and $[SO_4]$ tetrahedra with increasing temperature (Figure 1). Fitting of the measured cell volumes yields a coefficient of thermal expansion, $\alpha = \alpha_0 + \alpha_1 T$, where $\alpha_0 = 1.01 \times 10^{-4}$ K-1 and $\alpha_1 = -1.15 \times 10^{-7}$ K^{-2}. On heating, the hydrogen bonds, O1···D-O3, through which the (001) octahedral-tetrahedral sheets are held together, become weakened, as reflected by an increase in the D···O1 distance and a concomitant decrease in the O3-D distance with increasing temperature.

On further heating to 575 K, jarosite starts to decompose into nanocrystalline yavapaiite and hematite (Figure 2), a direct result of the breaking of the hydrogen bonds that hold the jarosite structure together. This study has, for the first time, unraveled the atomistic mechanisms of thermal expansion and decomposition of jarosite and provided important insights into its further applications. (To be published by *Physics and Chemistry of Minerals* **37**:73-82, February 2010).

Experimental and computational studies on collective hydrogen dynamics in ammonia borane: incoherent inelastic neutron scattering

On-board hydrogen storage has been described as a technological bottleneck for transition to a hydrogen-based fuel economy. One particular class of compounds, amine borane and ammonia borane, NH3BH3, in particular, have recently received a great deal of attention given the high gravimetric and volumetric density of hydrogen and the promise to meet many of the technical benchmarks required of solid-state hydrogen storage materials for fuel cell powered vehicles.

Researchers S. M. Kathmann, V. Parvanov, G. K. Schenter, A. C. Stowe, L. L. Daemen, M. A. Hartl, J. Linehan, N. J. Hess, A. Karkamkar, and T. Autrey have suggested that materials composed of protonic and hydridic hydrogen appear to release or desorb hydrogen at lower temperatures. This suggestion lead to interest in approaches to study how dihydrogen bonding interactions affect the structure and dynamics of ammonia borane.

The overarching goal of their research at the Lujan Center is to develop complementary experimental and computational approaches to gain fundamental insight as to how dihydrogen bonding affects the structure and dynamics of hydrogen-rich materials. Specifically, how intermolecular interactions between neighboring protonic and hydridic hydrogens' dihydrogen bonds in a molecular crystal are coupled to the intramolecular interactions within NH_3BH_3 using experimental neutron vibrational spectra and computed power spectra.

First principles molecular dynamics simulations provide a means to calculate the Fourier transform of the velocity autocorrelation function. This novel computational method differs from the usual harmonic approximation, and includes all anharmonic effects at finite temperature. Partial vibrational spectra are easily obtained, which helps with the spectral interpretation problem. The dynamics of NH_3BH_3, NH_3BD_3, and ND_3BH_3 at 10 K were computed using the CP2K ab initio molecular dynamics simulation package (Figure 1). Separately deuterating the boron or nitrogen end of NH_3BH_3 allows the rotational dynamics of each end of the molecule to be investigated.

Figure 2 shows a comparison between the measured neutron vibrational spectra (black circles) at 10 K and computed green curve at 10 K for NH_3BH_3. The green curve where all the hydrogen atoms on each molecule are correlated, can be decomposed into two components: correlating the hydrogen atoms on the B end of NH_3BH_3 (magenta dashed curve), and correlating the hydrogen atoms on the N end of NH_3BH_3 blue dot–dash curve. The computed spectrum is in excellent agreement with the measured peak at 340 cm^{-1}, as well as the broad peak from 50 to 250 cm^{-1}. The neutron vibrational spectra and calculated spectrum agree extremely well with the previously measured Raman spectra.

The decomposition of the spectrum into B and N components shows that the majority of the observed intensity 340 cm^{-1} is due to the hydrogen atoms on the boron end. However, there is also an appreciable contribution to the 340 cm^{-1} mode from the hydrogen atoms on the nitrogen end. These dominant contributions to the motions are reversed for the broadband ranging from 50 to 250 cm^{-1}, where the hydrogen atoms on the N end contribute more than the hydrogenatoms on the B end. The rotational motions of the BH3 end of the molecule are strongly correlated with the motion of the NH_3 end of the molecule. The minor

peaks 100, 150, and 210 cm^{-1} within this broad range are consistent with contributions from the hydrogen atoms on the N end and are well reproduced in the computed spectrum.

The agreement found between experiment and calculated spectra is excellent and illustrates the power achieved by combining measured inelastic incoherent neutron spectra and ab initio power spectra to understand the vibrational dynamics in hydrogen-bonded materials. This study contributes to the understanding of the nature of the cohesive energy of the molecular crystal by comparing the dynamics of an "isolated" NH_3BH_3 molecule to that of the molecular crystal. In bulk ammonia borane, the intermolecular interactions are dominated by dihydrogen bonding and one expects that similar behavior would be seen in other dihydrogen bonded systems. Some mode assignment for the hydrogen motion is possible, however, it is found that the lowest modes are dominated by collective motion. (*J. Chem.Phys.* **130**, 024507 (2009).)

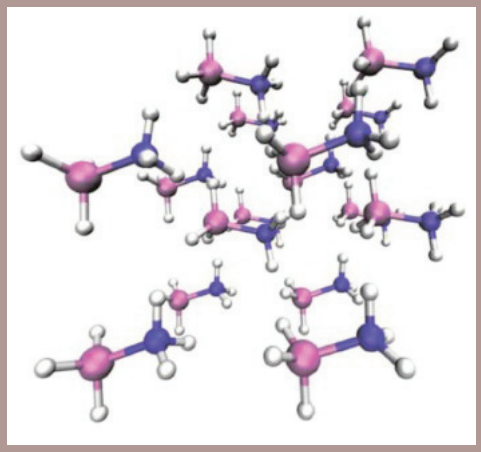

Figure 1. A snapshot taken along the NVE CP2K trajectory of 16 NH_3BH_3 molecules: Nitrogen = blue, boron = magenta, and hydrogen = white.

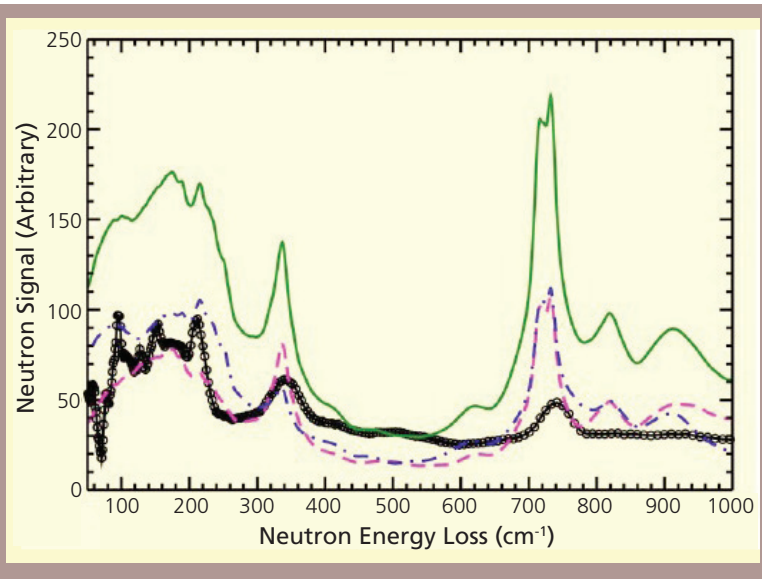

Figure 2. A comparison between the measured neutron spectra (black circles) at 10 K and computed spectrum (green curve) for NH_3BH_3 at 10 K correlating all the hydrogen atoms on each molecule. Note the spectrum correlating the hydrogen atoms on the B end of NH_3BH_3 (magenta dashed curve), and spectrum correlating the hydrogen atoms on the N end of NH_3BH_3 (blue dot-dash curve).

Morphotropic phase boundary in piezoelectric perovskites

The best piezoelectric materials are solid solutions in the vicinity of the steep morphotropic phase boundary (MPB) separating rhombohedral and tetragonal phases in the composition-temperature plane. A classical example is the lead zirconate titanate [Pb(Zr*x*Ti1-*x*)O3, PZT] system, with x ≈ 0.52, where the two phases are separated by a boundary extending from the lowest temperatures up to several hundred degrees. Also at x ≈ 0.52, PZT features an extremely large dielectric constant, making PZT-based materials one of the most prominent and useful electroceramics.

The origin of MPB has been under keen studies for 40 yrs and has not been well understood. High-pressure neutron diffraction offers an ideal probe into this problem because neutrons are sensitive to light elements, notably the oxygen octahedral tilting in crystal structure,

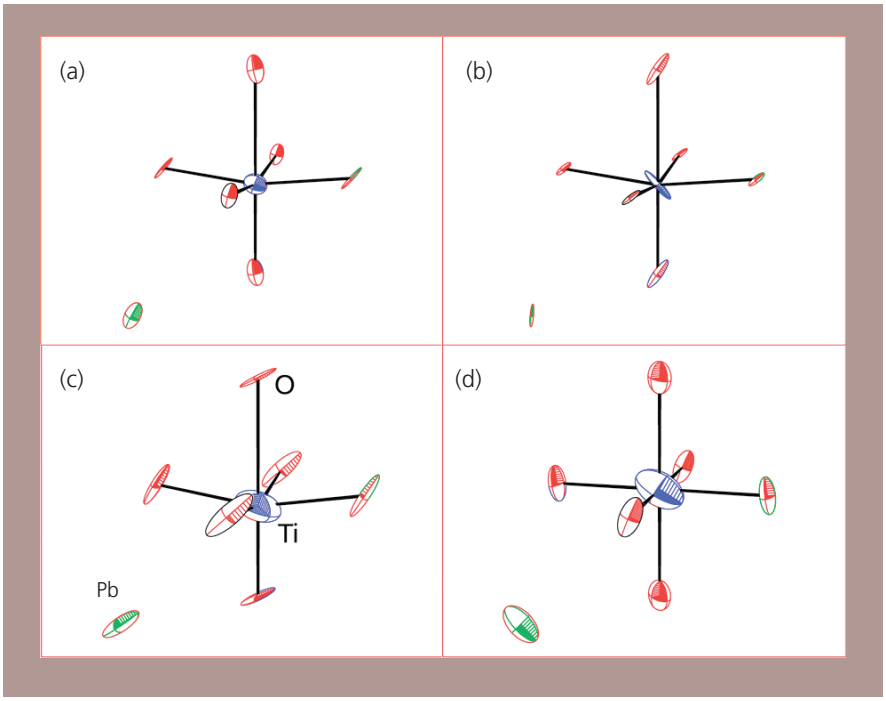

Figure 1. Atomic displacement ellipsoids at (a) 300 K and 0.8 GPa of pressure, (b) at 300 K and 2.5 GPa of pressure, (c) at 300 K and 8.3 GPa of pressure, and (d) at 600 K and 3 GPa of pressure. The tendency of oxygen ions to move along the (101) direction is clearly observed. Also, the elongation of the Ti displacement ellipsoid is clear and is similar to the well-known displacements of Pb ions. This demonstrates the crucial role that oxygen octahedra tilts play.

and because pressure mimics the "chemical pressure" arising from the cation substitution (such as Zr for Ti in PZT).

Recently, researchers J. Frantti, Y. Fujioka, and R. M. Nieminen (Helsinki University of Technology, Fi), and J. Zhang, S. C. Vogel, Y. Wang, and Y. Zhao (LANL) conducted experiments using TAP-98 on PbTiO3, a simplified PZT system, at Lujan Center's High Pressure Preferred Orientation (HIPPO) spectrometer. A combination of experimental results and density functional theory computations demonstrates that the competition between two important factors determines the MPB. The first is the oxygen octahedral tilting (Figure 1), giving advantage for the rhombohedral *R*3*c* phase. The second is the entropy, which in the vicinity of the MPB favors the tetragonal phase above 130 K. The balance of two factors over a large temperature range results in a steep phase boundary in the pressure-temperature space.

Not only do these findings provide a mechanism underlying the origin of MPB, they also underscore practical guides for the design of new, lead-free piezoelectric materials. (*Journal of Physical Chemistry B* **113**, 7967-7972, 2009.)

Enhanced hydrogen uptake in Ti-doped SBA-15

Among the two principle, current candidates for potential hydrogen storage materials for use in mobile applications, those based on chemical storage possess very high hydrogen-densities. However, these materials suffer from the large expense in energy that is required to retrieve hydrogen from the material and the even greater energy expended in regeneration of the storage material. On the other hand, materials with high porosity that use the sorption of molecular hydrogen are handicapped by the weakness of the guest-host interaction, which in turn imposes the use of high pressures and low temperatures to achieve practical storage capacities.

A considerable effort is, therefore, being made to improve the understanding of the nature of the interaction of hydrogen with porous hosts and their surfaces and to investigate more systematically the parameters that may enhance he binding of hydrogen in such materials. A large number of studies to date have focused on graphitic materials and hybrid materials such as metal-organic frameworks. Researchers A. I. Acatrinei, M. A. Hartl, J. Eckert, E. H. L. Falcao, G. Chertkov, and L. L. Daemen (LANL) used metal-doped SBA-15 as a platform for the study of many of the factors that may enhance hydrogen binding in porous materials with a large surface area, as it possesses an adjustable microstructure and is easily doped in controllable manner with a variety of metals.

Figure 1 shows that Ti-doping of the mesoporous silicate SBA-15 (6% Ti, nominal), which enhances the uptake of H_2 compared to undoped material. Inelastic Neutron Scattering (INS) at the Lujan Center sheds light on the interaction between adsorbed hydrogen and the (Ti-doped) silica surface. The broadband between 800 and 900 cm^{-1} can be attributed to bending modes of bridging hydroxyls on Ti-O-Si, or perhaps Ti-O-Ti bridges. The Ti concentration in the material is sufficiently high for some of those dimeric species to occur.

Calculations show the δ(Ti-OHbridge) to occur at 837 cm^{-1}, while this mode is known to occur at 1060 cm^{-1} for a Si-O(H)-Si bridge. Hydroxyl bending modes on mixed Si-O-Ti bridges could therefore readily fall in the range of the broad INS band at 890 cm^{-1} , depending on their actual geometry. The shoulders at 790 and 650 cm^{-1} then correspond to Ti-OH stretching modes, which will become visible in the INS because of the associated displacement of the H on the (Ti) O. Ti-H moieties do not appear to be present in significant numbers, as there is little evidence for the associated bending mode expected below or near 500 cm^{-1}.

The present system may therefore be viewed as another example of so-called hydrogen spillover, where molecular hydrogen dissociates at an active site on a surface (such as a metal cluster) and the resulting atomic H diffuses to and binds at other surfaces sites, or possibly in the interior of the material. The latter process appears to be involved in some recent potential hydrogen storage materials with very large gravimentric hydrogen capacities at room-temperature and elevated hydrogen pressures.

This research demonstrated that doping SBA-15 with Ti results in a significant improvement in the uptake of hydrogen at 77 K by the mesoporous silicate. Physisorption occurs at the hydroxyl groups and oxygen atoms of the pore surfaces. INS provides clear evidence for adsorption of H_2 in the vicinity of the Ti sites. Despite the fact that these sites represent, at most, 5% of silica entities in the material, they appear to be at least as effective as the more numerous hydroxyl groups in adsorbing hydrogen. An increase in hydrogen pressure above 10 bar results in a significant enhancement of hydrogen adsorption,

which exhibits a degree of hysteresis that increases with hydrogen pressure. INS vibrational spectroscopy suggests that this may be the result of activation of H_2 near the Ti site, followed by spillover to the immediate surroundings of that site.

These results open new possibilities to study the physisorption of H_2 in another class of porous materials with high specific-surface-area under pressure. The possibility of pressure activated spillover phenomena that can be chemically tuned may well enhance the utilization of this type of material for hydrogen storage. This is a rich array of physical and chemical parameters to study the adsorptive interaction of H_2 with the surface of doped SBA-15. (*J. Phys.Chem. C* **113**, 15634 (2009).)

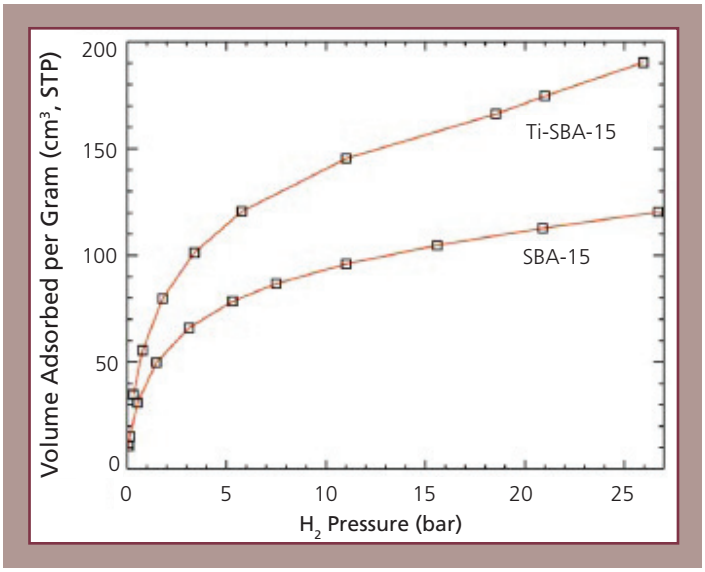

Figure 1. Hydrogen high-pressure adsorption isotherms (T = 77 K) for SBA-15 and Ti-SBA-15 (10% Ti doping). The lines are a guide to the eye. Notice that the slope of the Ti-SBA-15 isotherm at 25 bar is larger than the slope of the SBA-15 isotherm at the same pressure.

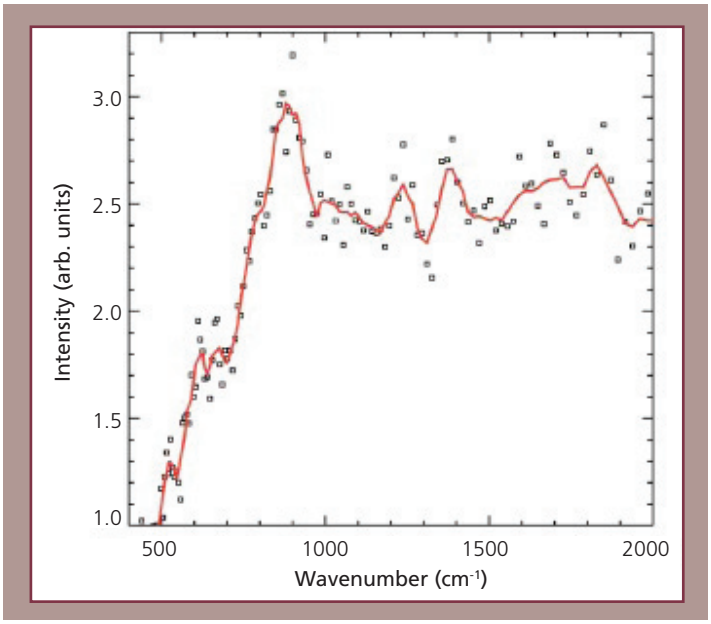

Figure 2. Neutron vibrational spectrum of H_2 adsorbed on Ti-SBA-15. The figure shows the difference between the spectrum collected for H_2 adsorbed on Ti-SBA-15 and H_2 adsorbed on SBA-15.

Determining the impact of radioactive decay on heating the Earth's core

Electron capture is a form of radioactive decay in which the nucleus "captures" an atomic electron from an inner shell. This type of radioactive decay may be subject to the influence of environmental effects, such as those due to chemical form and pressure. Greatly increased pressure increases the electron density near the nucleus and thus should increase the electron capture decay rate.

Such effects have been observed and documented for beryllium-7, with the largest observed effect

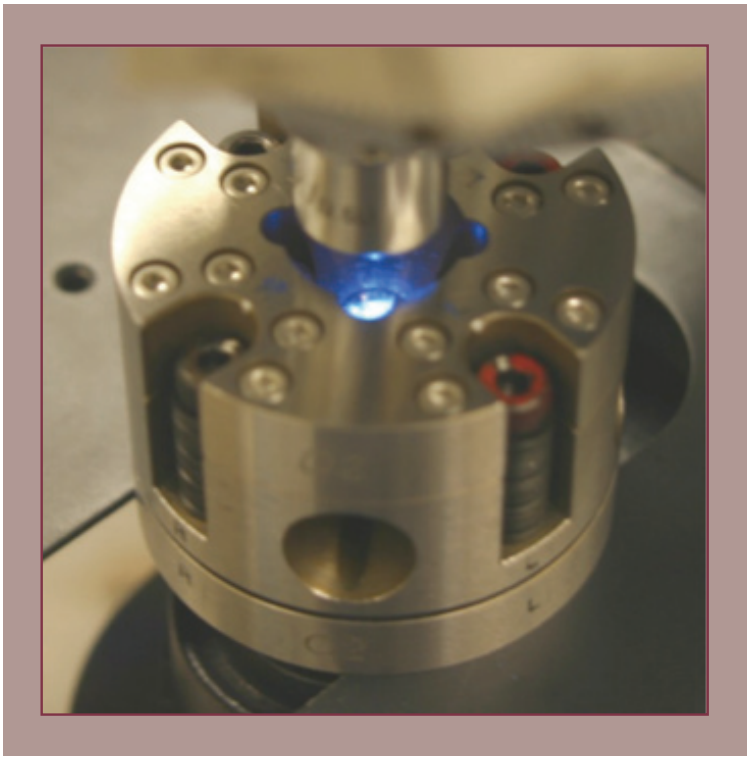

Figure 1. The center of the diamond anvil cell containing the sodium-22 sample is illuminated by blue light from an argon laser at the Lujan Center Raman Spectroscopy Laboratory. The laser is used to cause fluorescence in tiny ruby spheres in the cell. From a calibration of wavelength versus pressure, the internal pressure of the cell can be determined.

being about a 1% increase in the decay rate. Other radioactive decay processes, such as beta decay and alpha decay, generally are not expected to be influenced by the atomic environment, and have been shown to be insensitive to atomic effects.

A significant contributor of the Earth's heat comes from natural radioactive decay. A potentially important radionuclide is potassium-40, which may be alloyed at great pressure with iron in the Earth's core. Along with thorium and uranium, potassium may contribute substantially to the heating of the Earth's core. Although theoretical computations attempt to predict the change in the electron capture decay rate with pressure, there is, as yet, no data for potassium-40.

Because potassium-40 has a 1.25-billion-year half-life, direct measurements of the effect of pressure on decay are difficult. As a surrogate, chemically similar sodium-22 is being studied to test the theory. K. Lee (New Mexico State University) is leading a collaborative effort with R. O. Nelson and R. S. Rundberg (LANL) to conduct the measurement at LANSCE.

The experiment depends on Lee's expertise in loading and using diamond anvil cells (Figure 1) at the Raman Spectroscopy Laboratory at the Lujan Center (for pressure measurements), the use of highly enriched sodium-22 material, using the facilities of the Chemistry Division to grow a very small crystal, and use of counting instrumentation with two high-resolution gamma-ray detectors at LANSCE.

Because the expected effect is small (< 1%), the measurements are being made relative to gamma rays from cesium-137 located outside the pressure environment, but within a few millimeters of the compressed sample. Preliminary results indicate that the desired sensitivity is being achieved, and effects consistent with lifetime changes are being observed. If the effects are larger than predicted, there could be important consequences for our understanding of the Earth's internal heating.

These are the first measurements of the effects of pressure on sodium-22 decay. In addition to testing theory and improving our understanding of heating of the Earth's core, these measurements are of interest in a variety of applications, such as better calibrating potassium-40 decay as a long-time-scale chronometer and improving our knowledge of electronnucleus interactions.

Patent granted for "Ice method for production of hydrogen-clathrate-hydrates"

K. Lokshin and Y. Zhao (LANL) were granted U.S. patent # 7,371,907 for a method for hydrogen-clathrate-hydrate synthesis. Hydrogen-clathrate-hydrates are important for possible hydrogen fuel storage, and figure prominently in a hydrogen-based economy.

Lokshin's and Zhao's studies at LANSCE show that hydrogen clathrate (Figure 1) can trap hydrogen at mass fractions rivaling those of the best materials for hydrogen storage. In addition, they found a way to capture hydrogen in hydrogen clathrate in as little as a few minutes or less and release it at least as quickly.

A clathrate is an inclusion compound in which the guest species are enclosed on all sides of the host species forming a framework lattice. Clathrate hydrates are a subgroup of clathrates, with the host framework made up of hydrogen-bonded water molecules, and guest molecules trapped inside the polyhedral cages of the framework. Their invention is a novel method whereby the formation of

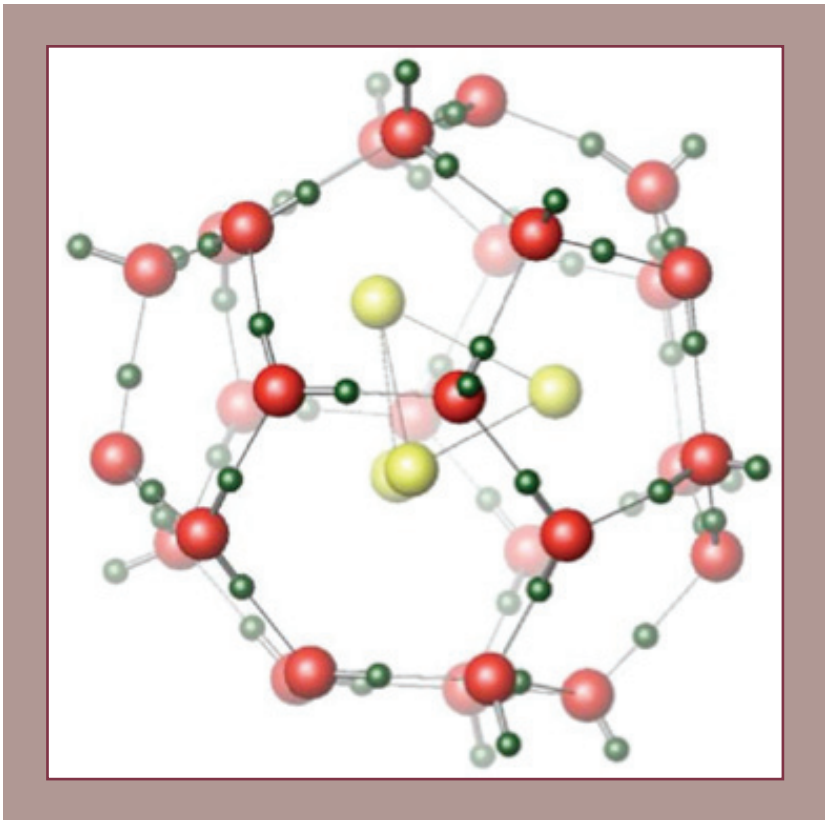

Figure 1. Large cage of hydrogen clathrate.

hydrogen-clathrate-hydrate occurs directly from ice and hydrogen, presenting a completely new technological means for hydrogen storage.

Ice-like polyhedral cage frameworks of clathrate hydrate can hold substantial amounts of guest molecular hydrogen—up to 3.77% of total mass at atmospheric pressure and moderately low-temperatures (140 K to about 200 K). Under higher pressures, these clathrates can hold greater amounts of hydrogen. The hydrogen storage capacity of clathrate hydrates is higher than the available hydrogen-storage metal hydrides, for example, Mg_2NiH_4 (3.59%) and $LaNi_5H_6$ (1.37%). A significant benefit of hydrogen-clathrate-hydrate is that by controlling pressure and temperature, it is possible to reversibly trap and/or release substantial amounts of molecular hydrogen.

Enzyme study at the Lujan Center explains detoxification of nerve agents

Organophosphorus molecules such as tabun, sarin, soman, VX, and diisopropyl fluorophosphate have the potential for devastating use as highly-toxic chemical-warfare agents. Scientists from Germany and LANL are collaborating to develop a biologically inspired defense against these deadly nerve agents.

Diisopropyl fluorophosphatase (PDFase), an enzyme found in squid, can detoxify these agents by breaking a chemical bond in their phosphate groups. DFPase is a prime candidate for development as a decontaminant because large amounts can be produced cheaply using bacterial expression systems, and it is very

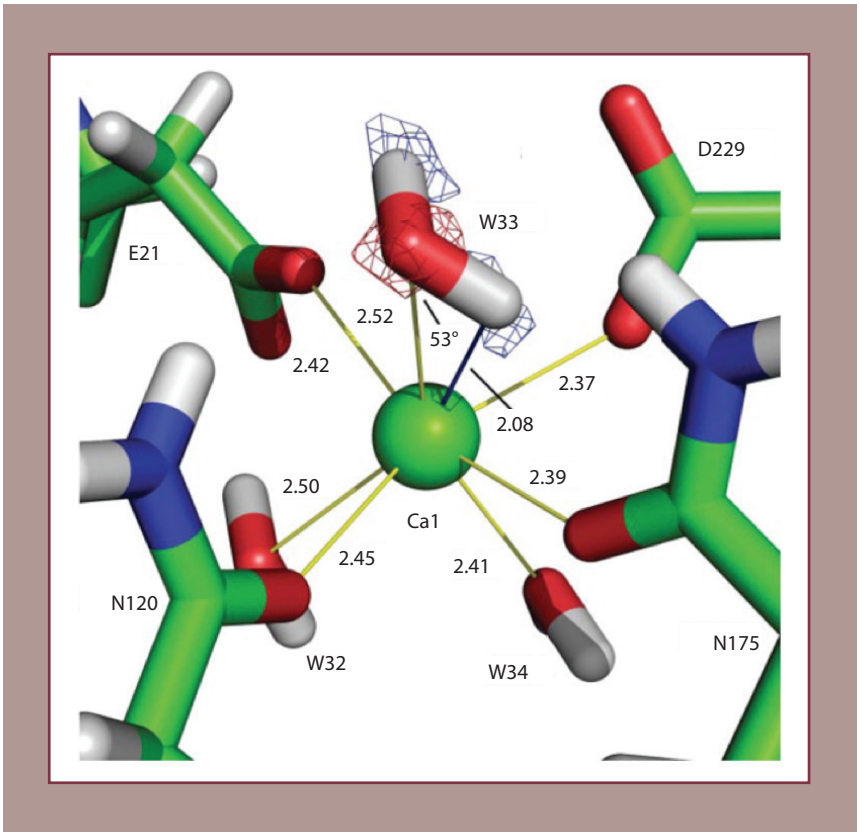

Figure 1. The active site environment of DFPase around the catalytic calcium ion, showing neutron scattering density from a functionally important solvent molecule (W33) that was expected to be an hydroxyl ion in the previously proposed catalytic mechanism and is demonstrated to be a water molecule in the newly proposed mechanism.

stable under a wide variety of environmental conditions. However, before DFPase can be used in the field, its efficiency and specificity against different nerve agents must be improved.

Engineering DFPase with improved performance against nerve agents requires understanding how DFPase binds the agents. Researchers M. Mustyakimov, B. Schoenborn, and P. Langan (LANL) and collaborators used a new computational approach and software developed at LANL to combine neutron diffraction data collected on the Protein Crystallography Station with x-ray data collected elsewhere.

The resulting joint x-ray/neutron structure of the DFPase active binding site is more accurate and complete than structures obtained by either technique alone. DFPase binds in an unexpected configuration, which rules out current ideas about its catalytic mechanism. It is the first protein for which neutron diffraction data report an extended network of internal water molecules, connected by hydrogen bonds in the form of a water tunnel in the center of a propeller-like structure.

The protonation states of DFPase side groups and solvent molecules in the active site support a newly proposed catalytic mechanism (Figure 1) involving a water molecule coordinating the catalytic calcium ion in a highly strained environment. This mechanistic insight enabled engineering improvements in DFPase for enhanced performance against nerve agents. (*Proceedings of the National Academy of Sciences USA* **106**:713-718 (2009).)

Neutrons reveal "sense-reversal" in twinning deformation of confined metal grains

If metals did not give before they break, as ceramics do, the Iron Age would not have happened and humanity would not have reached the level of science and technology characterized by the last two centuries of industrialization.

Metal forming is the macroscopic result of disrupting the atomic lattice in complex ways at the nanoscopic level. While analysis of this complex response has proceeded fruitfully by decomposing the deformation into basic

Figure 1. Top: SMARTS instrument. Bottom: HIPPO instrument.

elements, such as "slip" along crystallographic planes and "twinning" of grains, our emerging understanding is incomplete. Major complications arise because each grain is embedded in a matrix of other grains with semi-random orientations. B. Clausen, C. N. Tomé, and D. W. Brown (LANL), and S. R. Agnew (University of Virginia) have identified how deformations self-regulate the internal stress of a metal.

The scientists used neutron diffraction at the Lujan Center to identify a "sense-reversal" of the internal stress in twinned grains. A theory combining elastic and plastic modes of deformation describes this new feature and explains how texture variation—a reorientation of grains—due to twinning is sufficient to explain the observed macroscopic stress–strain response. The order in which slip and twinning are activated is important along with stress relaxation associated with twin propagation and neighbor constraints.

Twin propagation is similar to that of a crack: while a large local shear stress is required to initiate twinning, the stress for propagation is smaller. Once activated, twinning tends to lower the elastic energy by growing to a more energetically favorable size. In the new theory, the initial twin size "at birth" is assumed to occupy a "finite initial fraction" of the volume. Neutrons have a substantial advantage in determining the internal strains and structure of deformed metal. The SMARTS (Spectrometer for Materials Research at Temperature and Stress) instrument specializes in measurements during loaded deformation experiments at selected temperatures, and HIPPO (High- Pressure-Preferred Orientation neutron time-of-flight powder diffractometer) is suited to assessing average grain orientation or texture (Figure 1).

The scientists allowed for creation and growth of new twin grains with strain, while the parent grain's volume fraction concomitantly decreases. This feature alone enabled the evolution of yield stress, texture, and twin volume fraction with strain to be predicted correctly, which could not be accomplished with previous models. (*Acta Materiala* **56**:2456 (2008).)

First preparation and characterization of technetium bromides

Because technetium (Tc) and rhenium (Re) are members of the same group in the periodic table, the occurrence of analogous halide, oxide, coordination, and organometallic compounds is expected. However, the development of Tc chemistry has lagged behind that of Re because the inherent radioactivity of all Tc isotopes has limited the number of laboratories that can study Tc chemistry. Because most studies focus on the applications of the Tc-99m isotope in diagnostic nuclear medicine, there are some gaps in the knowledge of fundamental Tc chemistry.

Lujan Center graduate student E. Rodriguez (University of California, Santa Barbara) collaborated with former LANL employee A. Sattelberger (Argonne National Laboratory), T. Cheetham (Cambridge University), and F. Poineau, P. M. Forster, and K. R. Czerwinski (University of Nevada, Las Vegas) to make and characterize the first bromides of Tc to be reported in the past 40 years. The scientists synthesized the Tc bromides ($TcBr_3$ and $TcBr_4$) through reaction between Tc metal and elementa bromine.

The congruent formation of $TcBr_3$ and $TcBr_4$ could be due to inhomogeneous reaction conditions or kinetic considerations (that is, formation of $TcBr_4$ from $TcBr_3$ is faster than formation of $TcBr_3$ from Tc metal). $TcBr_3$ is the first trivalent Tc halide to be characterized.

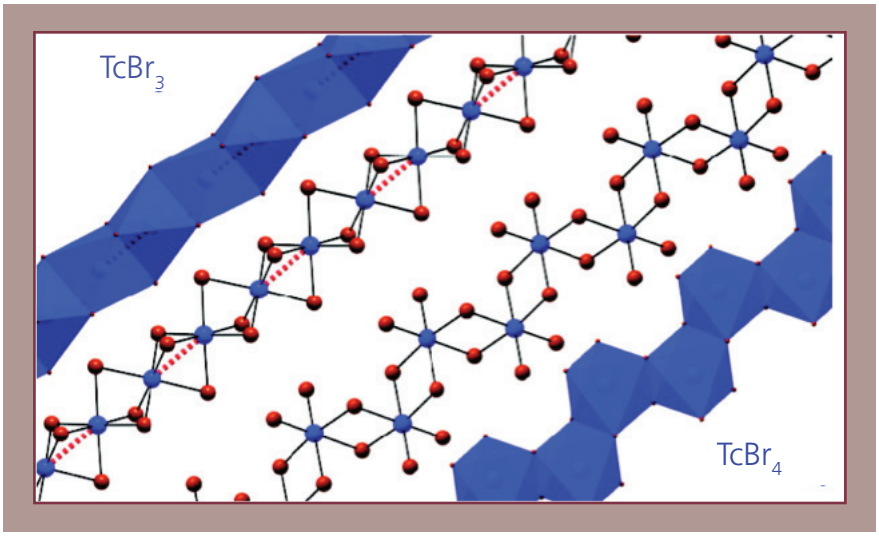

Figure 1. Structural representation of technetium bromide infinite chains.

The Tc bromides unexpectedly do not have extensive similarities with the bromides of neighboring Re. The reaction product between Re metal and bromine leads to a mixture of $ReBr_3$ and $ReBr_5$, and the structure of $TcBr_3$ differs significantly from that of $ReBr_3$ (Figure 1). This implies that much remains to be learned about fundamental Tc chemistry. (*Journal of the American Chemical Society* **131(3)**:910-911 (2009).)

Developing surrogate biomembranes

Supported lipid bilayers have long been used as surrogate membranes to facilitate physical measurements of model cellular interfaces. However, these surrogate membranes suffer from the disadvantage of constraining the lipid bilayers to planar or nearly planar geometry. Cellular membranes possess a three-dimensional, supple, and dynamic structure, which affects cellular adhesion processes and the dynamics and localization of transmembrane proteins.

LANL researchers H. L. Smith, M. S. Jablin, J. Saiz, A. J. Hurd, J. Majewski, and E. Watkins (also University of California, Davis), and collaborator A. Vidyasagar (University of South Florida) developed a polymer gel layer that provides a realistic, controlled environment to study biomembranes (Figure 1). The stable, cushioned membrane system is simple to prepare, robust, and enables control over both hydration of the supporting polymer and fluctuations of a supported lipid bilayer.

LANSCE neutron reflectivity and fluorescence microscopy studies showed that the surface-tethered polymer network undergoes a five-fold change in thickness over a 25–37 °C temperature range. As the polymer swells, it

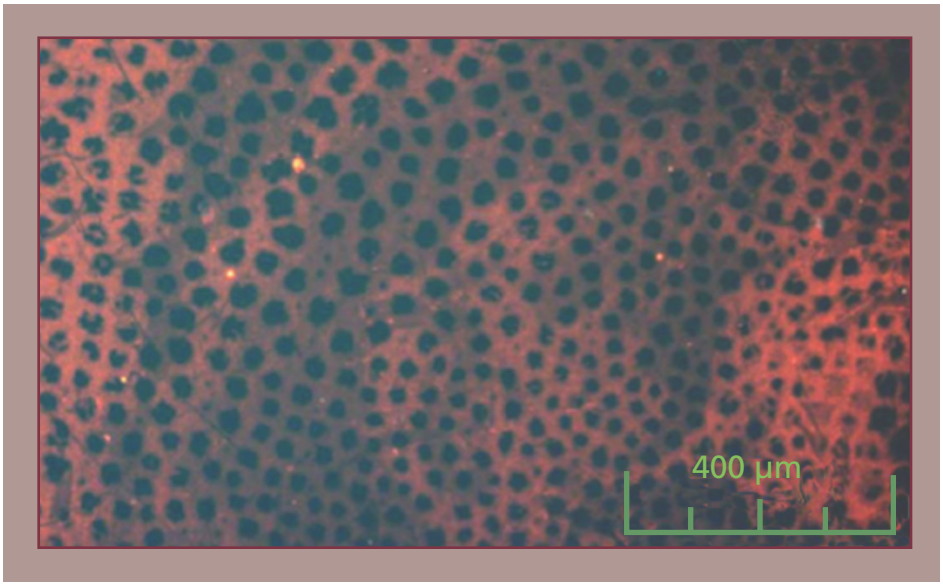

Figure 1. Fluorescence microscopy image of the supported bilayer on top of the polymer cushion. The red areas are regions of higher bilayer concentration. At 25 °C, the bilayer is fluid and preferentially phase segregates from the black polymer cushion gel domains.

promotes both in- and out-of-plane fluctuations of the supported membrane that mimic the properties of living cellular membranes.

The promotion of membrane fluctuations offers far-reaching applications as a surrogate biomembrane. This polymer-membrane system may facilitate otherwise difficult studies of lipid-protein interactions, transmembrane ionic transport, membrane structure, and membrane-based biosensors that previously have not been possible because of the limitations of existing models. (*Physical Review Letters* **102**:228102 (2009). The American Physical Society also selected the research to appear in the *Virtual Journal of Biological Physics Research*.

Structural details of self-organizing phospholipids revealed

Lipid bilayers and their self-organizing structures are used as models of cellular membranes and for their potential in biosensor applications. For the first time, the unprecedented structural details of a single, supported phospholipid bilayer at the solid-liquid interface were shown using high-resolution x-ray reflectivity and grazing incidence diffraction.

Researchers C. E. Miller and J. Majewski (LANL), E. B. Watkins (LANL and University of California, Davis), and D. J. Mulder and T. L. Kuhl (University of California, Davis) characterized the structure of single, supported bilayers by x-ray reflectivity and grazing incidence diffraction in bulk water. The scientists prepared bilayers on a solid support by fusion of small, unilamellar vesicles; Langmuir-Blodgett-Schaeffer (LBS) deposition. LBS bilayers display symmetric leaflets similar to monolayer structures, while vesicle fusion yields more inhomogeneous bilayers.

Diffraction showed that lipids are always coupled across the bilayer even when leaflets are deposited independently. This result indicates the existence of orientational texture. Bilayers formed by vesicle fusion have more disorder in the inner leaflet compared to structures prepared using the more controlled LBS technique. This methodology can be used to study more complicated biomembranes and their interaction with proteins. (*Physical Review Letters* **102**:238101 (2009).)

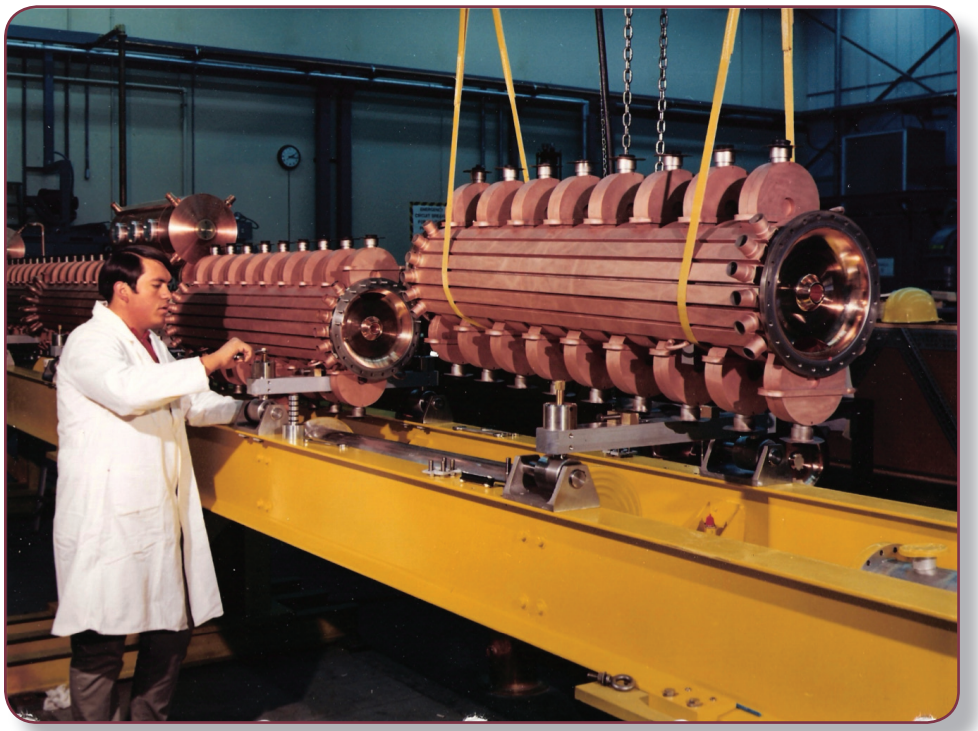

A section of the linear accelerator's drift tubes under construction in 1969.

Evidence discovered for lipid rafts in model biomembranes

There is increasing evidence that lipids comprising the plasma membrane are inhomogeneously distributed, forming liquid domains rich in cholesterol and saturated lipids. These domains, called "lipid rafts," are implicated in many cell functions including endocytosis, signaling, and lipid regulation. Driving forces for raft formation and the role cholesterol plays on membrane lipid organization remain unresolved.

J. Majewski (LANL) and collaborators from the University of Chicago, Max Planck Institute, and

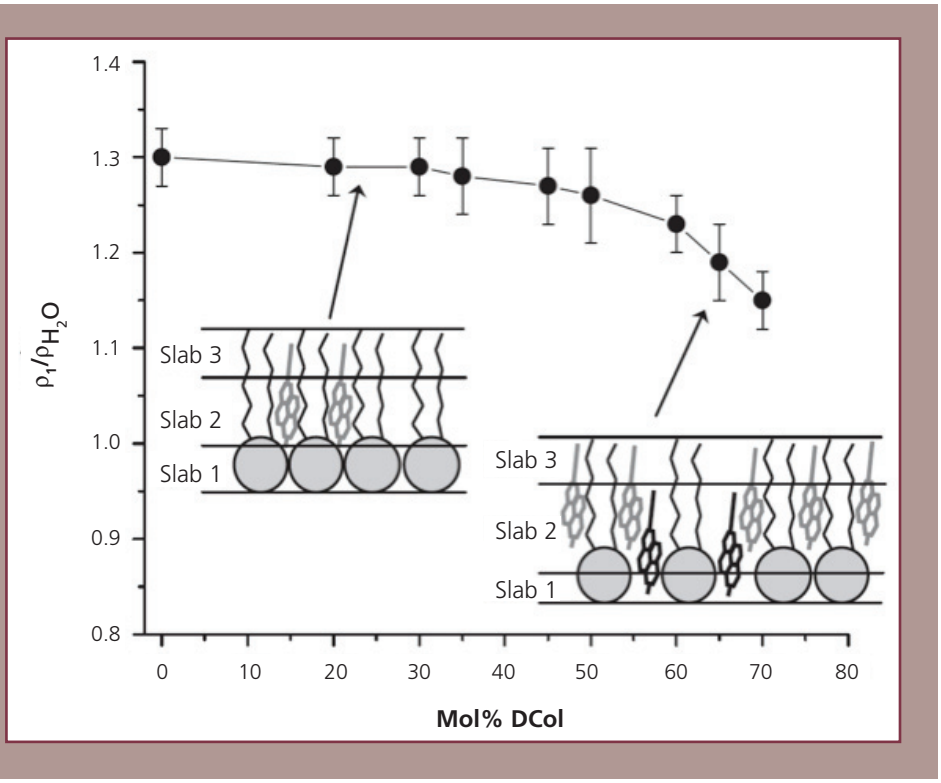

Figure 1. Dependence of normalized electron density of slab 1, normalized to the electron density of water, ρH_2O = 0.334 eρ/Å3, $\rho_1/\rho H_2O$, (defined as the SM head-group region) on DChol content. Values of ρ_1 were obtained from fitting the x-ray reflectivity data. The cartoons illustrate that ρ_1 decreases with the penetration of DChol into the head-group region at high DChol content, since electron density of the DChol sterol ring is lower than that of the lipid headgroup. Gray DChol denotes complexed DChol. Black DChol denotes free DChol with higher vertical mobility.

Niels Bohr Institute (University of Copenhagen), discovered the presence of lipid rafts in the structure of model biomembranes. The scientists analyzed lipid monolayers composed of different compositions of sphingomyelin (SM) and dihydrocholesterol (DChol), both of which are thought to be major constituents of lipid rafts, to examine lipid-cholesterol interactions.

Grazing incidence x-ray diffraction and x-ray reflectivity techniques probed lateral ordering and structural features of the model systems of mixed monolayers. Figure 1 shows that the electron density of slab 1 decreases with increasing DChol due to the mixing of the lower electron density DChol sterol rings into the higher electron-density SM head-groups. At low DChol content, DChol is localized in the SM tail-group region, exerting little effect on the SM head-group electron density. With the relatively large cross-sectional area of SM head-group compared to its tail-group, DChol can be readily accommodated in the predominantly SM film without perturbing the head-group region.

A more pronounced decrease in the electron density of slab 1 is found with increasing DChol beyond the cusp point. This is consistent with DChol penetrating into SM head-groups, lowering the electron density of the region. Thus the x-ray data reveal short-range (~25 Å) two-dimensional ordering.

The nanoclusters show two distinct regions: below the cusp point of the phase diagram (35 mol% DChol), a constant d-spacing was observed; above the cusp, the d-spacing increases linearly with DChol in accordance with Vegard's law for binary alloys. The components in this lipidic alloy are a 65:35 SM/DChol entity and excess DChol. X-ray reflectivity data indicate the emergence above the cusp of an uncomplexed DChol population with greater vertical mobility. (*Physical Review Letters* **103**:028103 (2009).)

How oxidative stress degrades cell membrane structure

Researchers J. Majewski, H. Smith, and L. Daemen (LANL) and collaborators from the University of California, Davis showed how oxidant assault—long suspected to be a factor in Alzheimers and Parkinson's disease, aging, and other maladies—affects cellular membrane structure.

Cellular membranes are complex, highly-organized structures a few nanometers thick consisting primarily of a double layer of phospholipid molecules, cholesterol, and transmembrane proteins and sugars. The membranes have important structural and functional roles in cells,

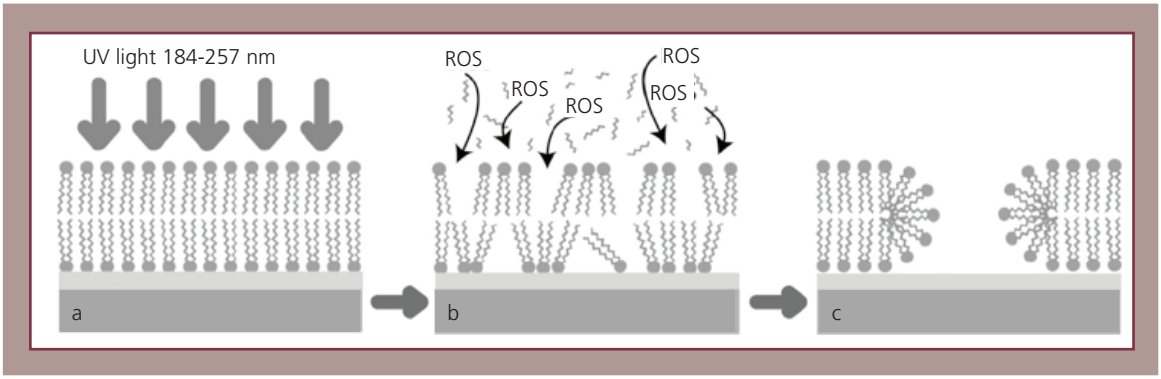

Figure 1. Schematic of the oxidation process occurring during exposure of the bilayer to UV. (a) The membrane is exposed to UV. (b) Reactive oxygen species enter the membrane, and lipid fragments enter solution. (c) The membrane rearranges to form pores where deuterated water enters.

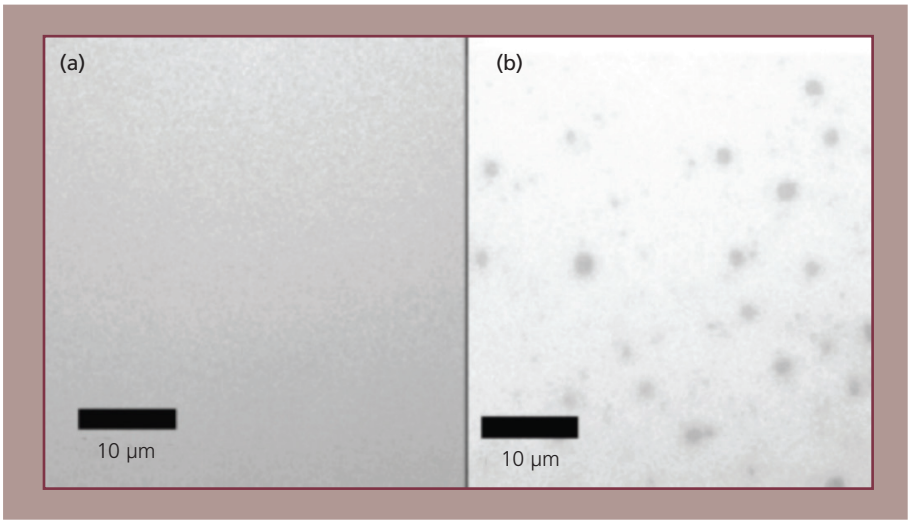

Figure 2. Fluorescent micrograph of a bilayer (a) before illumination, and (b) after exposure to UV light for 3 min. The black spots in the membrane indicate the formation of pores.

including acting as a semi-permeable barrier regulating the flux of materials into and out of the cell, controlling interactions with extra-cellular compounds, and providing a framework for the operation of cell-integral proteins.

The researchers used a model configuration of supported lipid bilayers at the solid-liquid interface and ultraviolet (UV)-generated reactive oxygen species to mimic the early stages of oxidative assault on a lipid biomembrane. Neutron reflectivity probed the structural changes.

The researchers concluded that the membranes become more permeable due to water channel formation during early phases of membrane degradation (Figures 1 and 2). An unusual graded interface at the membrane-water interface appears to be a gradient of oxidized material into bulk solution. Unsaturated lipids oxidize faster than saturated lipids, and the presence of the antioxidant L-ascorbic acid slows the rate of oxidation. (*Journal of the American Chemical Society* **131**:3631 (2009).)

Nanograins demonstrate extraordinary thermal stability

Nanoscale structure gives nanomaterials enhanced physical properties, compared with bulk materials. However, applications of some nanomaterials have a limited temperature range to prevent the growth of grain size. L. Daemen (LANL), M. Barsoum (LANL and Drexel University), and collaborators (Drexel University, Linkoping University, Sweden; University of Pennsylvania; and University of Delaware) discovered extraordinary thermal stability of magnesium nanograins in a titanium-aluminum-carbon-magnesium composite.

X-ray diffraction and neutron spectroscopy indicate that a thin, mechanically robust layer separates the magnesium nanograins and prevents them from growing (Figure 1). The layer is thin enough and mechanically robust enough to survive the melting and solidification stresses during the temperature cycling. The microstructure is so stable that heating the composite three times to 50 °C beyond the melting point of the bulk magnesium does not lead to growth of the grain size.

Making nanoscale materials economically and on an industrial scale is a challenge because nanosized powders must remain non-agglomerated and mono-dispersed during synthesis and consolidation. Processing the

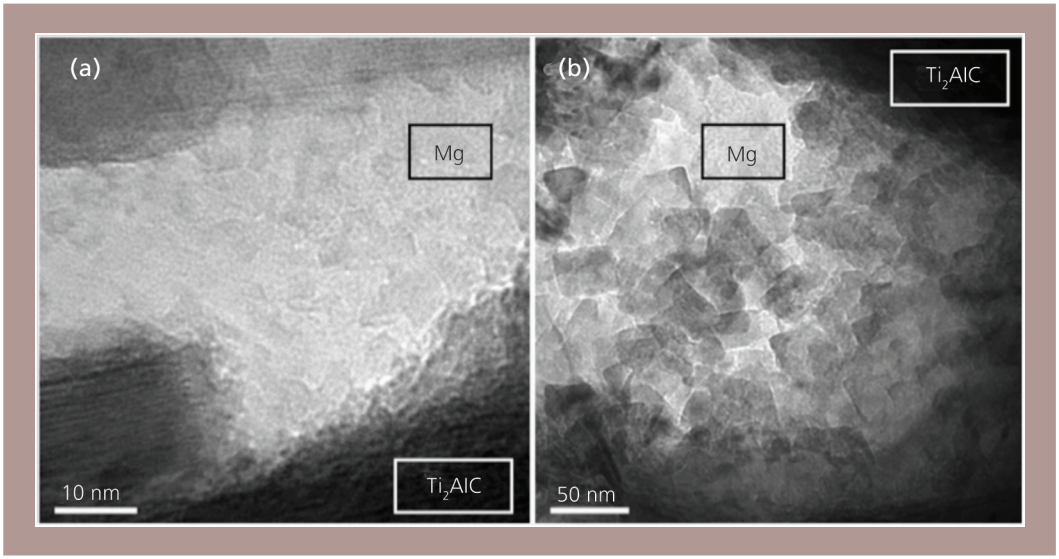

Figure 1. Transmission electron microscopy images of the magnesium nanograin matrix in the (a) hot pressing and (b) melt infiltration Ti_2AlC composite samples.

magnesium nanograin matrix composites is a simple process that uses pressure-less melt-infiltration, resulting in magnesium grains of ~20–40 nm in size. The material is readily machinable, light, relatively stiff, strong, and exhibits ultrahigh damping.

The material is readily machinable, light, relatively stiff, strong, and exhibits ultrahigh damping. The combination of excellent mechanical properties and thermal stability should provide a broad range of potential applications. (*Nano Letters* **9**:3082 (2009).)

Competitive adsorption of lung surfactant and albumin

Lung surfactant is a slippery, complex mixture of lipids and proteins that helps the lungs inflate with air and keeps the air sacs (alveoli) from collapsing. Acute respiratory distress syndrome (ARDS) occurs when pulmonary capillaries leak blood serum proteins (especially albumin) into the alveoli. The leakage prevents the lungs from filling with air and can result in a dangerously low level of oxygen in the blood. Understanding the fundamental biophysics and surface chemistry of lung surfactant can lead to therapeutic treatment. Clinical research shows that the presence of hydrophilic non-adsorbing polymers within the same subphase helps the lung surfactant overcome the effects of albumin.

C. Miller and J. Majewski (LANL), and collaborators (University of California, Santa Barbara; University of Chicago; and RisØ National Laboratory, Denmark) used x-ray reflectivity and grazing incidence x-ray diffraction to examine competitive adsorption of lung surfactant and albumin at the air-water interface as a model for behavior in the lung.

Equilibrium favors lung surfactant as it has the lower equilibrium surface pressure, but the smaller albumin is kinetically favored by faster diffusion. The scientists added Survanta, is a clinical lung surfactant used to treat acute respiratory distress syndrome. Survanta reduces the surface tension of fluids inside the lung, preventing collapse of the lung. Albumin induces a slightly larger lattice spacing and greater molecular tilt of the phospholipid phase fraction of Survanta, similar in effect to a small decrease in the surface pressure.

Adding the water-soluble polymer, polyethylene glycol (PEG), to the Survanta and albumin-containing subphase restores the characteristic Survanta electron density profile at the interface and confirms that PEG is depleted near the interface. Survanta has a more compact lattice corresponding to a small increase in the surface pressure.
These findings give insights into the biophysics and molecular basis for acute respiratory distress syndrome treatment: (1) albumin adsorption creates a physical barrier that inhibits lung surfactant adsorption, (2) PEG in the subphase generates a depletion attraction between the lung surfactant aggregates and the interface that enhances lung surfactant adsorption, and (3) the structure or properties of the lung surfactant monolayer are substantially unchanged.

The research will aid in the rational development of improved treatments for acute respiratory distress syndrome. (*Biophysical Journal* **97**:777 (2009).)

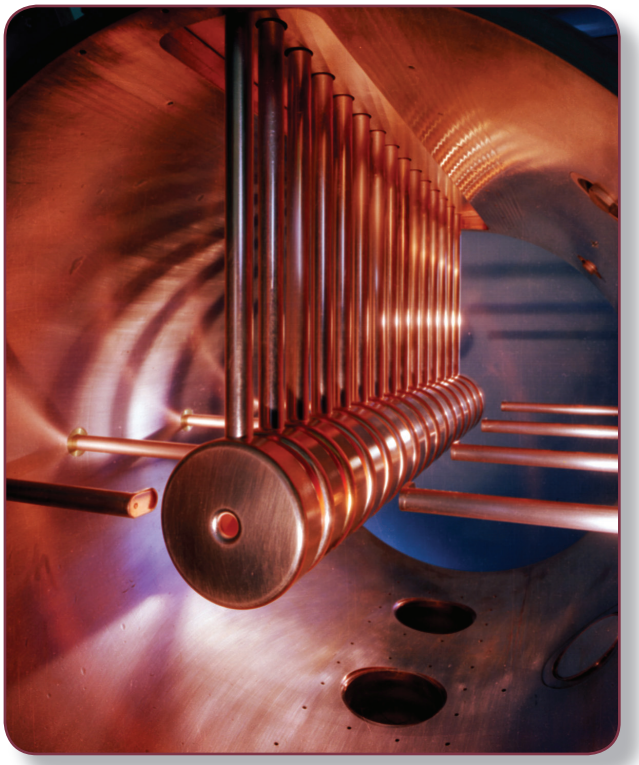

A section of the linear accelerator's drift tubes under construction in 1969.

Neutron reflectometry studies of nanostructural phenomena at the fuel cell interface

Polymer Electrolyte Fuel Cells (PEFCs) hold promise for energy production due to their high-energy density, high efficiency, and zero emissions. The active power-producing center of a PEFC is the catalyst-coated membrane, which consists of anode and cathode catalyst layers coated onto either side of an ion-exchange polymer (or ionomer) membrane.

The triple-phase interface of a PEFC electrode is comprised of three co-mingled two-dimensional interfaces: a platinum-carbon interface (for electron transport and catalyst particle dispersion), a platinum-ionomer interface (for proton transport to reaction sites), and an ionomer-carbon interface (for high dispersion of catalyst-support aggregates, electrode structural integrity, and high porosity for oxygen/hydrogen diffusion).

Understanding the basic structure of ionomers across length scales, from molecular to nanostructural to bulk, is important to comprehend water transport, proton transport, and the oxygen reduction reaction mechanism occurring at the triplephase interface. This information will assist in improving the efficiency of PEFCs.

J. Chlistunoff, R. Borup (MPA-11), and J. Majewski (LANL), and D. Wood (Oak Ridge National Laboratory) used neutron reflectometry at the Lujan Center to examine the interactions of PEFC materials comprising the triple-phase interface. They studied a commercially available ionomer, Nafion. The scientists used smooth, idealized layers of Nafion on glassy carbon and platinum surfaces as an experimental model for the PEFC electrode interfaces.
Separate hydrophobic and hydrophilic domains formed within the Nafion layer when equilibrated with saturated deuterated water vapor. The thicknesses of the hydrophobic and hydrophilic domains changed to the same magnitude when a platinum oxide layer was present compared to a thin hydrophobic domain in contact with platinum. The findings are direct experimental evidence that both the interfacial and long-range structural properties of Nafion are affected by the material with which it is in contact.

Evidence of physical changes of aged Nafion films show a permanent increase in the thickness of the Nafion film and a decrease in scattering length density. The researchers attribute these results to irreversible swelling of the Nafion film. (*Journal of the American Chemical Society*, in press.)

A view of the Lujan Center's Experimental Room #2 showing various instruments that rely on neutron scattering for research.

Neutron reflectometry provides first sub-nanometer visualization of live cell adhesion

Neutron reflectometry (NR) at LANSCE is used to probe the structure of thin films at various interfaces. Over the past 30 years, NR has evolved to become key in the characterization of thin films. Typically, NR measurements are performed on model systems in which samples are homogeneous over large areas. Because of their complexity and inhomogeneity, the measurement of live objects, such as cells adherent to a solid

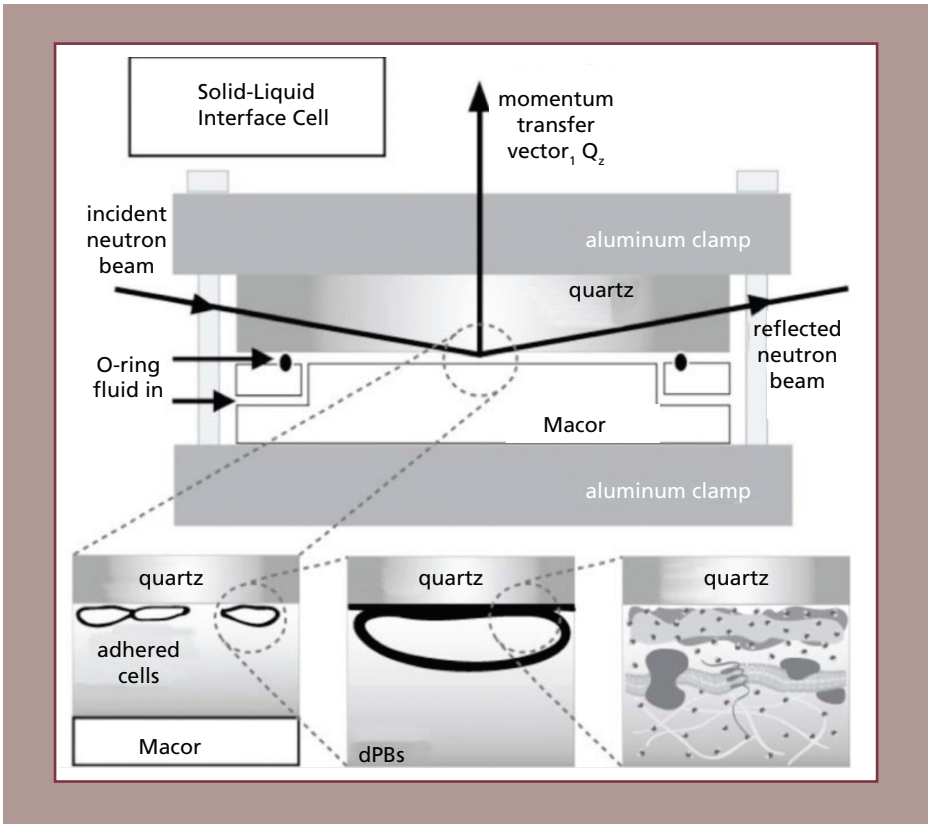

Figure 1. Schematic of the NR measurements. The quartz substrate with adherent cells is clamped against a Macor disk with a 0.2–0.3-mm-thick gap where the subphase (deuterated phosphate buffered saline, dPBS) is injected. The neutron beam penetrates the lateral face of the quartz substrate to reach the solid-liquid interface where the cells reside. Insets show a cartoon representation of how the cells behave in the adherence region. Immediately adjacent to the quartz substrate is a layer of adherence proteins (~120-Å thick), on top of which sits the membrane region (~80-Å thick), followed by a diffuse profile representing the interior of the cell. Small dots in the far right panel represent deuterated water molecules as a function of distance from the quartz substrate.

substrate, is a radical departure from a typical system measured via NR.

However, in situ NR measurements of biologically relevant objects are needed to study the detailed structure and biophysics of cell attachment. H. Smith, M. Jablin, J. Majewski, J. Hickey, A. Trujillo, and J. Freyer (LANL) used NR to examine living mouse fibroblast cells adherent on a growth media coated quartz substrate (Figure 1). This is the first visualization and quantization of the interface between live cells and a substrate with sub-nanometer resolution using NR.

The Figure 1 inset panels are a representation of how the cells behave in the adherence region. The membrane region, ~80-Å thick, contains the membranes of cells that are inhomo-geneously distributed or undulating, likely conforming to the non-planar geometry of the supporting adherence proteins. (*Biophysical Journal*, in press.)

X-ray studies reveal how plants defend against bacterial invaders

Purothionins are low-molecular-weight plant-polypeptides that appear to have an important role in defense against bacterial invaders.

Their toxic effect may arise from lysis (disruption) of the membranes of the attacking cells. To clarify how purothionins lyse the bacterial phospholipid membranes, J. Majewski (LANL) and B. Stec (Burnham Institute for Medical Research, La Jolla, CA) used synchrotron x-ray scattering methods (x-ray reflectivity and grazing incidence x-ray diffraction) to investigate the

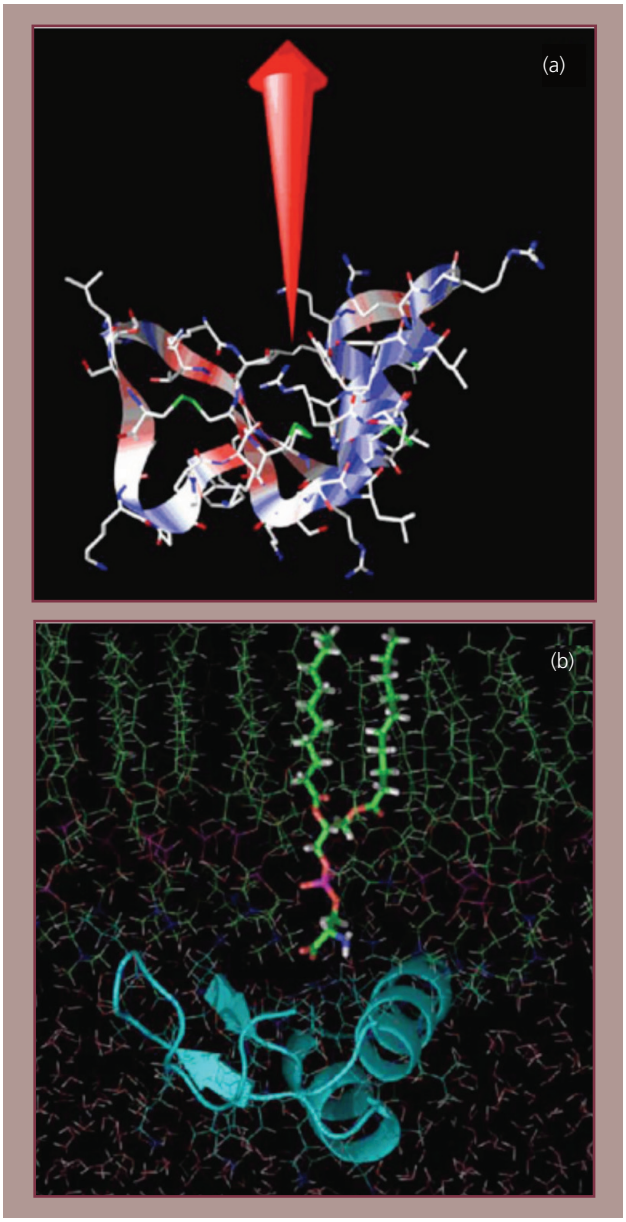

Figure 1. (a) Ribbon representation of beta-purothionin superposed onto bond-stick model showing the distribution of positively charged amino acids. The vector of the electric field originating at the site of binding of a small molecule entity (glycerol, serine, phosphate, etc.) detected in each crystal structure of thionins that is proposed to be the phospholipid binding suite is depicted by the red arrow. (b) Snapshot of a molecular dynamics simulation illustrating the possible attachment of the charged phospholipid to the purothionin.

interactions of purothionins with a model lipid membrane (Figure 1).

The results suggest that purothionin transiently binds to the surface of phospholipid membranes in the liquid phase and withdraws some of the membrane's components. Information gained from research into the mechanism of bacterial cell lysis could give insight into how antibiotics function and the development of new classes of antibiotics from plants. (*European Biophysics Journal*, in press.)

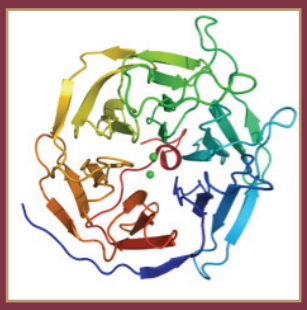
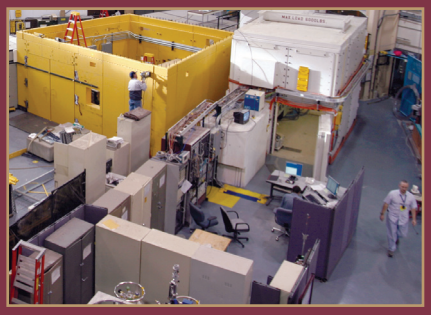
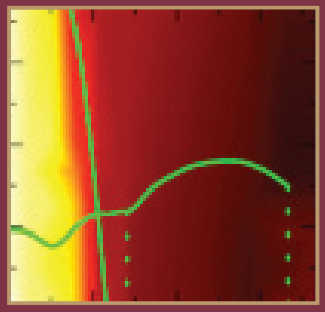
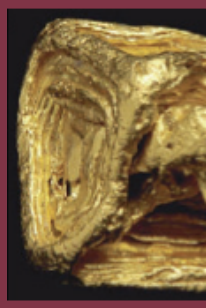

Lujan Center Published Article Reprints

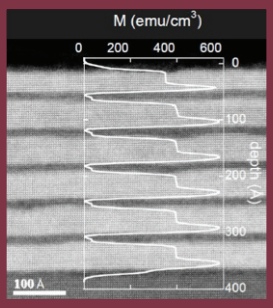

Published Article Reprints

Understanding the insulating phase in colossal magneto-resistance manganites: shortening of the Jahn-Teller Long-Bond across the phase diagram of $La_{1-x}Ca_xMnO_3$

E. S. Bozin, A. J. DeConinck, G. Paglia, and S. J. L. Billinge (Michigan State University); M. Schmidt and P. G. Radaelli (ISIS, Rutherford Appleton Laboratory); J. F. Mitchell (Argonne National Laboratory); T. Chatterji (Institute Laue-Langevin, FR); Th. Proffen (Los Alamos National Laboratory)

Introduction

One approach for establishing a correlation between inhomogeneities and electronic properties is to study the complete phase diagram of interesting systems. We set out to examine the local structure of the $La_{1-x}Ca_xMnO_3$ (LCMO) manganite family [1]. This is an archetypal system for such studies because of the strong electron-phonon coupling, through the Jahn-Teller (JT) effect, resulting in a large structural response to electronic phase separation. We have used the atomic pair distribution function (PDF) measured from neutron powder diffraction data to probe this effect. When the charges are localized in a polaronic insulating phase, the JT-long-bond is seen. A two-phase fit of an undistorted and distorted phase to the low-r region of the PDF can thus yield a quantitative measure of the phase fraction of each phase as a function of *T* and *x* in the system $La_{1-x}Ca_xMnO_3$. Contrary to the canonical understanding, we found that the length of the Jahn-Teller long-bond in the insulating phase decreases continuously with increasing doping in this system.

Experimental

A series of 13 powdered LCMO samples with compositions spanning $0 \leq x \leq 0.5$ were prepared using standard solid state synthesis methods and annealed to ensure oxygen stoichiometry and characterized by resistivity and magnetization measurements. Two additional finely pulverized single crystal samples (x=0.075, x=0.1), grown by the floating zone method utilizing image furnace, were also used to increase coverage of the phase space under the study. Neutron powder diffraction measurements were carried out at the NPDF diffractometer at Los Alamos Neutron Scattering Center and at the GEM diffractometer at the ISIS facility at the Rutherford Appleton Laboratory in the UK.

The samples, of approximately 6-g. each, were loaded into extruded vanadium containers and sealed under He atmosphere. The data were collected for all the samples at a consistent set of seven temperatures between 10 °K and 550 °K using a closed-cycle helium refrigerator. The data were processed to obtain PDFs [2] using the program PDFGETN [3] by a sine Fourier transform of the total scattering structure function *F(Q)* up to a value of Q_{max} of 35 $Å^{-1}$. This high Q_{max}, coupled with the excellent statistics from NPDF and GEM, result in high-quality PDFs with minimal spurious low-r ripples and negligible termination ripples.

Results and Discussion

The PDF analysis involves both direct data evaluation and structural modeling using the program PDFFIT [4]. Results of complementary average crystal structure modeling, carried out using the program GSAS [5], are also presented. All refinements were carried out using the

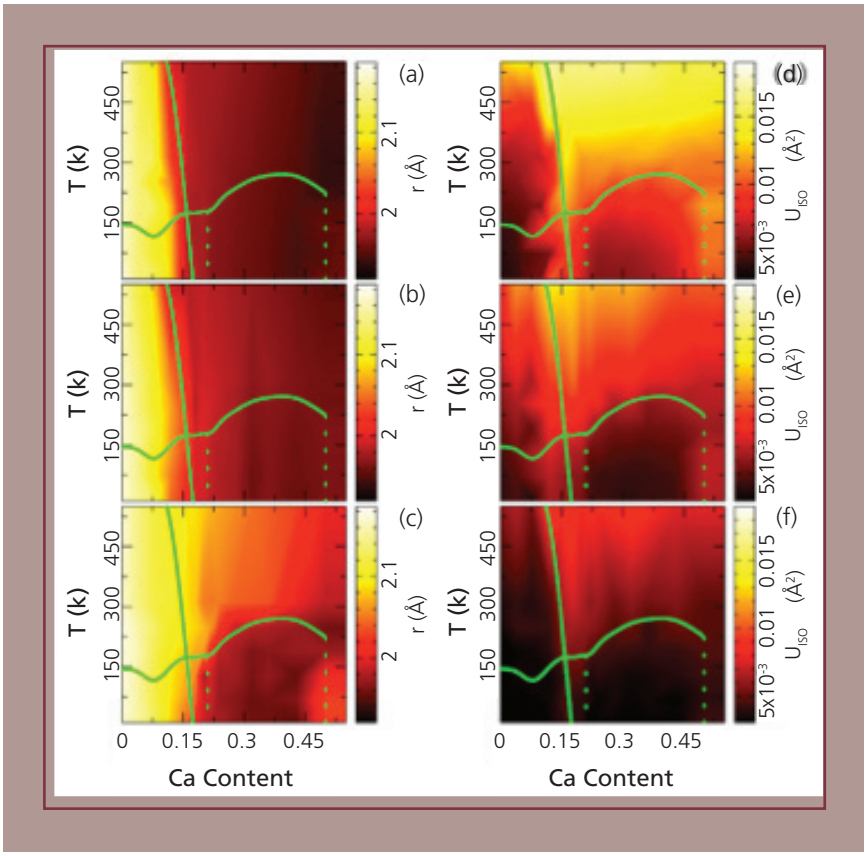

Figure 1. Contour plot of the JT distortion (long Mn-O distance) in (x,T) parameter space as obtained from (a) Rietveld analysis and PDF analyses over (b) 20-Å and (c) 6-Å ranges, respectively. Contour plot of the isotropic displacement parameter of oxygen, U_{iso}(O2) in Pbnm setting, as obtained from (d) Rietveld analysis, and PDF analyses over (e) 20-Å and (f) 6-Å ranges. In all the panels the solid curves indicate TJT and T_c phase lines, while dotted vertical lines indicate IM phase boundaries, as determined from the sample characterization measurements.

O or O′ structural models in the Pbnm space group with isotropic displacement parameters. Our analysis does not address the ordering of localized charges such as observed in the charge ordered state at x=0.5 [6]. Main results are summarized in Figures 1 and 2.

In the orthorhombic O phase, the local JT distortion amplitude (the length of the JT-long-bond) is the same as the average long range ordered value. The distortion is constant with temperature for fixed Ca content, but decreases linearly with increasing Ca content. Upon crossing into the pseudocubic O′ phase, the average JT distortion (assessed through Rietveld and 20-Å PDF refinements) disappears abruptly. However, this effect is accompanied by the anomalous increase of the isotropic thermal parameters on oxygen sites. This is consistent with the understanding that the pseudocubic O′ phase in the insulating

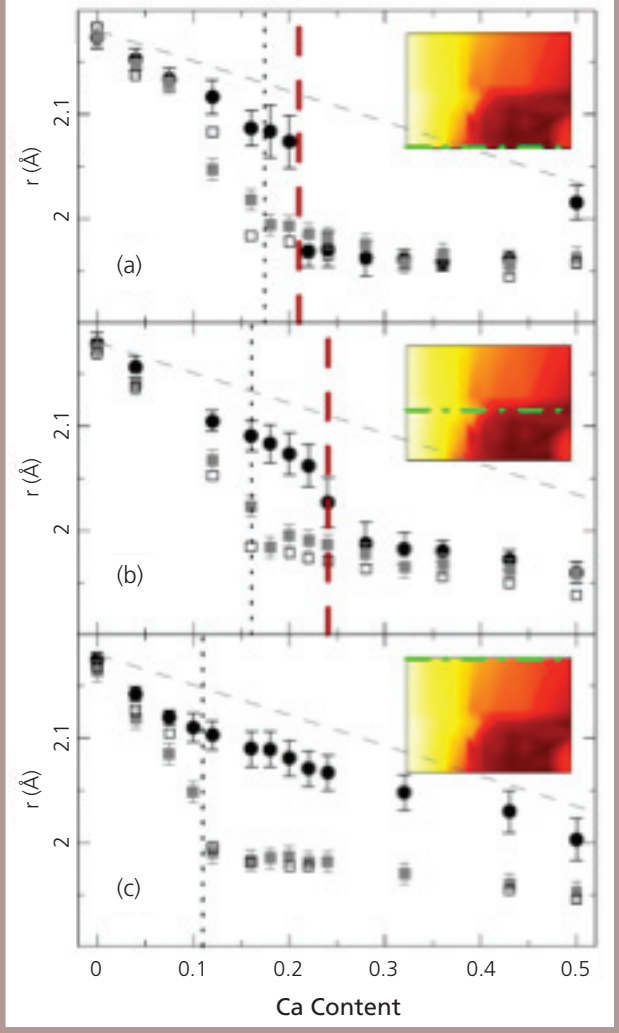

Figure 2. Length of the longest Mn-O distance in the MnO_6 octahedron vs doping at (a) 10 K, (b) 250 K, and (c) 550 K. Open squares denote Rietveld result; Solid squares and circles show results of PDF refinements over 20-Å and 6-Å ranges, respectively. Sloping dashed lines denote Vegard's law behavior for Mn-O longbond interpolating between the values for $LaMnO_3$ and $CaMnO_3$. Dashed vertical lines mark the IM transition, while the dotted vertical lines denote the orthorhombic to pseudocubic phase transition.

state consists of orbitally disordered, JT distorted, octahedra, and that this picture can be extended to finite doping.

In the ferromagnetic metallic (FM) phase, the average JT-long-bond disappears, but there is no significant enlargement of the refined oxygen thermal parameter showing that the local JT-long-bond is also absent. Structural refinements to the PDF data over a wide range of r (up to 20 Å) mimic the Rietveld results rather closely. This shows that the average structure result is already obtained for a PDF refinement over a 20-Å range, suggesting that the size of local orbital ordering correlations is limited to this range. By fitting the PDF over a narrow r range of 6 Å, the length of the local long Mn-O bond has been obtained. The local JT distortion is present in the entire insulating part of the phase diagram, but that it is effectively removed for the metallic compositions at lowest temperatures. Second, it is seen that the magnitude of the local JT distortion has a relatively strong doping dependence at lower Ca concentrations, with the bond length versus concentration curve flattening at higher Ca doping levels.

Selected constant temperature cuts are shown in Figure 2, for 550 °K, 250 °K, and 10 °K, respectively. The square symbols show the behavior of the average structure. The JT-long-bond decreases with doping in the orbitally ordered O phase, but then abruptly shortens at the structural phase transition, indicated by the dotted line in the figure. In contrast, the local JT bond is insensitive to the structural transition, but disappears abruptly when the sample goes through the insulator-metal (IM) transition. This is consistent with the widely held current view. What is less expected is the observation that the length of the local JT-long-bond shortens with increasing doping in the insulating state, which is in disagreement with the small polaron picture for the insulating state.

Conclusions

The detailed evolution of the magnitude of the local Jahn-Teller (JT) distortion in $La_{1-x}Ca_xMnO_3$ is obtained across the phase diagram for $0 \leq x \leq 0.5$ from high-quality neutron diffraction data using the atomic pair distribution function method. A local JT distortion is observed in the insulating phase for all Ca concentrations studied. However, in contrast with earlier local structure studies, its magnitude is not constant, but decreases continuously with increasing Ca content. This observation is at odds with a simple small-polaron picture for the insulating state. (*Physical Review Letters* **98**:137203 (2007).)

References

[1] Bozin, E. S., et al., *Phys. Rev. Lett.* **98**, 137203 (2007).

[2] P. F. Peterson et al., *J. Appl. Crystallogr.* **36**, 53 (2003).

[3] P. F. Peterson et al., *J. Appl. Crystallogr.* **33**, 1192 (2000).

[4] T. Proffen and S. J. L. Billinge, *J. Appl. Crystallogr.* **32**, 572 (1999).

[5] A. C. Larson and R. B. Von Dreele, Los Alamos Laboratory Report No. LAUR-86-748, 1987.

[6] P. G. Radaelli et al., *Phys. Rev. B* **55**, 3015 (1997).

Suppression of nuclear polarization near the surface of optically pumped GaAs

M. R. Fitzsimmons, B. J. Kirby, N. W. Hengartner, D. L. Smith, and F. Trouw (Los Alamos National Laboratory); M. Erickson, S. D. Flexner, T. Kondo, C. Adelmann, C. J. Palmstrøm, and P. A. Crowell (University of Minnesota); W. Chen, T. R. Gentile, J. A. Borchers, C. F. Majkrzak, (National Institute of Standards and Technology); R. Pynn (Indiana University)

Introduction

Proposed applications of spin-polarized transport, such as the spin-field-effect-transistor [1], require populations of spin- polarized electrons and precise control of their spin dynamics and relaxation. In zinc-blende semiconductors such as GaAs, non-equilibrium populations of spin-polarized electrons can be optically [2,3] or electronically [4,5] produced. Electron spin lifetimes in GaAs can be long [6] enough to allow magnetic fields of a few Gauss to influence electron spin dynamics. Since effective magnetic fields due to the hyperfine interaction between the electron and nuclear spin systems can be thousands of Gauss, such fields can profoundly affect electron spin lifetimes. The interaction strength is strongest when spin-polarized carriers are localized, for example in quantum wells [7] or at donor sites [8]. Since the electron density and spin polarization can vary rapidly due to quantum confinement, doping profile, or to the presence of interfaces, the nuclear polarization and resulting effective hyperfine field may be non-uniform [9]. Thus, an independent means of determining the spatial distribution of nuclear polarization is desirable in order to better understand the effects of hyperfine interactions in semiconductors.

We measured the spin dependence of polarized neutrons reflected by a GaAs sample as it was optically pumped. This dependence was correlated with the helicity of the circularly polarized light and found to oscillate with neutron wavevector transfer. The data provide definitive evidence that optically induced nuclear polarization in GaAs is not uniform with depth. Quantitative analysis of the data shows that nuclear polarization is suppressed for tens of nanometers near the surface of GaAs.

Experimental

For the PNR experiment, samples (area ~2 cm^2) were cooled to 20 K in a He vapor cryostat. A sample could be rotated about the y-axis inside the cryostat such that the sample's surface normal was parallel to the incident laser light, (i.e., $\alpha = 0$,), independently of the alignment of the sample with respect to the neutron beam. Circularly polarized light entered the cryostat through a pair of fused silica windows. The incident power density on the sample was 0.25 W/cm^2. A magnetic field $B_A = 265 \pm 15$ G was applied to the sample along its surface normal by permanent magnets.

The intensity of the reflected neutron beam normalized to that of the incident beam for neutron beam polarization parallel (+) and antiparallel (–) to the net nuclear spin of GaAs yielded the reflectivities $R^{\pm}(Q)$. To assess the spin dependence of the neutron reflectivity, we define a quantity called the neutron spin asymmetry

$$A_i = \frac{R_i^+ - R_i^-}{R_i^+ - R_i^-}$$

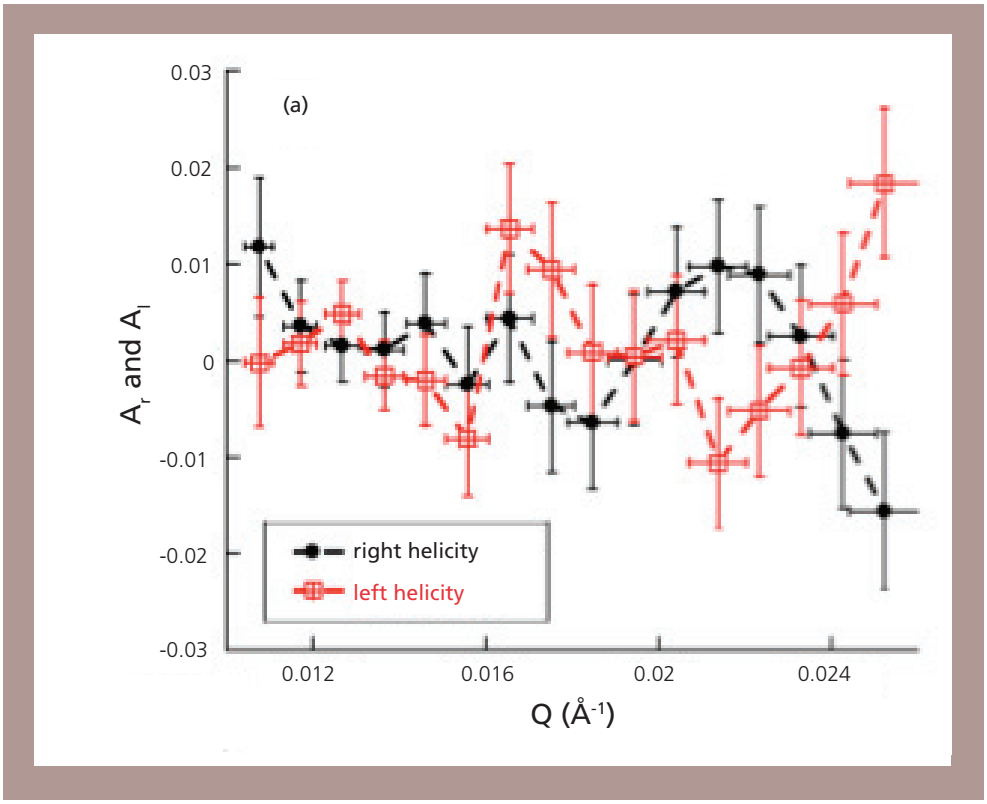

Figure 1. Neutron spin asymmetry vs. wave vector transfer for left and right circularly polarized light.

where the subscript i is either "*r*" or "*l*". The neutron spin asymmetries Ar and Al are shown for Sample A in Figure 1 as circle and open-cross-square symbols, respectively (dashed curves connect the symbols). Since PN is reversed when the helicity of the CPL is reversed, the relationship $R_r^{\pm} = R_l^{\mp}$ leads us to expect that $A_r = -Al$ in the absence of instrumental (non-light-polarization-induced) effects.

Results and Discussion

$A_{POL} = (A_r - A_l)/2$ (Figure 2) is the part of the neutron spin asymmetry that depends upon light polarization (and hence P_N), since the influence of "right" and "left" circularly polarized light reinforce each other (and the instrumental effects cancel each other). The systematic variation of A_{POL} with Q is direct evidence for a non-uniform distribution of nuclear polarization with depth. The simplest representation of such a distribution consistent with A_{POL} (Q) is to ascribe different neutron spin-dependent scattering lengths to the top and bottom parts of the sample (thus introducing a second interface [the first is the sample's surface], inset Figure 2). The change of the scattering length across the two interfaces gives rise to a modulation of *A(Q)*.

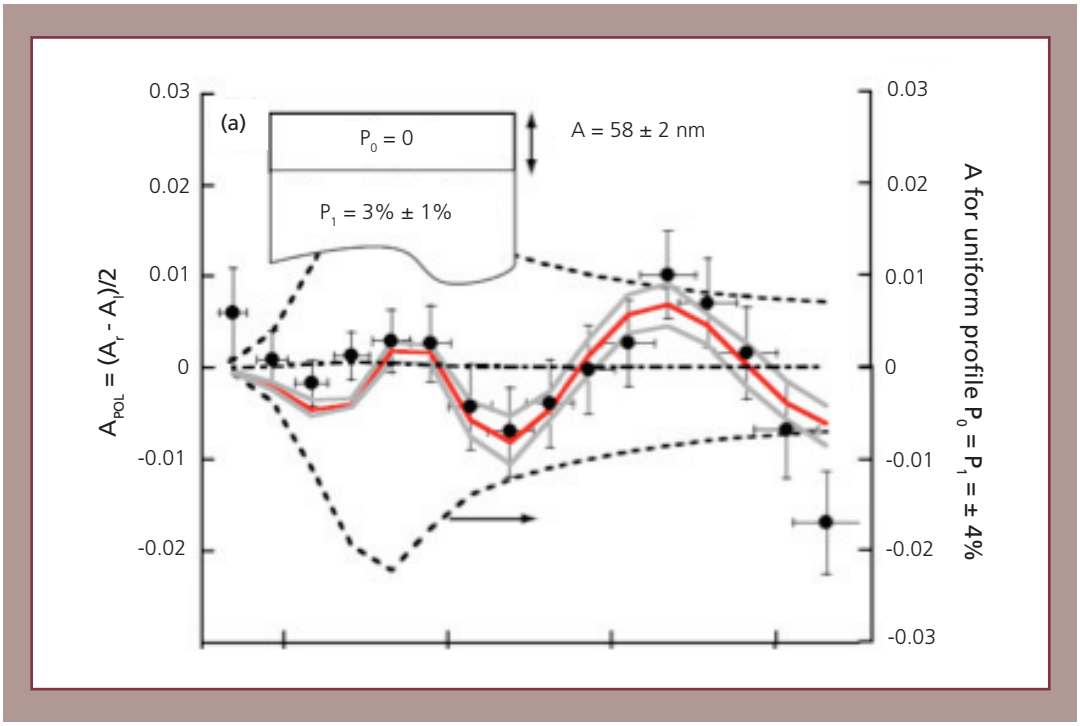

Figure 2. The neutron spin asymmetry due to the influence of polarized light sans instrumental effects. Inset: The model of nuclear polarization in GaAs that gives rise to the calculated neutron spin asymmetry (red curve) consistent with the observations.

In summary, we have detected nuclear polarization of GaAs by measuring the scattering of polarized neutron beams. The wave vector dependence of the neutron spin asymmetry enables us to conclude that nuclear polarization is not uniform across the depth of the GaAs sample. A profile of nuclear polarization that is suppressed within ~60 nm of the GaAs surface and then increases to ~3% in the GaAs bulk explains the neutron data and is consistent with measurements of bulk nuclear polarization inferred from luminescence. The suppression of nuclear polarization near the GaAs surface is a probable consequence of the absence of DNP near the surface (due to unoccupied donor sites) and the relatively short nuclear spin diffusion length in compensated p-type GaAs that precludes diffusion of nuclear polarization into the surface region. Suppression of nuclear polarization near the GaAs surface (and by extension to any interface that is accompanied by a modest electric field) suggests the influence of nuclear polarization on electron spin dynamics near the surface (or interface) should be minimal. (*Physical Review B* **76**:245301 (2007).)

References

[1] S. Datta and B. Das, *Appl. Phys. Lett.*, **56**, 665 (1990).
[2] G. Lampel, *Phys. Rev. Lett.* **20**, 491 (1968).
[3] R.R. Parsons, *Phys. Rev. Lett.* **23**, 1152 (1969).
[4] R. Fiederling, et al., *Nature* **402**, 787 (1999).
[5] Y. Ohno, et al., *Nature* **402**, 790 (1999).
[6] J.M. Kikkawa and D.D. Awschalom, *Phys. Rev. Lett.* **80**, 4313 (1998).
[7] S.W. Brown, T.A. Kennedy, D. Gammon and E.S. Snow, *Phys. Rev. B* **54**, R17339 (1996).
[8] D. Paget et al., *Phys. Rev. B* **15**, 5780 (1977).
[9] A.K. Paravastu and J.A. Reimer, *Phys. Rev. B* **71**, 045215 (2005).

Neutron and x-ray structural studies of short hydrogen bonds in photoactive yellow protein (PYP)

S. Z. Fisher, A. Y. Kovalevsky, and P. Langan (Los Alamos National Laboratory); J. F. Domsic (University of Florida); P. Thiyagarajan and A. J. Schultz (Argonne National Laboratory)

Introduction

Photoactive yellow protein (PYP) is a small (125 amino acids) soluble 14 kDa blue light receptor and is found in Halorhodospira halophila. It is thought to mediate blue-light phototaxis of the organism through a covalently bound chromophore, para-coumaric acid (pCA) [1]. PYP absorbs a photon in the ground state (P) and converts to a red-shifted intermediate species (I1) that is rapidly converted to the blue-shifted state (I2). Eventually it returns to the P state, completing the photocycle. The pCA isomerization causes not only changes in the overall structure of the protein, but also the hydrogen-bonding (H-bonding) pattern in the active site. These H-bonds are crucial to photocycle kinetics and PYP serves as a model system for the understanding of similar reactions in larger, more complex systems [1]. These short H-bonds could represent short strong H bonds (SSHB) or even low-barrier H bonds (LBHB), which are known to be very important in enzyme reaction mechanisms. A characteristic of these kinds of bonds is that the donor O-H bonds is lengthened and leads to disorder of the H between two Os. Despite the availability of high-resolution X-ray structures of PYP, the exact location and H-bond donors and acceptors in the active site are still unknown [2]. To this end, neutron studies of PYP were initiated as neutrons are readily scattered by H atoms and as a result H positions are easily obtainable with these methods.

Experimental

Wild type PYP was expressed in *H. halophila* as a His-tagged apoprotein. It was affinity purified and concentrated to 30 mg/ml [2]. Crystals were prepared by microseeding using 2.6 M ammonium sulfate, 50 mM sodium phosphate pH 7.0. A single, large crystal of PYP (1.8 x 0.7 x 0.6 mm; ~0.8 mm^3) was mounted in a quartz capillary. The crystal was subject to H/D exchange for at least a month by replacing the stabilization buffer with 3.2-M perdeuterated ammonium sulfate made in D_2O.

Time-of-flight neutron Laue data were collected at the Protein Crystallography Station (PCS) at the Los Alamos Neutron Science Center (LANSCE). Each exposure was 22 hrs; 15 different settings were collected. Data were processed to 2.5-Å resolution using a modified version of *d*Trek*. The structure was refined using nCNS, a modified version of CNS that has been adapted to enable joint x-ray and neutron refinement [3]. The starting model used for refinement was a room-temperature x-ray structure of PYP (PDB ID 1otb; [2]). Table 1 shows the data collection, refinement, and final model statistics.

Results and Discussion

From the neutron data it is clear that the phenolate O atom of pCA accepts H-bonds from protonated Glu-64 and Tyr-42 side chains (Figure 1). These interactions are stabilized by Thr-50 acting as a H-bond donor to Tyr-42 and as an acceptor from Arg-52. The H atom

Table 1. PCS neutron data collection and model refinement statistics. Values in parentheses for the highest resolution shell.

Space group, unit cell (Å)	$P6_3$, a = 66.8, c = 40.9
Resolution (Å)	30.0 – 2.5 (2.64 – 2.50)
Total no. Reflections / Unique	10615 (1103) / 3172 (410)
Redundancy	3.3 (2.7)
Completeness (%)	88.8 (79.3)
$\langle I/\sigma(I)\rangle$	3.4 (1.7)
R_{sym}	0.312 (0.413)
No. Protein / Solvent atoms	1105 / 77
R.m.s.d. Bond Lengths / Angles (Å, °)	0.005 / 0.922
Ave. B Factor Main / Side / Solvent pCA (Å^2)	15.5 /17.9 / 30.0 / 12.8
R_{cryst} / R_{free} Joint XN	0.216 / 0.232
R_{cryst} / R_{free} Neutron / x-ray	0.262 / 0.273; 0.214 / 0.232

of Thr-50 N-alpha did not exchange to a D, suggesting a very stable H-bond between Thr-50 and Glu-46.

There is strong nuclear density, corresponding to the presence of D atoms, between Thr-50 and Tyr-42 side chains, and between Glu-46 and pCA. This indicated that Glu-46 is indeed protonated at this pH, as previously thought. A series of omit nuclear density maps confirmed that pCA is deprotonated. Additionally, the D atom between Tyr-42 and pCA is only partially occupied and this suggests that the D atom on Tyr- 42 is either mobile or disordered between short, strong H-bonds to pCA and Thr-50. These features were not previously visible using just x-ray data alone, and the neutron data, even at modest resolution, gives a direct view of the protonation states in the active site of PYP. The results of the H-bonding distances to pCA, though not conclusive, are consistent with the short H-bond possibly acting like a LBHB.

Conclusions

PYP is an important protein that serves as model for the characterization and elucidation of light-dependent signal transduction and photocycles. Using neutrons to investigate the short H-bonds in the chromophore-binding pocket yields unique information not attainable with other, conventional methods. The results from this study support previous data that showed pCA involved with short, strong H-bonds to Glu-46. Also, it appears that the D atom from Tyr-42 is not exclusively H-bonded to pCA and may in fact fluctuate between pCA and Thr-50. The size of the crystal used in this study was relatively small and represents a significant success.
(*Acta Crystallogrpahica Section D Biological Crystallography* **63**:1178-1184 (2007).)

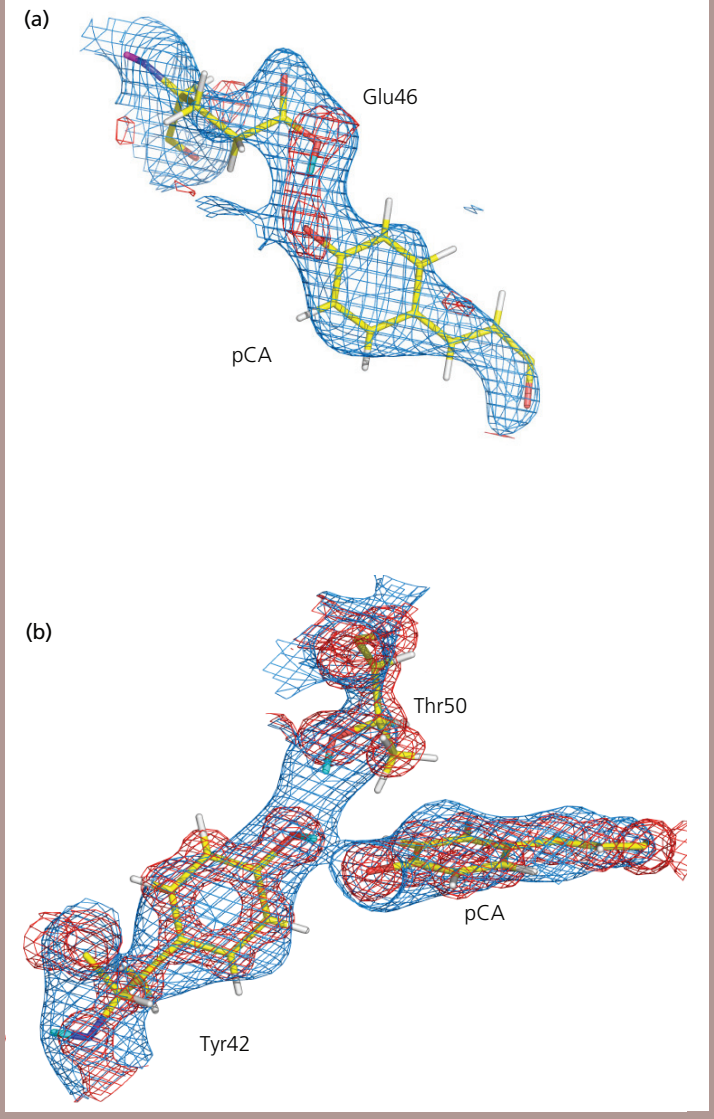

Figure 1. Nuclear and electron density maps of the active site of PYP. (a) The H-bond between Glu-46 and pCA, blue $2F_o$-F_c nuclear map is contoured at 1.2σ, and the omit F_o-F_c nuclear map is shown in red; (b) The H-bond pattern between Tyr-42, Thr-50, and pCA, blue $2F_o$-F_c nuclear map is contoured at 1.2σ, the $2F_o$-F_c electron density map is shown in red mesh.

References

[1] Imamoto, Y et al., Photochem. *Photobiol.*, **83**, 40-49 (2007).

[2] Anderson, S. et al., *Acta D* **60**, 1008-1016 (2004).

[3] Adams, P.D. et al., *Acta D* **65**, 567-573 (2009).

Quantifying interfacial ferromagnetism in $LaMnO_3/SrMnO_3$ superlattices

S. J. May, S. G. E. te Velthuis, S. D. Bader, and A. Bhattacharya (Argonne National Laboratory); A. B. Shah, J.-M. Zuo, X. Zhai, and J. N. Eckstein (University of Illinois, Urbana-Champaign); M. R. Fitzsimmons (Los Alamos National Laboratory)

Introduction

Interfaces in perovskite oxide heterostructures can exhibit electronic, magnetic, and structural properties that are not present in the adjoined compounds [1,2]. However, quantitative measurements of interfacial phenomena are challenging due to the difficulty of fabricating abrupt oxide heterostructures and directly measuring the properties of buried interfaces. In this study, we use polarized neutron reflectometry (PNR) to quantify the magnitude and spatial extent of interfacial ferromagnetism in manganite superlattices.

In bulk form, $LaMnO_3$ (LMO) and $SrMnO_3$ (SMO) are antiferromagnetic with $3d^4$ and $3d^3$ Mn electronic configurations, respectively. By doping Sr into $LaMnO_3$, a mixed Mn valence is established leading to double-exchange mediated ferromagnetism in $La_{2/3}Sr_{1/3}MnO_3$. At $LaMnO_3/SrMnO_3$ interfaces, it is believed that charge is transferred from the $LaMnO_3$ layer to the $SrMnO_3$ layer, creating a mixed valence condition at the interface [3,4]. The aim of this work is to determine if this charge transfer leads to interfacial ferromagnetism and, if so, how do the magnetic properties depend on the distance between adjacent interfaces.

Experimental

Manganite superlattices with a nominal composition of $(LMO)_{2n}/(SMO)_n$ were deposited on $SrTiO_3$ substrates using ozone assisted molecular beam epitaxy. X-ray reflectivity and diffraction measurements were used to quantify the superlattice composition and to confirm that interfacial mixing is limited to length scales of less than one unit cell. To obtain the magnetic depth profile of the superlattices, PNR measurements were performed on the ASTERIX instrument at the Lujan Center. Measurements were carried out under saturating applied magnetic fields.

Results and Discussion

A $[(LMO)_{11.8}/(SMO)_{4.4}]_6$ superlattice was chosen due to its large superlattice period. This sample exhibits ferromagnetism below ~190 K. Room-temperature PNR measurements were performed to determine the nuclear scattering length densities of LMO and SMO, which were within 4% of their calculated values. The sample was then cooled to 10 K in a field of 5.5 kOe. The low temperature PNR data is shown in Figure 1(a). Magnetic Bragg reflections are present at q = 0.1 and 0.2 $Å^{-1}$, indicating that the magnetic potential is repeating with each superlattice period (62.8 Å).

The magnetic structure is revealed by fitting the PNR data using Parratt's dynamical formalism. The model that best fits the data consists of an enhanced moment (3.8 μ_B/Mn) at the LMO/SMO interfaces extending over three unit cells with the LMO layer. In contrast, the SMO/LMO interfaces do not exhibit interfacial ferromagnetism. A sizable moment (2.6 μ_B/ Mn) within the non-interfacial LMO is present, while the moment within the non-interfacial SMO regions is negligible. Scanning transmission electron microscopy (TEM), performed on the same sample as the PNR measurements, reveals a likely structural origin of this magnetic asymmetry. The interfaces where LMO is grown

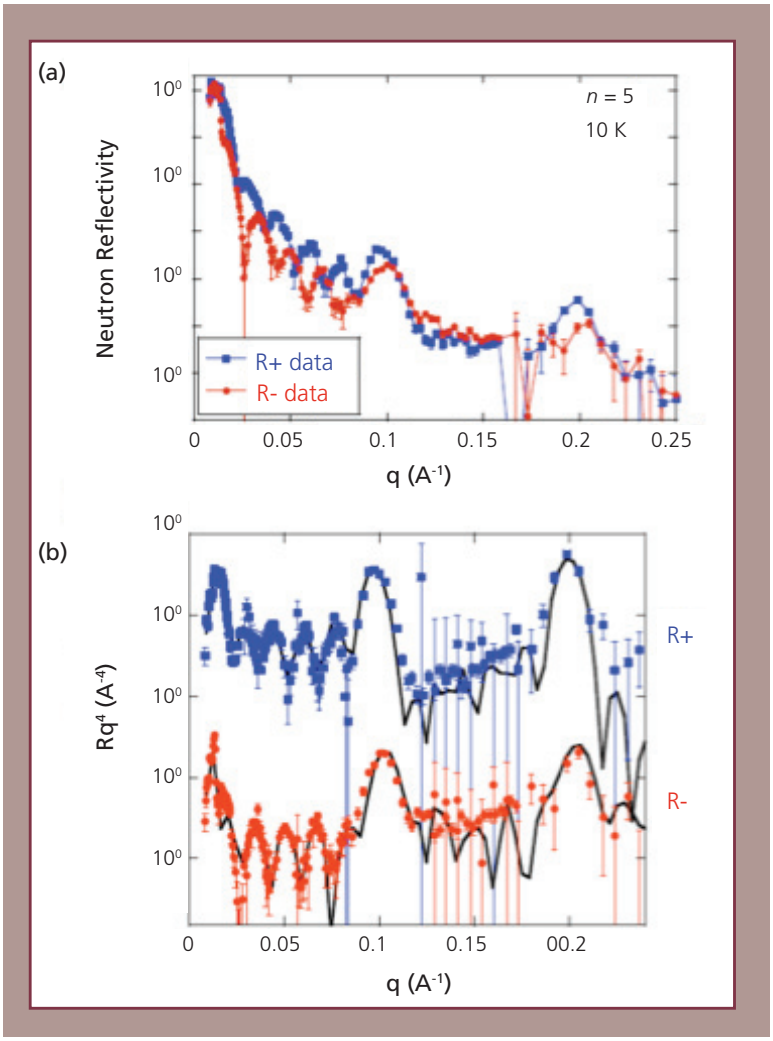

Figure 1. PNR data measured at 10 K (A); the same data with the fitting results (B), adapted from [5] for the different crystallographic modifications.

on SMO (LMO/SMO) are atomically smooth over tens of nanometers, while the SMO/LMO interfaces exhibit roughness of 1–2 unit cells. A comparison of the magnetic profile with the TEM image (Figure 2) suggests that this roughness destabilizes the interfacial ferromagnetism [5].

To understand how the magnetic structure changes as the interfaces are moved closer together, a $(LMO)_6/(SMO)_3$ superlattices was also measured with PNR at 10 K. For this sample, the moment within the LMO layers is roughly 2.6 μ_B/Mn; however, a moment of 0.8 μ_B/Mn is present in the SMO layers [6]. In a $(LMO)_2/(SMO)_1$ superlattice, the magnetization and resistivity data closely resemble that of a random alloy $La_{2/3}Sr_{1/3}MnO_3$ film, suggesting that the charge is uniform throughout the superlattice.

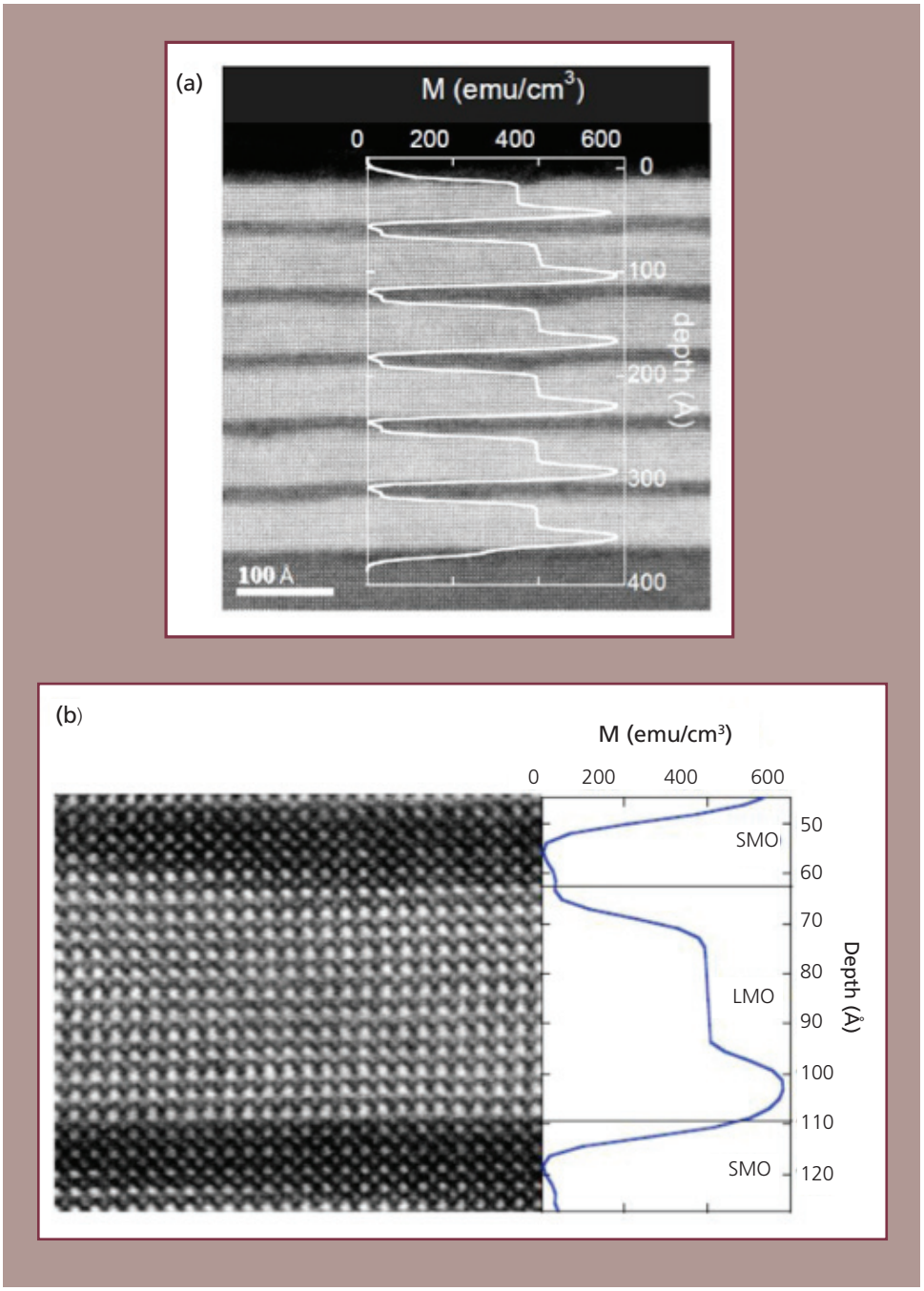

Figure 2. The magnetic profile of the [$(LMO)_{11.8}$/$(SMO)_{4.46}$] superlattice overlaid on a TEM micrograph of the same sample (A). A high-resolution comparison of the structural and magnetic profile (B), adapted from [5].

These results indicate that the amplitude of the magnetic modulation decreases as the interfaces are pushed closer together, consistent with the interfacial charge transfer mechanism.

Conclusions

Using PNR, we have quantified the interfacial ferromagnetism in a large period $LaMnO_3$/$SrMnO_3$ superlattice. We find that the magnetic profile is asymmetric about the interfaces, and that this asymmetry is correlated with a morphologic asymmetry of the interfaces. Additionally, we have determined how the magnetic profile depends on the superlattice period. These results illustrate the ability of PNR to directly probe the magnetic properties of oxide interfaces, allowing for a deeper understanding of the interfacial electronic and magnetic reconstructions that occur in complex oxide heterostructures. (*Physical Review B* **77**:174409 (2008) and *Physical Review Letters* **100**:257203 (2008).)

References

[1] Ohtomo, A., et al., *Nature*, **419**, 378-380 (2002).
[2] Bousquet, E., et al., *Nature*, **452**, 732-737 (2008).
[3] Lin, C., et al., *Phys. Rev. B*, **73**, 041104(R) (2006).
[4] Smadici, S., et al., *Phys. Rev. Lett.*, **99**, 196404 (2007).
[5] May, S. J., et al., *Phys. Rev. B*, **77**, 174409 (2008).
[6] Bhattacharya, A., et al., *Phys. Rev. Lett.*, **100**, 257203 (2008).

Local structural origins of the distinct electronic properties of Nb-substituted $SrTiO_3$ and $BaTiO_3$

K. Page and R. Seshadri (University of California, Santa Barbara), T. Kolodiazhnyi (National Institute for Materials Science, Japan), Th. Proffen (Los Alamos National Laboratory), and A. K. Cheetham (University of Cambridge)

Introduction

The perovskite $SrTiO_3$ becomes metallic with 0.03% to 0.1% Nb substitution on the Ti site, while $BaTiO_3$ remains insulating above 10% Nb substitution. The distinct properties are amply illustrated by considering the temperature dependence of the electrical resistivity and the magnetic susceptibility of the solid solution series $Sr_{1-x}Ba_xTi_{0.9}Nb_{0.1}O_3$ displayed in the panels of Figure 1. As the value of x (the amount of Ba) is increased across the solid solution, the resistivity (Figure 1(a)) displays an upturn at low

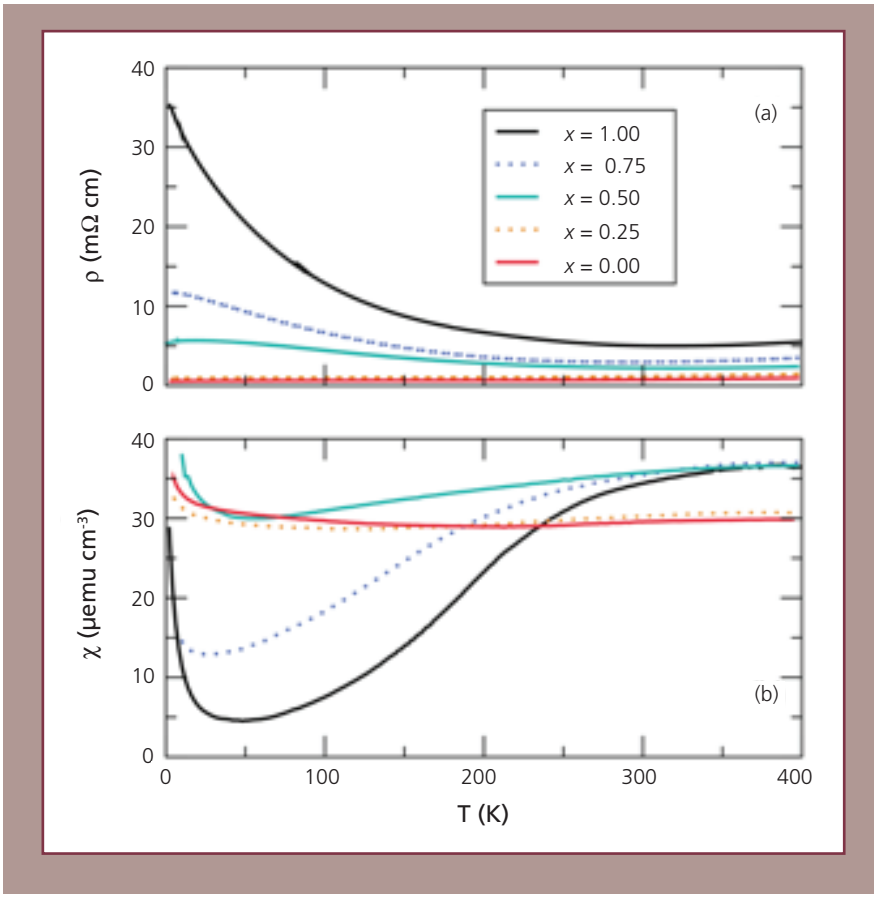

Figure 1. Resistivity (a) and magnetic susceptibility (b) as a function of temperature for samples of $Sr_{1-x}Ba_xTi_{0.9}Nb_{0.1}O_3$.

temperatures; the change from a positive to negative temperature coefficient of resistivity takes place between $x = 0.25$ and $x = 0.50$. In correspondence with electrical transport, the magnetic susceptibility of the Sr-rich side of the solid solution is largely temperature independent, in keeping with its metallic transport properties, while the Ba-rich samples display stronger temperature dependence, characteristic of moments on localized electrons. Given the nearly identical structure and electron counts of the two materials, the distinct ground states for low substitution were a long-standing puzzle. In this work, we describe from neutron studies of average and local structure the subtle yet critical difference that we believe underpins the distinct electronic properties in these fascinating materials [1].

Experimental

Samples were prepared from high-purity (99.99%) $Ba(Sr)CO_3$, TiO_2, and Nb_2O_5 powders purchased from Sigma Aldrich. Pellets of stoichiometric amounts of the starting materials were calcined at 1100 °C for 20 hrs in flowing H_2, at a flow rate of 50 cm_3/min, with a second regrinding or repelletization at 1350˚C for 20 hrs in flowing H_2. Four-probe resistivity was measured on 95% dense ceramic samples cut into 2×2×9 mm^3 parallelepipeds. Magnetic susceptibility in the 2 K –400 K range was measured with a Quantum Design Magnetic Property Measurement System XL. High-*Q* resolution neutron powder diffraction data were collected on the $SrTi_{0.875}Nb_{0.125}O_3$ and $BaTi_{0.875}Nb_{0.125}O_3$ samples on the NPDF instrument at the Lujan Center [2] at room temperature and at 15 K. Rietveld refinement of the diffraction data was carried out in the GSAS-EXPGUI [3] suite of programs. The experimental pair distribution function was extracted from neutron total scattering data using the program PDFGETN [4]. The wave vector cutoff Q_{max} used for the transform was 40 $Å^{-1}$. Pair distribution function (PDF) refinements were carried out using the PDFGUI program [5].

Results and Discussion

In Figure 2, we compare the 15 K data and PDF fits to the average tetragonal structure of (a) $SrTi_{0.875}Nb_{0.125}O_3$ and the average cubic structure of (b) $BaTi_{0.875}Nb_{0.125}O_3$ to a maximum vector length of 50 Å. Both compounds are remarkably well described by their average structures over this range, suggesting that local effects due to Nb substitution have a small correlation length. However, significant anomalies were found in the isotropic displacement parameters Uiso for the two compounds. Both in Rietveld and PDF refinement results, $SrTi_{0.875}Nb_{0.125}O_3$ was found at room temperature to have a large Uiso value on the A site (Sr) compared to the value found for Ba in $BaTi_{0.875}Nb_{0.125}O_3$. This is a signature of the tilting instability that drives the cubic compound to transform to a tetragonal ground state, whereupon all values of Uiso at 15 K are somewhat more reasonable.

In $BaTi_{0.875}Nb_{0.125}O_3$, on the other hand, it is the (Ti/Nb) site that has an anomalously large Uiso, both at 300 K and at 15 K. Figure 3(a-d) displays the short r PDFs of $SrTi_{0.875}Nb_{0.125}O_3$ and $BaTi_{0.875}Nb_{0.125}O_3$ at room temperature and at 15 K. For $BaTi_{0.875}Nb_{0.125}O_3$ at 300 K, and more markedly at 15 K, the first coordination shell is clearly bimodal. In contrast, the local structure of $SrTi_{0.875}Nb_{0.125}O_3$ is undistorted and well described by the crystallographic model. Comparison with calculated shortest Ti-O distances in the different crystallographic modifications of $BaTiO_3$ [6] in Fig. 3(e) reveals rhombohedral-like local Ti/Nb-O symmetry for $BaTi_{0.875}Nb_{0.125}O_3$, explaining the larger Ti/Nb site Uiso seen in cubic structure refinements. Why is the off-centering incoherent? The introduction of random potentials via Nb substitution on the Ti site in $BaTiO_3$, in addition to the introduction of charge carriers due to the aliovalent nature of the substitution, suppresses dipole-dipole correlations.

In systems where the substitution is isovalent, for example, $BaTi_{1-x}Sn_xO_3$, ferroelectricity is suppressed only somewhat slowly [7]. In keeping with ideas of "ferroelectric metals" (and their

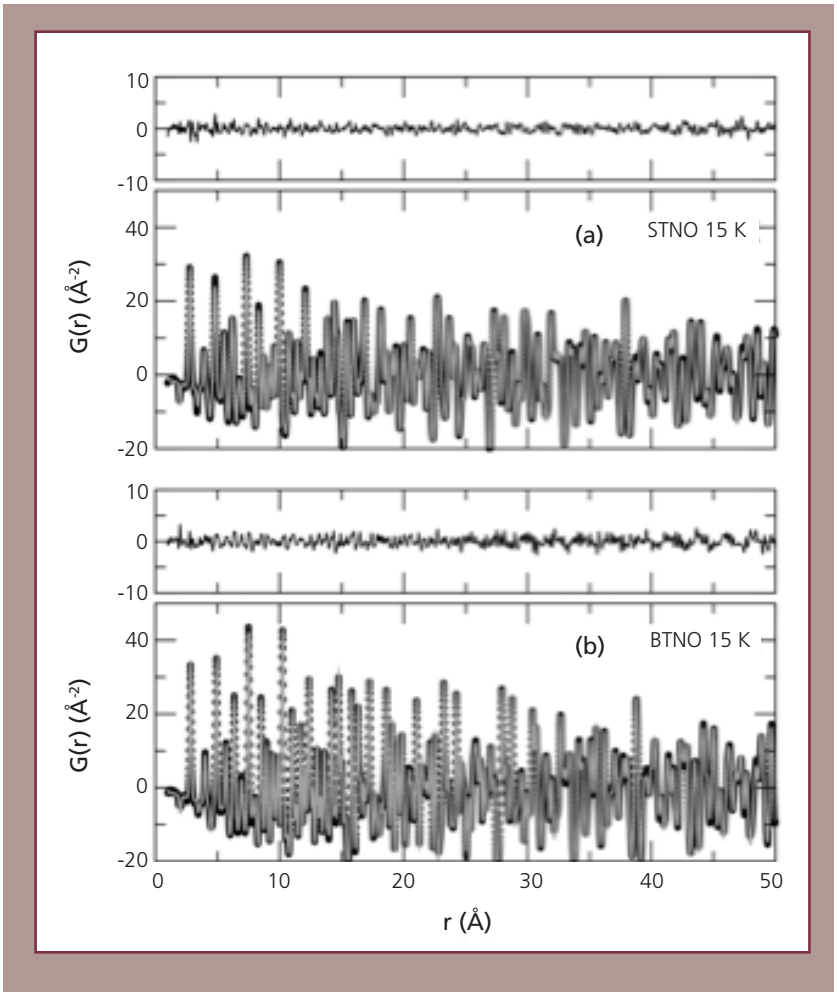

Figure 2. Neutron PDF of (a) $SrTi_{0.875}Nb_{0.125}O_3$ and (b) $BaTi_{0.875}Nb_{0.125}O_3$ acquired at 15 K. Circles are data and lines are fits to the average tetragonal (a) and cubic (b) structures.

scarcity), charge carriers screen the long-range electrostatic interactions responsible for ferroelectric order [8,9]. However, local effects that are responsible for off-centering, namely, the second-order Jahn-Teller distortion on Ti^{4+}, are quite robust to changing electron counts, and persist even when long-range ordering of dipoles has been suppressed. Importantly, since transport occurs through states involving (Ti/Nb) *d*-orbitals, the incoherent nature of the off-centering induces electrons to localize. In $BaTiO_{3-\delta}$, metallic ground states are obtained even in systems where Ti displacements are seen, provided they are coherent [10], clearly pointing to the importance of incoherency in determining the electronic ground state in $BaTi_{0.875}Nb_{0.125}O_3$.

Conclusions

This work demonstrated while $SrTi_{0.875}Nb_{0.125}O_3$ possesses a distorted noncubic structure at

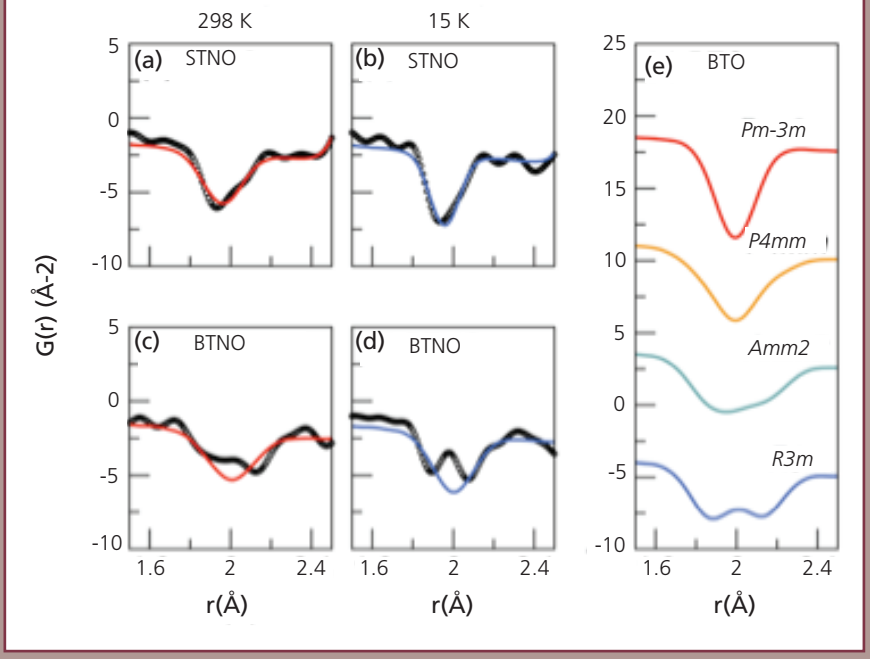

Figure 3. Shortest Ti/Nb-O distances in (a,c) 15 K PDFs and (b,d) 300 K PDFs for $SrTi_{0.875}Nb_{0.125}O_3$ and $BaTi_{0.875}Nb_{0.125}O_3$, respectively. (e) Calculated shortest Ti-O distances in $BaTiO_3$ for the different crystallographic modifications.

15 K, Ti/NbO_6 octahedra in the structure are regular. $BaTi_{0.875}Nb_{0.125}O_3$, on the other hand, shows evidence for local cation off centering while retaining a cubic structure. We believe this probed distortion is responsible for an insulating ground state in $BaTi_{0.875}Nb_{0.125}O_3$– since transport occurs through states involving (Ti/ Nb) *d*-orbitals, the incoherent nature of the off-centering induces electrons to localize. In $SrTi_{0.875}Nb_{0.125}O_3$, where no distortions are found, Ti/Nb t_{2g} electronic degeneracy is retained, and there is no disorder induced localization. (*Physical Review Letters* **101**:205502 (2008).)

References

[1] Page, K., et al., *Phys. Rev. Lett.* **101**, 205502 (2008).
[2] Proffen, Th., et al., *Appl. Phys. A* **74**, S163 (2002).
[3] Toby, B. H., et al., *J. Appl. Crystallogr.* **34**, 210 (2001).
[4] Peterson, P.F., et al., *Appl. Crystallogr.* **33**, 1192 (2000).
[5] Farrow, C. L. et al., *J. Phys. Condens. Matter* **19**, 335219 (2007).
[6] Kwei, G. H., et al., Ferroelectrics 164, 57 (1995).
[7] Nakamura, T. et al., Jpn. *J. Appl. Phys.* **5**, 1191 (1966).
[8] Anderson. P. W, et al. *Phys. Rev. Lett.* **14**, 217 (1965).
[9] Sergienko, I. A., et al., *Phys. Rev. Lett.* **92**, 065501 (2004).
[10] Kolodiazhnyi, T. *Phys. Rev. B* **78**, 045107 (2008).

Hydrogen location in stages of an enzyme-catalyzed reaction: Time-of-flight neutron structure of D-Xylose isomerase with bound D-Xylulose

A. Y. Kovalevsky, M. Mustyakimov, S. Z. Fisher, B. P. Schoenborn, and P. Langan (Los Alamos National Laboratory); A. K. Katz, H. L. Carrell, and J. P. Glusker (Fox Chase Cancer Center); L. Hanson (University of Toledo); L. Coates (Oak Ridge National Laboratory); G. J. Bunick (University of Tennessee)

Introduction

The metallo-enzyme D-Xylose isomerase (XI, named also D-glucose isomerase) inter-converts aldose sugars, D-glucose and D-xylose, into their ketose isomers, D-fructose and D-xylulose, using the active-site that binds two divalent metal cations (Mg^{2+}, Co^{2+} or Mn^{2+}). It, therefore, found commercial applications in the production of sweeteners and, recently, bio-fuels [1]. The reaction is known to proceed in three stages: 1) substrate sugar ring opening; 2) aldo-keto isomerization and 3) product ring closure; however, many questions remain about how exactly the enzyme catalyzes this reaction [2]. A number of hydrogen atoms are moved during the reaction involving changes in protonation states of the XI active-site residues and the substrate. However, how exactly that happens and what the roles are of different residues and solvent molecules is not completely understood even after ultra-high resolution structures of XI have now become available [3].

Three possible mechanisms, involving cis-ene diol intermediate [4], a hydride shift [5] and a metal-mediated hydride shift [6], have been proposed. Understanding the details of the XI-catalyzed reaction will help in protein engineering efforts to improve its industrial performance and, ultimately, combined with other advancements, to lower the cost of biofuels.

We have used the Lujan Center's Protein Crystallography Station (PCS) to study the XI mechanism with the time-of-flight (TOF) neutron diffraction method. Neutron diffraction is advantageous for locating hydrogen (H) and deuterium (D) atoms in proteins before x-ray crystallo-graphy. D's scatter neutrons as well as other common protein atoms, carbon, nitrogen, and oxygen. But H and D are virtually invisible to x-rays, even at better-than-atomic resolution of 1 Å. Thus, neutron protein crystallography is becoming a vital technique for studying enzyme reactions, in which Hs and solvent molecules play essential roles.

Table 1. Neutron crystallographic data collection. Values in parentheses are for the highest resolution shell.

Space Group	**$P2_1$**
Unit Cell (Å)	a = 94.6 b = 100.0 c = 104.0
Resolution	100 – 2.20 (2.32 – 2.20)
# refls	118062 (9409)
# Unique refls	21892 (2863)
Redundancy	5.4 (3.3)
Completeness	89.4 (81.3)
$\langle I/\sigma(I)\rangle$	5.8 (2.0)
R_{sym} †	0.25 (0.38)
R_{work}/R_{free}	0.25 / 0.29

Experimental

A crystal of XI with two Mg^{2+} ions in the active site suitable for neutron diffraction analysis was grown at pH of 7.6 and then soaked in D_2O buffer containing per-deutrated D-xylose. The substrate was enzymatically converted to per-deuterated D-xylulose. The neutron diffraction data were collected on the PCS to 2.2-Å resolution and overall completeness of 89.4% (Table 1). The data were processed with the software [7] modified for neutron diffraction data and *CCP4i* [8]. The neutron structure was refined with nCNS [9].

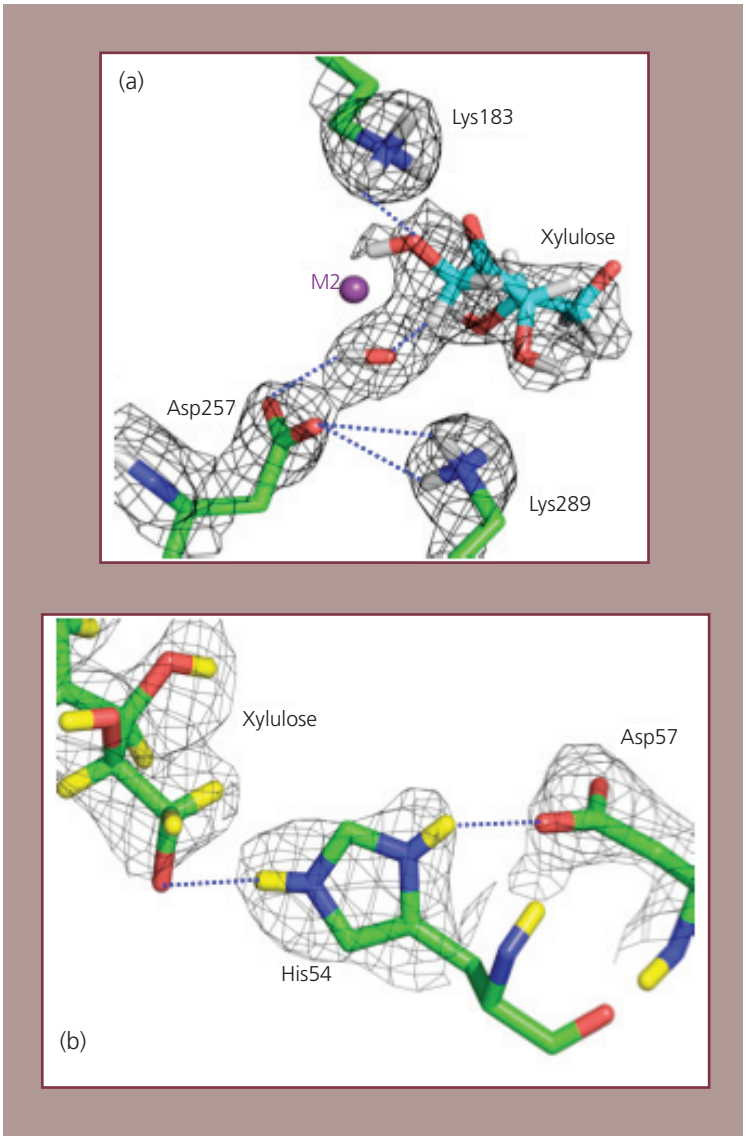

Figure 1. Binding of xylulose to the XI active site. 2FO-FC nuclear density maps around M2 (a) and His-54 (b).

Results and Discussion

The XI-xylulose neutron structure was refined using the x-ray coordinates from PDB entry 4XIS as the starting point. The Mg2+ metal positions, referred henceforth M1 (structural metal) and M2 (catalytic metal), were fixed in the same locations found in 4XIS. Mg is relatively weak neutron scatterer, but is a good x-ray scatterer, and its position is more accurately obtained from an x-ray crystal structure.

Several important differences and similarities were observed in the active site of XI-xylulose neutron structure compared with the published neutron structure of native XI-Co, which contained two $Co2^{+}$ cations and no substrate/product bound [3]. First, the catalytic solvent species is a hydroxyl anion (OD^{-}) in XI-xylulose (Figure 1a), while it was a water molecule (D_2O) in XI-Co. This implies that during the reaction this D2O has to be deprotonated. Second, Lys-289 is protonated, having ND^{3+} ε-amino group, and H-bonded with the negatively charged deproto-nated carboxylic moiety of the nearby Asp-257 (Figure 1a). In the native enzyme Lys- 289 is neutral (ND_2), is rotated away from Asp- 257 and is disordered over two positions. Third, in both structures His-54, the essential residue for the ring-opening step, is protonated, with both side-chain nitrogens connected to D atoms (Figure 1b), and is H-bonded with Asp- 57. Fourth, His-220 is neutral (D on Nε1) in XI-xylulose and binds to M2 with Nε2, whereas this N is protonated half of the time in Xi-Co and has virtually no binding to M2. Other important findings in XI-xylulose are: i) the terminal oxygen O5 of the linear product is deprotonated ($O5^{-}$) and is involved in a salt-bridge with the charged His-54 (Figure 1b); ii) O2 has lost and O1 and C1 have gained hydrogen atoms, providing evidence that the isomerization reaction occurred in the active site; and iii) Lys-183 is protonated in both native and XI-xylulose neutron structures.

These observations shed new light on the mechanism of XI. The ring-opening does not proceed with a permanent H transfer to O5, while Lys-289 gains a proton, possibly from the sugar's O1 hydroxyl group. This, and the proto nation of Lys-183, contradicts previous proposals for the mechanism [10,11] and suggests the potential involvement of Lys-289 in the first step of the reaction. Interactions of the OD– with the xylulose's C1 and O1 suggest that the hydroxyl ion might protonate C1, which would be consistent with enediol mechanism, or O1, which would produce a carbocation stabilized by the OD–, while the next step, isomerization, may proceed via hydride shift from C2 to C1.

Conclusions

In summary, the comparison of the neutron structures XI-xylulose and the published native complex XI-Co suggest that, after the sugar substrate's ring is opened, involving the His-54 Asp-57 pair, it extends and is anchored in the active site by H-bonds with Lys-183 and His-54. At some stage catalytic D2O is deprotonated, and Lys-289 is protonated. The isomerization step may occur via enediol intermediate or hydride shift. Precise movements of H atoms during this step remain to be determined. (*Biochemistry (Rapid Reports)* **47**:7595-7597 (2008).)

References

[1] Bhosale, S. H., *et al., Microbiol Rev.,* **60**, 280-300 (1996).

[2] Asboth, B., Naray-Szabo, G., *Curr. Prot. Pept. Sci.,* **1**, 237-254 (2000).

[3] Katz, A. K., et al., *Proc. Natl. Acad. Sci.,* **103**, 8342-8347 (2006).

[4] Rose, I. A., et al., *Biochim Biophys. Acta,* **178**, 376-379 (1969).

[5] Collyer, C. A., Blow, D. M., *Proc. Natl. Acad. Sci.,* **87**, 1362-1366 (1990).

[6] Fenn., et al., *Biochemistry,* **43**, 6464-6474 (2004).

[7] Helliwell, J. R., et al., *J. Appl. Cryst.*, **22**, 483-497 (1989).

[8] Weiss, M. S., *J. Appl. Cryst.*, **34**, 130-135 (2001).

[9] Adams, P., et al., *Acta Crystallogr. D*, **65**, 567-573 (2009).

[10] Lee, C., et al., *J. Biol. Chem.*, **265**, 19082-19090 (1990).

[11] Collyer, C. A., et al., *J. Mol. Biol.*, **212**, 211-235 (1990).

Rapid determination of hydrogen positions and protonation states of diisopropyl fluorophosphatase by joint neutron and x-ray diffraction refinement

M.-M. Blum (Goethe University Frankfurt, GR, and Blum Scientific Services); K. Kehe (Bundeswehr Institute of Pharmacology and Toxicology); M. Mustyakimov, B. Schoenborn, and P. Langan (Los Alamos National Laboratory); H. Rüterjans and J. C.-H. Chen (Goethe University Frankfurt, GR)

Introduction

Diisopropyl fluorophosphatase (DFPase) from *Loligo vulgaris* is a calcium-dependent enzyme (35 kDa) capable of rapidly hydrolyzing a wide variety of organophosphorus nerve agents, including soman, sarin, and tabun, and is a prime candidate for enzymatic decontamination. The enzyme has been extensively studied with regards to its structure and mechanism; an atomic resolution x-ray crystal structure is available, and the structures of more than 15 site-directed mutants have been solved (Figure 1, left). Mass spectroscopic analysis of the reaction products under single- and multiple-turnover conditions in $H_2{}^{18}O$ demonstrated that the hydrolysis reaction proceeds via a phosphoenzyme intermediate, indicative of direct nucleophilic attack on the substrate by the protein [1]. To offer a detailed view of the hydrogen atoms and protonation states of residues and solvent molecules in the active site, neutron diffraction data were collected at the Lujan Center's Protein Crystalography Station (PCS) and the structure solved.

Experimental

Crystals of hydrogenated DFPase were grown by hanging drop vapor diffusion from 11 % PEG 6K, 0.1 M MES, pH 6.5. After several weeks, a number of large crystals appeared. One crystal measuring 2.4 x 0.5 x 0.36 mm (0.43 mm^3) was mounted in a glass capillary, and exchanged against deuterated mother liquor for one week prior to recording the first test diffraction images. Data were collected to 2.2-Å resolution over the course of approximately one month at the PCS, with a total of 37 settings and ~24-hr exposures per image. Data were integrated and scaled in d*TREK modified for time-of flight data, with good statistics (R_{sym} = 0.199, 81.8% overall completeness, 5.9-fold redundancy, Mn(I)/sd = 4.0) [2].

The structure was refined using a new implementation of joint x-ray and neutron data refinement, *nCNS*, developed at LANL and Lawrence Berkeley National Laboratory. The room temperature apoenzyme structure and structure factors (PDB: 2gvw) were used for the x-ray data portion of the joint refinement. Occupancies of labile hydrogen/deuteriums were refined to reflect the degree of exchange, and cycles of model building and positional, temperature factor, and simulated annealing refinement yielded a final structure with a R_{free} of 25.1% and 31.6% for the x-ray and neutron datasets, respectively (PDB: 3byc) [3].

Results and Discussion

Two features of the active site nuclear density maps have a particular bearing on the reaction mechanism. Calcium-coordinating residue Asp-229, previously identified as a

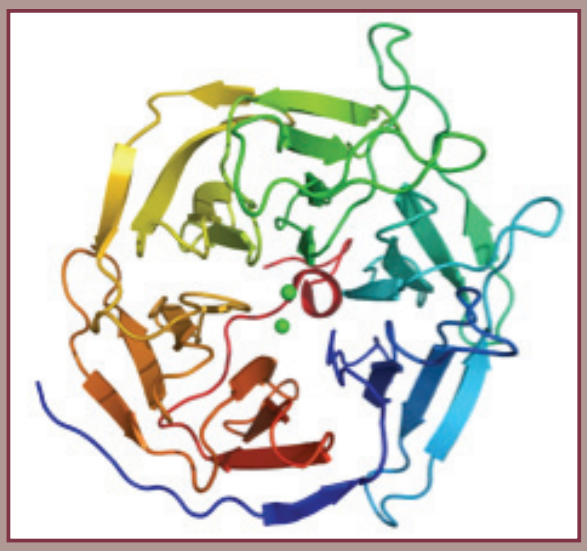

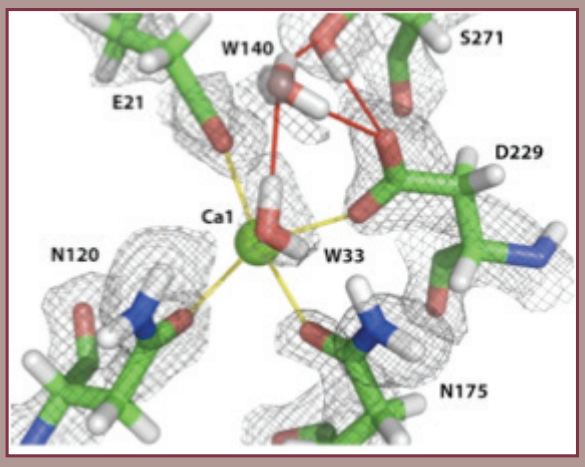

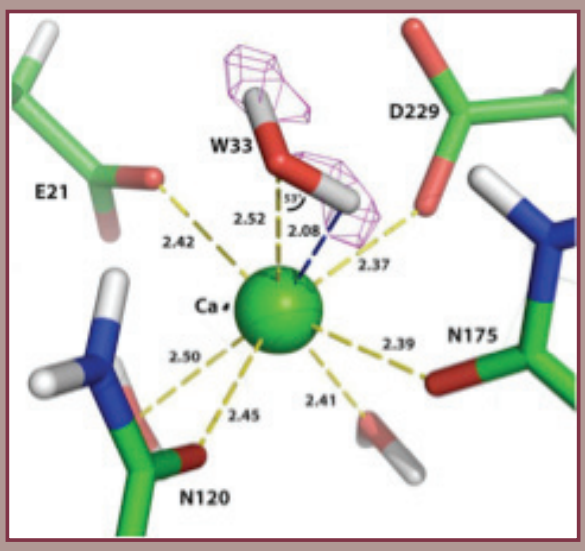

Figure 1. Left: Overall structure of DFPase, colored from N-terminus (blue) to C-terminus (red). The two calcium ions are shown as green spheres. Center: Nuclear density in the active site. W33 is water, and Asp-229 is deprotonated. Right: Nuclear density omit map for W33 (pink). The deuteriums were omitted, and reappear as difference peaks of equal intensity. Distances between the catalytic calcium and its coordinating atoms are indicated in Å. Highlighted in blue is the calcium - deuterium distance and the Ca - O - D angle.

potential nucleophile, is deprotonated, and calcium-coordinating solvent molecule W33 is identified as water, and not a hydroxide (Figure 1, center). These features are consistent with direct nucleophilic attack, and inconsistent with metal-assisted water activation. To confirm the identity of W33 as a water, a simulated annealing neutron omit map was calculated, omitting the two deuterium atoms. Two difference peaks appear, at equal intensity, in the geometry of a water molecule (Figure 1, right). Furthermore, W33 resides in an unusual orientation, with a Ca - O - D angle of 53 degrees and a closest distance of Ca - D of 2.08 Å, well beyond those observed for small molecule calcium hydrates (Figure 1, right). This orientation in the context of the active site environment is unfavorable, but may minimize even more unfavorable orientations. These structural features were clearly visible by neutron diffraction at moderate (2.2 Å) resolution; the 0.85-Å x-ray maps were not able to reveal these critical features.

Conclusions

The 2.2-Å neutron structure of DFPase presents the most detailed picture of the active site environment to date. Putative nucleophilic residue Asp-229 is deprotonated, while solvent molecule W33 is water, and not hydroxide. The mechanism most consistent with the neutron structure and the mass spectroscopic data is shown in Figure 2.

On a technical level, this structure represents a major advancement in data collection. The crystal size used in this study was 0.43 mm^3, which is among the smallest crystals used for neutron diffraction. Furthermore, this is one of the largest protein structures and unit cells/asymmetric units to be studied by neutron crystallography [2].

The neutron structure and recent mechanistic studies on DFPase will allow for efforts to re-engineer the enzyme to accommodate a wide variety of substrates, and also for efforts

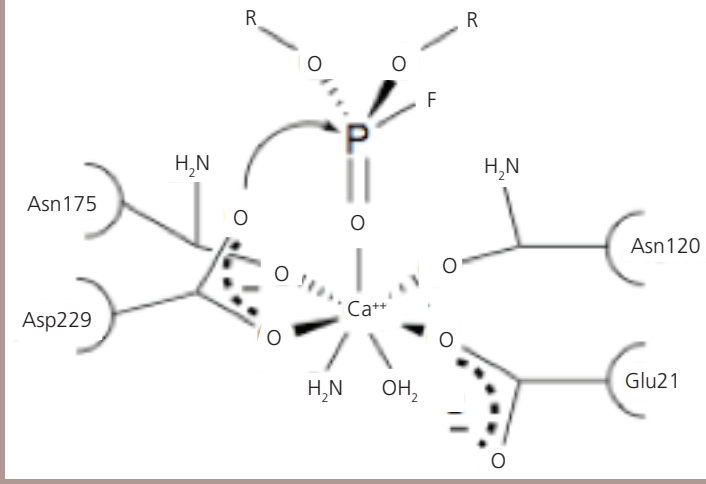

Figure 2. Proposed mechanism involving direct nucleophilic attack of the Asp-229 carboxyl oxygen on the phosphorus of the substrate.

to augment its activity and detoxification properties. A first round of optimizing the active site has yielded a modified enzyme with reversed enantioselectivity against the more toxic stereoisomers of the nerve agents [4]. Further efforts are underway to optimize the enzyme's activity and substrate range. (*Proc. Natl. Acad. Sci. USA* **106**:713-719 (2009).)

References

[1] Blum, M.M., et al., *J. Am. Chem. Soc.* **128**, 12750-12757 (2006).

[2] Blum, M.M., et al., *Acta Cryst.* **F63**, 42-45 (2007).

[3] Blum, M.M., et al., *Proc. Natl. Acad. Sci. USA,* **106**, 713-719 (2009).

[4] Melzer, M., et al., *J. Am. Chem. Soc.* **131**, 17226-17232 (2009).

Development of spin echo scattering angle measurement (SESAME) on Asterix

R. Pynn, R . Ashkar, P. Stonaha, and A. Washington (Indiana University); M. Fitzsimmons (Los Alamos National Laboratory); W. T Lee (Oak Ridge National Laboratory)

Introduction

Over the past few years we have been developing a new neutron scattering technique which uses Larmor precession of a neutron spins to encode the angle through which neutrons are scattered by a sample. Most of this development has made use of the Lujan Center's Asterix reflectometer, which provides a suitable polarized incident neutron beam and is also equipped for polarization analysis. The goal of this project is to allow measurements of elastic scattering to be made with good momentum resolution without requiring the tight beam collimation and monochromatization that is usually required with traditional neutron scattering techniques and which results in a substantial intensity penalty. We expect the new method to allow neutrons to make measurements that have hitherto been impossible. When applied to surface scattering, the method—normally referred to as Spin Echo Grazing Incidence Scattering (SERGIS) in this context—will allow lateral structure of surfaces and layers with length scales between ~25 nm and ~1000 nm to be probed in the GISANS (Grazing Incidence Small Angle Neutron Scattering) geometry. Because the method naturally produces a real space correlation function rather than the traditional Q-space scattering function, it turns out to be very useful for measuring long-range correlations in bulk materials. Another interesting feature is that the method naturally accounts for multiple scattering, yielding the pair correlation function even in cases where multiple scattering is dominant, provided all of the scattering can be captured by the neutron detector employed. This makes the method useful for studies of concentrated systems such as colloidal glasses or ceramics, which are often difficult to study with neutrons because accurate data correction cannot be guaranteed.

Experimental

The equipment used in these experiments has been built by graduate students at Indiana University (Ashkar, Stonaha, and Washington) and is designed to be mounted on any neutron instrument that provides a suitable polarized neutron beam and polarization analysis. Pictures of some of the equipment are shown in Figure 1. The operational principle of the method is summarized in Figure 2. Each pair of triangular cross-section solenoids is similar to the device shown in Figure1C and causes the two spin states to be refracted along different paths, just as a pair of Wollaston prisms splits a light beam into its two principal polarization components. In the absence of a sample, the two neutron polarization states recombine at the pi/2 flipper on the right of Figure 2 and the full neutron polarization is retrieved as a spin echo. When the sample is present, the two spin states visit different parts of the sample that are separated by a distance called the spin echo length (the distance between the red and blue trajectories in Figure 2). When they recombine this information is encoded in the resultant neutron polarization. In fact, the polarization is given by the cosine Fourier transform of the usual scattering function along the coding direction, which is perpendicular to the neutron beam and in the plane of Figure 2.

For technical reasons, closed solenoids like that shown in Figure 1c do not work well and one

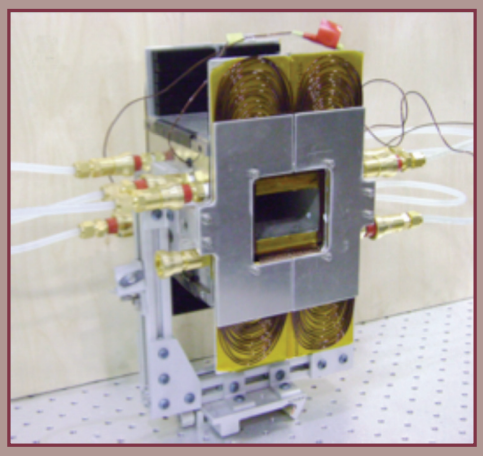

(a)

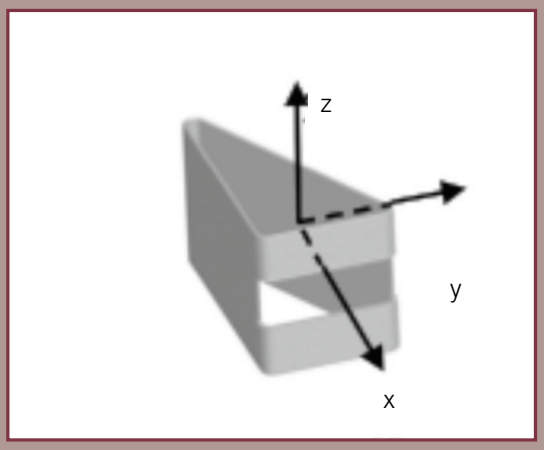

(b)

(c)

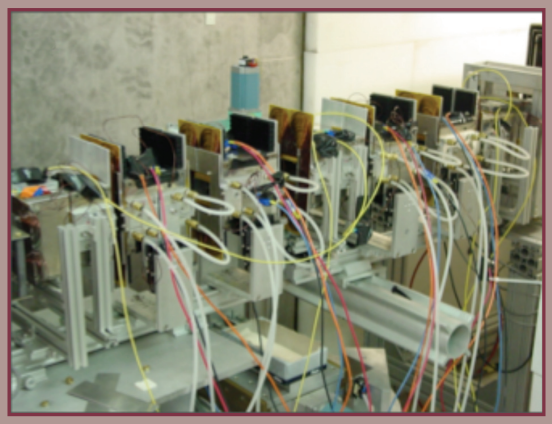

(d)

Figure 1. (a) Water-cooled, triangular-cross-section solenoids; (b) schematic of a single gapped solenoid; (c) early model closed triangular solenoid with one side of the mumetal flux return path removed; (d) equipment mounted on Asterix

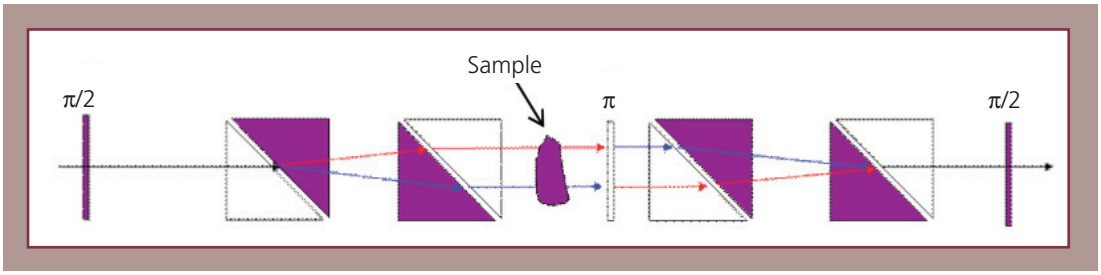

Figure 2. Schematic diagram of SESAME method. The triangular shapes are solenoids producing magnetic fields either into (magenta) or out of (white) the plane of the paper. The arrows indicate schematically the trajectories of the two neutron spin states while pi/2 and pi indicate neutron spin flippers.

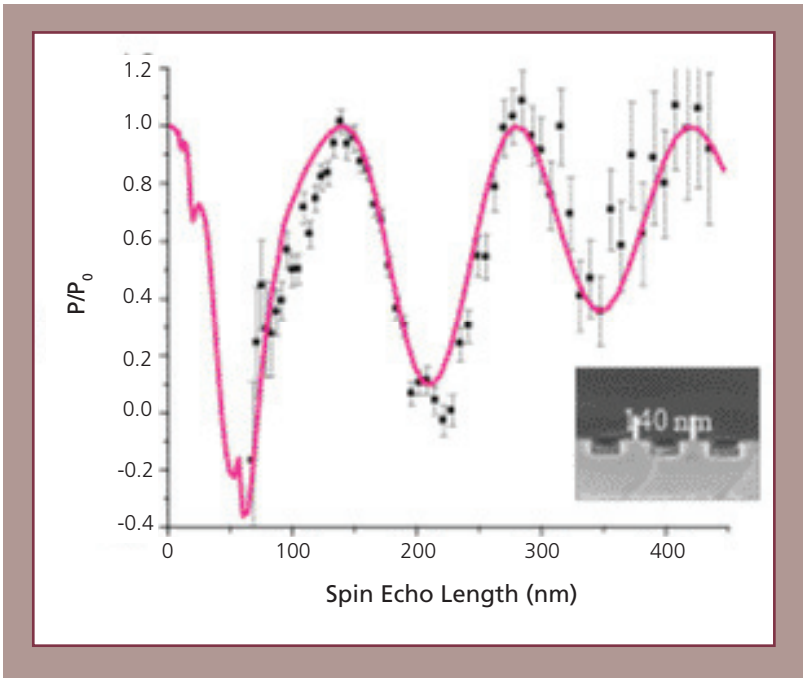

Figure 3. Spin echo polarization for scattering from a silicon diffraction whose profile is shown in the inserted TEM image. The polarization has been normalized against the echo pollarization from a smooth silicon wafer, P_0. The echo polarization is plotted against the spin echo length which is the correlation distance probed in the sample. Peaks in P/P_0 are expected (and observed) at multiples of the grating spacing. The red curve is the result of a full dynamicaltheory calculation without any adjustable parameters.

is obliged to introduce gaps in the solenoids, as indicated schematically in Figure 1b.

Results and Discussion

Figure 3 shows an example of a recent result obtained a silicon diffraction grating.

Because the SERGIS technique measures a Fourier transform of the scattering function, we expect Figure 3 to resemble the autocorrelation function of the grating profile. Since the latter is rectangular (as shown in the inset of Figure 3), the echo profile might be expected to be a series of isosceles triangles with peaks at multiples of the grating period (140 nm in this case). In fact, to explain the detailed shape of the profile, a complete dynamical scattering theory is required: neither of the approximations used previously (the Distorted Wave Born Approximation and the Phase Object Approximation) is adequate in this case. We have succeeded in developing such theory (as shown by the red curve in Figure 3) which, unlike previous similar theories, is stable to all orders. (*Rev. Sci. Instrum.* **79**:063901 (2008); *J. Appl. Cryst*. **41**:897 (2008); *Physica B* **404**:2582 (2009).)

Tunable ($\delta\pi$,$\delta\pi$)-type antiferromagnetic order in α-Fe(Te,Se) superconductors

W. Bao (Renmin University of China); Y. Qiu and M. A. Green (National Institute of Standards and Technology and University of Maryland); P. Zajdel (National Institute of Standards and Technology and University of Silesia); M. R. Fitzsimmons and M. Zhernenkov (Los Alamos National Laboratory); Q. Huang and S. Chang (National Institute of Standards and Technology); B. Qian, E. K. Vehstedt and Z. Q. Mao (Tulane University); M. Fang (Tulane University and Zhejiang University); J. Yang (Zhejiang University); H. M. Pham and L. Spinu (University of New Orleans)

Introduction

Recently discovered ferrous superconductors differ from phonon-mediated conventional superconductors in an important way: when the nonmagnetic La in LaFeAs(O,F) families is replaced by magnetic a lanthanide, TC increases from 26 K to as high as 55 K [1-5]. A La(O,F) "charge reservoir" layer turn is not required for superconductivity and can be completely absent in the α phase of Fe(Se,Te). The common iron layer contributes dominantly to the electronic states at the Fermi level in these families of materials, which thus share similar quasi-two dimensional Fermi surfaces with a nesting wave vector (π, 0) in the reciprocal Fe square lattice. The antiferromagnetic order in those families of materials has been predicted by nesting spin-density-wave (SDW) mechanism [6]. It is known that nesting condition is lost when adding electrons or holes to the system which destroys the SDW order well before the optimal superconducting state is established. Moreover, despite the same (π, 0) SDW order being predicted for α-FeTe in theory, we observed a completely different antiferromagnetic order with the in-plane propagation vector ($\delta\pi$, $\delta\pi$) along the diagonal direction of the Fe "square" lattice. The δ is tunable from an incommensurate 0.38 to the commensurate 0.5. Therefore, experimental results reported here call for a better understanding of the mechanism of magnetism and its role in superconductivity for the ferrous superconductors.

Experimental

In the compound α-FeTez as a function of z, there exist two distinct types of transport behaviors in the low temperature phase: for $z \geq 0.90$ the samples change from a semiconductor to a metal, while for $z < 0.90$ the samples remain semiconducting. Therefore, we selected a typical composition from each range of z for this study, FeTe0.82 and FeTe0.90. For superconducting α-Fe(Te, Se)$_z$, we chose the highest TC $\approx$ 14 K compound $Fe(Te_{0.6}Se_{0.4})_{0.82}$. As parent compounds we have chosen $Fe_{1+y}Te$ with y = 0.141 and 0.076. The neutron powder diffraction study was done using BT1 instrument at NIST, single crystal neutron diffraction was performed with TAS BT9 at NIST, and the polarized neutron scattering was performed using reflectometer, Asterix, at the Lujan Center.

Results and Discussion

The high-resolution powder diffraction spectra of polycrystalline samples showed that the high-temperature phase of these samples indeed has the tetragonal P4/*nmm* structure, however, the more appropriate formula for nominal α-$Fe(Te_{1-}x, Se_x)_z$ is Fe_{1+y} (Te_{1-x}, Se_x).

It was found while $Fe_{1.080}Te_{0.67}Se_{0.33}$ remains tetragonal in the superconducting state at 4 K, the parent compounds $Fe_{1.141}Te$ and $Fe_{1.076}Te$ experience a first-order magnetostructural transition. The semiconducting $Fe_{1.141}Te$ distorts to an orthorhombic *Pmmn* structure

below TS ≈ 63 K, with the a axis expanding and the b axis contracting. This results in the splitting of the (*h*0*k*) Bragg peaks of the high-temperature structure. The orthorhombic distortion here, however, does not double the unit cell. The metallic $Fe_{1.076}Te$ has a monoclinic $P2_1/m$ structure below TS ≈ 75 K. In addition to the differentiation of the *a* and *b* axis the *c* axis rotates towards the a axis to β ≈ 89.2°. Thus, the monoclinic distortion not only splits the (200) but also the (112) Bragg peak. In the weaker first-order transition of $Fe_{1.141}Te$, a mixed phase exists and at 55 K upon warming, 85% of the sample is orthorhombic and 15% tetragonal.

The additional magnetic Bragg reflections of the monoclinic metal were found and could be indexed with a commensurate magnetic wave vector q = (½0½). However, magnetic Bragg reflections of the orthorhombic semiconductor cannot be indexed by multiples of the nuclear unit cell. By performing single crystal neutron diffraction, we determined the incommensurate magnetic wave vector q = (±δ0½), where δ ≈ 0.380, for $Fe_{1.141}Te$. The q determines that magnetic moments in each row along the b axis are parallel to each other. The rows of moments in an Fe plane modulate with the propagating vector 2πδ/a, which is 45° away from that of FeAs materials. From one plane to the next along the c axis, magnetic moments simply alternate direction. This unusual coupling between the lattice and magnetic degrees of freedom (DOF) is consistent with multiple d-orbital magnetism [7].

To distinguish between lattice and magnetic DOF, we measured a $Fe_{1.141}Te$ single-crystal sample, aligned in the (*h*0*l*) horizontal scattering plane, using the polarized neutron beam spectrometer Asterix. The neutron spin is controlled to align either perpendicular to the (*h*0*l*) plane (VF) or parallel to the momentum transfer (HF). All four channels (++, --, +-, -+) in both the VF and HF configurations were measured for the (001) and (δ0½) Bragg peaks. The flipping ratio for the instrument configuration we used was 10.3 as measured at the nuclear (001) peak. The magnetic origin of the (δ0½) is demonstrated by spin-flip scattering in HF. The normalized intensity of (δ0½) in VF is 8.24(28) in the non-spin-flip (NSF) channels, and 4.13(20) in the spin-flip (SF) channels. Therefore $Fe_{1.141}Te$ has an incommensurate magnetic structure with $M = 0.76(2)\mu_B$/Fe.

To understand whether the incommensurate magnetic structure in the orthorhombic semiconducting phase is locked or tunable, we examined another sample $Fe_{1.165}(3)Te$ by powder diffraction at BT1, NIST. The incommensurability is greatly affected and measures at δ ≈ 0.346, despite no appreciable differences in the moment from $Fe_{1.141}Te$. Thus, δ can be tuned by varying the excess Fe in the orthorhombic phase, and it reaches a commensurate value ½ for the composition $Fe_{1.076}Te$ in the metallic monoclinic phase with less excess iron.

We also tried to determine if the new magnetic order survives in the optimal TC superconducting sample $Fe_{1.080}Te_{0.67}Se_{0.33}$. While there is neither long-range magnetic order nor structural transition, we observed pronounced short-range quasielastic magnetic scattering at the incommensurate wave vector (0.438, 0, ½) using SPINS at NIST. We found a short magnetic correlation length of 4 Å, approximately equal to twice the nearest-neighbor Fe spacing. The results are consistent with the expected diffusive nature of the short-range magnetic correlations. This is very different from the case of the (π,0) SDW which is completely suppressed in the optimal T_C FeAs samples [8].

Conclusions

To summarize, the α-Fe(Te,Se) shares a common electronic structure with the previously reported FeAs-based superconductor systems. Though the same (π, 0) SDW order has been predicted, we show the presence of a fundamentally

different ($\delta\pi$,$\delta\pi$) antiferromagnetic order which propagates along the diagonal direction. The incommensurability δ in the orthorhombic semiconducting phase is easily tunable with excess Fe and locks into a commensurate ½ in the monoclinic metallic phase. This magnetic order, which survives as short-range order even in the superconducting state, cannot be the result of Fermi surface nesting, which is along the (π, 0) direction which depends on electronic band filling. (*Physical Review Letters* **102**:247001 (2009).)

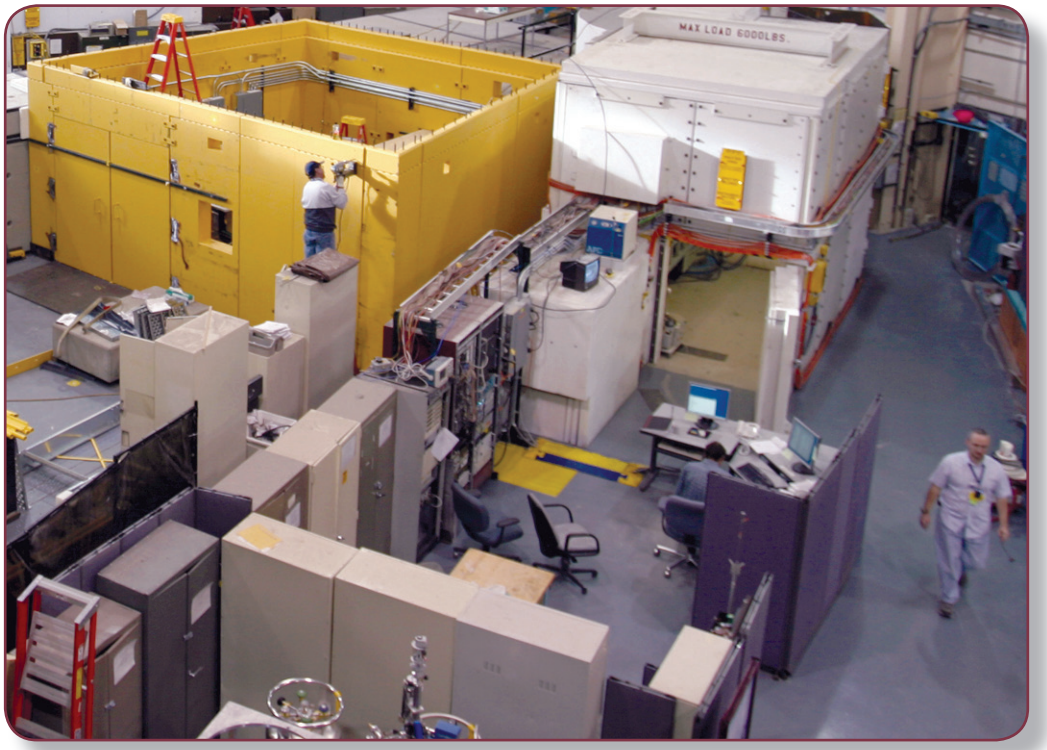

The Lujan Center's Experimental Room #2.

References

[1] Y. Kamihara et al., *J. Am. Chem. Soc.* **130**, 3296 (2008).

[2] X. H. Chen et al., *Nature (London)* **453**, 761 (2008).

[3] G. F. Chen et al., *Phys. Rev. Lett.* **100**, 247002 (2008).

[4] Z. A. Ren et al., *Chin. Phys. Lett.* **25**, 2215 (2008).

[5] A. A. Abrikosov et al., *Zh. Eksp. Teor. Fiz.* **39**,1781 (1960).

[6] F. Ma et al., *Phys. Rev. B* **78**, 033111 (2008);

[7] T. Yildirim, *Phys. Rev. Lett.* **101**, 057010 (2008).

[8] C. de la Cruz et al., *Nature (London)* **453**, 899 (2008).

Direct determination of protonation states of histidine residues in a 2-Å neutron structure of deoxy-human normal adult hemoglobin and implications for the bohr effect

A. Y. Kovalevsky, M. Mustyakimov, S. Z. Fisher, and B. P. Langan (Los Alamos National Laboratory); T. Chatake, T. Ishikawa, and Y. Morimoto (Kyoto University, Jp); N. Shibayama (Jichi Medical University, Jp); S.-Y. Park (Yokohama City University, Jp)

Introduction

The oxygen-transporting hemoglobin (Hb) reversibly binds oxygen (O_2), while changing its overall tetrameric structure in the process. The deoxygenated Hb has low affinity for O_2 and its structure is referred to as T (or tense)-state. Upon binding of four O_2 molecules, T-state undergoes tertiary and quaternary conformational changes leading to R (or relaxed)-state, which has high-oxygen affinity, as modeled in the allosteric Monod, Wyman, and Changeux (MWC) [1] and other more complex models [2, 3]. In addition, the allosteric T↔R transition is modulated by other small molecules, such as H^+, CO_2, Cl^-, phosphate ions—called heterotropic effectors. Hydrogen cations (H^+) play a key role in the allosteric regulation of human adult normal hemoglobin (HbA). Deoxy-HbA has a higher affinity for H^+ than oxy-HbA. This trend is demonstrated in the relationship between pH and oxygen binding in the *Bohr effect* [4]. In the alkaline *Bohr effect* at pH above six, more H^+ ions are bound to the T-state HbA than to the R-state. Thus, upon oxygenation, specific H^+ binding sites (Bohr groups) change their pKa. Structural studies by Perutz [5] suggested a few residues can be designated as Bohr groups, however, later research [6, 7] showed that a large number of residues might contribute to the *Bohr effect*. Largely, these are histidine (His) residues, whose side-chain imidazole rings can be protonated/deprotonated at the physiological conditions during T↔R transitions. Therefore, the knowledge of the protonation states of His residues is of great importance for our better understanding of how HbA functions.

Neutron diffraction is unsurpassed in its ability to image and determine the positions of hydrogens in a protein. Hence, we chose neutron protein crystallography technique to study the molecular mechanism of the *Bohr effect* in HbA, with the specific aim of determining protonation states of all 38 His residues in the deoxy-form of HbA. We

Table 1. Neutron crystallographic data collection. Values in parentheses are for the highest resolution shell.

Space Group	**$P2_1$**
Unit Cell a, b, c, (Å) β(°)	 a = 63.8, b = 84.5, c = 54.4 99.3
Resolution	53.7 – 2.00 (2.11 – 2.00)
# refls; unique	103065 (8463); 33302 (4142)
Redundancy	3.1 (2.0)
Completeness	86.7 (74.6)
$\langle I/\sigma(I)\rangle$	4.4 (1.5)
R_{sym}	0.203 (0.339)
R_{work}/R_{free}	0.25 / 0.30

succeeded in growing large 20-mm^3 deoxy-HbA crystals in D_2O and employed the time-of-flight (TOF) technique at the Lujan Center's Protein Crystallography Station (PCS) to collect a complete neutron crystallographic dataset to 2-Å resolution. We were able to unequivocally assign protonation states of 35 His residues and compared these results with previous 2D NMR measurements and discuss the implications for the *Bohr effect*.

Experimental

Hemoglobin was purified from human blood and the deoxy-HbA crystal was grown in D_2O as described elsewhere [8,9]. Forty-six TOF Laue diffraction images were collected at PCS to give an overall completeness of 87% to 2-Å resolution (Table 1). The data were processed with the software [10] modified for neutron diffraction data and *CCP4i* [11]. The neutron structure was refined using *nCNS* [12]. The protonation states of His were determined from omit $2F_O$-F_C and F_O-F_C nuclear density maps (Figure 1).

Results and Discussion

All carboxylic side-chains of ordered Glu and Asp residues were found to be deprotonated and hydroxyl groups of Tyr, Thr, Ser were protonated. The putative *Bohr groups*—α-termini of αVal1 and carboxylates of βGlu-43—were disordered and their protonation states remained undetermined. Of the 38 His residues, three were also disordered, therefore the protonation states of the remaining 35 were unambiguously assigned based on the presence or absence of peaks in the omit $2F_O$-F_C and F_O-F_C nuclear density maps (Figure 1).

The surprising result is that four pairs of surface (αHis-20, αHis-50, αHis-89, αHis-143), the terminal βHis-146 (Figure 2), and both pairs of distal His residues (αHis-58, βHis-63) revealed different protonation states between equivalent chains. For some this can be explained by crystal packing interactions that necessitate protonation or neutrality of a His residue. However, for distal αHis-58, βHis-63, and residues βHis-143 and βHis-146 at the C-termini, another justification is required. βHis-146 has the largest negative ΔpK_a, while βHis-143 has the largest positive ΔpK_a [6]. Thus, they are expected to be protonated and neutral, respectively.

This is the case in the α1β1 dimer (Figure 2), but in α2β2 the protonation states for these His residues are reversed. This finding and the fact that α2His-58 and β2His-63 are neutral, while they were protonated in our previous analysis [13], have led us to propose that α2β2 dimer is no longer in pure T- state. The finding that distal His and buried αHis-103 residues

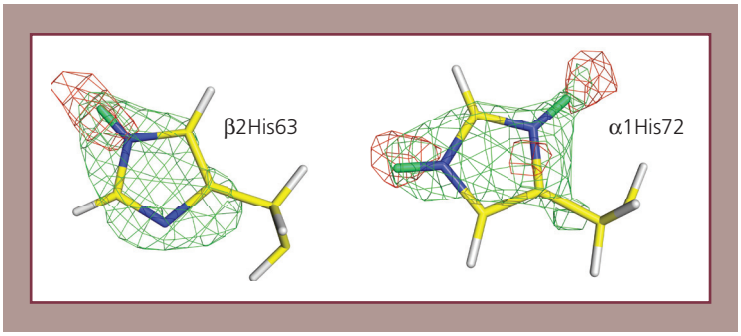

Figure 1. Examples of omit F_O-F_C (red) and 2FO-FC (green) nuclear density maps for His residues, showing the location of the D atoms.

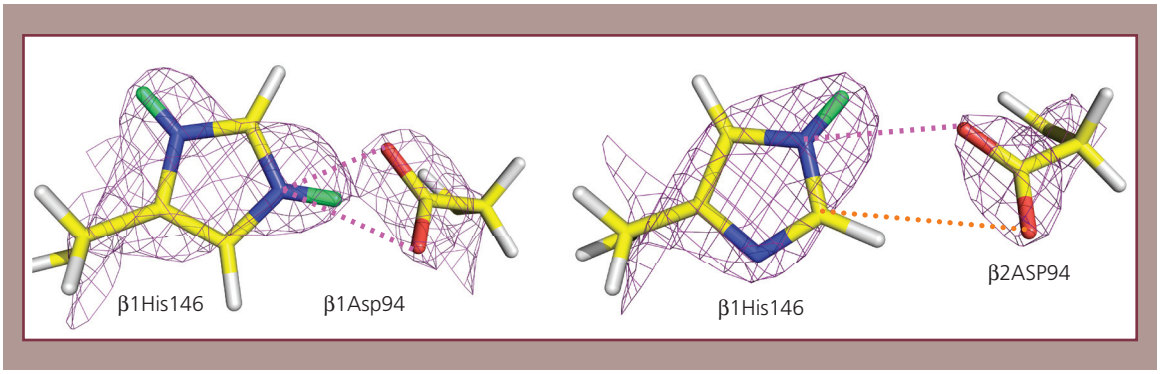

Figure 2. Protonation states and H-bonding of βHis-146.

are protonated and are able to change their charged state suggested their possible role in the *Bohr effect*, although their ΔpK_a values are not available from NMR [6].

Conclusions

The deoxy-HbA neutron structure revealed that distal His residues (αHis-58, βHis-63) and the buried αHis-103 might participate in the *Bohr effect*. This conclusion was not expected based on prior knowledge from solution data. We found, however, that α2β2 heterodimer may have departed from the pure T-state, because β2His-146 was neutral and β2His-143 was protonated, while the opposite protonation states were expected based on the ΔpK_a values from previous NMR studies [6]. (Research to be published by *J. Mol. Biol.* (2010).)

References

[1] Monod, J., et al., *J. Mol. Biol.,* **12**, 88-118 (1965).
[2] Perutz, M. F., et al., *Ann. Rev. Biophys. Struct.*, **27**, 1-34 (1998).
[3] Yonetani, T., et al., *J. Biol. Chem.*, **277**, 34508-34520 (2002).
[4] Wyman, J., *Adv. Protein Chem.,* **19**, 223-286 (1964).
[5] Perutz, M. F., Nature, 228, 726-739 (1970).
[6] Fang, T.-Y., et al., ***Biochemistry***, **38**, 13423-13432 (1999).
[7] Matthew, J. B., et al., *Biochemistry,* **18**, 1928-1936 (1979).
[8] Shibayama, N., et al., *Biochemistry*, **30**, 8158-8165 (1991).
[9] Kovalevsky, A. Y., et al., *Acta Crystallogr. F*, **64**, 270-273 (2008).
[10] Helliwell, J. R., et al., *J. Appl. Cryst.*, **22**, 483-497 (1989).
[11] Weiss, M. S., *J. Appl. Cryst.*, **34**, 130-135 (2001).
[12] Adams, P., et al., *Acta Crystallogr. D*, **65**, 567-573 (2009).
[13] Chatake, et al., *J. Am. Chem. Soc.*, **129**, 14840-14841 (2007).

The neutron structure of human carbonic anhydrase II: Implications for proton transfer

S. Z. Fisher, A.Y. Kovalevsky, M. Mustyakimov, and P. Langan (Los Alamos National Laboratory); J. F. Domsic, R. McKenna, and D. N. Silverman (University of Florida)

Introduction

Human carbonic anhydrase II (HCA II) is ~30 kDa cytosolic Zn-protein that catalyzes the interconversion of carbon dioxide and bicarbonate. Catalysis proceeds via a Zn-hydroxide mechanism and has 2 parts: a nucleophilic attack on incoming CO_2 to produce HCO_3-, followed by a proton transfer (PT) step to regenerate the active site. The CO_2-hydration step is fairly well understood, but the details of PT have been elusive. This PT step in catalysis occurs between Zn-bound H_2O via an ordered H-bonded network of waters to an internal proton shuttle, His-64. Several hydrophilic residues line the active site and order the water network through H-bonding interactions [1]. The orientation of the waters and the charged states of these hydrophilic residues has been unknown, due to the limitations of x-ray crystallography for observing H atoms. To elucidate the H atom positions in the HCA II active site, neutron studies were conducted to look at the nature of the Zn-bound solvent, the charged state of the proton shuttle His-64, if any of the residues that line active site are ionized/charged, and also to observe the orientation and H-bonding of the water network.

Experimental

A large, single crystal (1.2 mm^3 volume) of wild type HCA II was prepared by sitting drop vapor diffusion in a nine-well glass plate. The protein concentration was 15 mg/ml and the precipitant solution consisted of 1.15-M sodium citrate in 100-mM Tris-Cl pH 9.0. The crystal

Table 1. PCS neutron data collection and model refinement statistics. Values in parentheses for the highest resolution shell.

Space group unit cell (Å, °)	$P2_1$, a = 42.6, b = 41.6, c = 72.8, β = 104.6
Resolution (Å)	20.0 – 2.00 (2.11 – 2.00)
Total no. reflections	14136 (1760)
Redundancy	3.0 (2.0)
Completeness (%)	84.6 (72.8)
$\langle I/\sigma(I)\rangle$	3.8 (1.6)
R_{sym}	0.271 (0.384)
No. protein / solvent atoms	4072 / 232
R.m.s.d. bond lengths / angles (Å, °)	0.010 / 1.793
Ave. B factor main / side / solvent ($Å^2$)	21.5 / 24.2 / 38.7
R_{cryst} / R_{free} Neutron	27.5 /28.6
R_{cryst} / R_{free} x-ray	16.1 / 17.3

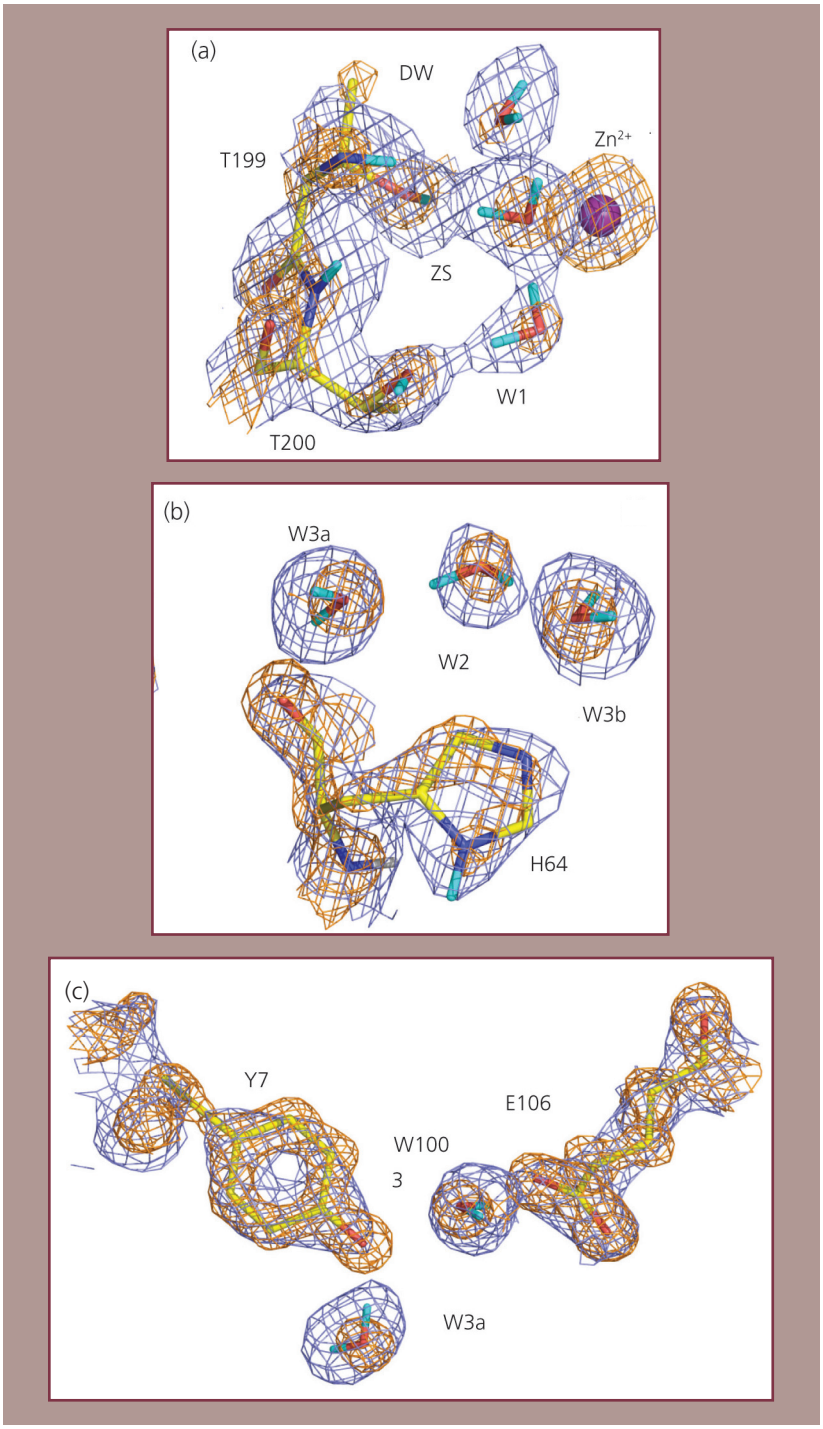

Figure 1. Active site of HCA II. (a) Zn-bound solvent and interactions with Thr199 and Thr200; (b) the proton shuttle His-64 and water orientations; (c) Tyr-7 is deprotonated. $2F_o$-F_c nuclear maps are in blue and are contoured at 1.5σ, electron density $2F_o$-F_c maps are in orange and are contoured at 2.5σ.

was sealed in a quartz capillary and allowed to undergo H/D exchange for three months prior to data collection. Neutron diffraction data was collected at the Lujan Center's Protein Crystallography Station (PCS) [2]. Diffraction data were processed and reduced with a modified version of *d*TREK*. Room temperature x-ray data from a similar crystal, also subjected to H/D exchanged, were collected on an in-house Rigaku RAXIS-IV^{++} diffractometer. Model refinement was performed with nCNS, a modified version of CNS that allows the simultaneous refinement of the model against both room-temperature x-ray and neutron data sets. Table 1 shows the data collection, data set, and model refinement statistics. Experimental data and model were deposited with the Protein Data Bank, PDB id 2kkx. The final model had standard geometry and neutron and x-ray R values for R_{cryst} of 27.5 and 16.1, and R_{free} of 28.6 and 17.3, respectively.

Results and Discussion

From the nuclear map, the deuterium atoms on the Zn-bound solvent (ZS) are clearly visible (Figure 1a), consistent with this species corresponding to a water molecule. This is unexpected as a predicted OH^- should be present based on the pK_a of 7.0 for ZS and the high-pH of crystallization. This is the first direct observation of the nature of ZS, and this has not been previously possible using x-ray data alone. Also, consistent with H_2O bound to the Zn, the proton shuttle His-64 appears neutral, with the unprotonated imidazole N pointing towards the active site, ready to pick up the excess H^+ during catalysis (Figure 1b).

The cluster of H-bonds between ZS, Thr-199, and Glu-106 serves to orient ZS and will likely help to stabilize the newly formed OH^- during catalysis. Tyr-7 is an important active site residue that helps to orient water W3a and forms part of the water network present in HCA II.

A surprising observation was the Tyr-7 appears deprotonated in the neutron structure. This suggests that Tyr-7 has an unusually low pKa and the functional significance is unclear. Mutagenesis of this residue to a Phe yielded a mutant HCA II that had enhanced PT activity compared to wild type [3]. Efforts to determine the deprotonation of this residue by NMR on 13C-Tyr labeled HCA II are underway. Such a negative species close to the proton conducting water network could have profound implications for how PT proceeds at high pH.

Conclusions

This is the first report of a neutron structure of any carbonic anhydrase. The structure sheds light on various active site features not previously known and these have implications for how PT proceeds in protein systems. For the first time the nature of the ZS is directly observed, as well as the details of the H-bonded waters and their orientations in the active site of HCA II. This data suggests that there has to be a reorientation of the active site waters to facilitate PT. The significance of deprotonated Tyr-7 remains to be elucidated and a lower-pH neutron structure of HCA II will be valuable to observed these residues in their charged state. (Research to be published in *Biochemistry* **49** (2010).)

References

[1] Silverman, D.N. and McKenna, R., *Acc. Chem. Res.* **40**, 669-675 (2007).
[2] Fisher, S.Z. et al., *Acta F* **65**, 495-498 (2009).
[3] Fisher, S.Z. et al., *Biochemistry* **46**, 3803-3813 (2007).

Weapons Neutron Research

Introduction

Research Highlights

Weapons Neutron Research

The Weapons Neutron Research (WNR) facility at LANSCE consists of a high-energy "white" neutron source (Target 4), a proton reaction area (Target 2), as well as the three nuclear physics flightpaths at the Lujan Center. The neutron beams produced at WNR are of much higher energy and have shorter pulse-duration than those produced at the Lujan Center.

Using the 800-MeV proton beam from the Linac, Target 4, a bare, unmoderated tungsten spallation source, produces neutron beams with energies ranging from about 0.1 MeV to more than 600 MeV. Because the proton beam is pulsed, the energy of the neutrons can be determined by time-of-flight (TOF) techniques. The time structure of the proton beam can easily be optimized for the requirements of particular experiments. Typically, Target 4 operates with a proton beam current of approximately 1.5 μA, 1.8 ms between pulses, and approximately 14,000 pulses/s. Target 4 is the most intense high-energy neutron source in the world. It has six flightpaths instrumented for a variety of measurements.

Samples at Target 2 (also known as the Blue Room) can be exposed to the direct 800-MeV proton beam or beam that has been compressed in time with the Proton Storage ring (PSR).

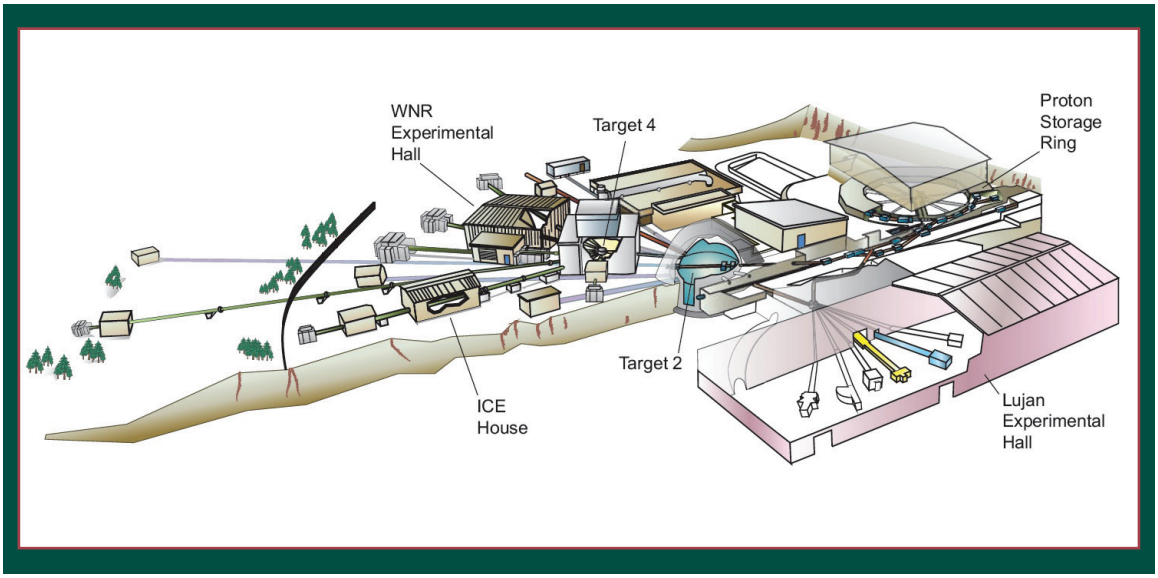

Figure 1. The Layout at WNR. The WNR houses Targets 2 and 4. The latter provides pulses of energetic neutrons to a flexible array of instrumented flightpaths. Target 4 is the most intense high-energy neutron source in the world, with six instrumented flightpaths.

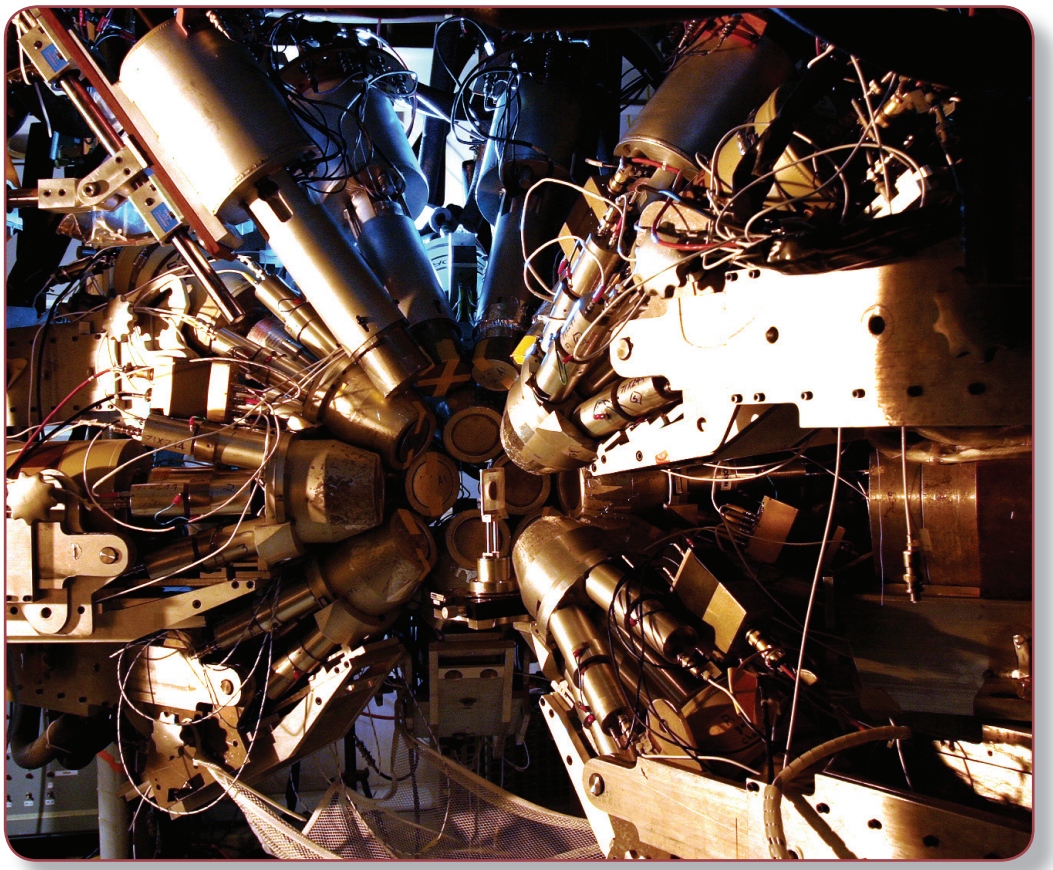

WNR's GEANIE spectrometer consists of approximately 26 compton-suppressed, high-resolution germanium gamma-ray detectors. GEANIE is located on an approximately 20-meter-long flightpath.

WNR's industrial users testing semiconductor-device reliability

The recent attention given to accelerator and braking failures in automobiles has highlighted concerns about the reliability of semiconductor devices. In fact, some in the semiconductor industry believe that the pervasive and ever-increasing use of semiconductor devices throughout modern life make improving device reliability the greatest challenge facing the industry.

The semiconductor industry believes the primary threat to semiconductor-device reliability comes from neutrons, which are produced when cosmic rays strike the atmosphere. Because neutrons are uncharged, these cosmic-ray-induced neutrons can travel long distances without being absorbed, reaching aircraft altitudes and even sea level. When neutrons strike the silicon atoms in semiconductors they produce a nuclear reaction and create charged particles. These charged particles can produce a range of failures from bit-flips that can corrupt data to latching-up the entire device, causing permanent device failures.

Concerns about semiconductor reliability are not new. In 1975, cosmic rays were suspected of causing certain electronic problems in satellites. In the early 1990s, the Boeing Company, as part of certifying the Boeing 777 airplane, recognized that neutrons cause failures in semiconductors at aircraft altitudes. To test their semiconductors, Boeing needed a way to bombard them with a neutron spectrum that closely mimics the spectrum produced by cosmic rays. WNR met these requirements.

Since then, the demand by semiconductor companies to use WNR to test semiconductor reliability has grown.

Figure 1. *Examples of WNR's industrial, academic, and national laboratory partners during 2007–2009.*

In 2004, in response to the high demand LANSCE completed construction at WNR of the Irradiation of Chips and Electronics (ICE) House. The ICE House is used primarily for semiconductor testing. The neutron beam at the ICE House closely matches the atmospheric neutron spectrum, but is one million times more intense (six orders-of-magnitude). The benefit of the ICE House's beam intensity is that more neutrons allows experiments to be completed much faster: one hour of testing in the ICE House is equivalent to over 100 years of actual use. No other facility in the world offers this intensity while closely matching the atmospheric neutron spectrum. Today, the list of WNR's industrial, academic, and other users (Figure 1) represents an international clientele and some of the world's most notable companies and organizations. (Because most of the semiconductor-reliability research performed at the ICE House is propriety it cannot be presented here.)

Neutron testing of semiconductors is also crucial to LANL. For example, much of LANL's national security and other research depends upon using some of the world's fastest supercomputers. LANL needs these supercomputers to be reliable. When they do not operate reliably it is important, strategically and economically, to understand the cause(s) and to prevent future failures.

One now-decommissioned LANL supercomputer, Q, is a case in point. This supercomputer had 8,192 microprocessors. As Q was being commissioned, a greater-than-anticipated number of node failures were observed. One cause was hypothesized to be single-event effects (SEE) caused by cosmic-ray-induced neutrons. The relevant hardware from Q was tested in the ICE House. The results were consistent with the hypothesis that the failures were due to neutron-induced SEEs. With this information, mitigation strategies could be explored.

LANSCE's WNR studies cavitation corrosion of the ORNL spallation neutron source target

The Spallation Neutron Source (SNS) at Oak Ridge National Laboratory (ORNL) will be the most powerful pulsed-neutron source in the world when the design specifications are achieved. With beam power greater than 1 MW, SNS will provide researchers with exceptional neutron intensities for material science research. The SNS project for the Department of Energy's Office of Science has a cost of over $1 billion.

A crucial element of the SNS success is the neutron production target. To achieve the specified intensity, the SNS neutron production target requires a flowing-liquid metal target to remove the deposited heat. Mercury was chosen for the target fluid because of mercury's high density, large atomic number, and thermodynamic properties. This is the first time such a target has been used.

The scientists and engineers from SNS use the pulsed-proton beam at WNR to test the performance of the SNS target because the LANSCE proton beam has energy density similar to what the SNS target will experience. During the target tests at WNR, pitting occurred in the walls of the mercury container. Cavitation bubbles, formed by the pressure wave from the very intense proton beam-pulse, appear to be the cause of pitting. This cavitation erosion may limit the lifetime of the SNS target.

To study this effect and to develop techniques to mitigate the problem, scientists initiated additional target studies at WNR. The goal of the experiments is to study the effect of target geometry, fluid flow, and energy density on the cavitation rate. The results of the experiments are key to developing a strategy to address the SNS target issues.

LANSCE's unique facilities are making an extremely important contribution to the success of SNS and to the basic understanding of liquid targets for pulsed neutron sources.

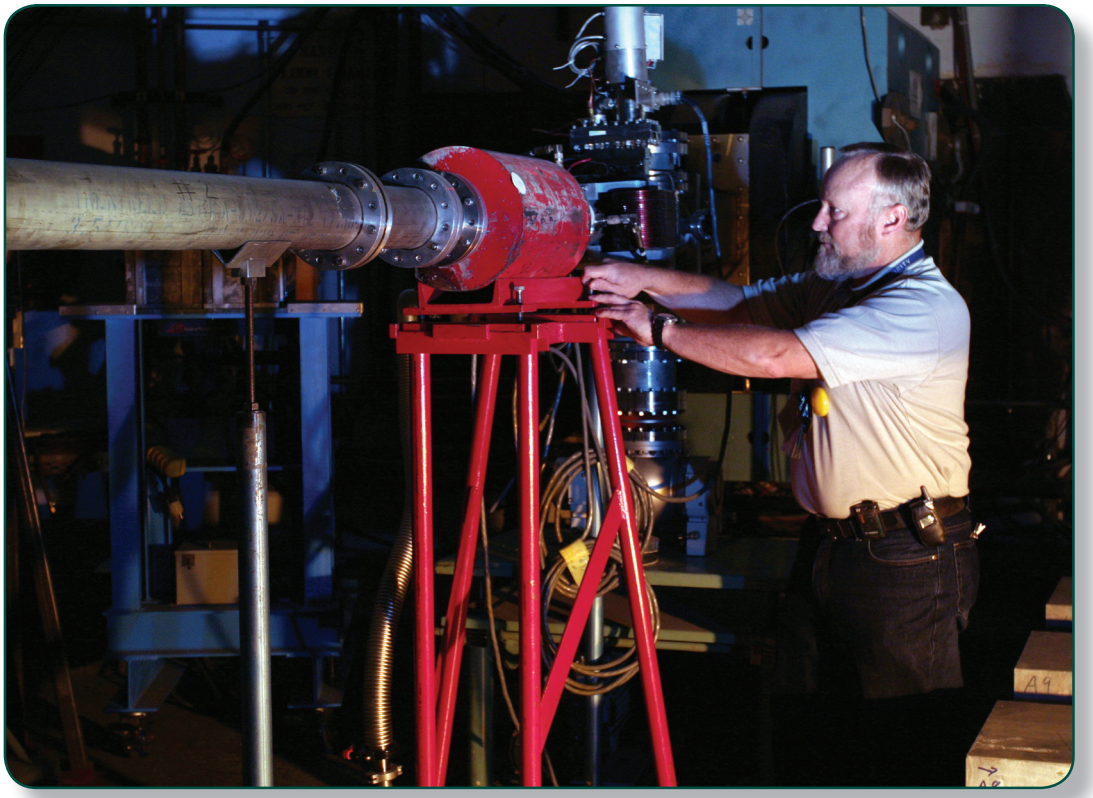

A scientist prepares an experiment in the Blue Room at WNR.

First demonstration of 197-MeV protons at LANSCE for isotope production: ability to transport multiple-energy protons beams is restored

The Isotope Production Facility (IPF) at LANSCE uses 100-MeV protons from the Linac to create radioisotopes though nuclear reactions. Staff LANL's Chemistry Division then separate and purify the radioisotopes for medical and research needs.

In an effort to produce new radioisotopes, scientists performed calculations for radioisotope production using other proton beam energies. Their calculations indicate that ~200 MeV protons are optimal to make desired new radioisotopes, such as gadolinium-153.

A cooperative effort between LANSCE, LANL's Accelerator Operations and Technology Division, and Chemistry Division personnel enabled the Linac to transport 197-MeV protons to the Blue Room experimental area of WNR. It has been many years since protons at an energy other than 800-MeV have been used in the experimental areas at LANSCE, and never at an energy less than 256-MeV at WNR.

As part of this effort, LANSCE also recovered the capability to transport multiple-energy proton beams (197-MeV and 800-MeV) simultaneously

WNR facility at LANCE; the concrete dome in the upper photo covers the main experimental area.

to different experimental areas. The capability to simultaneously transport multiple-energy proton beams is essential for simultaneously operating the Proton Radiography, Ultracold Neutrons, and the IPF program.

The capability to change the beam energy from pulse to pulse was in Louis Rosen's original design for LANSCE and built into the original accelerator controls, but the multiple energy controls have not been used in more than a decade. The system with the 197-MeV and 800-MeV beams worked on the first try and only required minor adjustments to achieve production-quality operation.

The 197-MeV beam "tune" will support experiments that Chemistry Division's IPF personnel run in the Blue Room at WNR. These experiments are expected to lead to developing a unique isotope production capability to complement the existing 100-MeV IPF facility at LANSCE.

Gamma-ray measurements with GEANIE at LANSCE for neutrinoless-double-beta-decay

R. Nelson, M. Devlin, N. Fotiadis, G. Chaparro, S. Elliott, V. Guiseppe, and M. Boswell (Los Alamos National Laboratory) M. Dolinski and R. Norman (University of California, Berkeley and Lawrence Livermore National Laboratory)

Our understanding of neutrino mass and its particle-antiparticle nature (whether the neutrino is its own antiparticle or not) is currently being investigated by a number of large international collaborations through attempts to observe the extremely rare neutrino-less-double-beta-decay ($0\nu\beta\beta$) process. In this process two betas are emitted, but no neutrino.

For the double-beta decay process, a peak in the energy spectrum at a single energy might be observed corresponding to the energy deposited by the two electrons (Figure 1). Observation of such a peak would indicate that neutrinos are their own antiparticles; lepton number is not conserved, and a measure of the effective mass of the electron neutrino with sensitivities below 100 meV is provided. A variety of collaborations exist that are working to make such measurements: CUORE, EXO, GERDA, Majorana, and NEMO-3 is a partial list.

A number of nuclei have been identified for which the neutrino-less, double-beta decay process would be energetically favorable. These nuclei include: calcium-48, germanium-76, selenium-82, molybdenum-100, cadmium-116, tellurium-130, xeneon-136, and

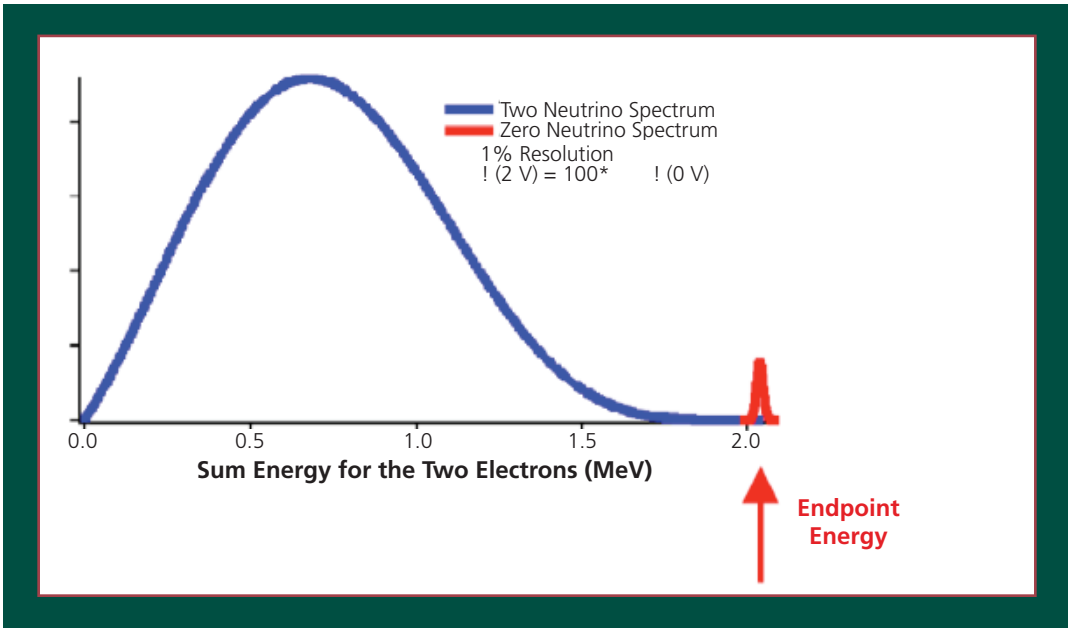

Figure 1. Energy spectrum for the 2 e-.

neodymium-150. At least 16 collaborations have proposed measurements and several efforts are underway based on one claimed result for a small germanium detector.

Because double-beta decay is an extremely rare events with lifetimes on the order of 10^{22} to 10^{25} years, very large samples and extremely low backgrounds are needed to perform a useful measurement. In some cases, such as germanium-76 and tellurium-130, the sample is also the detector, either a semiconductor detector or a cryogenically-cooled micro calorimeter/ bolometer. These samples/detectors require masses on the order of 100 kg to a ton or more of these materials to obtain good sensitivity. The detectors must be placed in deep underground laboratories to minimize backgrounds from cosmic rays and other sources. A goal is to have backgrounds below one-count-per-ton of material per year in the small energy region of interest.

A potentially important source of background in deep underground experiments is caused from the production of gamma rays by cosmic-ray-induced, high-energy neutrons. If neutrons interacting in the double-beta detector or its shielding produce gamma rays with energies in the region of interest, the reaction can seriously affect the sensitivity of the measurements. Typical shielding materials are high-purity lead or copper.

Because gamma-ray production due to high-energy neutron-interactions is not well known, it is important to search for such background lines as crucial information in designing the experiments. Measurements have been initiated using the high-energy WNR neutron source and the GEANIE detector, an array of 26 high-resolution germanium detectors to assess the background situation. The high-energy (>200 MeV) neutrons available at WNR and the array of germanium detectors make GEANIE an ideal place to perform such measurements.

The CUORE and Majorana collaborations have made high-energy neutron-induced gamma-ray measurements using GEANIE. First measurements were on tellurium-130 and natural tellurium by members of the CUORE collaboration. The Majorana collaboration has performed experiments on copper, lead (shielding materials), germanium-76 and natural germanium, which are the active detector elements. New experiments by the Majorana team are looking at backgrounds in argon and other detectors.

Neutron and gamma-ray production with low-energy beams

T. N. Taddeucci and R. L. Sheffield (Los Alamos National Laboratory) T. N. Massey, D. Carter, J. E. O'Donnell, C. R. Brune, D. Ingram, D. Jacobs, and A. DiLullo (Ohio Univeristy)

Proton, deuteron, and helium beams with energy of 4 MeV or less can be readily produced by small accelerators such as radio-frequency-quadrupole linear accelerators. High-energy (>10 MeV) neutrons and gamma rays can be produced with such beams by selecting nuclear reactions with large positive Q values. These high-energy secondary beams can be useful for nondestructive evaluation applications, such as radiography or interrogation of bulk containers for shielded fissile material.

We have considered a number of candidate source reactions capable of producing useful fluxes of both neutrons and high-energy gammas. One candidate reaction is of special interest. The bismuth (B)-11(d, nγ) reaction is well known as a prolific source of 15.1-MeV gamma rays, which is an ideal energy for photo fission production. This reaction has a Q-value of +13.73 MeV. Deuterons with energy greater than the threshold value E_{thr} = 1.63 MeV can excite the 15.1-MeV state in carbon (C)-12, which can then decay directly to the ground state as a strong M1 transition. In spite of the large cross section for production of the 15.1-MeV gamma ray, published cross-section values have relatively large uncertainties. Measurements made at Caltech by Kavanagh and Barnes [1] were assigned a normalization uncertainty of ±24%. Later measurements at Rice by Kuan et al. [2] were assigned an uncertainty of ±50%.

To confirm the suitability of the B-11(d, nγ) reaction for potential actinide-detection applications, we have performed new cross-section measurements at several beam energies in the range from 3–7.44 MeV using both stopping-thickness and thin targets. Neutron and gamma-ray angular distributions were measured simultaneously. The most significant result of these measurements was the discovery that previous B-11(d, nγ) cross sections were probably over estimated by almost a factor of two.

Measurements were made using the 4.5-MeV tandem Van de Graaff accelerator and beam-swinger facility [3] at the Ohio University John E. Edwards Accelerator Laboratory. Neutrons were detected with an array of three NE-213 liquid-scintillator detectors positioned about 8 m from the target in a well-collimated beam tunnel. Gammas were detected in a single 4-in-diameter by 4-in-thick bismuth-germanate (BGO) detector positioned approximately 2 m from the target. Three target samples consisting of sintered boron enriched to 97.15% in B-11 were obtained on loan from Indiana University. The thickest B-11 target was self-supporting and stopping thickness, with an areal density of 57.4 mg/cm^2. Two thinner samples with areal densities of 900 μg/cm^2 and 3.17 mg/cm^2 B were mounted on thin carbon + polystyrene backing foils.

Detailed excitation functions for the B-11(d,n) C-12($\gamma_{15.1}$) reaction were previously measured by Kavanagh and Barnes [1] and by Kuan et al. [2]. These two data sets agree well in shape, but not in magnitude. A comparison of our new data to the previous measurements is shown in Figure 1.

Cross sections derived from all three B-11 target samples are in good agreement. Normalization

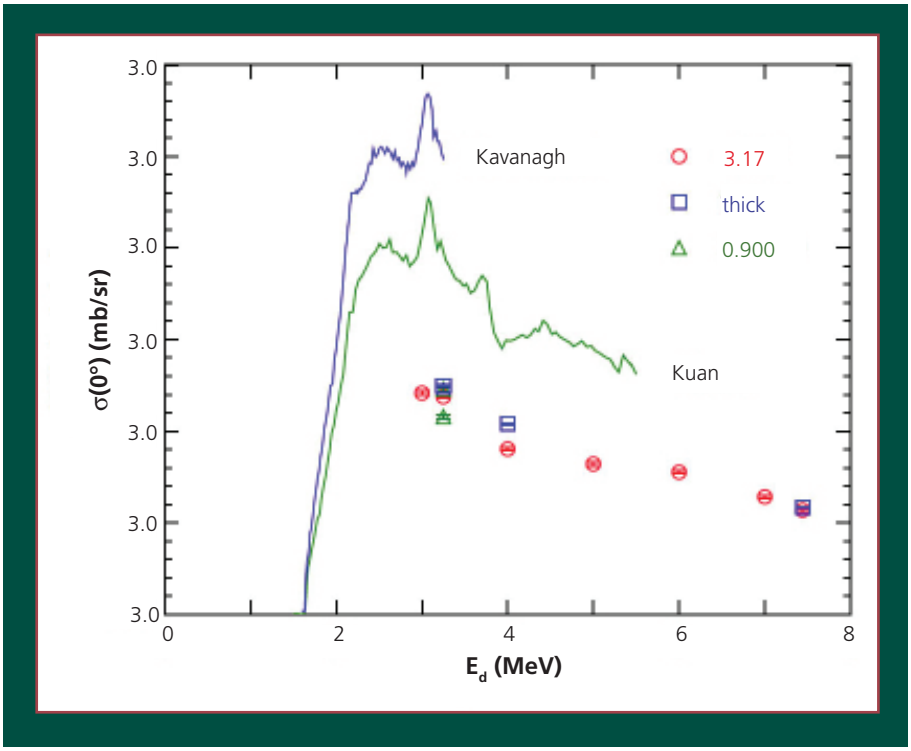

Figure 1. Cross section for the B-11(d,n) C-12($\gamma_{15.1}$) reaction as a function of deuteron energy. The solid curve labeled "Kavanagh" corresponds to data from [1], and the solid curve labeled "Kuan" is from [2]. New measurements correspond to three different sample thicknesses: 3.17 mg/cm² (circle), 0.900 mg/cm² (triangle), and stopping thickness (square).

of the BGO data (beam integration, solid angle, etc.) was also checked by comparing yields for fluorine-19(p,αγ) at Ep = 3 MeV to results from previous measurements [4] with a NaI detector. Agreement was better than 10%.

Our new cross-section values are about a factor-of-two smaller than the previous measurements. The explanation for this difference likely lies in how the gamma-ray line shape is treated in extracting total yields from the measured gamma-ray spectra.

Our new measurements have three advantages over previous work. The BGO detector has very high effciency (≈ 97%), so multiple-scattering and escape-peak effects are minimized. The large (≈ 2 m) stand-off distance of the BGO detector from the target position allowed for very effcient time-of-flight gates to be imposed on the data. This results in a very clean spectrum free from secondary gamma-ray and neutron contributions. Finally, modern Monte Carlo codes and fast computers allow for a very precise calculation of the gamma-ray pulse-height distribution (line shape) for a given gamma energy.

Gamma yields for the 15.1-MeV transition were extracted from the measured pulse-height spectra using a line shape calculated with the

Monte Carlo code MCNP5 [5]. The MCNP5 calculations were folded with a Gaussian resolution function adjusted to match the observed width of the 15.1-MeV line. This width corresponds to a detector resolution of $\Delta E/E = 0.033$. The calculation included absorbers such as the target-chamber wall and the air path from target to detector, the aluminum casing of the BGO detector, and the acrylic light guide behind the BGO crystal.

The MCNP5 line shape is compared to a measured pulse-height spectrum in Figure 2. This spectrum was obtained with the thin (900 μg/cm^2) B-11 target. Agreement between calculation and experiment was excellent.

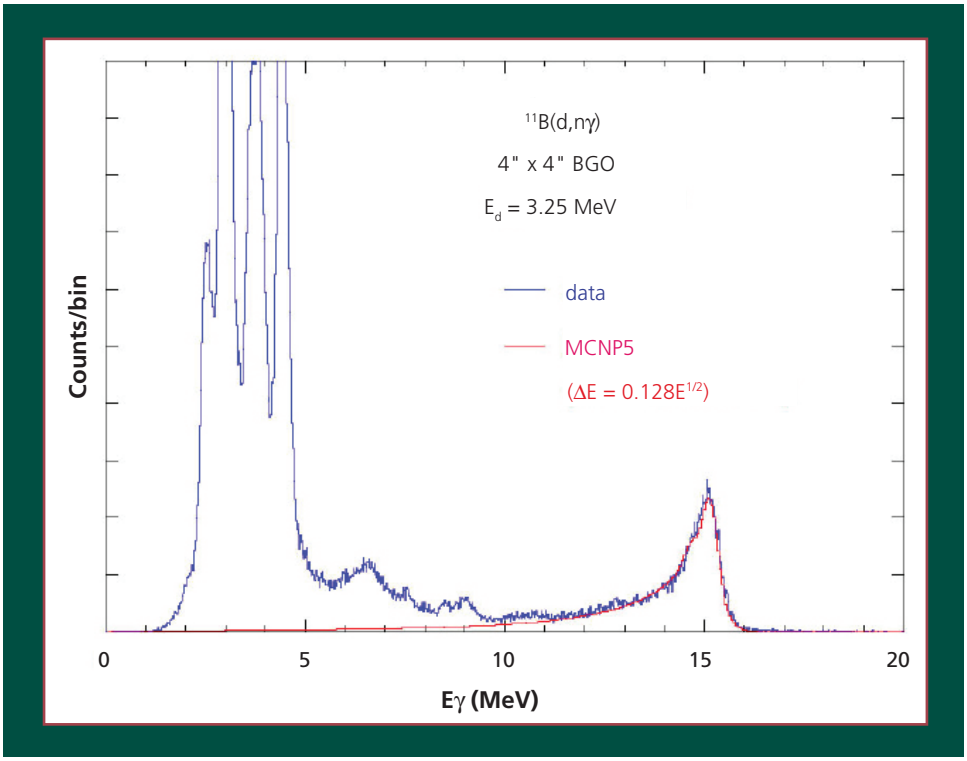

Figure 2. Comparison between measured (blue) and calculated (red) line shapes for the B-11(d, n) C-12($\gamma_{15.1}$) transition.

References

[1] R. W. Kavanagh and C. A. Barnes. 1958. *Phys. Rev.* **112**:503.

[2] H. Kuan, P. R. Almond, G. U. Din, and T. W. Bonner. 1964. *Nuclear Physics* **60**:509.

[3] R. W. Finlay, C. E. Brient, D. E. Carter, A. Marcinowksi, S. Mellema, G. Randers-Pherson, and J. Rapaport. 1982. *Nucl. Instrum. Methods* **198**:197.

[4] A. Fessler, T.N. Massey, B.J. Micklich, D.L. Smith. 2000. *Nucl. Instrum. Methods A450*:353.

[5] Computer code MCNP 5.1.40, Los Alamos National Laboratory, Los Alamos, New Mexico. (available URL: http://mcnp-green.lanl.gov/index.html).

Biological effects of high-energy neutrons studied at WNR facility

W. W. Kuhne and W. S. Dynan (Medical College of Georgia, Augusta, GA), B. B. Gersey and R. T. Wilkins (Prairie View A&M University, Tx), H. Wu (NASA Johnson Space Center), and S. A. Wender (Los Alamos National Laboratory)

Cosmic radiation produces secondary radiation in the form of high-energy neutrons when the radiation interacts with the atmosphere, spacecraft structures, and planetary surfaces. These high-energy neutrons can be a significant contributor to the neutron dose received by crewmembers and passengers during commercial aviation travel and astronauts during space missions. Our knowledge of the biological damage produced by high-energy neutrons is poor.

Because of the similarity of the neutron energy spectrum delivered to WNR to the secondary neutron-energy spectra found both in the Earth's upper atmosphere and onboard the Soviet/Russian Mir and on the International Space Station, WNR is an ideal place to study the biological effects of high-energy neutrons. An experiment designed to investigate the biological effects of high-energy neutrons was recently conducted at WNR's ICE House experimental station. The experiment was sponsored by the Department of Energy's Low-Dose Radiation Research Program and NASA.

Specifically, the experiment was designed to determine the biological damage expressed in developing embryos of the Japanese medaka fish (*Oryzias latipes*) exposure to low doses of neutron radiation. The medaka was chosen as the vertebrate model for a variety of reasons. During its entire embryonic development, the medaka embryo is transparent. This transparency allows the use of a DNA-binding counter stain as a visual aid in the investigation of the quantity and spatial distribution of the damage within the embryo. The DNA damage and repair processes in response to ionizing radiation are similar to those found in mammals. Over the past 20 years, the response of the medaka to ionizing radiation has been a subject of intense study and has resulted in a significant body of literature. However, only a few papers have resulted from studies that specifically investigated the response of the medaka to high-LET (linear energy transfer) radiation—radiation with large energy deposition per unit-track-length, such as from alpha particles and heavy ions. This was the first medaka study using a high-energy neutron beam.

Medaka embryos were exposed in vivo at ~48-hrs post-fertilization with doses of 0 to 50 cGy (50 rad) at a dose rate of 1.5 cGy/h. After neutron exposure and release following a radiation survey, the embryos were shipped to the Medical College of Georgia for further processing. To further explore the dose response, medaka embryos were exposed to similar doses of low-LET gamma radiation at the Medical College of Georgia. Results of this work will significantly advance the understanding of the biological effects of high-energy neutron radiation. All experiments were conducted following Animal Care and Use Committee approvals at LANL and the Medical College of Georgia.

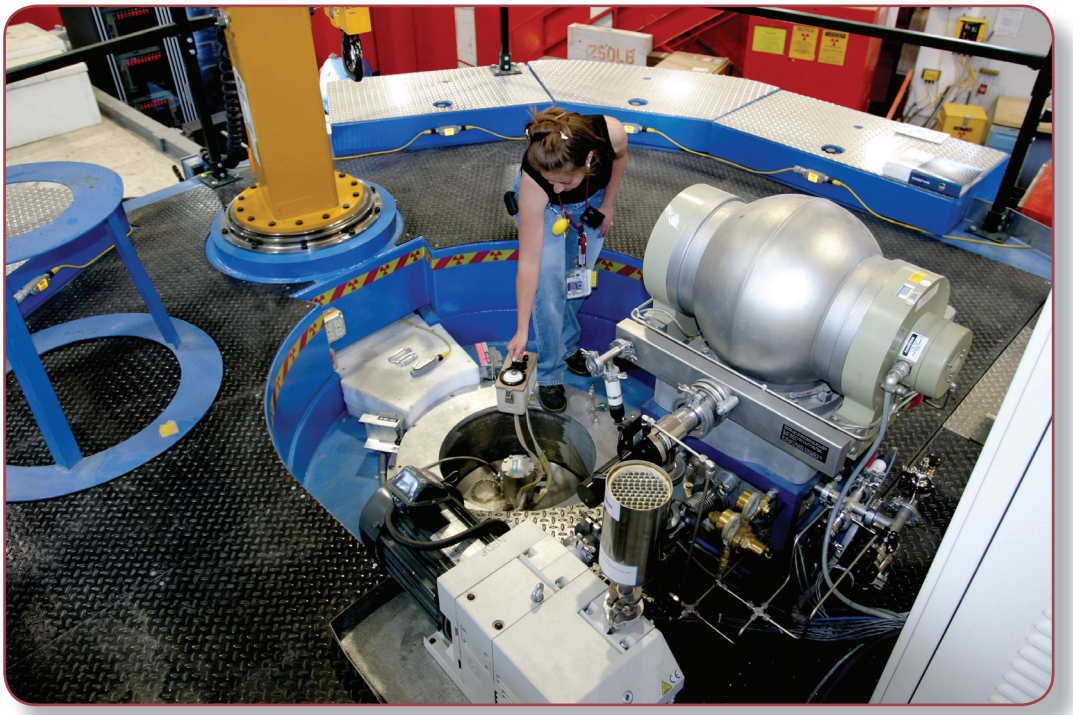

Radiological technicians regularly check the safety of LANSCE's instruments and equipment.

A new measurement of neutron capture on americium-241 with DANCE at LANSCE

M. Jandel, T. A. Bredeweg, M. M. Fowler, E. M. Bond, R. S. Rundberg, D. J. Vieira, J. B. Wilhelmy, J. L. Ullmann, A. J. Couture, J. M. O'Donnell, R. Reifarth, J. M. Wouters, M. B. Chadwick, and R. R. Clement (Los Alamos National Laboratory), U. Agvaanluvsan, R. A. Macri, S. A. Sheets, C. Y. Wu, and J. A. Becker, (Lawrence Livermore National Laboratory)

Yields of nuclear reactions on americium (Am)-241 are being proposed as sensitive new radiochemical diagnostics for past nuclear weapons tests. To use these diagnostics to greatest benefit, a precise knowledge of the cross sections for a variety of nuclear reactions, including (n,γ), (n,2n), and (n,fission), on the Am isotopes is needed. These data also are important for understanding the burn-up of Am in advanced nuclear reactors, as part of the Global Nuclear Energy Partnership (GNEP), and in nuclear forensics. The measurement of the cross section for Am-241 (n,γ) reported here was made as part of a LANL Laboratory Directed Research and Development project for developing the ΔA radiochemical diagnostic.

This work represents the first absolute cross-section experiment performed for neutron capture on Am-241. The measurement spans seven orders-of-magnitude in neutron energy range from below thermal to 300 keV. In addition, the experiment is a significant advancement over past measurements because WNR's Detector for Advanced Neutron Capture Experiments (DANCE) detector measures the full energy of the gamma-ray cascade following capture. This permits

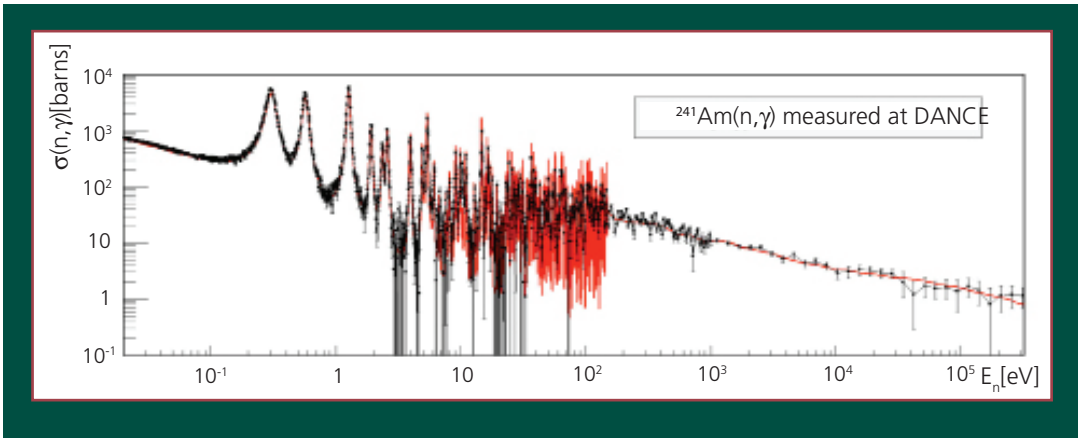

Figure 1. Am-241 (n,γ) cross-section measured using the DANCE detector (black points) compared to the ENDF/B-VII evaluation (red). The larger uncertainties at 40 and 180 keV are due to resonance absorption of the neutron flux by the flightpath windows. At lower energies the compound nuclear resonances are evident.

positive identification of the capture reaction and minimizes experimental backgrounds.

The DANCE detector is a 4π array of 160 barium fluoride (BaF2) scintillators located on Flightpath 14. The radioactive Am-241 target consists of 219 μg of 99.9% pure Am-241 electroplated on to two 2.5-μm-thick titanium foils, sandwiched back to back. The deposit had a thickness of 691 μg/cm^2. The neutron flux was measured using a BF_3 ion chamber, which uses the well-known $^{10}B(n,\alpha)^7Li$ reaction as a standard.

The measured cross section is shown in Figure 1, compared to the ENDF/B-VII evaluation. The overall uncertainties in the measurement are typically 4% near thermal (0.025 eV), 6% near 1 keV, and 18% above 10 keV. The measurement in general confirms the cross section in the evaluation. A detailed analysis of the resonances below 20 eV using the SAMMY resonance analysis code has been done, and the measured neutron widths show some potentially significant deviations from the previous data and the evaluation.

The results of this measurement significantly reduce uncertainties in the radiochemical chain for Am. Neutron-reaction cross-section measurements on other elements in the Am radiochemical chain are planned.

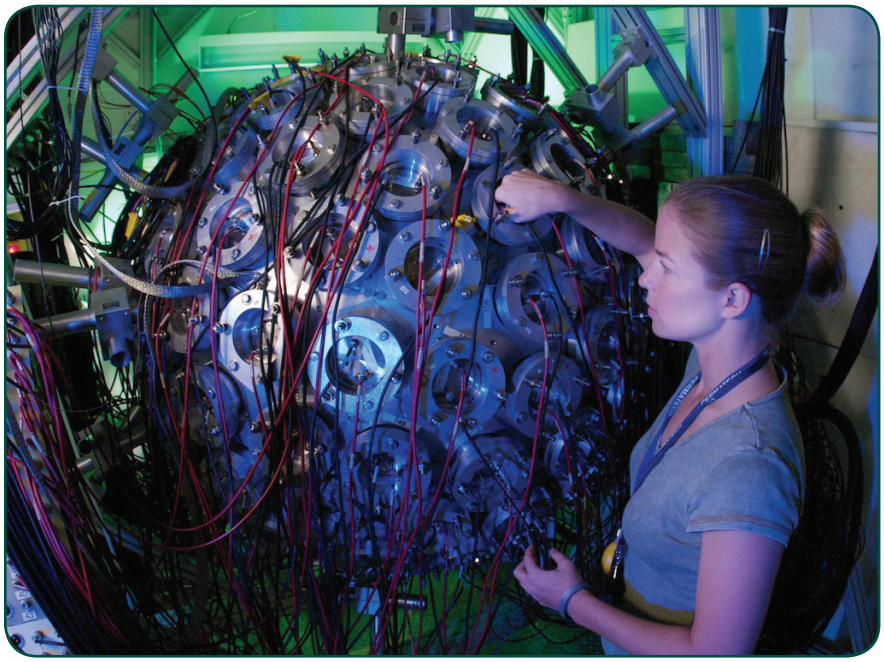

A student helps prepare WNR's DANCE instrument for a experiment.

First measurement of neutron capture on metastable americium-242m with DANCE at LANSCE

M. Jandel, E. M. Bond, T. A. Bredeweg, R. S. Rundberg, D. J Vieira, A. J. Couture, R. C. Haight, J. M. O'Donnell, and J. L. Ullmann (Los Alamos National Laboratory), C.Y. Wu, M. Stoyer, M. M. Fowler, P. Wilk, W. E. Parker, J. A. Becker, R. Macri, and U. Agvaanluvsan (Lawrence Livermore National Laboratory)

A detailed knowledge of neutron capture probabilities on the 141-year-half-life metastable state of americium (Am)-242 (Am-242m) is important, both as part of the reaction network for radiochemical diagnostics for past weapons tests and for calculating neutron balance in advanced reactors and nuclear waste transmutation systems. Am-242m is produced by neutron capture on Am-241. The ground state has a half-life of 16 hrs and is produced in 70% to 80% of all neutron captures, while the 141-year

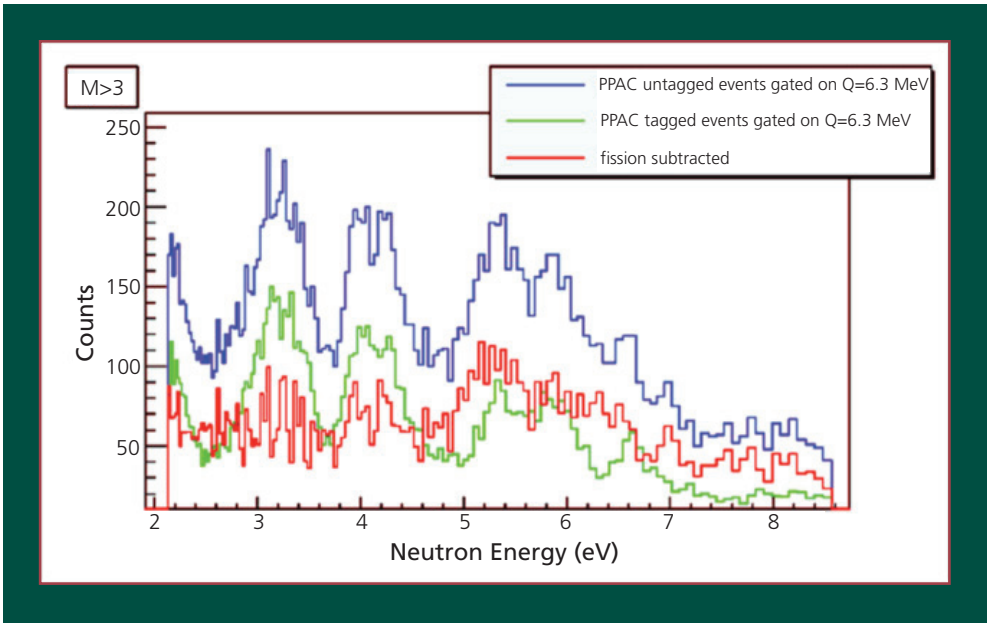

Figure 1. The blue curve shows the total counts corresponding to neutron capture (at least three gamma rays detected) plus fission on Am-242m. Typical neutron resonances are observed in this energy range. The green curve shows the fission-tagged events, and the red curve shows neutron capture, obtained by subtracting the tagged fission events from the total. The red curve provides preliminary capture yields with a shape that, for some energies, is noticeably different from the fission yields (green). Note: instrumental backgrounds have not been subtracted.

metastable state, Am-242m, is produced in an estimated 20% to 30% of the captures.

In a collaborative effort, LANL and Lawrence Livermore National Laboratory (LLNL) scientists used WNR's unique Detector for Advanced Neutron Capture Experiments (DANCE) instrument at the Lujan Center to measure the latter reaction.

There is only a very small amount of isotopically-separated Am-242m in the world. This sample was produced by irradiation in a nuclear reactor, followed by isotopic separation (a major effort for LLNL), over 50-years ago. The target material must be chemically purified just before use to remove the 163-day-half-life decay product, curium-242, the alpha decay of which produces a major source of experimental background. The material was chemically separated and electroplated on titanium foils at LLNL.

Am-242m has a large fission cross section, estimated to be one to two orders-of-magnitude larger than capture cross section. Several measurements of the fission cross section in the neutron energy range from thermal to tens of MeV have been made. However, neutron capture has never been measured because, in the past, the experimental requirement for large quantities of sample material could not be met. However, the highly-efficient DANCE detector, a ball of 160 barium fluoride (BaF2) scintillators, coupled with the large neutron-flux at the Lujan Center, make it possible to measure neutron capture on a very small quantity of sample material. Because the fission cross section is typically much larger than the capture cross section, a fission-tagging detector must be used to separate the fewer capture events from the many fission events.

To tag the Am fission events, a specially constructed fission-counter is inserted into the center of the DANCE ball. The titanium foils containing the Am-242m formed part of the fission-counter. Data in two narrow energy ranges were obtained and a preliminary analysis has been completed. These first results, representing about one-third of the total data acquired, are shown in Figure 1. This is the first measurement of neutron capture on Am-242m. Besides providing crucial information for the weapons diagnostics, the data is important for advanced reactor concepts because it allows accurate calculation of the buildup and destruction of minor actinides, which can play a large role in the potential radioactive waste and criticality issues.

Fission measurements of plutonium in support of the global nuclear energy partnership

T. Hill, F. Robeson, and F. Tovesson (Los Alamos National Laboratory)

The neutron-induced fission cross sections of four plutonium (Pu) isotopes (239–242) have been measured at WNR in support of the Global Nuclear Energy Partnership (GNEP). The GNEP program is a presidential initiative aimed at developing safe, carbon-free, and economically competitive nuclear energy to meet increasing energy needs and reduce the world's dependence on fossil fuel. The vision is a closed-nuclear-fuel-cycle, where spent fuel is re-used to reduce nuclear waste and nuclear proliferation concerns. To achieve these goals, an intensive research and development effort is dealing with different aspects, such as nuclear fuel service, appropriately-sized reactors, and nuclear safeguards.

A technology for reducing waste generation from nuclear power plants is the proposed fast-burner reactor. Different from traditional light-water reactors, the neutron flux of fast-burn reactors burns not only the fissile isotopes (uranium-235, Pu-239) but also the minor actinides, such as Pu-240 and Pu-242, which are produced by nuclear transmutation in the fuel material. These and other minor actinides are responsible for most of the radiotoxicity and long half-life of light-water reactor waste. By using a reactor type in which they are incinerated through fission, much of the waste problem is solved.

To reduce operational margins, and hence, costs of these advanced reactors, high-precision nuclear data is essential. Sensitivity studies performed as part of the GNEP program have shown the need to improve the precision of neutron-induced fission cross sections, as well as other nuclear data, of certain actinides and other materials. An experimental program to provide these cross sections with high accuracy has been developed at LANSCE, and makes use of both the WNR and the Lujan Center.

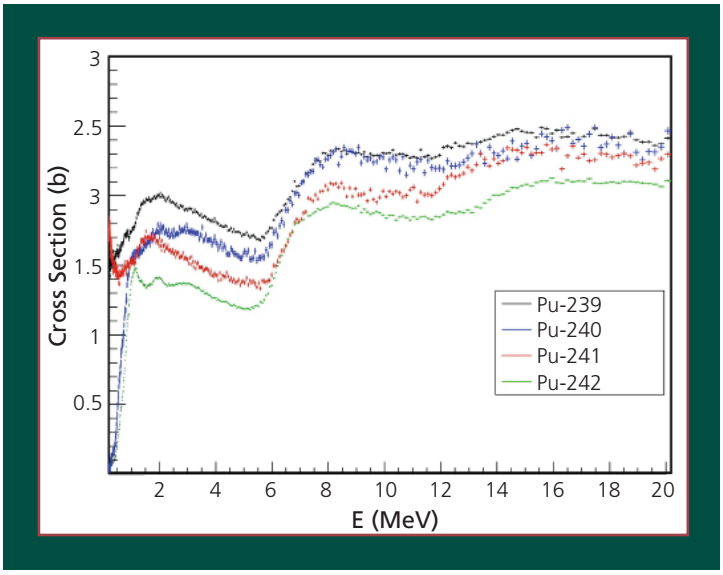

Figure 1. Neutron-induced fission cross-sections of plutonium isotopes measured at LANSCE. This is only part of the energy range that was investigated, which spanned from thermal energies to 200 MeV. Note that only statistical uncertainties are shown.

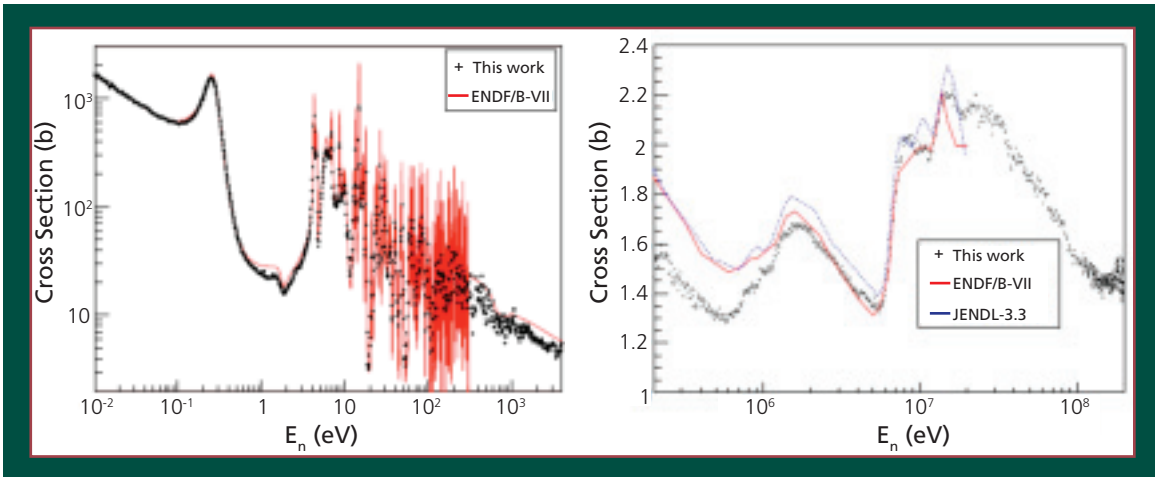

Figure 2. This shows the Pu-241 data in comparison with the U.S. ENDF/B-VII and Japanese JENDL-3.3 evaluated data libraries. The differences between the new data and the evaluations are evident.

The fission measurements performed at LANSCE are unique in that they span 12 decades of neutron energy, from sub-thermal to hundreds of MeV. At most facilities, these cross sections have been measured either in the thermal and resonance region, or in the MeV-region, but not both. This has led to problems when preparing cross-section evaluations that are used in nuclear reactor calculations. Mismatches between high- and low-energy data have caused discrepancies in the keV region of the evaluations, which is of particular importance to the fast-reactor technology considered for GNEP. The new measurements from LANSCE resolve these issues by providing continuous data over the full energy-range of interest.

Recent results for four important Pu isotopes are shown in Figure 1. This plot illustrates the data in one particular energy region, but the full data set extends from 0.01 eV to 200 MeV. The data on Pu-239 are in good agreement with much of the previous data and help to resolve some discrepancies at higher neutron energies. The Pu-242 results are of particular importance for GNEP, because they resolve a discrepancy in the evaluation at 10 keV. The presence of a 2.3 eV resonance was also confirmed by the measurements. This resonance was missing from the previous evaluation. Improvements such as these reduce, the uncertainties in the evaluated data libraries and thus reduce the uncertainties in the reactor simulations.

Measurements on Pu-241 are especially challenging due to its relatively short 14.4-year half-life and the backgrounds associated with its decay. These data offer a significant improvement over the few previously available results, and differ from current evaluations by as much as 30%. Figure 2 shows the Pu-241 data in comparison with the U.S. ENDF/B-VII and Japanese JENDL-3.3 evaluated data libraries. The differences between the new data and the evaluations are evident.

Using the current technique, measurements of other actinides important to GNEP are planned. There is also ongoing development to reduce uncertainties in the cross-section measurements. One promising technique is to use a Time-Projection Chamber, a detector commonly used in high-energy physics, which is expected to provide enough detailed information so that new levels of precision can be achieved.

Nuclear level densities studied through neutron reactions at FIGARO

B. Haight (Los Alamos National Laboratory)

Experiments at the WNR facility are designed to quantify the number of nuclear levels, as a function of excitation energy, in isotopes of importance to weapons development and nuclear energy. This nuclear-level density is often the largest uncertainty in the input to nuclear-reaction model codes used to calculate reaction rates for Laboratory programs.

The approach is to use neutron-induced reactions and look at the emitted neutron spectrum (Figure 1). Researchers use the FIGARO array of gamma-ray and neutron detectors (Figure 2) with WNR's source of fast neutrons. The researchers "tag" the reaction by detecting a gamma ray emitted by the excited residual nucleus and this signal is the "stop" signal of the time-of-flight of the incident neutron from the WNR source. The energy of this incident neutron is thus determined by its time-of-flight. The same gamma-ray signal is the "start" signal for the emitted neutrons, which are detected by an array of neutron detectors.

With the continuous-in-energy neutron source at WNR, researchers can focus on a range of excitation of the target nucleus (Figure 3). This unique way of measuring neutron-emission spectra also opens the possibility for gating the neutron spectrum on a specific gamma-ray transition that selects a certain set of levels that feed this transition, thereby allowing tests of the angular-momentum distribution of levels as functions of excitation energy.

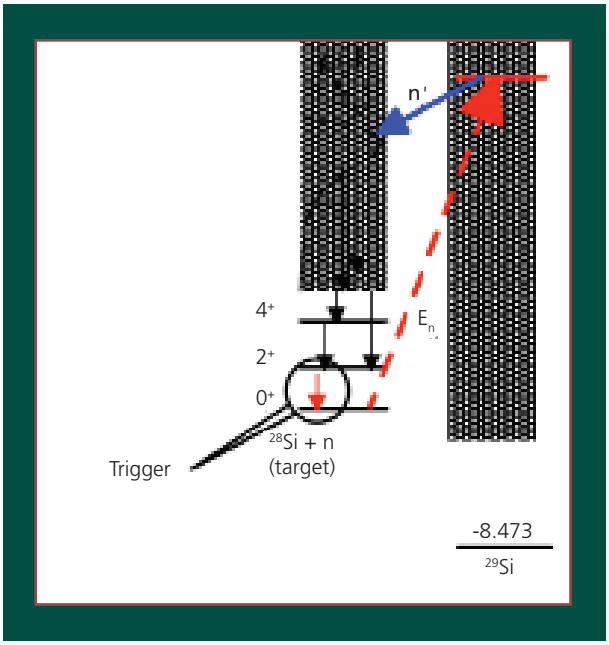

Figure 1. Simplified energy diagram of a fast neutron of energy E_n interacting with a silicon (Si)-28 nucleus, forming a compound, excited Si-29 nucleus, which decays by neutron emission. Neutrons are emitted to populate a range of excitation energies in Si-28 according to the density of excited levels, which is not well known. The energy of the emitted neutron specifies the excitation energy in Si-28, and these levels decay by gamma-ray cascades to reach the low-lying states of known spin and parity. Nearly all of the cascades pass through the 2^+ state, and so researchers can use the $2^+ \rightarrow 0^+$ gamma-ray transition to trigger the event and start the clock for a time-of-flight measurement of the energy distribution of the emitted neutrons.

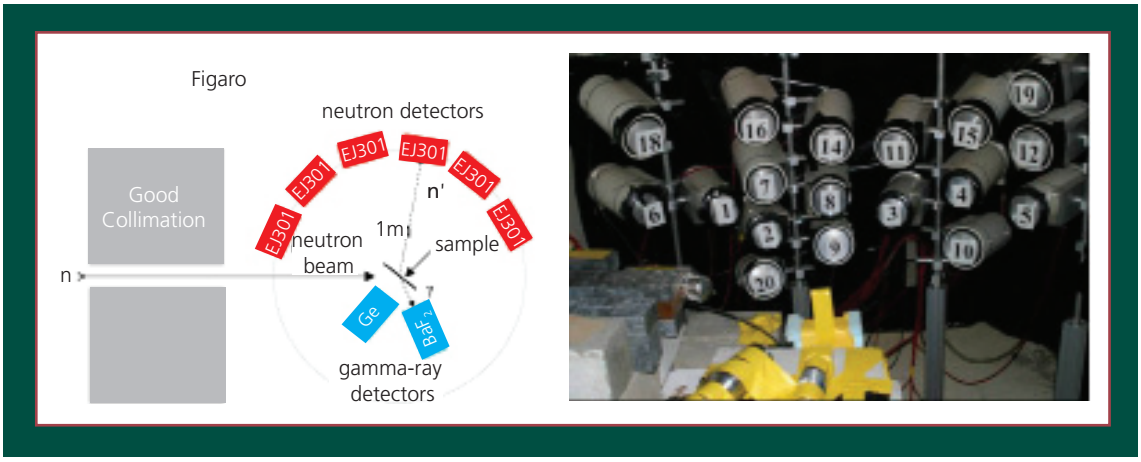

Figure 2. (a) Schematic layout of FIGARO with gamma-ray detectors (blue) and neutron detectors (red). The gamma-ray detectors tag the reaction and serve as start signals for the time-of-flight of the neutrons from the sample to the neutron detectors. (b) The array of neutron detectors has been increased from the original number of 6 to 20.

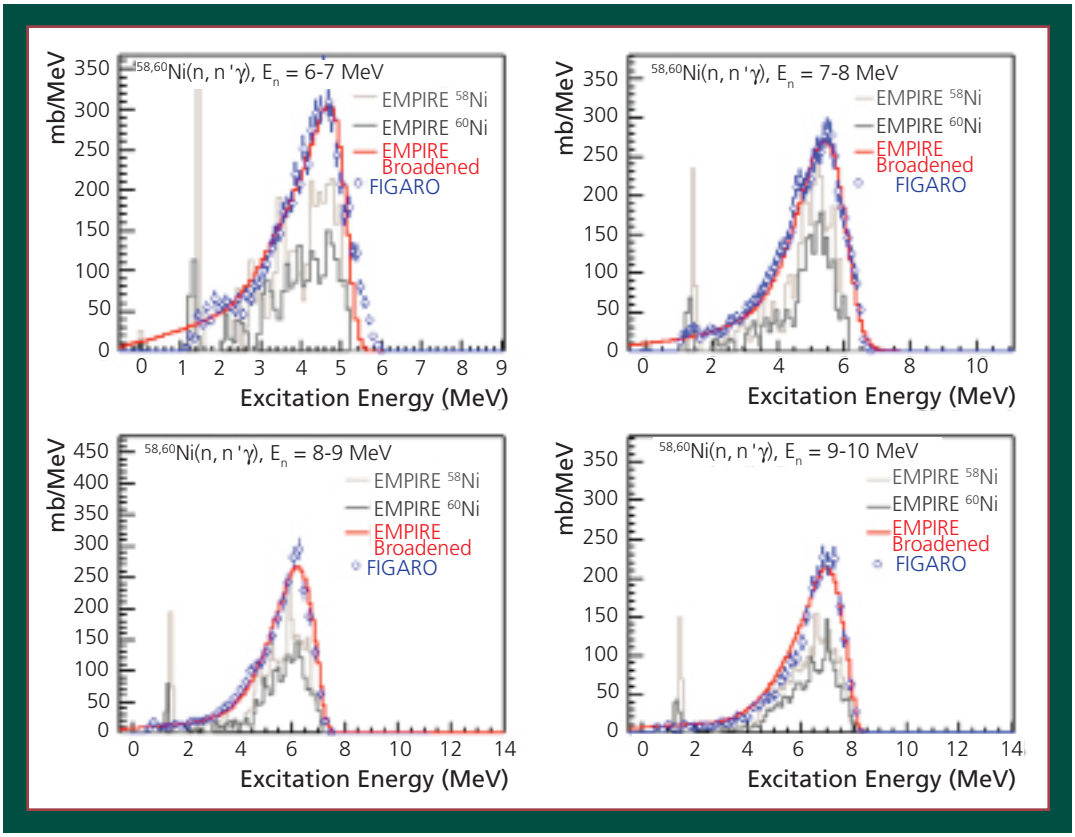

Figure 3. Neutron emission spectra from nickel bombarded with neutrons of energies from 6 to 10 MeV. The calculations with the code EMPIRE used a modified level density.

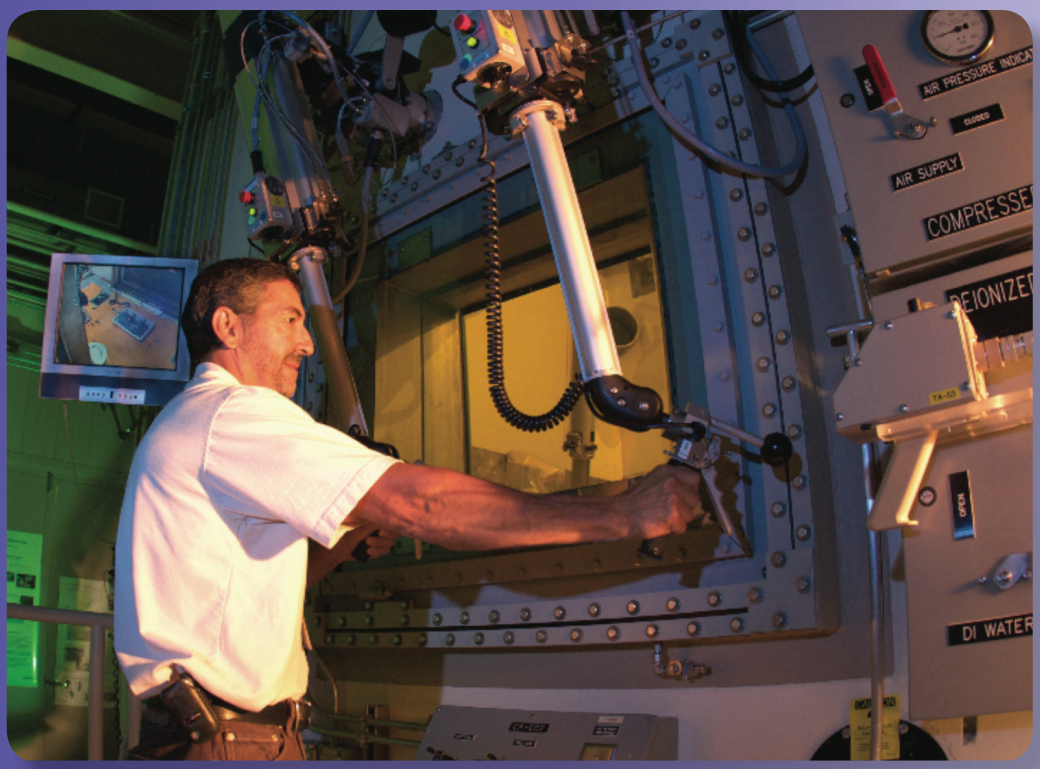

Isotope Production Facility

Introduction and Highlights

Isotope Production Facility

Introduction

Beginning in 1974, before the current Isotope Production Facility (IPF) (Figure 1a) could be built, isotope production at LANSCE occurred at the end of the beamline just prior to the beam dump (Figure 1b). This meant isotopes were produced somewhat inefficiently: only during the months when the entire Linac was running, and only at more or less full power.

Eventually funding was secured, and by 2005 Louis' vision was realized: LANSCE's state-of-the-art IPF was completed and in production (Figure 2). Today, IPF is integral to LANSCE producing short-lived and other isotopes critical to research in nuclear physics and nuclear weapons, and to other programs across the Laboratory. The Isotope Production and Applications Program's (IPAP's) infrastructure also includes hot-cell-processing, waste handling, and storage and disposal facilities (Figure 3).

In addition, IPF is an important part of the DOE's National Isotope Program (Figure 4).

IPF is the DOE's newest isotope production facility providing a noncommercial source of radioisotopes for the nation and the world, filling a niche that commercial isotope suppliers cannot. IPF's isotopes are used in millions of medical procedures every year in the U.S. and worldwide, as well as in industry, homeland security, and environmental research. IPF's customer base historically consists of more than 250 hospitals, research institutions, and private sector companies. IPAP routinely and successfully delivers isotope products to customers: between 150 and 200 isotope shipments annually.

The DOE isotope program coordinates the production and output of the DOE-supported Virtual Isotope Center (Figure 5). This concept was born at LANL in the early 1990s, based upon its collaborations with TRIUMF in Vancouver, Canada, and the Institute of Nuclear Research in Troitsk, Russia. The Virtual Isotope Center includes the iThemba Laboratory in Cape Town, South Africa, and the Paul Scherrer Institute in Villigen, Switzerland. The Virtual Isotope Center

Figure 1. Aerial view of LANSCE with IPF today (a) and prior to 2005 (b).

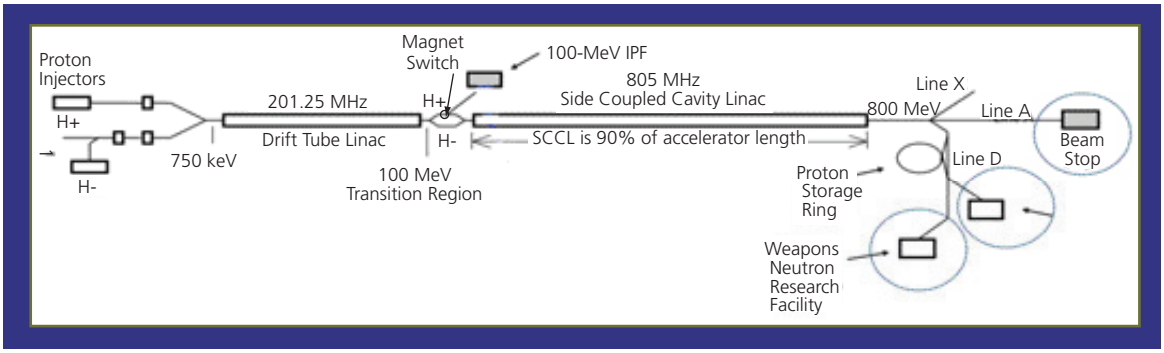

Figure 2. Louis Rosen provided a space between the 100-MeVsection and the 700-MeV section of the accelerator where a magnet could be installed to deflect the 100-MeV beam into what would become a radioisotope facility.

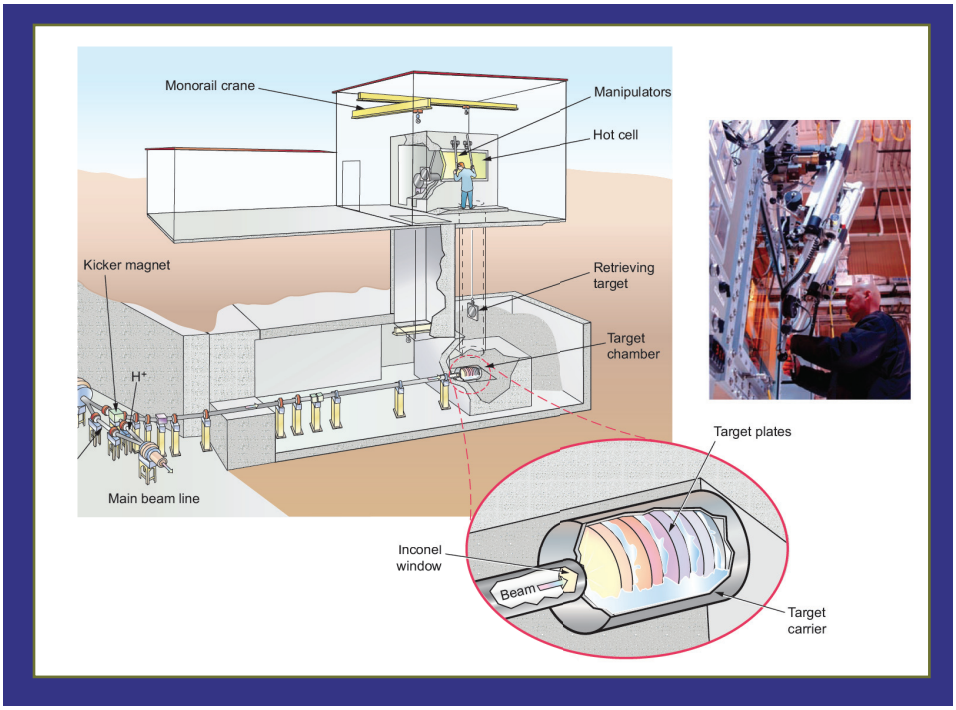

Figure 3. Interior of the IPF. The drawing shows an operator standing at the hot cell on the upper level of the IPF, remotely manipulating targets and equipment. The remote-controlled chain-drive shuttle system is visible, and a stack of targets is in the cave on the lower level, being irradiated with protons. The blowup shows the proton beam entering the target chamber through an inconel window and cooling water flowing through the spaces between the stacked targets. The photo shows a technician remotely manipulating targets in the hot cell.

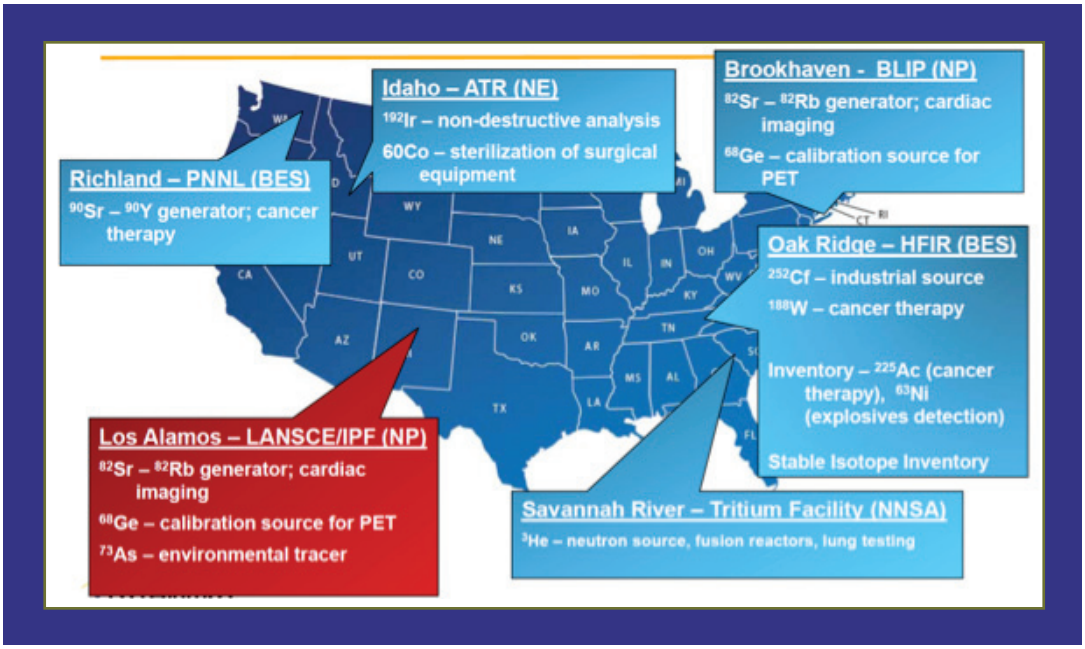

Figure 4. IPF is an important part of the DOE's National Isotope Program. IPF is the DOE's newest isotope production facility providing a noncommercial source of radioisotopes for the nation and the world.

logistics are challenging; targets are irradiated at these international accelerator facilities, packaged into appropriate transportation containers and shipped to LANL (or Lawrence Berkeley National Laboratory (LBNL)) for separation of the isotopes from the target material in the hot-cell facility, then distributed to DOE customers.

Activity Highlights

From 2007 through 2009, IPF continued to supply, worldwide, strontium (Sr)-82 for cardiac imaging (benefiting on average 10,000 patients per month) and germanium (Ge)-68 for the calibration of Positron Emission Tomography (PET) instruments. Ge-68 is used to calibrate every PET scanner in clinical use: over 800 scanners in the U.S. and over 1200 worldwide.) IPF isotope production aids the healthcare of millions of patients every year.

The demand for IPF isotopes continues to grow (Table 1). IPF produced over 50% of the National Isotopes Program's accelerator-based isotopes in 2007. In 2009, it produced approximately 60% of the isotopes. In 2010, IPF expects to produce approximately 70% of the isotopes. For example, Sr-82 production is projected to increase because of a critical shortage of molybdenum (Mo)-99, which is the primary isotope used (90%) for cardiac imaging. Mo-99 is reactor-based and its primary supplier (in Canada) is out of production. It is unknown when Mo-99 production will resume. To meet Sr-82 production demands, in 2009, the DOE requested IPF dedicate operations beyond regularly scheduled productions, in May 2010 and January 2011, for increased Sr-82 production.

Due to an increased interest and use of Ge-68's daughter, gallium (Ga)-68, which is used for medical imaging, the production of Ge-68 has

Figure 5. The DOE National Isotope Program coordinates the production and output of the DOE-supported Virtual Isotope Center (above). This concept was born at LANL. The Virtual Isotope Center logistics are challenging; targets are irradiated at these international accelerator facilities, packaged into appropriate transportation containers and shipped to LANL or LBNL for separation of the isotopes from the target material in the hot-cell facility, then distributed to DOE customers.

Table 1. IPF Radioisotope Production Continues to Increase

Fiscal Year	**2007**	**2008**	**2009**
Sr-82 units shipped (Ci)	59	41	66
Ge-68 units shipped (Ci)	6.5	7.9	10
Beam hours (delivered)	2911.7	3200	3255
Beam reliability	80.2	86%	95%
(Note: the increased trend in beam reliability is tied to investments in the H^+ injector.)			

been steadily increasing. This trend is expected to continue in 2010 and beyond.

Program Highlights

In 2009, the National Isotope Program, which funds IPF, transitioned from the DOE's Office of Nuclear Energy to their Office of Science, Nuclear Physics. This transition has resulted in a renewed commitment to balance commercial isotope production with research isotope production. Developing research areas include the following:

- Medical applications—a key focus on the production of alpha-emitting isotopes, strengthening university partnerships, and integrating isotopes into nanomaterials.
- Nuclear physics applications—leveraging capabilities for cross-section measurements using LANSCE instruments (LSDS and DANCE).
- National security applications—improving the unique overlap of isotope production capability and national security research.
- Improving isotope production R&D—a special focus on IPF targets to take full advantage of available current and improving isotope-processing methods.

Production and Facility Updates

Since IPF was commissioned in 2005, it has increased the production of Sr-82 by roughly 350%. In 2009, IPF operated at full current: 250 mA at 40-MeV primary beam energy. This capability opens a variety of new possibilities for isotope production, and addresses recommendations outlined in DOE's Nuclear Science Advisory Committee's (NSAC's) recently issued NSAC-I reports. Specific isotopes that could be produced at this energy are copper (Cu)-64 (which will leverage IPF's expertise in Cu-67 production), yttrium (Y)-86, zirconium (Zr)-89, iodine (I)-124, and lead (Pb)-203.

In 2009, IPF demonstrated that it could provide 355-mA beam at 100-MeV primary beam energy. This will result in higher production rates once advances in targets are developed and implemented; current target designs fail above 255 mA.

Research Highlights and Accelerator Highlights

In 2009, IPF is the only U.S. high-energy proton facility capable of irradiation of actinide targets. IPF received funding to explore the accelerator-based production of actinium (Ac)-225 from a natural-abundance thorium (Th)-232 target. Ac-225 shows great promise as a cancer therapy isotope. The project will assess production yields and product purity by production at 100, 200, and 800 MeV.

In addition, IPF intends to investigate other actinide-target-based isotopes for national security research. These efforts will be performed in conjunction with WNR.

In 2009, IPF, in a joint effort with the Missouri University Research Reactor, also received research funding in 2009 to explore the production of arsenic isotopes for imaging and therapy applications. The primary objective of this effort is to cross-train students, postdocs, and staff in the production and processing of accelerator- and reactor-produced isotopes.

IPF Users

IPF continues to supply isotopes to a variety of industrial and academic users. High-volume customers include General Electric (GE) Healthcare, DraxImage, Eckert & Ziegler, MDS Nordion, Sanders Medical Products, and Siemens Molecular Imaging. University customers include the State University of New York, Stony Brook; University of Nevada; University of Alberta (Canada); University of Miami; University of Wisconsin; Yale University; and the University of Zaragoza (Spain).

Other non-academic customers include the U.S. Environmental Protection Agency, NASA, the National Institutes of Health, Siemens Medical, Jeroen Bosch Hospital (Netherlands), Perkin-Elmer, the National History Museum (UK), Institute for Energy Technology (Norway), Isotope Technologies (Germany), and Rothamsted Research (UK).

A patient readied for treatment in 1979 as part of LANSCE's nuclear medicine program using isotopes produced at LANSCE.

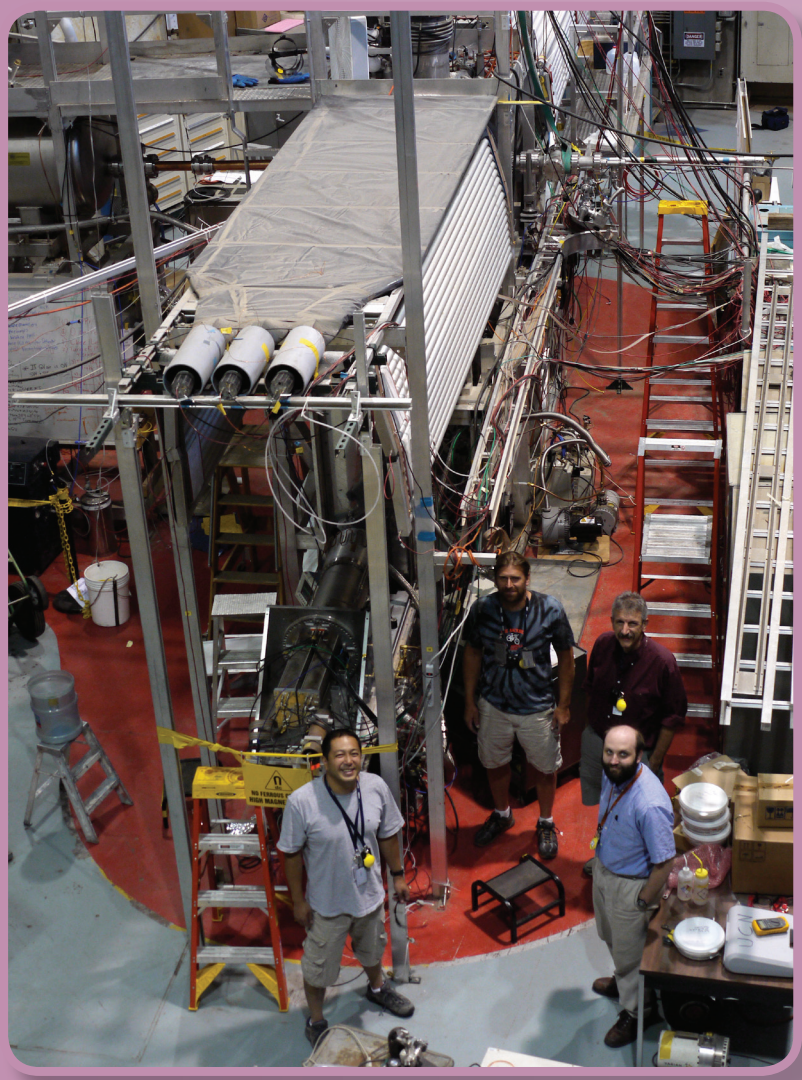

Ultracold Neutrons Facility

Introduction and Highlights

Ultracold Neutrons Facility

Today at LANSCE, fundamental nuclear science is strongly represented by research being done at the Ultracold Neutrons (UNCs) facility (Figure 1). UCNs are neutrons with such low kinetic energy (0 to 8 m/s; they travel about as fast as a human can run) that they can be stored for many hundreds of seconds or even transported over long distances in special containers to be used in experiments.

In 2009, LANSCE was the only source producing extracted UCNs in the U.S. LANSCE produces the highest density of UCNs of any source in the world. LANSCE researchers are using UCNs to probe physics beyond the Standard Model. By researching UNC beta-decay they are investigating what is called the weak nuclear force.

The weak nuclear force is one of the four fundamental forces in nature, which include gravity, electromagnetism, and the strong nuclear force. Measuring the weak nuclear force's parameters is one of the best ways to improve our understanding of the fundamental physics laws of the universe.

When a neutron decays, it emits a proton, electron, and a neutrino in a process known as beta decay. Measurement of the A-correlation, the correlation between electron beta-decay and the initial polarization of the neutron, provides one of the most accessible windows and reveals details into the weak nuclear force. Previous measurements of the A-correlation have been plagued by systematic uncertainties and

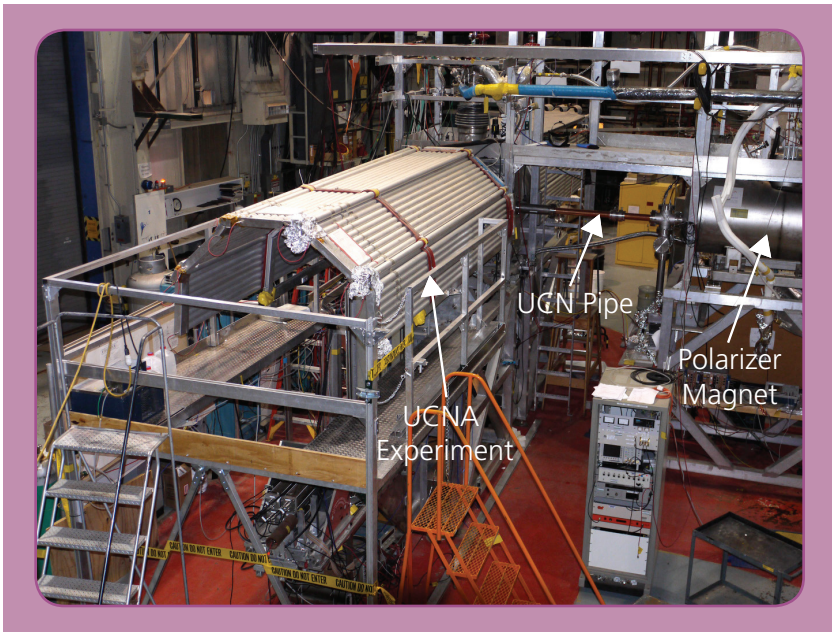

Figure 1. The UCNA project at LANSCE. UCNs are created by the proton beam and the UCN source. Neutrons are piped across the room, polarized by the central magnet, then trapped in the experiment on the left. There, the decay electrons are counted and the A-correlation is measured.

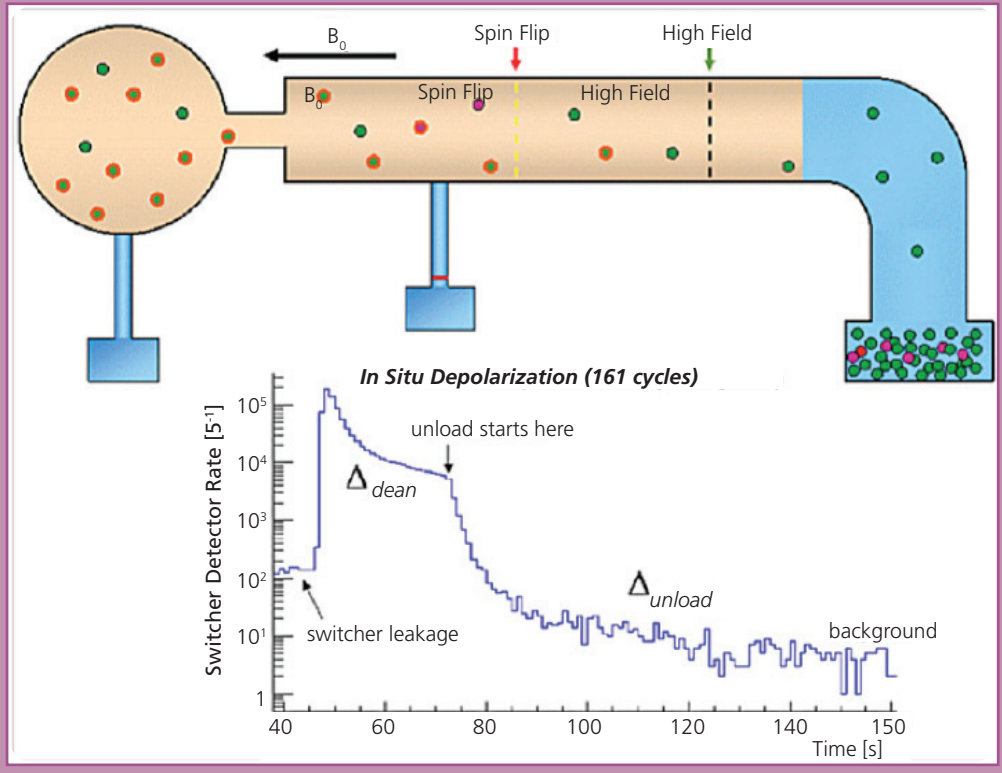

Figure 2. UCNA project. Schematic of a test measurement of neutron depolarization. The experiment is shown as the circle on the left. The neutrons (depicted as dots) flow through the experiment and into a detector on the right. Bottom: The graph shows a typical depolarization measurement, which traps depolarized neutrons in the experiment while cleaning out the properly polarized ones. Any depolarized neutrons would show up as a peak under the label "Δ unload." The number of detected depolarized neutrons was consistent with zero, with sufficiently high precision to show that depolarization will not limit the precision of the final project results.

backscatter, but have hinted at a new physics beyond the Standard Model. The three leading systematic uncertainties are the depolarization of the neutrons in the experiment, the energy loss of the beta-decay particles while they are detected, and the undetected backscatter of the beta-decay particles from their detectors.

UCN's Asymmetry project (UCNA), which consists of LANL and its collaborators at North Carolina State University, Cal Tech, Virginia Tech, University of Washington, and Idaho State University, is designed to better measure beta-decay (Figure 2). The project can 100% polarize the UCNs—100% polarization allows much lower uncertainties— and observe their decay electrons (Figure 3). UCNA has negligible backscatter above that caused by cosmic rays or other natural sources. UCNA and its dedicated source for UCNs began construction and commissioning in 2003. Today, UCNA's beta-decay measurements are comparable in precision to the measurements planned at the Large Hadron Collider at CERN, Switzerland.

In 2007, UNCA completed the world's first measurement of the A-correlation using UCNs (Figure 4). The experiment yielded a 4% uncertainty. Between 2007 and 2008, UCNA accumulated statistics with a low 1% uncertainty.

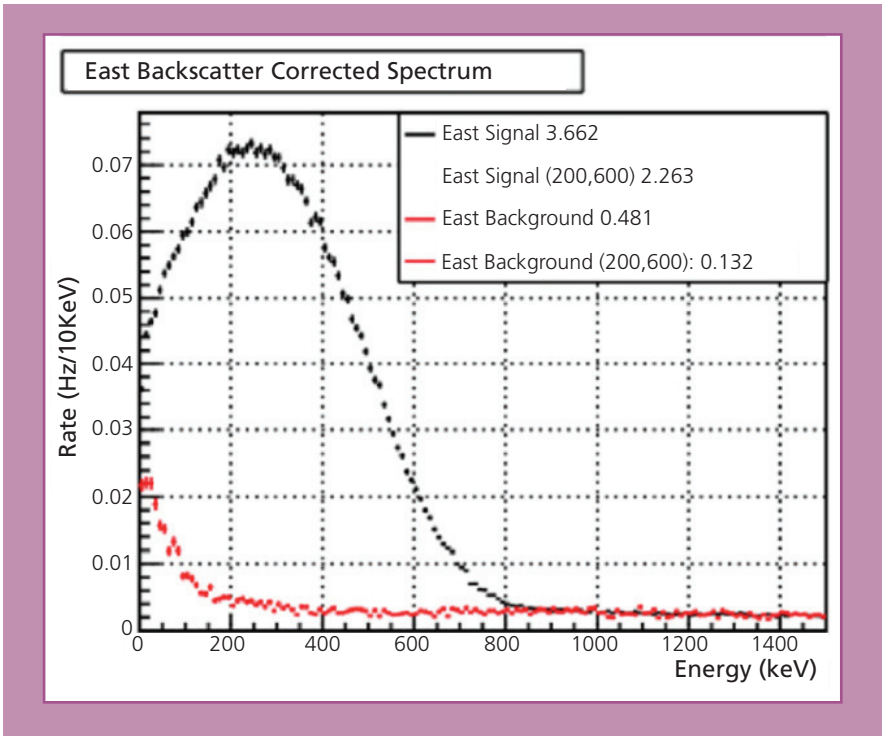

Figure 3. UCNA neutron beta-decay spectrum. The electron energy is shown on the horizontal axis and the number of detected electrons on the vertical axis. The signal + background is shown in black and the measured background in red.

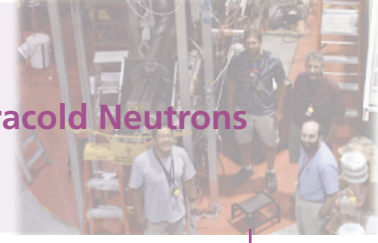

The ultimate goal of the project is to decrease the total uncertainty to about 0.25%. To achieve this, two advances are necessary: 1) a significant increase in the detected neutron decay rate over that seen in previous years, and 2) measurement of the main sources of systematic uncertainty to prove that they are as low as originally thought.

In 2009, the project made considerable progress in both. The decay rate approximately doubled, compared to 2008, by improving the ratio of detected decays to incident UCNs. In addition, all the leading systematic uncertainties were studied and established to be sufficiently low. ("First Measurement of the Neutron β Asymmetry with Ultracold Neutrons." *Physical Review Letters* **102**:012301 (2009).)

As a result of the engineering run during 2009, when an additional three-million decay events were detected at the higher rates needed for the statistics of the final measurement, the UCNA project is positioned to achieve the world's best measurement of the A-correlation during the 2010 accelerator cycle.

Proton Radiography Facility

Introduction

Research Highlights

Proton Radiography Facility

Proton radiography (pRad) was invented at LANSCE. pRad uses high-energy protons to take movies of the dynamic behaviors of materials in extreme environments, such as implosions (Figure 1). pRad is a perfect example of an important advancement in both nuclear science and technology brought about by Louis Rosen's vision: that LANSCE be a unique facility where purely basic nuclear science research would be kept partnered with the practical needs and applications of national security.

The drive to develop pRad came from the nuclear weapons program's need to interrogate weapons materials and the materials interactions before, during, and after implosion. This knowledge is needed to better understand how nuclear weapons work, how well they will work in various contexts, and to support the Stockpile Stewardship Program.

In the absence of nuclear testing, which the U.S. voluntarily ceased in 1992, the U.S. sought new methods to interrogate nuclear weapons implosions. These methods use surrogate implosion assemblies to generate data to reduce the uncertainties inherent in current simulation codes, calculations, and computer models. LANSCE scientists recognized that the penetrating power of high-energy protons makes them an excellent probe for a wide range of materials. The ability of the LANSCE accelerator to produce multiple proton pulses, and in a wide range of timing sequences, meets the specific needs of studying diverse materials in dynamic experiments. Powerful magnets are used like focusing lenses to precisely manipulate the positively charged proton pulses (Figure 1). Each proton pulse produces one radiographic image; a series of images make a movie of the experiment. The invention at LANSCE of specialized cameras capable of capturing dynamic images of proton-probed materials makes it possible to take these movies.

In addition to providing movies of dynamic experiments (Figure 2), pRad offers other huge advantages for imaging. For example, pRad can obtain detailed images of experiments conducted in sealed metal containment vessels (Figure 3). The image location is far enough away from the interaction region that background noise from scattered protons is minimized, while explosives from the experiment do not damage the detectors. This characteristic is useful, for example, studying damage features in explosively shocked samples (Figure 4). The sealed vessel provides the safety needed to study shocked samples of hazardous materials such as beryllium and plutonium. pRad is also used to perform classified and unclassified experiments to determine equation-of-state (EOS) for high explosives (HE) and materials, damage and fracture, material properties of explosives, and hydrodynamics.

There have been more than 400 dynamic experiments performed since 1997. The pRad program began in 2004. On average, 40 experiments were performed in 2007, 2008, and 2009 (Figure 5). Two-thirds of these experiments are related to weapons physics and one-third study specific weapons engineering issues or enhance the pRad measurement capabilities.

The invention of imaging proton radiography at Los Alamos (pRad) is the direct result of the synergy between defense mission and basic science research scientists at Los Alamos. The penetrating power of high energy protons, like that of x-rays makes them an excellent probe of a wide range of materials. But the incredible efficacy and versatility of pRad stems from the ability to produce multiple proton pulses in an accelerator and use magnets to manipulate the proton beam. The LANSCE accelerator meets the specific needs of each experiment by providing a wide range timing sequences for the proton pulses in the beam. Each proton pulse results in one radiographic image; a series of images make a movie. In this picture, the proton beam enters from the left-hand side.

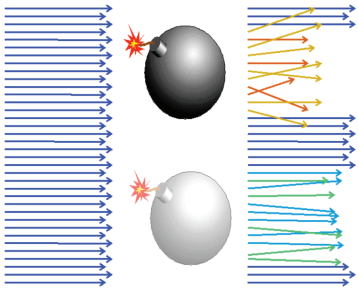

The interaction region is in a containment vessel specially designed to withstand the explosions that occur during experiments. Here, protons pass through the test object. This schematic illustrates (in an exaggerated manner) that protons transversing thicker or denser parts of the object lose more energy and are deflected more than those passing through thinner parts.

Strong magnets are used as lenses for the proton beam. In this picture, the magets are the orange blocks—four magnets with drift regions make up one lens that images the interaction region. This imaging process gives protons huge advantages over x-rays for imaging: The image location is far enough from the interaction region that background noise from scattered protons is minimized and explosives from the experiment do not damage the detectors. Different lens configurations can be used to magnify the view—3x and 7x magnifiers have been built and used at LANSCE. Highly radioactive objects can be imaged without their radiation "fogging" the image.

Figure 1. Proton radiography facility.

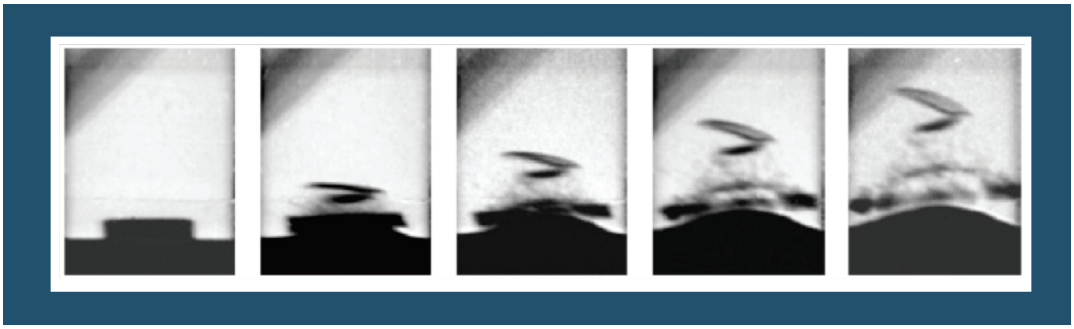

Figure 2. A time series (movie) of radiographs of tin that can be used to compare its behavior to model predictions. In this series, the proton beam enters from the left-hand side. The penetrating power of protons makes this type of imaging possible.

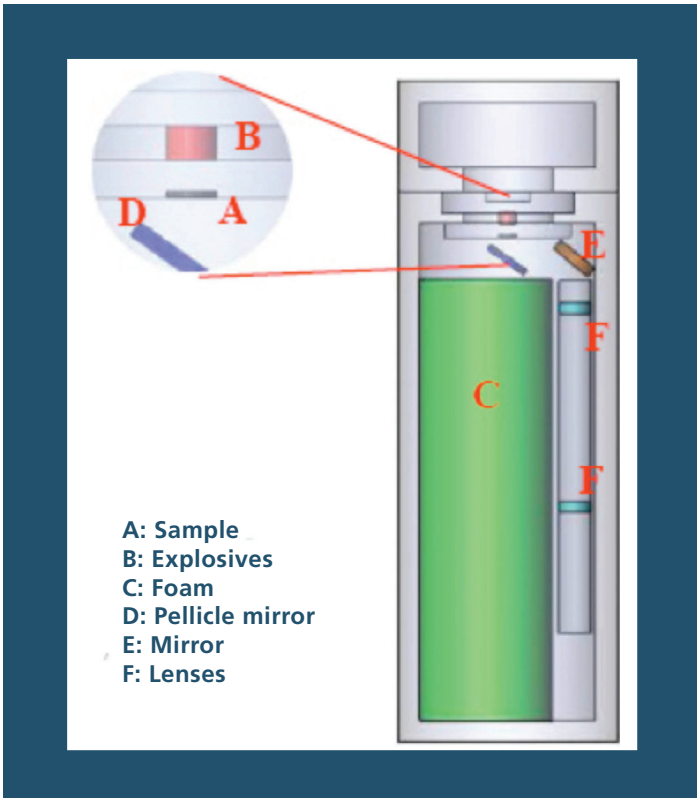

Figure 3. Schematic showing a sealed metal containment vessel designed to catch the shocked sample in foam for later metallographic examination. This vessel also allows for optical velocimetry of the front surface of the sample.

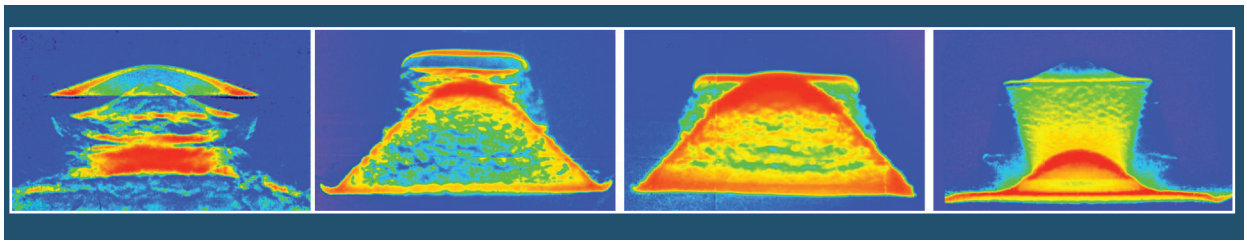

Figure 4. A series of proton radiographs of disks (left to right) aluminum, copper, tantalum, and tin that have been explosively shocked from below. The radiographs reveal the internal structure of the materials in these extreme conditions. For example, the aluminum sample shows the formation of layers of spall while the tin sample displays characteristics of melting.

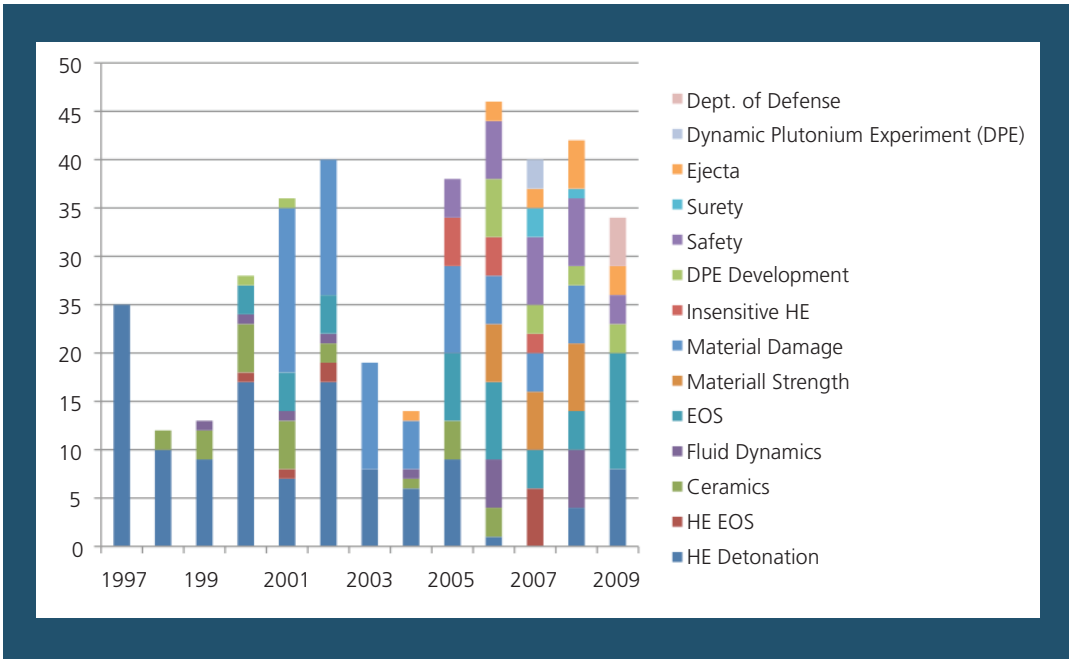

Figure 5. The diversity of the types of pRad experiments is increasing. Currently, about 40 dynamic experiments are performed each year.

Key highlights during 2007–09 include the following:

- In 2007, the team started an effort to improve the proton beam alignment. By 2009, the alignment was significantly improved, leading to improvements in imaging resolution (Figure 6).
- The program developed an improved camera technology, "Camera on a Chip" Figure 7). Camera on a Chip is a 2-cm x 2-cm hybrid chip; a combination of a microelectronic chip having a 720 x 720-pixel array of silicon photosensors, together with a metal-oxide-semiconductor (CMOS) chip having a corresponding array of control-and-processing circuits. Together they achieve a performance far exceeding that possible with either of those technologies alone. It has light-detection (quantum) efficiency of greater than 90% from 450 to 650 nm, a minimum exposure time of 50 ns, and a minimum interframe time of 300 ns. The camera can be triggered to capture frames at the times of greatest interest during a fast event or an event with changing time scales. It also stores three frames "on-chip" and is relatively insensitive to the stray radiation normally present in radiography experiments. It gives scientists a single sub-microsecond imaging tool. This achievement won an R&D 100 award in 2007.
- The electronics controlling the timing and firing system were upgraded to a modern, simple, and easier to maintain programmable-logic-chip-based system (Figure 7). The new system eliminates days of maintenance down-time that had previously plagued the program. The new system was designed and built in 2007, tested in 2008, and implemented in 2009.
- A new confinement vessel is in design to do future plutonium experiments.
- Increased operational experience is improving efficiency and data quality. For example, the number of days needed to prepare a shot has decreased from approximately six in 2005 to less than 3.5 in 2009 (Figure 8).
- Due to improved capabilities, the demand for access to pRad is twice what pRad can provide; with additional funding the program could double in size.
- The diversity of the types of pRad experiments is increasing (Figure 5).

Figure 6. Improvements to pRad's proton beam alignment, and thus its imaging resolution, were made between 2007 and 2009. Note the improved beam alignment in these images.

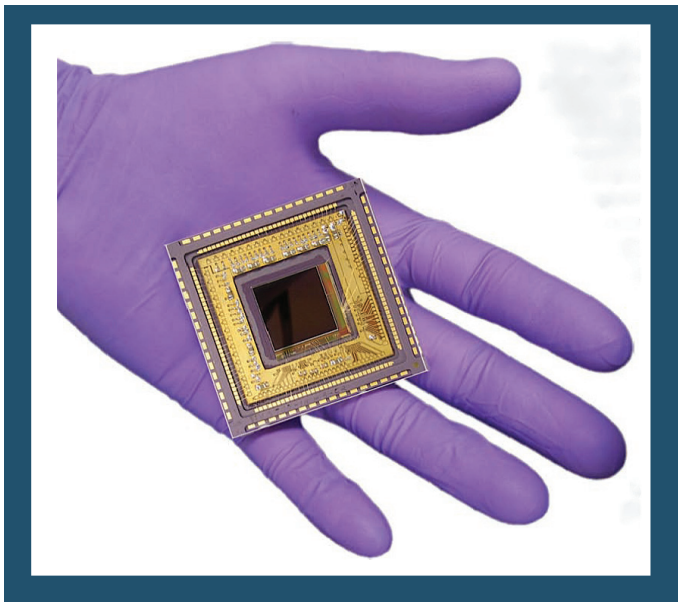

Figure 7. The pRad Camera on a Chip that won an R&D 100 Award in 2007.

Visualizing bubble distributions in mercury flow with proton radiography

When fully operational, the Spallation Neutron Source (SNS) at Oak Ridge National Laboratory will be the most intense pulsed neutron source in the world with a proton beam power of greater than 1 MW. To handle these power levels and maintain good neutron production efficiency, the SNS team adopted the concept of a flowing mercury target. Such a design reduces the stress on the target material, but raises issues about the integrity of the mercury container. Experiments at the Weapon Neutron Research (WNR) facility at LANSCE using the intense pulsed beam from the Proton Storage Ring (PSR), show that the beam pulse creates a shock in the mercury and causes

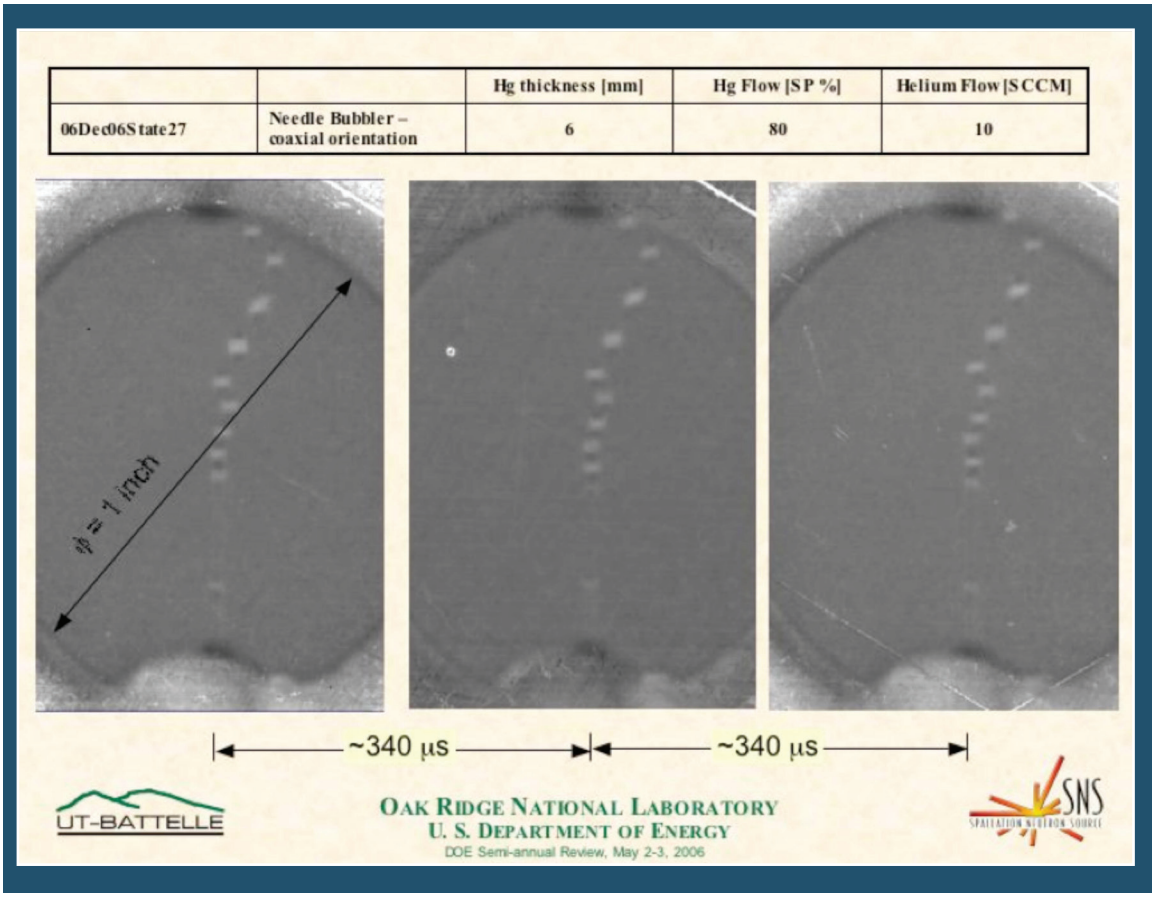

Figure 1. Three frames from a movie of bubbles streaming out of a needle in the flowing mercury. The bubbles originate about mid-frame. The image is looking through 6 mm of mercury and the field of view is approximately 0.7-in across by 1.2-in high. The bubbles are approximately 1 mm in diameter. As noted on the slide, the frames are separated by 340 μs. The bubbles are moving at approximately 1 m/s.

cavitation that erodes the walls of the target container. This cavitation damage erosion (CDE) may limit the lifetime and power level of the SNS target.

One strategy being pursued to reduce CDE is the pre-beam introduction of small gas (helium) bubbles that could absorb and attenuate the pressure pulse. Previous in-beam experiments at WNR with bubble injection succeeded in reducing damage, but the degree of reduction was unsatisfactory. Acoustic and x-ray radiography techniques used at the time to assess the generated bubble population failed to determine whether the desired bubble population goal was achieved prior to irradiation. The goal of the pRad experiment was to visualize the generated bubble populations under a range of mercury flow and gas injection rates, and to ultimately quantify these populations to compare performance.

The test conditions included the same operating parameters as used in the WNR tests; therefore, observed damage results may now be correlated to the introduced bubble population. Test conditions also included the use of single-needle bubblers directly in the beam object region. Data from these radiographs will be valuable in benchmarking two-phase-computational-fluid-dynamics simulations and first-principles predictions for bubble production.

The needle bubbler tests were motivated from the SNS collaboration with the Japan Proton Accelerator Research Complex/Japan Spallation Neutron Source project in Japan.

More than 400 radiographs and several movies imaging the dynamic flow of the bubbles in the flowing mercury were taken during the pRad experiment. Bubbles could be seen in these test conditions (Figure 1.) The smallest observed bubbles were between 200- and 300-μm in diameter, while some of the larger bubbles were 3 or 4 mm.

A preliminary analysis of images from one condition indicated a total gas-void fraction of about 1%, which was larger than expected. This estimate did not include bubbles smaller than the 200-μm detectable limit, which are the most important bubbles for absorbing an intense beam pulse and reducing damage. Nevertheless, the data obtained are vastly more detailed than any prior bubble diagnostic, and its interpretation has advanced this important line of CDE mitigation R&D. Complete analysis and quantification of the populations will be done at SNS.

The SNS experimenters are encouraged by this success and are considering various follow-up tests at both pRad and WNR. Further development of the pRad 7x magnifier might enable bubble visualization to sizes below 100 μm. Including fiducial points in the object region of fixed density that would enable void fraction estimation from bubbles below the spatial resolution limit. Improved bubble generators and concepts for gas-wall-mitigation (another approach to reducing CDE) might also be investigated in the future. pRad could also be a valuable tool to benchmark acoustic or other laboratory diagnostics.

Proton radiography makes over-constrained measurements of the equation-of-state in shock compression experiments

The pRad program has developed a new radiographic technique using multiframe 800-MeV pRad to measure over-constrained equations-of-state for shock-loaded samples. By synchronizing the 800-MeV proton beam pulses to a coupling between a 40-mm-bore powder gun and the pRad system, quantitative, real-time measurements of shock wave and particle velocities, as well as shocked and unshocked material densities, were measured directly from the multiple-time radiographs. Results for aluminum and copper symmetric-impact experiments were obtained (Figure 1). Measured density values lie on Hugoniots (Figure 2).

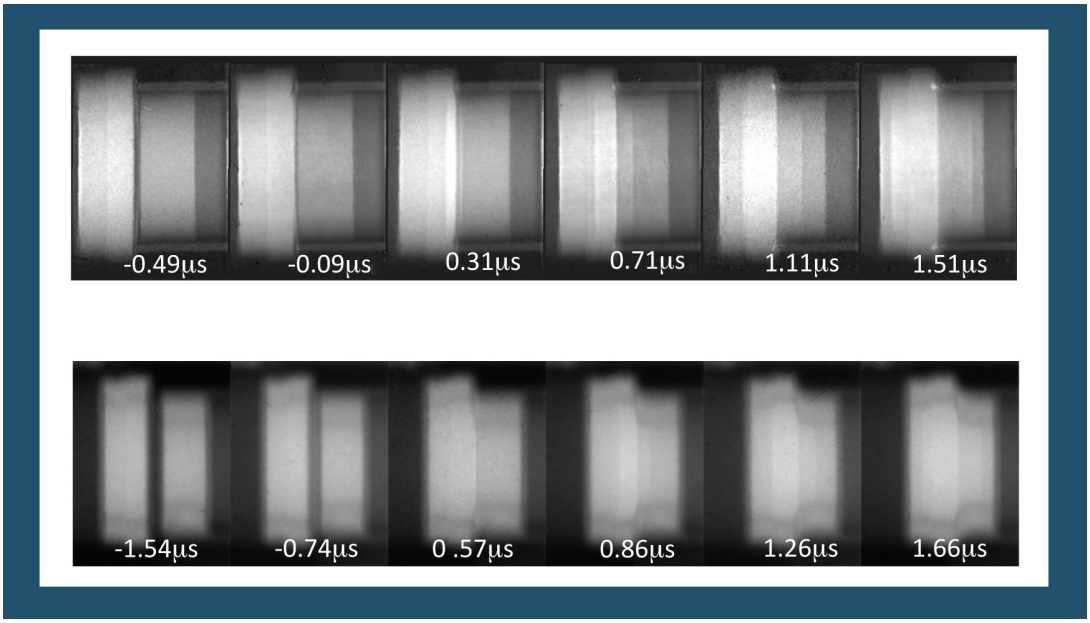

Figure 1. Top: Radiographs of the aluminum flyer approaching from the left and impacting an aluminum target. The shock wave can be observed progressing over time. The edges of the flyer and the shock front can be determined to within 30 μm. The change in density behind the shock front causes a change in contrast, which is then quantified as a density value in the material to within 1% of the accepted value. Bottom: Similar radiographs for copper.

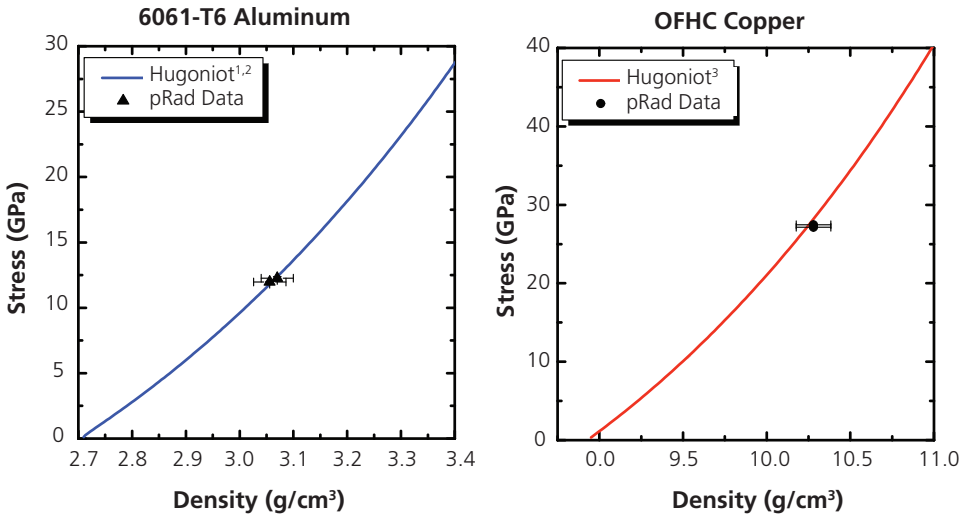

1. C. D. Lundergan and W. Herrmann, J. Appl. Phys. 34, 2046 (1963).
2. W. M. Isbell and D. R. Christman, Tech. Rep. MSL-69-60, General Motors (1970).
3. R. G. McQueen, S. P. Marsh, J. W. Tayor, et. al., High Velocity Impact Phenomena (Academic Press, New York, 1970).

Figure 2. Measured density for aluminum and copper lie on Hugoniots.

Dynamic proton radiography experiments study plutonium damage

A series of six pRad experiments were completed at LANSCE to study the damage evolution of small samples of plutonium driven by small quantities of high explosives. These experiments were an extension of the Thermos series of experiments previously fired at the Nevada Test Site. Three dynamic experiments were performed as confirmatory experiments in preparation for the plutonium series. Early-time dynamic radiographs from one confirmatory experiment, in which a lead sample was used, are shown in Figure 1. These radiographs were collected at 200-ns intervals and divided by a static radiograph to compress the dynamic range for display purposes. In these radiographs the expanding high-explosives products can be seen as well as the resulting shock passing through the lead sample.

Late-time dynamic radiographs from the same event are shown in Figure 2. In this series of radiographs, the damage process formed multiple spall layers in the lead sample. The lead and plutonium samples were stopped in a foam recovery system for post-shot analysis of the damaged material.

Surface velocities of each sample were also measured in these six experiments using VISAR and photon Doppler velocimetry. These data provide a fully diagnosed set of dynamic experiments for comparison to model predictions. Scientists expect to learn valuable information about the dynamic damage evolution of plutonium from the radiographs and velocimetry, in combination with results from the post-shot studies of the damaged materials. This new capability will provide new insights into the dynamic properties of high-explosives-driven materials of interest to the weapons program.

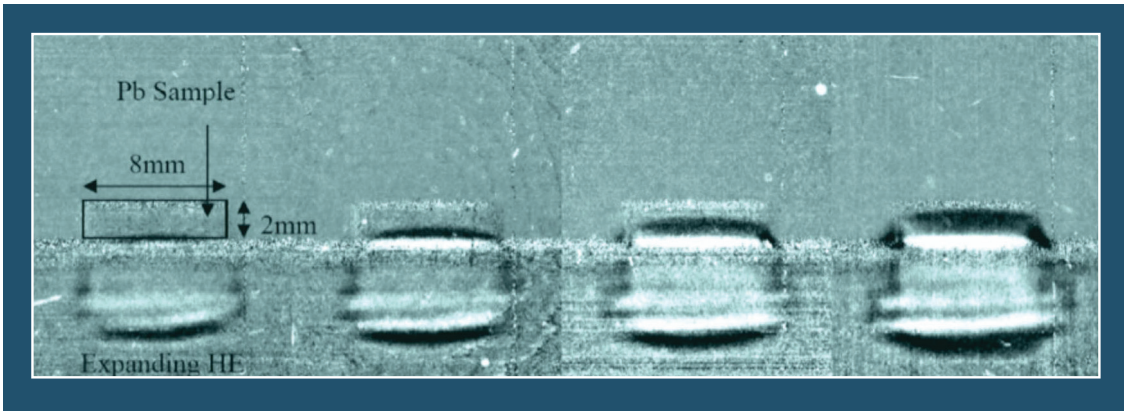

Figure 1. Early-time dynamic radiographs, divided by a static radiograph, collected at 200-ns spacing, showing the expansion of high explosives and the resulting shock traversing the lead sample.

Figure 2. Late-time dynamic radiographs of the same event as shown in Figure 1, showing the damage evolution of the lead sample.

Proton radiography richtmyer-meshkov instability experiments

pRad used to study experiments at LANSCE are Richtmyer-Meshkov instability formation and evolution in shocked tin. A Richtmyer–Meshkov instability occurs when an interface between fluids of differing density is impulsively accelerated, for example, by the passage of a shock wave. The development of the instability begins with small amplitude perturbations, which initially grow linearly with time, followed by a nonlinear regime (Figure 1).

The goal of these pRad experiments is to develop a physics-based ejecta model for implementation into LANL computational programs. Examination of the Richtmyer-Meshkovi instability into gases, as compared with a vacuum, improves the understanding of ejecta transport. When a high-velocity flyer plate impacts a stationary tin target, instabilities form in the tin as the shock wave releases on the backside of the target (the portion of the target that interfaces with either xenon gas or a vacuum).

pRad completed experiments of Richtmyer-Meshkov instability into vacuum and into gas (Figure 2). This work focused on studies of multiple-sinusoidal mode targets.

The study also includes an investigation of two mode targets to evaluate bubble saturation theory. The Richtmyer-Meshkov instability

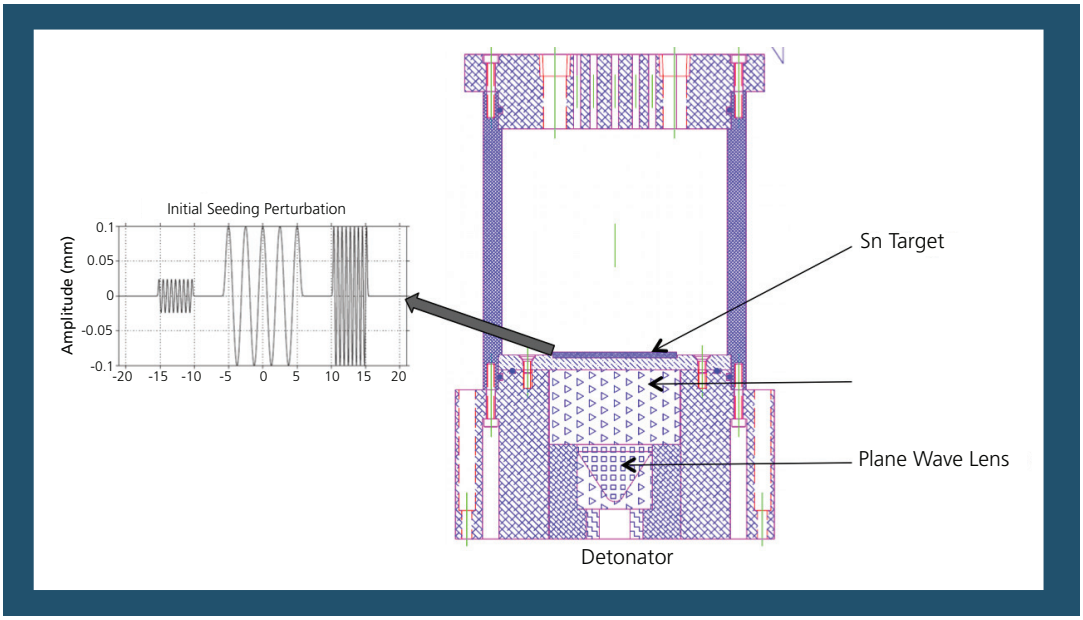

Figure 1. Left: experimental setup showing tin target. The development of the instability begins with small amplitude perturbations, which initially grow linearly with time, followed by a nonlinear regime.

experiments address transport, particle breakup, and bubble saturation. The United Kingdom's Atomic Weapons Establishment (AWE) has modeled one Richtmyer-Meshkov instability experiment. LANL is also modeling the experiments. Study tools include package modeling to inform experimental design, pRad, the Forest Flyer, and optical velocimetry. LANL collaborators from AWE and LLNL are interested in the experimental data and in modeling the data. AWE presented their results at the *International Workshop on the Physics of Compressible Turbulent Mixing Conference* in Santa Fe, NM.

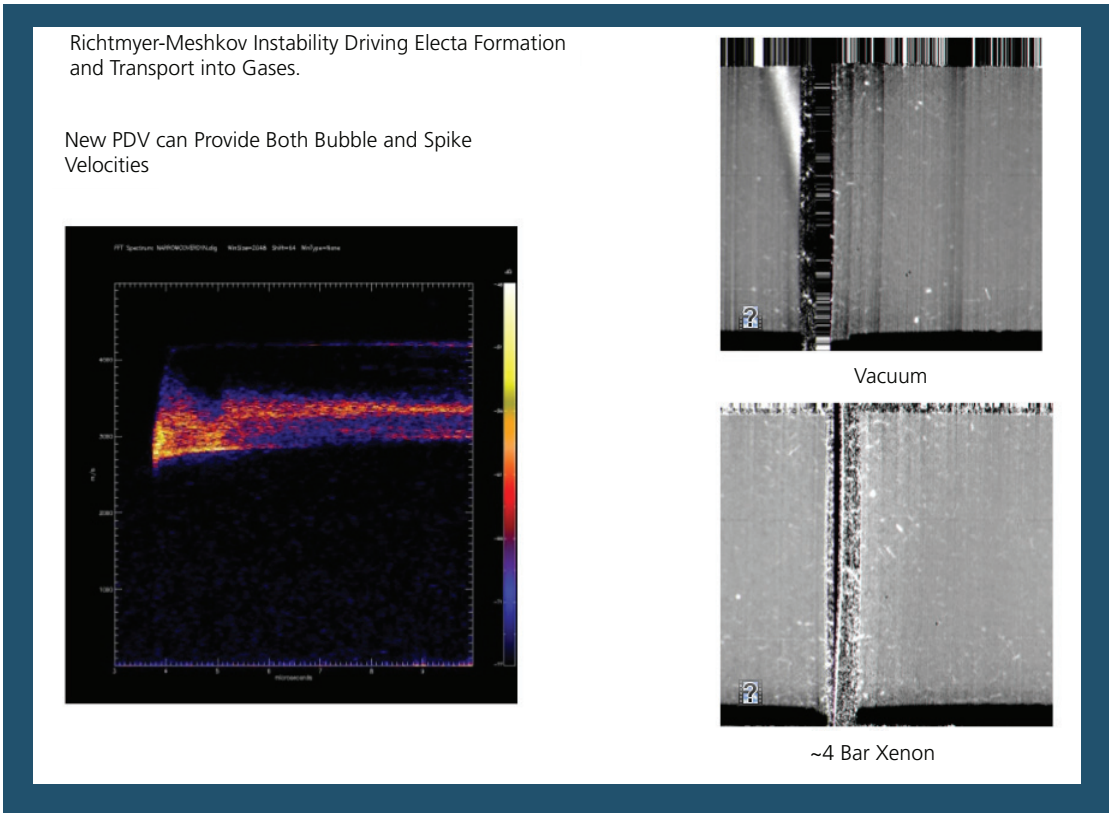

Figure 2. Richtmyer-Meshkov Instability growth into vacuum (above) and into gas (below).

High-explosive equation-of-state and dynamic material properties

High explosives are usually initiated with detonators, but it is important to understand the properties of explosives as they are heated, and when the temperature is high enough to cause a thermal explosion. The understanding of thermal explosions has been hindered, compared to that of detonations, by the difficulty of predicting the exact time of the event. pRad can illuminate the events at the center of a thermal explosion but requires the ability to control ignition time to within a hundred microseconds.

A technique has been developed for synchronizing a thermal explosion at the center of a heated explosive with hundred-microsecond accuracy at the end of a several hours of heating. The accomplishments required to achieve this technique included controlling the location of ignition and measuring the temperature at the ignition location. Once thermal runaway begins, synchronization is achieved by using a fiber-coupled laser to provide a temperature perturbation within the ignition volume. The pRad team used a convergent heating geometry, and a carefully chosen heat profiles to determine the ignition location, and then embedding a fiber optic at that location to provide the temperature jump (using a free-running YAG) to conduct the experiment. An image of the onset of burning in the explosive and subsequent case expansion were recorded. This allows a better understanding of thermal explosion and opens up the field of thermal explosion research to previously inaccessible diagnostics.

The quasi-static images taken during heating show that the volume expansion from the phase change is accommodated in the shot (Figure 1). From the dynamic images at ignition, it is possible to put together a model for burn propagation that includes cracking, convection, and conductive consumption of material.

The thermal explosion appears to originate at a hot spot and quickly propagates through cracks in the material. The material between the cracks then reacts more slowly (Figure 2). Figure 2 is a composite of two experiments showing the initiation of the reaction of the high explosive.

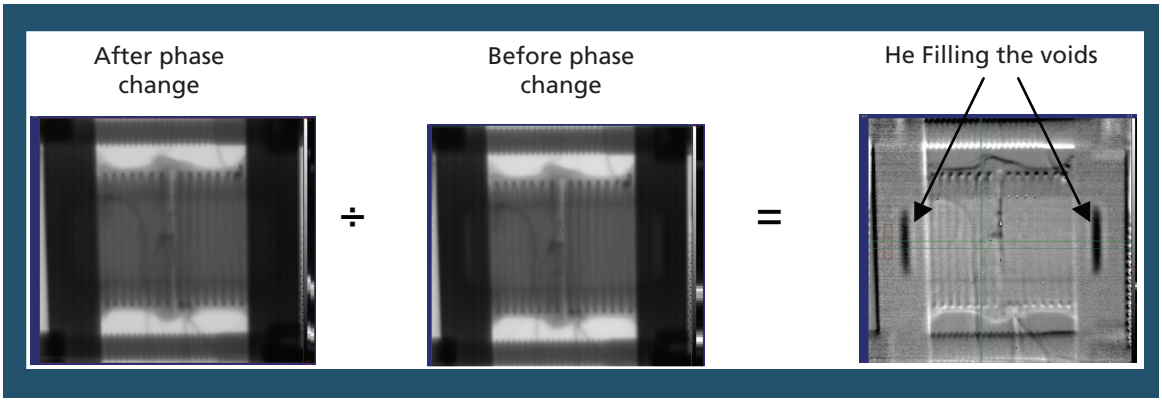

Figure 1. Cookoff experiments showing phase measurable phase change of high explosives during heating.

The relative offset in time has been established by looking at the metal motion in later time data. Figure 3 shows the proton transmission recorded along a diameter in the radial view. The data are normalized to one for transmission through the initial solid explosive and vertically offset to display proton transmission at different times.

Data from a sequence of 13 images are shown at 14 μs intervals starting at 2 μs subsequent to ignition. The solid lines are calculations of normalized density using a model of convective propagation of ignition and consumption by conductive burning. (*Physical Review Letters* **100**:228301 (2008).)

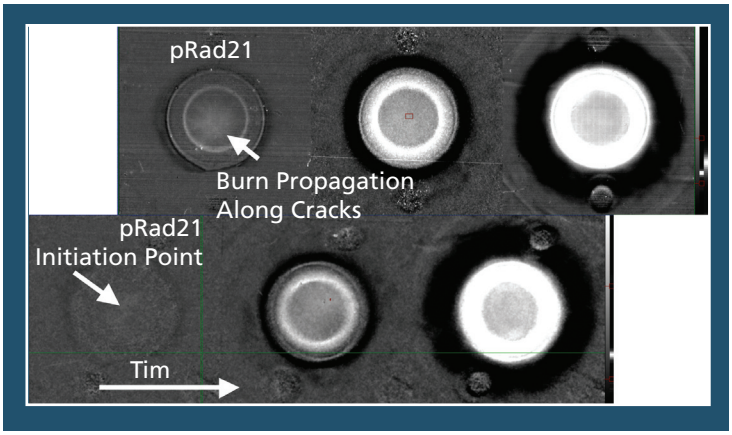

Figure 2. Two cookoff experiments (top and bottom) showing initiation of heated high-explosives along cracks.

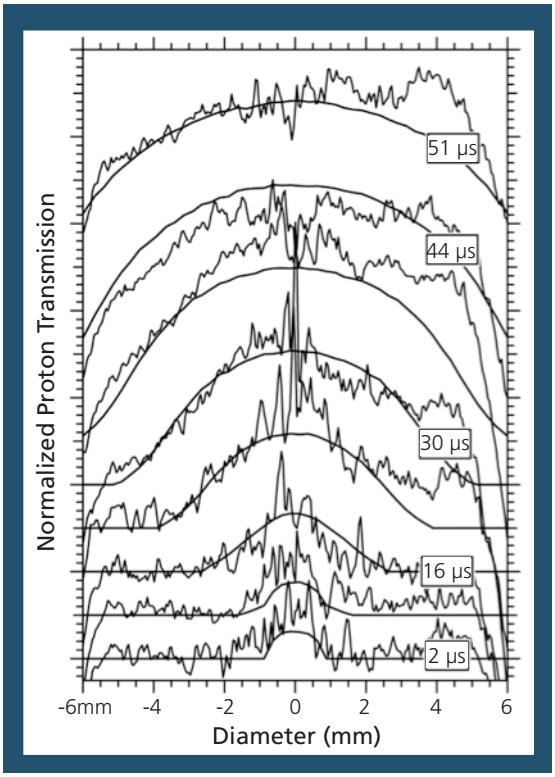

Figure 3. Proton transmission recorded along a diameter in the radial view. The solid lines are calculations of normalized density using a model of convective propagation of ignition and consumption by conductive burning.

Proton radiography makes computed tomography images of surrogate nuclear fuel rods

There is great interest in understanding the structural degradation mechanism of nuclear fuel rods under the extreme radiation and temperature conditions that exist in reactors. Such understanding will enable scientists to build better fuel rods and solve technical issues related to nuclear reactors.

Radiography is an important diagnostic tool to observe the degradation process of fuel rods. The pRad team, with other LANL collaborators, carried out computed tomographic (CT) imaging of surrogate fuel rods (sintered hafnia pellets). The sample was mounted on a goniometer and step-rotated in synchronization with the proton beam pulses to enable complete tomographic reconstruction (Figure 1).

Although the pRad magnetic imaging lens system was not fully optimized for this task, the resulting CT images revealed unexpected voids in the surrogate fuel rods (Figure 2). The team determined that relative-density measurements have less than 4% error. The use of more sophisticated CT reconstruction algorithms will improve resolution and determine small density variations.

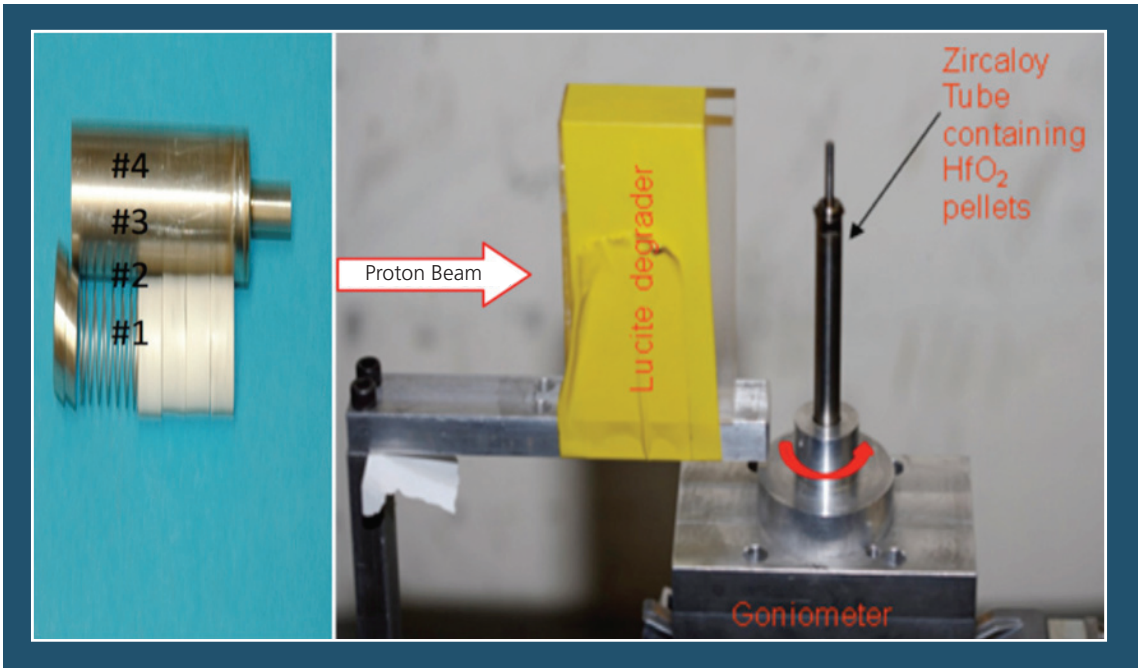

Figure 1. Left: four hafnia pellets and zircaloy tubing. Pellets #2, #3 and #4 were in the field of view of the pRad imaging lens. Right: photo of experimental apparatus. The zircaloy tube containing the pellets was rotated about its cylindrical axis. The degrader mitigates imaging blur from chromatics.

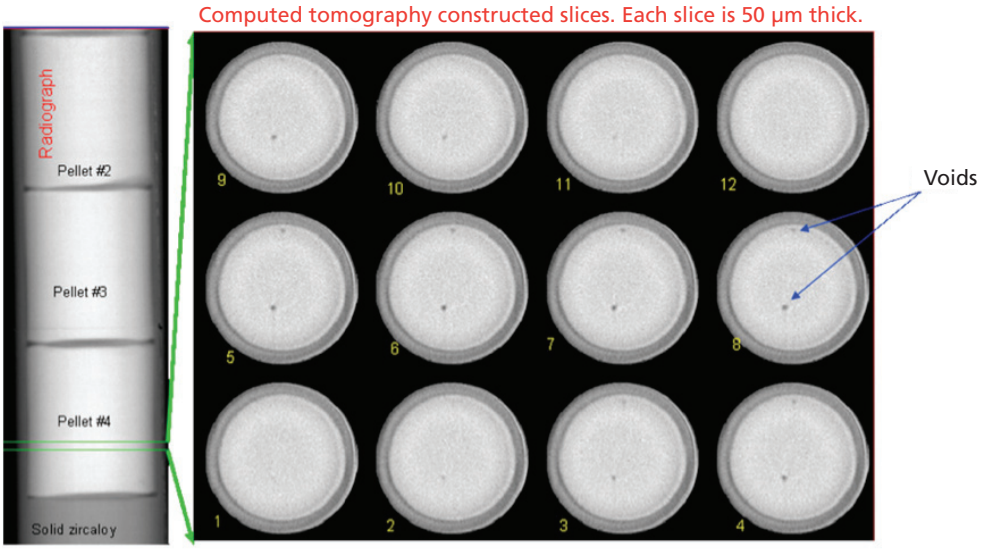

Twelve contiguous slices of a section of pellet #4 with voids at two locations. One of the voids has a diameter of ~225 μm and a length of ~450 μm. This is only one of several regions in pellet #4 with such voids.

Figure 2. Left: radiograph. Right: twelve CT reconstructed slices of 50-μm thickness. Contiguous slices of a section of pellet #4 reveal voids at two locations. One of the voids has a diameter of ~25 μm and a length of ~450 μm. This is only one of several regions in pellet #4 with such voids.

Material equation-of-state under shock-loading

B. Haight (Los Alamos National Laboratory)

Results of a series of dynamic experiments were published in late 2008 demonstrating the ability of 800-MeV proton radiography (pRad) to directly measure points on the Hugoniot with <1% dynamic density errors. These were the results of proof-of-principle experiments, placing points on the Hugoniot of well-known materials, copper and aluminum (Table 1 and Figure 1).

Since then further experiments have been performed studying material equation-of-state (EOS), focusing on solid-solid phase transitions. Figure 2 shows results from the alpha-epsilon phase transition in iron. The driving pressure of this experiment was designed to split the shock and phase transition waves, resulting in the two-wave structure shown in these radiographs. These results have been presented at various conferences and seminars and follow on work was performed in 2009 for publication in early 2010.

The work focused on EOS measurements on materials driven by a supported shock. More recently, experiments have been performed to investigate the potential for measuring EOS in materials driven by high explosives (HE), with the goal of identifying solid-solid and solid-liquid phase boundaries. Because of the high resolution and multiple pulse capability of 800-MeV proton radiography, the average shock velocity between radiographic frames and the density behind the shock discontinuity can be measured simultaneously. In a high-explosively-driven sample, the shock pressure decreases as it traverses the sample, allowing for multiple measurements of points along the Hugoniot.

A demonstration experiment was performed using this technique. In this experiment, a cylinder of high explosives was used to drive a Taylor wave shock into a tin sample. The series of radiographs from these experiments are shown in Figure 3, with the points along the Hugoniot-determined-through-density measurements and shock-velocity measurements from the multiple time-radiographs.

The development of these techniques is being refined on known materials in preparation for experiments on materials with unknown properties. Successful development of this technique will result in a single experiment capable of mapping out the Hugoniot from the peak pressure attainable with high explosives all the way down to nearly sound-wave velocities. (*Physical Review B* **77**:220101 R (2008).

Table 1. Summary of the experiments with the uncertaintes for each quantity shown in parentheses.

Experiment	Impactor/ Sample	Impactor Velocity (mm/μs)	Peak Stress (GPa)	Initial Density (g/cm³)	Calculated Density (g/cm³)	Measured Density (g/cm³)	Agreement
1	Al 6061-T6	1.452 (0.012)	12.27 (0.11)	2.710 (0.003)	3.067 (0.005)	3.070 (0.025)	0.1%
2	Al 6061-T6	1.422 (0.002)	11.98 (0.03)	2.710 (0.003)	3.060 (0.004)	3.056 (0.020)	0.1%
3	OFHC Cu	1.30 (0.04)	28.59 (0.91)	8.928 (0.003)	10.30 (0.05)	10.28 (0.08)	0.2%
4	OFHC Cu	1.249 (0.002)	27.16 (0.06)	8.928 (0.003)	10.241 (0.006)	10.28 (0.08)	0.4%

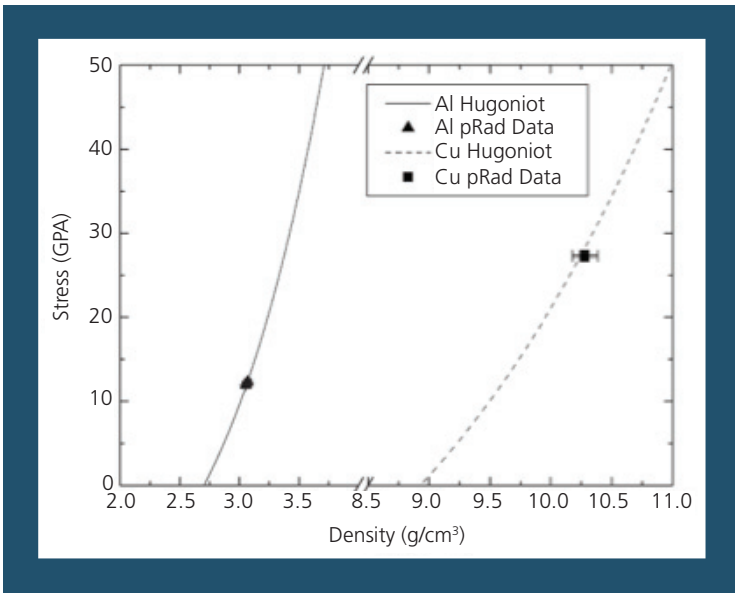

Figure 1. Results of proof-of-principle experiments demonstrating <1% density reconstructions from dynamic pRad experiments.

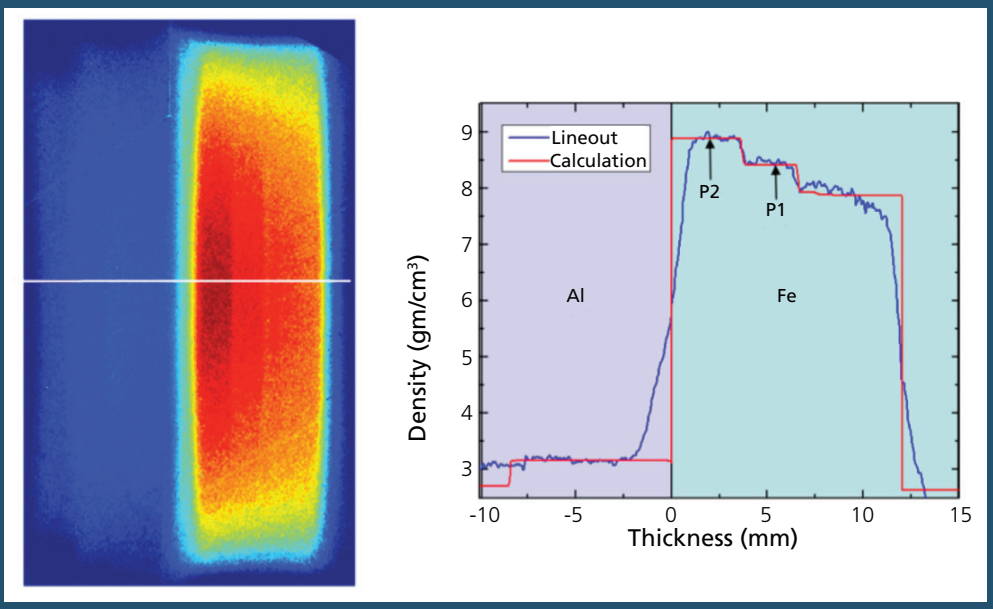

Figure 2. Left: color enhanced density distribution (red being the highest density) from a radiograph of an iron cylinder driven by an aluminum flyer, which was traveling from left to right. The leading density jump is the P1 wave and the second density jump is the phase transition or the P2 wave. Right: a lineout through the density distribution showing the agreement between model simulations and the radiographic density reconstructions.

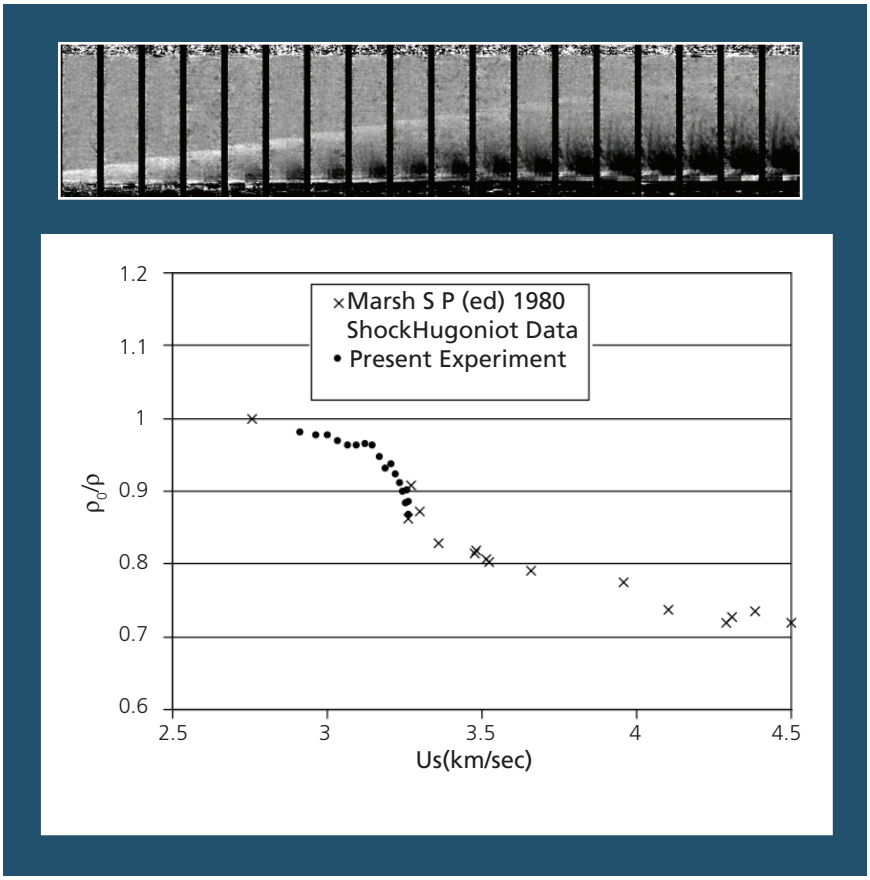

Figure 3. Top: multiple time radiographs of an HE-driven shock traversing a tin sample. The shock velocity between each radiograph, as calculated from a measurement of the leading edge of the shock and the inter-frame spacing of the radiographs. The density was inferred from the transmission of the radiographs.

Materials Test Station

Introduction and Updates

Project overview

Introduction

The U.S. Department of Energy (DOE) is developing technologies needed to reduce the quantity of high-level nuclear waste bound for deep geologic disposal. Central to this mission is the development of high burn-up fuel with significant inclusion of plutonium and minor actinides. Different fuel forms (for example, nitrides, oxides, and metal matrix) and composition are under study. The success of these materials cannot be judged until they have been irradiated and tested in a prototypic fast-neutron-spectrum environment.

LANL proposed a materials test station (MTS) to perform candidate fuels and materials irradiations in a neutron spectrum similar to a fast-reactor spectrum be built at LANSCE as one alternative to meet these mission needs. In 2005, Congress authorized funding for the design.

Mission

In fiscal year (FY) 2008, the DOE's Office of Nuclear Energy (NE) approved Critical Decision (CD)-0 for a Fast-Neutron Test Capability that defines the mission needs.*

To address the need for a domestic source of fast neutrons and to enhance nuclear science and engineering capabilities, the following mission needs must be met:

- A fast-spectrum neutron irradiation capability for the safe testing of advanced fuels and materials in an environment prototypical of fast spectrum reactors.
- A fast-neutron user facility to support university researchers and other DOE programs.

The MTS will comprise a spallation neutron source installed in an existing experimental hall (Area A), which is located at the end of the LANSCE linear accelerator (Linac) (Figure 1). Therefore, an experimental facility is available and ready for modification.

MTS, as currently conceived, will utilize a 1-MW proton beam from the Linac to generate an intense neutron flux with an intensity that is one-third to one-half that of the world's most intense research fast-reactors (Table 1).

When completed, MTS will offer the nation the only fast-spectrum irradiation capability in North America and Europe. In addition, researchers would not have to rely on securing and paying for irradiation time at foreign reactors. MTS will have lower capital costs than building a domestic fast-reactor, come on-line significantly sooner than building a domestic fast-reactor, and would fill the gap by doing critical research in the absence of a domestic fast-reactor.

MTS could be operated as a National User Facility and contribute significantly to the education and training of new generation of nuclear engineers and scientists. Most importantly, MTS will support research and development of vital closed-proliferation-resistant nuclear fuel cycles.

The proposed MTS is unique among fast-spectrum irradiation facilities in that the source of neutrons is not fission, but rather spallation. The facility is driven by a high-power (1 MW), medium-energy (800 MeV) proton beam, which produces neutrons through nuclear interactions with tungsten nuclei. About 15 neutrons are produced for every proton incident on the tungsten target. When properly configured, a

*Memorandum from D. Spurgeon, DOE-NE, to P. Bosco, DOE-OECM (28 November 2007).

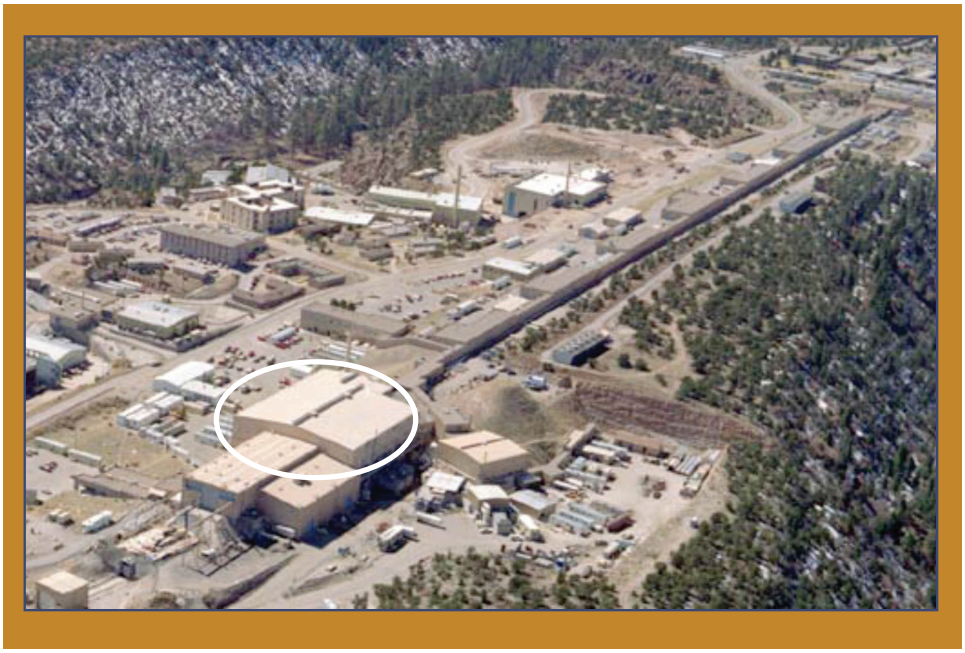

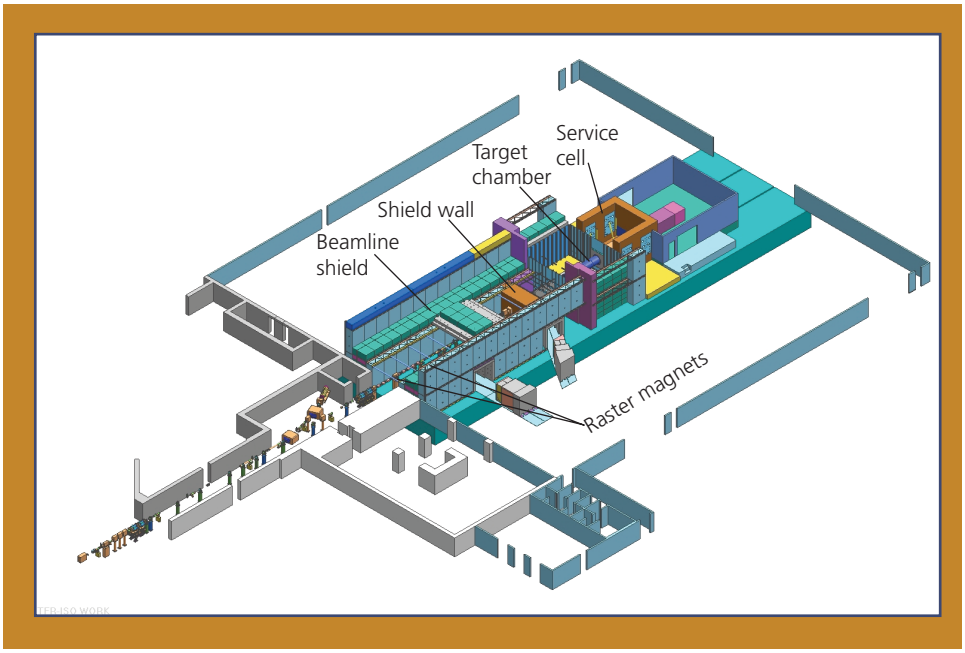

Figure 1. Top: A photograph of Area A, which is located at the end of the LANSCE linear accelerator beamline. Bottom: A schematic of the physical layout of the MTS in Area A. The beam-raster system paints a uniform beam exactly on the target. Independent fuel rodlets and multiple sample-cans allow different samples and configurations and short or long-term irradiations. Irradiated samples are transferred to shipping casks in the service cell.

Table 1. MTS Flux Level Approaches the World's Most Intense Research Fast-Reactors.

Facility	Peak Fast Flux (10^{15} n/cm^2/s)	Peak Annual Fast Fluence* (10^{22} n/cm^2/y)	Peak Annual Displacement Rate* (dpa/y)
MTS (USA)	1.3	2.1	17
BOR-60 (Russia)	2.8	4.6	24
JOYO	4.0	6.9	36

*Accounts for facility availability.

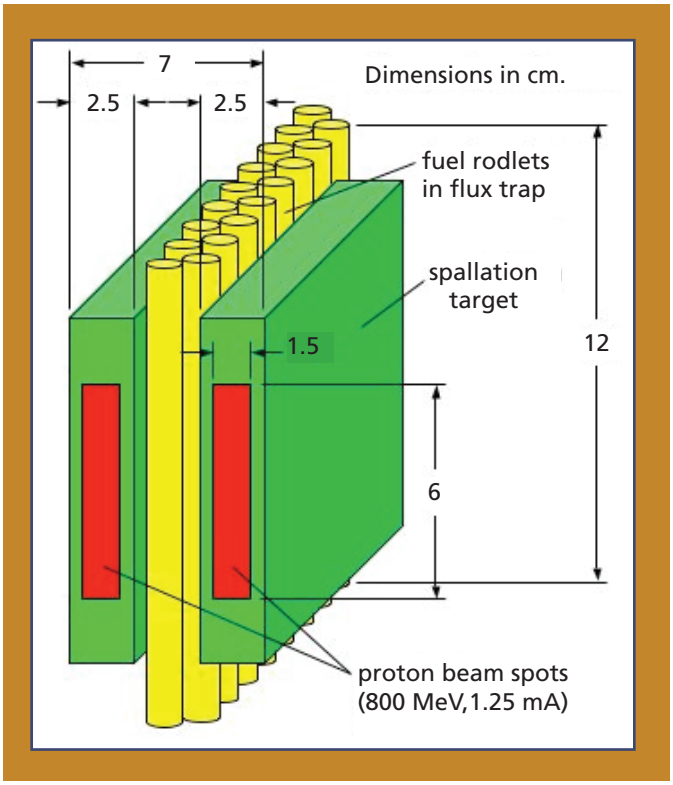

Figure 2. Basic concept of the MTS spallation target and fuel irradiation region.

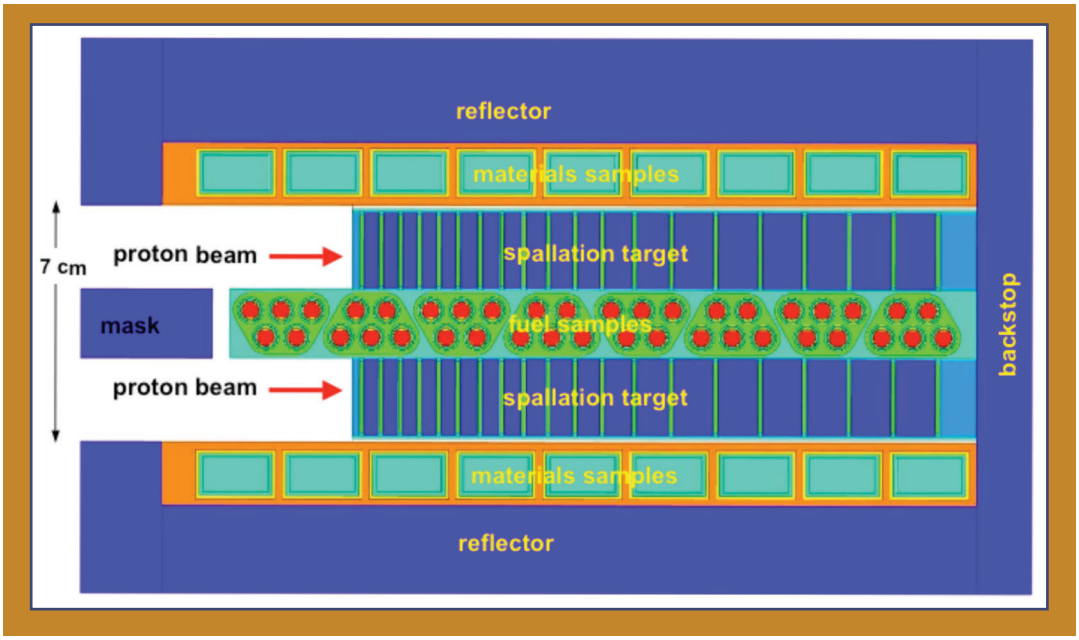

Figure 3. Horizontal cut through the target assembly.

1-MW proton beam can generate a fast neutron flux comparable to that of the world's most powerful research fast reactors. The irradiation volume is sufficient to accommodate several dozen 12-cm-high fuel rodlets, thus making it useful for testing nuclear fuels and cladding materials. MTS' capabilities will be sufficient to achieve 3.5% burnup per calendar year in highly-enriched fuel.

The target assembly (Figure 2) forms the heart of MTS. The target consists of two spallation target sections separated by a fuel irradiation region. The active fuel height of the fuel rodlets in the fuel irradiation region is 12 cm.

A horizontal cut through the target assembly is shown in Figure 3. The spallation target modules are comprised of a series of ever-thicker tungsten plates separated by 1-mm coolant channels. The coolant in both the spallation target modules and in the fuel module is lead-bismuth eutectic (LBE), which has a melting temperature of 125 °C. The primary motivation for selecting LBE to cool the fuel module is that it allows irradiation temperature of the fuel clad up to 550 °C. At temperatures over ~400 °C, active control of oxygen concentration in the LBE must be employed to control corrosion.

LANL has developed oxygen-control expertise through the operation of the Delta Loop; this experience will be applied to the design and operation of the LBE loops used in the MTS.

Lead-bismuth was recently demonstrated in a spallation target application in the successful MEGAPIE experiment at the Paul Scherrer Institute in Sweden. Two primary LBE loops are employed for cooling: one cooling the target modules and the other cooling the fuel module and backstop. The fuel module and spallation target modules share common sidewalls that allow active removal of decay heat from neighboring modules should either of the primary LBE loops fail during operation.

To provide nearly uniform neutron flux over typical pellet dimensions of 5-mm diameter by 5-mm

height, alternate macropulses of the proton beam are directed onto the two spallation-target sections. This design generates a time-averaged flux in the fuel irradiation region with a low gradient in all three transverse dimensions.

The beam pulse structure for nominal MTS operation will consist of 750-μs macropulses delivered at a 100-Hz repetition rate. A beam raster system, composed of a series of 10 magnets (up to 60-kHz raster frequency), delivers a time-averaged beam spot on each target section of nearly uniform 70-μA/cm^2 proton current density with dimensions 15-mm wide by 60-mm high (Figure 1).

The Linac is slated to undergo a major refurbishment that will assure stable and reliable beam delivery to the MTS. Once completed, the MTS is expected to receive 1.25-mA beam current for at least 4400 hrs annually.

MTS Accomplishments

FY07

- Received $3.8 M in funding. The MTS Mission Need Statement was updated and submitted to DOE-NE for review and approval.
- Significant progress was made on the pre-conceptual design of the MTS. LBE was selected as the coolant for the fuel and the spallation targets. A compact, five-pack structure was developed for holding the test fuel rodlets, allowing 40 rodlets to be irradiated simultaneously. The design mounts the target assembly and nearby shielding on a stalk with 40-in-diameter cross section that is extracted into a downstream service cell for servicing (Figure 1). The service cell walls and observation windows are sized to allow the target to be withdrawn from its operating position without a cool-down period following operation.
- An experiment was conducted to confirm that water could be used to cool the spallation target. The experiment confirmed the thermal hydraulic conditions sufficient to accommodate the design level heat flux of 600 W/cm^2.
- DOE-NE approves CD-0 for a Fast Neutron Test Capability. MTS is identified as one option for meeting this mission need.

FY08

- The MTS conceptual design was completed and the Conceptual Design Report was started using carryover funding from FY07. Its completion awaits project re-start.
- A 40%-scale compact heat-exchanger was built and installed on the Delta LBE Loop to confirm the novel features of the MTS primary heat exchangers.
- The Preliminary Hazards Analysis (PHA) for the MTS (TA53-SB-PHA-113-007.R1) was completed and submitted to the DOE's Los Alamos Site Office (LASO) for review and approval.
- LASO reviewed and approved the MTS-PHA and issued a Safety Evaluation Report (SER-LANSCE-MTS.01 Rev 0).
- Under separate funding ($11.9 M), the Area A cleanout project was initiated to remove experimental equipment from the experimental hall where the MTS will be built (Figure 4). A subcontract to perform the cleanout work was developed, competitively bid, and awarded to Demco, Inc.

FY09

- Significant progress was made on cleaning out the Area A experimental hall. In all, 1,205 tons of activated steel shielding were removed, packaged, and shipped to LANL's Waste Disposal Facility at TA-54. Another 10,488 tons were removed and stored on-site. Saving this material for future use as shielding won the project a LANL Pollution Prevention Award. Another 213 tons of beamline components, some of them highly radioactive, were removed, packaged, and shipped to TA-54 for disposal.

Figure 4. Left column to right column showing a time-lapse series of photographs of cleaning out of Area A in preparation of MTS construction.

User Program

LANSCE user program

LANSCE's User Program ensures the research it oversees represents the cutting edge of nuclear and materials science and technology. The User Program plays a key role in training the next generation of top scientists, attracting the best graduate students, postdoctoral researchers, and early-career scientists (defined as those less than 40-years old).

The User Program typically begins the first week of May and continues through December 23.

The User-Program Advisory Committee (PAC) members have the difficult task of reviewing, ranking, and recommending the best research proposals. Researchers from universities, industries, and federal laboratories worldwide submit proposals in a tight, competitive review process. The demand for beam time far outstrips LANSCE's ability to accommodate all of the proposals received. PAC members reported that the quality of proposals during 2007–09 was excellent, making their job even more challenging, and exciting.

User Demographics

The User Program's demographics count user visits and unique-user visits. User visits are the total number of visits by all users. A unique-user visit is defined as counting a user only once—the first time they come to LANSCE during a calendar year. In 2007, together the Lujan Center and WNR facilities hosted 1098 user visits, in 2008, 1074 user visits, and in 2009, 1160 user visits (Figures 1, 2).

The institutional affiliations of the unique users of the Lujan Center and of WNR are shown in Figures 3 through 8.

Note the largest segment of unique-users at the Lujan Center came from the academic community; at WNR the largest segment of unique-users came from industry in 2007, but from academia in 2008 and 2009. The majority of the WNR industry users are from firms that produce or use semiconductor devices. The semiconductor industry relies on WNR's unique capabilities to test their latest generation of chips for resistance to neutron-induced upsets.

Student Training and Research at LANSCE

LANSCE actively encourages student involvement in neutron science research and has programs to provide training and financial assistance to conduct experiments. The Student Travel Opportunities for Neutron Experiments (STONE) program is part of this effort. The STONE program offers students up to $500 in financial assistance toward travel expenses, lodging, and meals. By providing instrument access, training, and economic support to student users, the STONE program broadens the user community. For more information contact the LANSCE User Program Office.

LANSCE Neutron Scattering School

The annual LANSCE Neutron Scattering School began in 2004. The main goal of the school is to provide in-depth neutron-scattering training to graduate students, in their early stage of thesis research, and to postdocs. A particular emphasis is put on selecting a diverse student body to foster a cross-institutional, cross-disciplinary, and multicultural learning environment. The school provides a combination of classroom lectures by subject matter experts from around the world, and hands-on experience in conducting neutron scattering experiments.

Louis Rosen Prize

The Louis Rosen Prize honors the student with the most outstanding Ph.D. or M.S. thesis

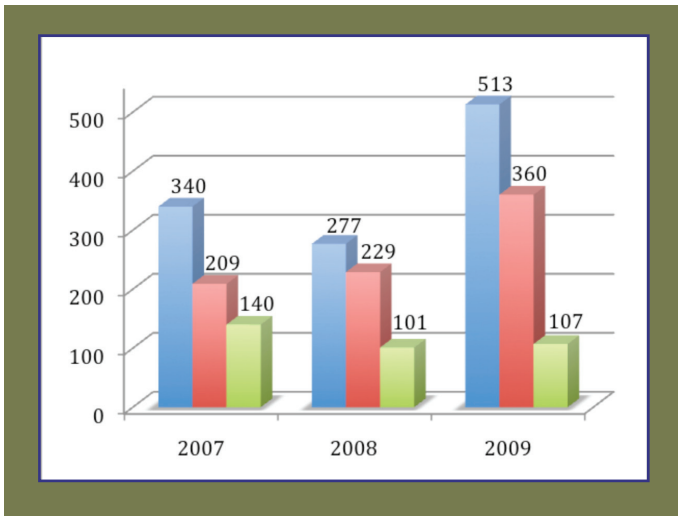

Figure 1. The user visits and unique-user visits to the Lujan Center from 2007–2009.

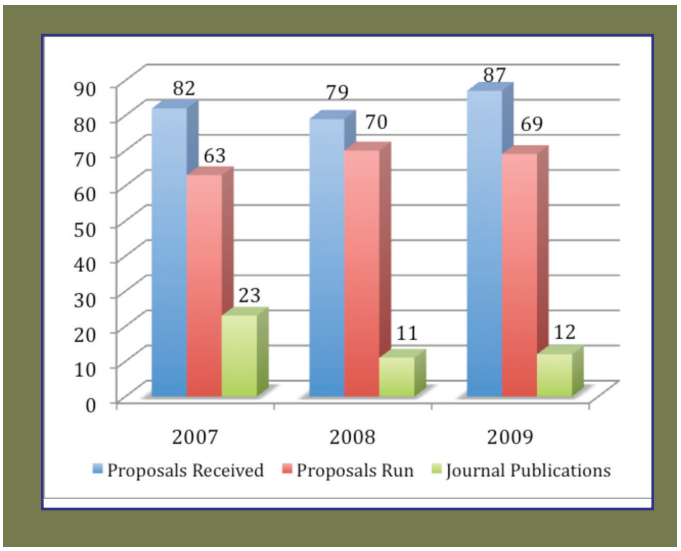

Figure 2. The user visits and unique-user visits to WNR from 2007–2009.

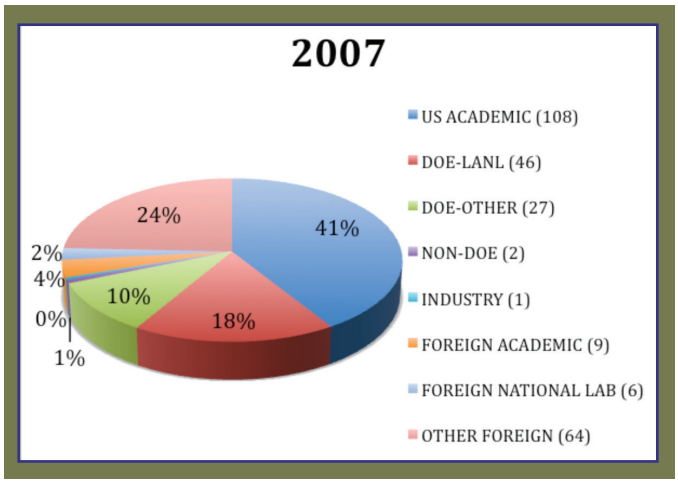

Figure 3. Institutional affiliation of the Lujan Center's unique-users in 2007.

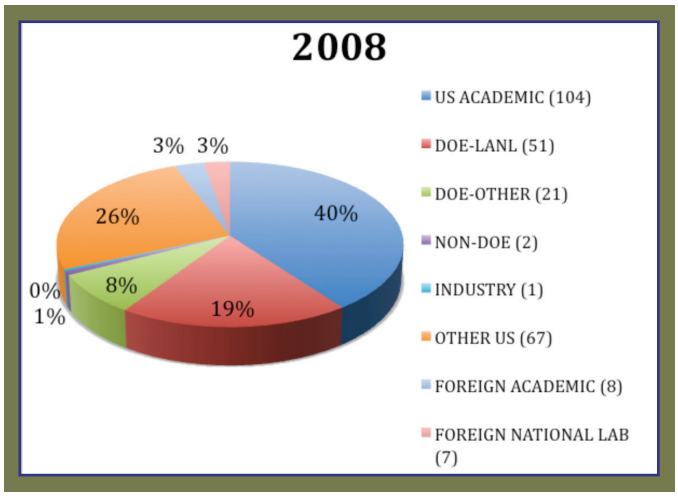

Figure 4. Institutional affiliation of the Lujan Center's unique-users in 2008.

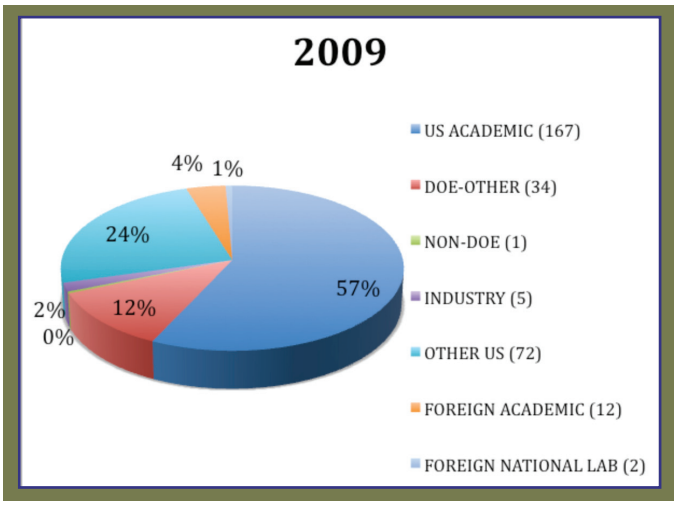

Figure 5. Institutional affiliation of the Lujan Center's unique-users in 2009.

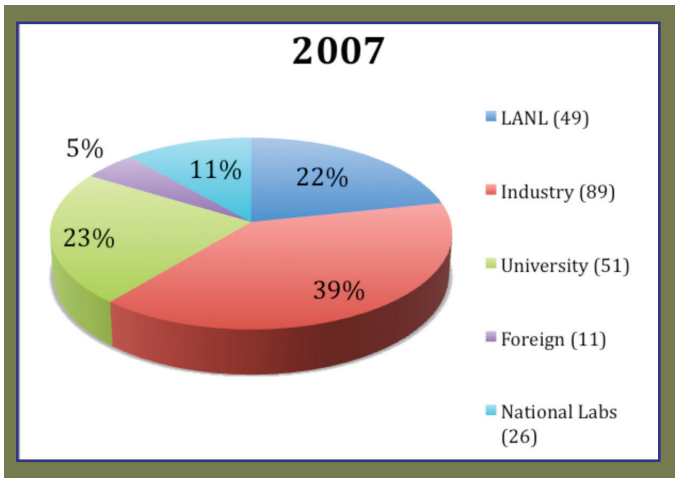

Figure 6. Institutional affiliation of the WNR's unique-users in 2007.

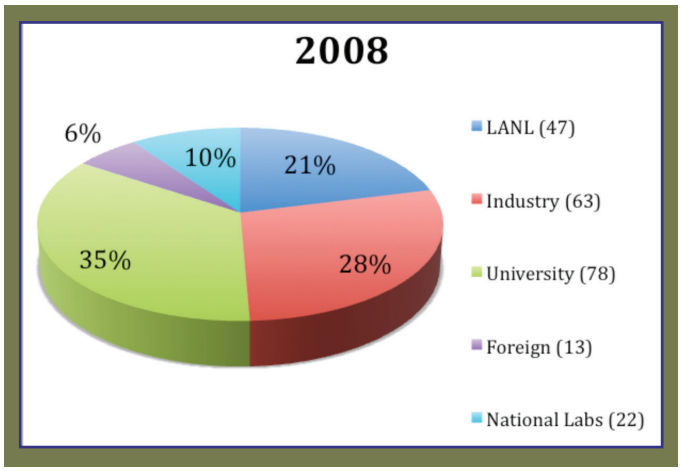

Figure 7. Institutional affiliation of the WNR's unique-users in 2008.

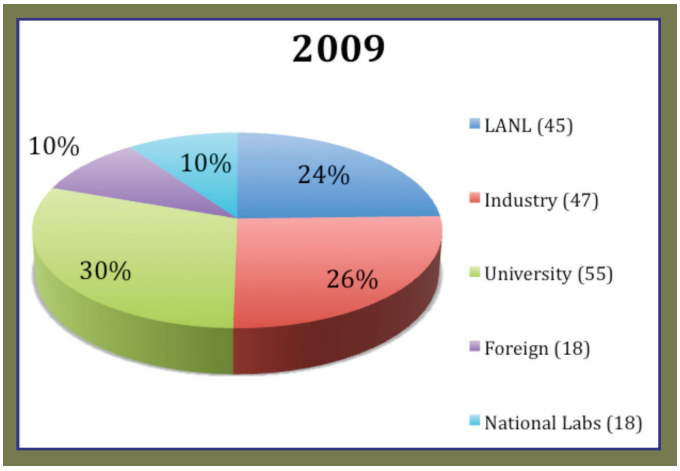

Figure 8. Institutional affiliation of the WNR's unique-users in 2009.

based upon experimental or theoretical research performed at LANSCE. Criteria include the originality and scientific impact of the research and the student's contribution to the research. The prize is $1000 and a commemorative plaque. For more information contact the LANSCE User Program Office.

Communicating with Our Users

Input from the user community is vital to continue to improve the user program. The LANSCE User Satisfaction Survey provides users the opportunity to comment about their User Program experience and to suggest ways to improve the user experience. All users are given the opportunity to complete the survey after completing their visit. The 2007, 2008, and 2009 survey results are summarized in Figures 9, 10, and 11. Note that overall the users are satisfied or very satisfied with the user program.

LANSCE User Group

The LANSCE User Group (LUG) is comprised of current users. LUG provides direct input to LANSCE management, primarily through LUG's Executive Committee. The LUG Executive Committee is comprised of twelve members; one member is a student or postdoctoral researcher. Committee members serve two-year terms (the student/postdoctoral member serves for one year). Membership terms are staggered to maintain continuity. The members are elected by the vote of the LUG membership, with candidates chosen to reflect the principle scientific activities at LANSCE.

The LUG Executive Committee and LANSCE management have monthly conference calls. These calls provide an opportunity for management to keep the Executive Committee apprised of the status of LANSCE activities

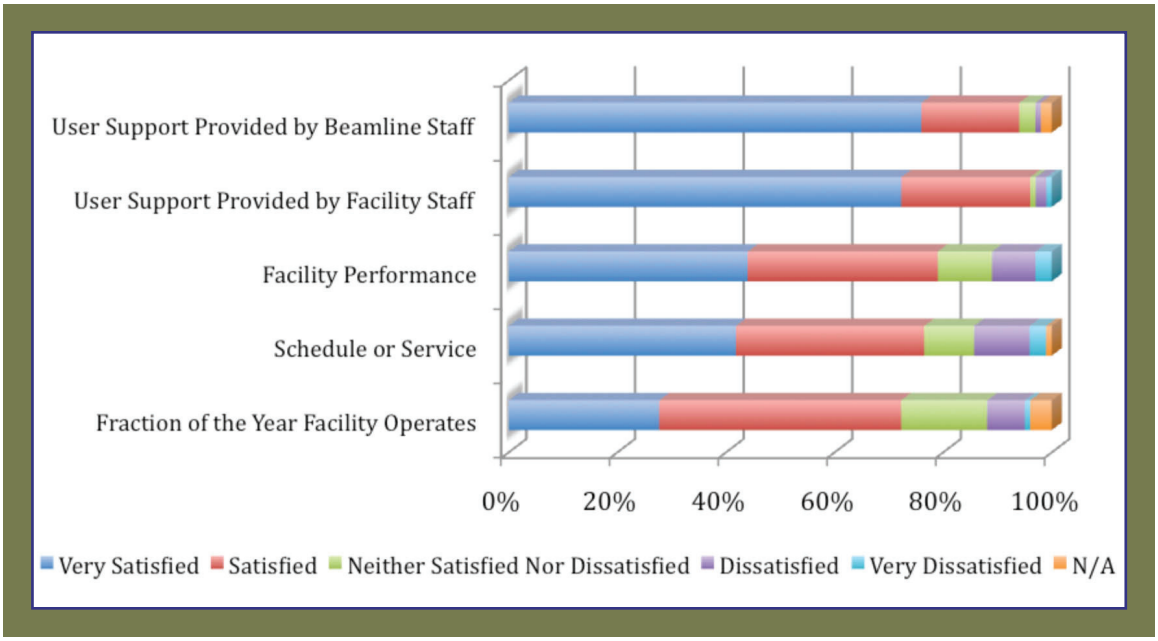

Figure 9. Summary of User Satisfaction Surveys for the LANSCE 2007 run cycle.

Figure 10. Summary of User Satisfaction Surveys for the LANSCE 2008 run cycle.

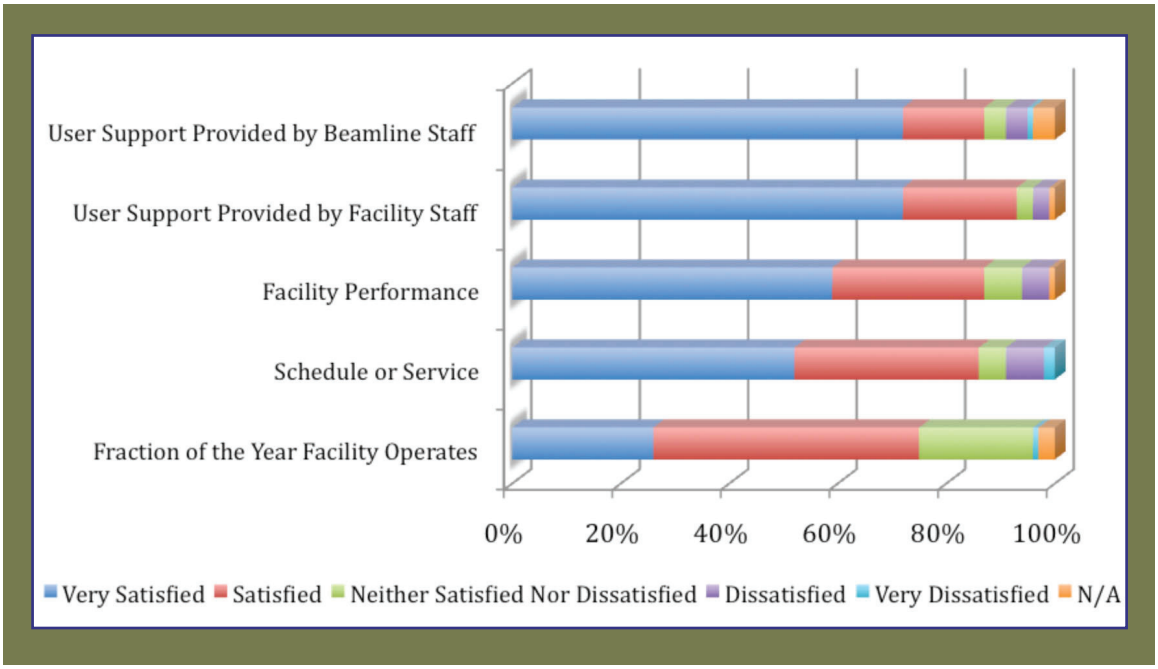

Figure 11. Summary of User Satisfaction Surveys for the LANSCE 2009 run cycle.

and for the Executive Committee to bring user issues to management's attention. The calls are also used to discuss strategies for the future of LANSCE facilities.

The LANSCE User Team

The LANSCE User Team is responsible for coordinating the users with LANSCE instrument scientist and the facility. Users contact the User Team weeks before they arrive at the LANSCE Visitor Center at Technical Area 53. Among there many responsibilities, the team issues the call for proposals, coordinates proposal experiment schedules, directs users to the training center, issues badges and dosimeters, helps to arrange tours of the facilities, handles the shipments of experimental samples, and assures that users paperwork is complete.

LANSCE User Team from left to right: Lisa Padilla, Leilani Conradson, Tanya Herrera, and Aundrea Espinoza.

The LANSCE User Group 2009 meeting poster. LUG provides direct input to LANSCE management, primarily throgh LUG's Executive Committee.

LANSCE neutron scattering school

Each summer the LANSCE Neutron Scattering Center School invites approximately 30 of the brightest future neutron scattering users to the Lujan Center for an intensive nine-day program of lectures and hands-on experiments in neutron scattering. The school topics rotate through a series of subjects for which neutron scattering is well suited and has made a major impact. The main goal of the school is to provide in-depth neutron-scattering training to graduate students in their early stage of thesis research, and to postdocs. A particular emphasis is put on selecting a diverse student body to foster a cross-institutional, cross-disciplinary, and multicultural learning environment.

The school is typically over-subscribed by a factor of two. A committee is charged with making the final selection based upon applications, which include a research statement and letters of recommendation. The National Science Foundation, the DOE's Basic Energy Sciences program, New Mexico State University, and LANL sponsor the school.

The first Neutron Scattering Center School was in 2004. The subject was Applications of Neutron Scattering to Magnetism. Subsequent subjects were Neutron Scattering and Structural Materials (2005), Neutron Scattering in Soft Condensed Matter and Structural Biology (2006), and Neutron Scattering Applications on Hydrogen in Materials (2007). In 2008, the school returned to the highly successful subject of Magnetism and Nanomaterials. In 2009, the subject was Phase Transitions.

The school draws from a wide spectrum of U.S. and foreign universities and institutions. Figure 1 shows the states and countries of origin for

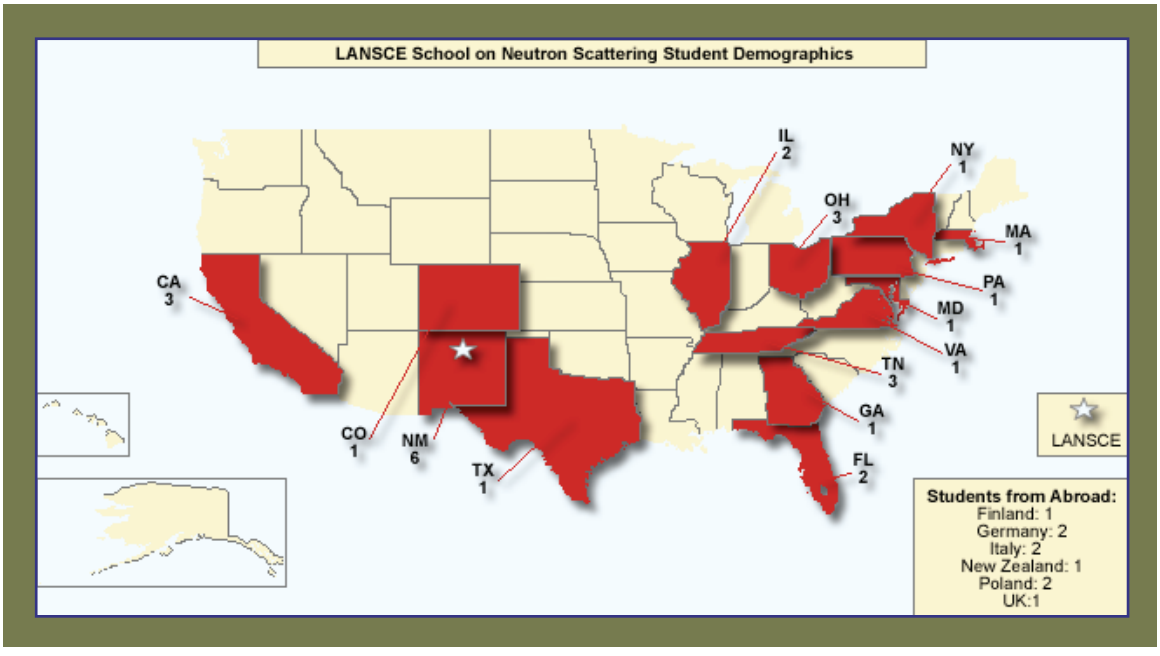

Figure 1. Student demographics of the LANSCE Neutron Scattering School.

a typical year. About 70-80% of the students do their thesis research at a U.S. university. However, typically only 40% (or fewer) are U.S. citizens. Women account for 25% to 30% of the students.

The school offers morning lectures by international experts in neutron scattering, followed by an afternoon of hands-on experiments using four or five of the Lujan Center's world-class neutron scattering instruments. The students analyze their data under the guidance of the Lujan Center's instrument scientists. On the final day of the school, the students assemble into groups and each group makes a formal half-hour presentation on the results of their research experience. These are professional presentations that are constructively reviewed by the school's faculty and the other students.

The students are accorded a day off on Sunday for an excursion to the famous archeological site Bandelier National Monument, or to some of the museums in nearby Santa Fe. An evening banquet is provided at the popular Pajarito Ski Hill.

Students and lecturers provide evaluations. These data are used to improve or modify the organization of future schools. On a scale of one to five, the students typically rank the question "Value to their professional future" as 4.7–4.8. A rank of 4.9 is usually given in response to, "Would you recommend this school to your colleagues."

Louis Rosen tutors a Scattering School student.

Class of 2007.

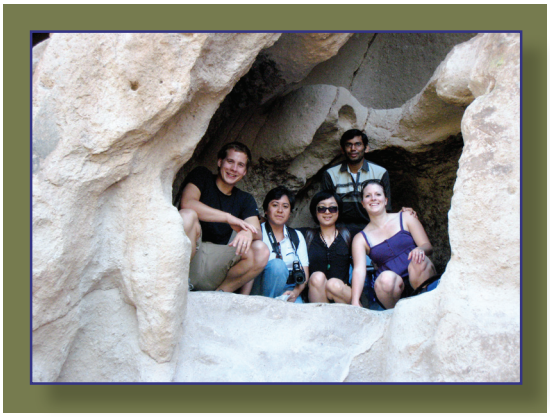

Students at Bandelier National Monument.

Students in class.

Accelerator Operations and Technology

2007-2009 Accelerator operations overview

J. Erickson and K. Jones (Los Alamos National Laboratory)

The Los Alamos Neutron Science Center (LANSCE) had three successful production runs during 2007–2009. Each year began in early January with the regularly scheduled accelerator maintenance period. Each outage was planned during the last quarter of the previous year. This both coordinates and levels personnel resources across selected major outage tasks. LANSCE uses project management tools to optimize work planning during the extended outages. Key projects and activities were assigned priorities. Accelerator, facility, and experimental area maintenance activities were completed within the allotted schedule.

After these extended maintenance outages and beam-delivery tune-ups, the accelerator facility is successfully returned to production status on or about May 1 of each year. Beam delivery to all experimental areas and the Isotope Production Facility (IPF) continues up until the holidays at the end of December.

The major factors contributing to reduced beam-availability during these years were difficulties with the 1L target hydrogen-moderator system, the 201-MHz amplifier systems, and site-power outages. Operations were continually challenged throughout these years because it was necessary to recycle the H^- source between scheduled maintenance periods due to shortened source-filament lifetimes.

Key Maintenance Activities in 2007

Due to resource availability, the 2007 outage maintenance was primarily limited to general repair and preventive maintenance for all accelerator systems. There were 398 maintenance activities completed in 2007. Maintenance activities focused on inspection, cleaning, and documentation of deficiencies, such as condition assessment. As funds were available for parts, line organizations responsible for systems made necessary repairs within the available budget. Major tasks completed during the 2007 outage include the following:

- Performed essential (Priority 1) accelerator, facility and experimental area maintenance.
- Completed extensive Accelerator Operations Manual (AOM) revisions.
- Integrated the AOM revisions with the Target Operations Manual (TOM).
- Reviewed and updated safety procedures and documentation.
- Successfully completed H^- ion-source development aimed at extending lifetime and improving source output.
- Installed new beam plugs and controls at Istotpe Production Facility (IPF).
- Replaced the coil on ring magnet SRBM11 using effective ALARA principles.
- Installed new access control systems (EPACS) on Weapons Neutron Research (WNR) flightpaths 15L and 60R.
- Facility and Infrastructure Recapitalization Program (FIRP) projects were assigned to Sector B (electrical), Sector M (water), and Building 7 (HVAC).
- Performed optional (Priority 2/3) accelerator, facility and experimental area maintenance.
- Developed and implemented a Safety Assessment Document and Accelerator Safety Envelope as required by *DOE Order 420.2B*.
- Revised and integrated the Accelerator Operations Manual and Target Operations Manual to incorporate all organizational changes, the conversion to *DOE Order 420.2B*

compliance, and the new roles of Area Managers and other key individuals.

- Repaired, in situ, the 1L Target TMRS to the extent possible with available technology and funds to extend the lifetime of the target.
- Made mechanical system improvements to the drift tube linear accelerator components.
- Improved the ready spare and in-service situation for 201-MHz final-power-amplifiers subject to delivery and satisfactory test-stand performance of new tubes from the vendor.
- Repaired water manifold leaks in the storage ring and on Module 40 in the accelerator.
- Repaired ring stripper foil actuators and replace ring stripper foils.
- Understood poor H^- ion source performance and developed a solution that permits delivery of 100 μA of average current at 20 Hz, 625 μs to the Lujan Center target with a source lifetime of four weeks.
- Procured a rebuilt inductrol voltage regulator (IVR).
- Installed IPF beam plugs as required by the Radiation Safety Committee.
- Designed and procured components for the 1L Mark III TMRS and establish staging space for assembly and testing.
- Completed scheduled FIRP projects, specifically Sector B water and power and MPF-7 HVAC improvements.
- Designed and procured components for an upgrade to the 1L target cooling water systems.
- Implemented new lock out/tag out implementation support documemt.

Key Maintenance Activities in 2008

There were 629 maintenance activities completed in 2008. These tasks were selected based on planning by the LANSCE User Facility Director, LANSCE Division, AOT Division, and Facility Operations Director representatives. The scoping process was designed to ensure selected tasks had sufficient resources (budget and personnel), were set with the right priority, and did not represent high schedule-risk for accelerator restart. Major tasks completed during the 2008 outage include the following:

- Focused on developing, measuring, and improving routine maintenance schedules and defining required resources for repetitive outage activities, while conducting oversight of regular maintenance activities not included in the tasks below.
- Completed and implemented a Safety Assessment Document and Accelerator Safety Envelope as required by *DOE Order 420.2B*.
- Procured/fabricated and assemble components for the new 1L Mark III TMRS for installation at a later date.
- Developed and implemented a column refurbishment plan agreed to by C-IIAC to assure reliable H^+ injector operation for IPF in 2008.
- Supported LANSCE Refurbishment (LANSCE-R) CD-1 work in accordance with LANSCE-R project schedule.
- Assembled a 201.25-MHz diacrode test stand.
- Continued to aggressively pursue H^- ion source development in both IB and ISTS in support of full 120-Hz operation.
- Received and tested a rebuilt IVR.
- Installed IPF beam shutter.
- Maintained PACS certifications as possible.
- Continued FIRP design and acquisition for execution in following outages.

Key Maintenance Activities in 2009

There were 341 maintenance activities completed in 2009. Maintenance activities

focused on inspection, cleaning, and documentation of deficiencies, such as condition assessment. As funds were available for parts, line organizations responsible for systems made necessary repairs within the available budget. Major tasks completed during the 2009 outage include the following:

- Implemented the new and approved Safety Assessment Document and Accelerator Safety Envelope as required by *DOE Order 420.2B*.
- Supported the new 1L Mark III TMRS project as necessary to proceed with installation in the 2010 outage.
- Continued to assemble a 201.25-MHz diacrode test stand.
- Supported LANSCE-R CD-1 work in accordance with the LANSCE-R project schedule.
- Resolved measurement and stability issues with the 201-MHz phase and amplitude controls.
- Made cryo-pump/post coupler water-system modifications.
- Continued to aggressively pursue H^- ion source development in both IB and ISTS to support full 120-Hz operation.
- Performed practical 1L Target maintenance necessary to minimize the risk of target failure prior to commencement of Mark III target installation in 2010.
- Maintained PACS certifications.
- Continued developing, measuring, and improving routine maintenance schedules and defining required resources for repetitive outage activities.

Operations, beam delivery, and reliability

Operations

Restarting the facility, on schedule, is complex and so always a major accomplishment. Beam delivery began on schedule in early May of each year. During operation, LANSCE personnel continued to maintain statistics addressing availability of critical systems. Identified sources of Lujan Center beam down time continue to support historical trends

Beam Delivery and Reliability

The overall beam-delivery and beam-reliability to LANSCE users is presented in Tables 1, 2, and 3. It is important to note the following:

- Lujan Center reliability exceeded 85% in 2009 and recorded the highest average-current since inception.
- IPF production for 2007 was seriously affected by gradual failure of the 750-kV accelerating column.
- IPF production in 2008 benefited from the replacement of the 750-kV column during the 2008 extended outage. This was a major accomplishment.
- The accelerator radio-frequency (RF) repetition rate, historically at 120 Hz, was limited to 60 Hz during all three years. This reduction was due to unresolved manufacturing problems with the 201-MHz-final-stage power amplifier. However, the 60-Hz limit helped reduce costs for power consumption for these years. The Weapons Neutron Research (WNR) scientific program suffers the brunt of the reduced RF duty-factor impact.

Table 1. 2007 Run-Cycle Beam Delivery and Reliabiltiy. Statistics			
Area	Scheduled Hrs	Delivered Hrs	Reliability
IPF	3628.9	2911.7	80.2%
Lujan Center	3255.2	2642.9	81.2%
pRad	753.7	716.9	95.1%
UCN	982.1	846.0	86.2%
WNR-T2	90.4	77.1	85.3%
WNR-T4	3226.9	2809.1	87.1%
Total	**11937.2**	**10003.7**	**83.8%**

Table 2. 2008 Run-Cycle Beam Delivery and Reliabiltiy. Statistics			
Area	Scheduled Hrs	Delivered Hrs	Reliability
IPF	3729.4	3200.4	85.8%
Lujan Center	3532.4	2741.0	77.6%
pRad	753.7	699.2	84.4%
UCN	2090.6	1719.4	82.2%
WNR-T2	336.1	293.9	87.4%
WNR-T4	3159.5	2582.8	81.8%
Total	**13676.0**	**11236.7**	**82.2%**

Table 3. 2009 Run-Cycle Beam Delivery and Reliabiltiy. Statistics			
Area	Scheduled Hrs	Delivered Hrs	Reliability
IPF	3420.6	3255.1	95.2%
Lujan Center	3329.8	2838.8	85.3%
pRad	1240.9	1138.3	91.7%
UCN	1038.7	880.7	84.8%
WNR-T2	194.7	178.2	91.5%
WNR-T4	3219.8	2895.8	89.9%
Total	**12444.5**	**11186.9**	**89.9%**

New design of the LANSCE injectors (2008-2009)

Presently, the LANSCE injectors comprise H^+ and H^- ions sources and separate Cockcroft-Walton (CW) accelerators to provide 750-keV beams for injection into the Linac. These beams are manipulated in long, low-energy beam transports (LEBTs) between the CWs and the 201.25-MHz, 100-MeV drift tube Linac (DTL). A double-buncher scheme is used to prepare these beams to maximize the accelerated beam current.

Unfortunately, the H^+ CW is over 35-years-old. Concerns over its useful lifetime and operational reliability have sparked interest in replacing it (and the H^- CW) with a modern equivalent, based upon radio-frequency-quadrupole (RFQ) accelerator technology.

A study was undertaken to develop a basic layout for a new H^+ injector that would replace the present H^+ CW and LEBT, leaving the H^- transport intact. This new injector would employ the existing H^+ duoplasmatron ion source and 750-keV, 201.25-MHz RFQ and be capable of delivering a fully bunched beam with peak currents over 21 mA. The new injector design is quite compact and produces a better quality beam, which is expected to increase capture and reduce losses along the Linac.

Since this layout was the result of merging the new H^+ injector with the existing H^- LEBT, a cursory look at the upgrading the H^- injectors was also done. To meet or exceed the present level of performance with the H^- beams, a solution employing two RFQ-based H^- injectors was considered: one injector for the WNR micropulse beam and a second injector for the remaining H^- beams for the Lujan Center, Proton Radiography (pRad), and Ultracold Neutrons (UCN) facilities. Both injectors would be relatively compact and produce better quality beam than presently available from the current injectors. If both injectors are replaced, the integrated design could be optimized for all beams.

The Particle Accelerator Conference poster from 2009. This well established conference series is of particular importance to the staff of AOT.

Pulse stacking (2008)

Experimenters at the WNR facility use time-of-flight techniques to measure the energy of neutrons produced in the nuclear reactions they study. The spacing between arrival times (typically 1.8 μs) of the proton pulses on the neutron spallation target dictates the range of neutron energies they observe.

Recently, there has been interest in performing measurements at lower neutron energies, which implies larger separation between arrival time of sequential proton pulses on target. The usual way to implement this increased pulse spacing is to remove one or more pulses from the sequence up at the low energy injector. Unfortunately, this reduces the average beam current, which then increases the time it takes to collect a specific amount of data.

In an effort to improve this situation, a new "pulse stacking" technique was proposed and successfully demonstrated at WNR. This technique employs the 800-MeV Proton Storage Ring (PSR) (Figure 1) at LANSCE to stack individual WNR micropulses from the Linac in the PSR into a single high-intensity bunch that is delivered many times a second. In the demonstration, the charge of the final bunch was increased 240 times over a single WNR micropulse, while the full-width half-maximum size of the bunch grew only to about 6 ns. These pulses were extracted with a 25-μs spacing and directing onto the WNR target.

Although this was demonstrated with the use of existing hardware, an idealized system would require a new PSR RF-buncher for creating more narrow, high-charged bunches, a new fast solid-state modulator for the PSR fast-extraction kickers (to allow on-demand extraction and more continuously-variable pulse-spacing), and a slow-kicker in the PSR extraction line to allow PSR to simultaneous provide beam to both the Lujan Center and WNR.

Figure 1. A view of the Proton Storage RIng at LANSCE.

Particle Accelerator Conference 2009

The 2009 Particle Accelerator Conference (PAC09) took place in Vancouver, British Columbia, from May 4th to 8th, 2009. PAC09 was hosted by TRIUMF, and was jointly sponsored by the NPSS (IEEE) and the DPB (APS).

This well-established conference series is of particular significance to accelerator scientists, engineers, atudents and industrial vendors interested in all aspects of particle accelerator technology. The Scientific Program comprises invited speakers, contributed orals, poster sessions, an Industrial Forum and an exciting Student Program. PAC09 is committed to reaching out to young researchers in the field, and has set a budget to partially support a limited number of qualifying accelerator students.

Abstracts for papers presented by AOT staff are summarized below.

Dissolved Gas-in-Oil Analysis to Assess the Health of the LANSCE High Voltage Systems

K. Young, G. O. Bolme, J. Lyles, D. Rees, A. Velasquez

The LANSCE linac RF system consists of four 201.25 MHz RF stations that supply RF power to the drift tube linac(DTL), and forty-four 805 MHz RF stations, that supply RF power to the coupledcavity linac(CCL). There are four large high voltage power supplies for the DTL RF systems. Seven high voltage power supplies provide the power for the 805 MHz klystrons. All power supplies consist of a transformer/rectifier, Inductrol Voltage Regulator (IVR) and a capacitor bank with crowbar protection. After 39 years of operation, some components are approaching the end of life and will be refurbished through the LANSCE-R project to ensure the reliability of the machine until 2025. An analysis of the oil in the high voltage power supply units was done to assess their health to determine if units need to be replaced or repaired as part of LANSCE-R. Since 1998 the oil in each unit has been sampled and tested annually, and reprocessed when required. Gas-in-oil data for these units from 1998 to present was analyzed. The levels of each gas component, trends in the data and the significance of the each dissolved gas are discussed. The health of the units is assessed.

Dual-Energy Operations at LANSCE for Proton Induced Nuclear Cross Section Measurements

M. Gulley, L. Bitteker, A. Couture, C. Pillai, A. Seifter, J. Ullmann, S. Wender, H. Bach, R. Gritzo, F. M. Nortier, D. Smith, F. O. Valdez

The WNR facility at LANSCE is preparing for a set of proton induced cross section measurements in support of the LANL Isotope Production Program. To determine the best way to produce particular isotopes, it is necessary to measure the production rate's energy dependence. The first measurements will use a 197-MeV proton beam, which prompted recovery of the facility's ability to transport multiple energy proton beams simultaneously to different experimental areas to ensure that an 800-MeV beam is available for Proton Radiography or Ultra-Cold Neutron experiments while a sample is irradiated with a lower energy beam for the cross section measurements.

The ability to change the beam energy pulse-to-pulse was built into the original accelerator controls, but the multiple energy controls were unused for over a decade and the system was re-commissioned for this effort. These experiments form part of an effort to establish a capability for the measurement of cross sections in the 197 to 800 MeV energy range.

The experiments are expected to provide the needed data for activities that may develop into a unique isotope production capability to compliment the existing 100-MeV IPF facility.

Full Temperature Mapping System for Standard 1.3 GHz 9-cell Elliptical SRF Cavities

T. Tajima, A. S. Bhatty, A. Canabal, G. V. Eremeev, F. Krawczyk

A temperature mapping system with 4608 100-ohm Allen-Bradley resistors has been built and tested at LANL. With this temperature mapping system we were able to locate lossy regions in the 1.3 GHz 9-cell SRF cavity due to field emission and direct heating. The results of the temperature mapping have been correlated with the inside surface inspection of the cavity and will be shown together with Q-E curves. A brief description of the mapping system and improvements that have been made in the recent months will also be mentioned in the paper.

SRF Cavity High-Gradient Study at 805 MHz for Proton and Other Applications

T. Tajima, A. S. Bhatty, G.V. Eremeev, F. Krawczyk, R. J. Roybal

805 MHz elliptical SRF cavities have been used for SNS as the first application for protons. At LANL, an R&D started to explore a capability of getting high-gradient cavities (40-50 MV/m) at this frequency for the future applications such as proton and muon based interrogation testing facility added to the LANSCE accelerator and a power upgrade of the LANSCE accelerator for the fission and fusion material test station. Optimized cell designs for "standard", "low-loss" and "reentrant" shapes, cavity test results for "standard" single-cell cavities with temperature mapping as well as surface inspection results will be presented.

Studies on the Effect of Coating Nb with Thin Layers of Another Superconductor such as NbN and MgB2

T. Tajima, A. Canabal, G. V. Eremeev (LANL), I. E. Campisi (ORNL), X. Xi (Penn State University), V. Dolgashev, S. G. Tantawi (SLAC)

We are currently testing the effect of coating Nb with a thin layer of another superconductor such as NbN and MgB_2. Gurevich's theory of multi-layered coating predicts an enhancement of the critical magnetic field, giving us hope to increase the achievable accelerating gradient to above 50 MV/m in elliptical cavities. CW test results of 3-GHz Nb single-cell cavities coated with ~100 nm NbN at LANL and 11.4 GHz <1 ˜s high-power pulsed test results of 2" Nb disk samples coated with ~100 nm MgB_2 will be presented.

Tune Measurements in the Los Alamos Proton Storage Ring

R. C. McCrady

Precise measurement of the tunes in the Los Alamos Proton Storage Ring (PSR) is difficult because the beam is normally extracted immediately after accumulation, preventing the use of continuous-wave radio frequency measurements. Presented here is a method that takes advantage of the phase information in the response of the beam to a transverse oscillatory driving voltage. This technique offers much greater precision than using the amplitude spectrum alone.

Prototype Beam Position and Phase Monitoring Electronics for LANSCE

J. F. Power, J. D. Gilpatrick

Future improvements to the Los Alamos Neutron Scattering Center (LANSCE) include new Beam position and phase measuring systems that

operate at 201.25 to 805 MHz. An effort is underway to build and test prototype electronics for these applications. We plan to use direct down conversion to 35 to 115 MHz followed by COTS FPGA hardware for in-phase and quadrature-phase (I/Q) signal processing. Self- calibration and system diagnostics circuits will be included. We are reporting on the status of these efforts.

cRIO-Based Wire Scanner Motion Control

J. D. Sedillo, J. D. Gilpatrick

The Compact Reconfigurable Input/Output (cRIO) hardware manufactured by National Instruments (NI) is evaluated as a wire scanner motion controller. This particular configuration utilizes a NI cRIO-9074 system combined with various C-series modules for wire scanner motion control I/O. Programs for this system have been written in LabVIEW and a majority of the motion-control functionality has been programmed into the cRIO's FPGA in order to provide the fastest motion control processing possible with cRIO. Additional topics of interest include, cRIO-based resolverto-digital conversion and closed-loop, stepper-based motion control.

Orbit Response Matrix Measurements in the Los Alamos Proton Storage Ring

J. Kolski (IUCF, Bloomington, Indiana; LANL), R. J. Macek, R. C. McCrady, T. Spickermann (LANL)

Orbit response matrix techniques have been used in numerous electron storage rings to elucidate various optical properties of the machines. Such measurements in a long-pulse accumulator ring have unique complications. We present here the techniques and results of such a measurement at the Los Alamos Proton Storage Ring*. We also show the deficiencies in previous models of the ring and a comparison of the beta-functions as fit by the orbit response method to direct measurements by quadrupole magnet variations.

Recent Observations, Experiments and Simulations of Electron Cloud Buildup in Drift Spaces and Quadrupole Magnets at the Los Alamos PSR

R. J. Macek, R. C. McCrady, L. Rybarcyk, T. Zaugg (LANL), A. A. Browman (TechSource, Santa Fe, New Mexico)

Recent beam studies have focused on understanding the main sources and locations of electron clouds (EC) which drive the observed e-p instability at the Los Alamos Proton Storage Ring (PSR). Strong EC signals are observed in drift spaces and quadrupole magnets at PSR which together cover ~65% of the ring circumference. New results making use of two longitudinal barriers to isolate the drift space electron diagnostic provide definitive evidence that most of the drift space EC signal is "seeded" by electrons ejected longitudinally by ExB drifts from adjacent quadrupole magnets. This result can explain why weak solenoids and TiN coatings in several drifts spaces had no effect on the e-p instability threshold. Modeling of EC generation in 3D quadrupoles using a modified version of the POSINST code shows that a sizeable fraction of the electrons generated in the quadrupoles are ejected longitudinally into the adjacent drifts. The experimental findings and simulation results will be presented.

LENS Proton Linac: 6 Kilowatt Operation

T. Rinckel, D. Baxter, A. Bogdanov, V. P. Derenchuk, P. E. Sokol (IUCF, Bloomington, Indiana), W. Reass (LANL)

The Indiana University Cyclotron Facility is operating a Low Energy Neutron Source, which provides cold neutrons for material research and neutron physics as well as neutrons in the MeV energy range for neutron radiation effects studies. Neutrons are being produced by a 13 MeV proton beam incident on a Beryllium

target. The LENS Proton Delivery System (PDS) is routinely operating at 13 MeV and 25 mA at 1.8% duty factor. The RF system, consisting of three Litton 5773 klystron RF tubes at 425 MHz and 1 MW each, power the AccSys Technology PL-13 Linac. The proton beam delivers 6 kilowatts of power to the Beryllium target. Details of the beam spreading system, target cooling system, and accelerator operations will be discussed.

Development of IH Accelerating Structures with PMQ Focusing for Low-Beta Ion Beams

S. Kurennoy, J. F. O'Hara, E. R. Olivas, L. Rybarcyk

We are developing high-efficiency room-temperature RF accelerating structures based on interdigital H-mode (IH) cavities and the transverse beam focusing with permanent-magnet quadrupoles (PMQ), for beam velocities in the range of a few percent of the speed of light. Such IH-PMQ accelerating structures following a short RFQ can be used in the front end of ion linacs or in stand-alone applications such as a compact deuteron-beam accelerator up to the energy of several MeV. New results from our detailed electromagnetic 3-D modeling combined with beam dynamics simulations and thermal-stress analysis for a complete IH-PMQ accelerator tank, including the end-cell design, will be presented.

Simulation of Large Acceptance Linac for Muon

H. Miyadera, A. J. Jason, S. Kurennoy

Muon accelerators are proposed world wide for future neutrino factory, muon colliders and other applications. One of the problems with accelerating muons is their large emittance as well as huge energy spreads. We carried out some simulation works on large acceptance muon linear accelerator that operates at mixed buncher / acceleration mode. The designed linac has following features: iris structure of 12 cm diameter, inject ~100 MeV muon beam and accelerates to several 100 MeV, 700 MHz and 25 MV/m peak field. Further acceleration of the muon beam can be easily done by extending the muon linear accelerator. According to the simulation, our linac can accelerates DC muon beam of 20 - 100 MeV range with 20% phase acceptance.

Use of a Debuncher Cavity for Improving Multi-Beam Operations at LANSCE

L. Rybarcyk, S. Kurennoy

The Los Alamos Neutron Science Center simultaneously provides both H^- and H^+ beams to several user facilities. Opposite polarity beams are usually accelerated in the linac during the same macropulse when beam-loading limitations are not exceeded. Presently, the Weapons Neutron Research (WNR) H^- and Isotope Production Facility (IPF) H^+ beams are accelerated simultaneously during the same macropulse. The amplitude of the cavity field in the last 201-MHz buncher, located in the common transport just upstream of the DTL, is a compromise between the optimal values for each beam. Recent beam dynamics studies have shown that implementing a debuncher cavity in the H^- low-energy beam transport would allow for more optimal operation of both beams. For this application where space is limited, a compact 201-MHz quarter-wave cavity will be used. This paper will report on the beam dynamics simulations performed and the quarterwave cavity design being developed to address this issue.

AOT & LANSCE The Pulse

May 2009

Eric Pitcher

Fueling a career in nuclear energy science

By Kirsten Fox
Communication Arts and Services

While fishing on Lake Michigan as a child, Eric Pitcher was intrigued by the looming nuclear power plant along the shoreline.

"I thought, 'wow, that's so cool. I wonder how that works?' " he said. From that moment on, Pitcher's aspiration was to launch a career focused on nuclear energy science. For Pitcher, serving as project manager for the Materials Test Station fuels that focus.

More efficient energy for the future

Pitcher, a scientist at the Los Alamos Neutron Science Center (LANSCE-DO), is helping construct the facility that could make nuclear energy cleaner and more efficient and also help solve the associated challenge of nuclear waste storage.

The test station will support the U.S. Department of Energy's participation in the Global Nuclear Energy Partnership, an international initiative aimed at meeting energy demands, reducing greenhouse gases, and preventing nuclear weapon proliferation. Slated to be complete by 2014, the Materials Test Station will be used in fuel and materials irradiation studies, aiding nuclear fuel recycling, and supporting materials science capabilities.

Nuclear energy supplies 20 percent of the nation's electricity and does not emit greenhouse gases. However, nuclear waste accumulates at temporary facilities near 104 U.S. reactors—and the nation does not have an immediately viable underground facility designated for long-term storage. Department of Energy Secretary Chu announced renewable energy and nuclear waste disposal a priority.

continued on page 4

Los Alamos National Laboratory • Est. 1943 ***The Pulse****—Newsletter of the Los Alamos Neutron Science Center and Accelerator Operations and Technology Division*

Tours, News, Conferences, & Celebrations

LANSCE tours

Throughout the year, LANSCE hosts a variety of visitors, many of who request tours of the accelerator, instruments, and laboratories. These visitors are either U.S. or foreign citizens and can represent, for example, academia, industry, national laboratories, and local, tribal, state, or the federal government. As a National User Facility, LANSCE encourages visitors and encourages visitors to schedule tours. Tables 1–3 provide lists of the number of visitors, and the institutions they represented, that toured LANSCE during 2007–2009. To schedule a tour of LANSCE simply contact the LANSCE User Office.

Table 1. Institutions and the Number of Visits to LANSCE in 2007

Institution	Number of Visits
Abilene Christian University	1
Argonne National Laboratory (ANL)	4
Bechtel Corporation	2
Boiz Allen	1
Boy Scouts of America	1
Brookhaven National Laboratory (BNL)	1
Caltech	3
Case Western Reserve University	2
Central New Mexico College	1
Decision Sciences Corporation (DSC)	7
Defense Nuclear Facilities Safety Board	1
Defense Threat Reduction Agency (DTRA)	2
Department of Energy Headquarters (DOE)	7
Department of Homeland Security	2
Espanola Valley High School	1
Hanford University	1
Idaho National Laboratory (INL)	5
Indira Gandhi Center	1
J&B Technologies	1
JB Henderson	1
Jefferson Lab	1
Kansas City Plant	1
Lawrence Berkeley National Laboratory (LBNL)	2
Lawrence Livermore National Laboratory (LLNL)	2
Los Alamos High School	2
Los Alamos Side Office (LASO)	3
Massachusetts Institute of Technology (MIT)	2

Table 1 (cont.). Institutions and the Number of Visits to LANSCE in 2007	
Institution	**Number of Visits**
Michigan State University	3
National Institute of Standards and Technology (NIST)	1
National Nuclear Security Administration (NNSA)	4
National Science Foundation (NSF)	1
National Security Technologies (NSTec)	4
Nature Magazine	1
Nevada Teawatt Facility	1
New Mexico State University	1
New Mexico Tech	1
North Carolina State University	2
Northrop Grumman Group	1
Oak Ridge Associated University (ORAU)	1
Oak Ridge National Laboratory (ORNAL)	4
Pueblo Electric Incorporations	1
Qwest	1
Remote Sensing Laboratory (RSL)	3
Russian Federal Nuclear Center (RFNC-VNIEF)	1
Rutgers Jersey State University	1
Saint-Gobain	1
San Ildefanso Pueblo	1
Sandia National Laboratories (SNL)	1
Snow College	1
SpecTal Consultants	1
Spectra Glass	1
Stanford University	1
Sun Microsystems	1
Texas A&M	1
Tidwell Cancer Treatment Center	1
U.S. Senate Energy	1
United Kingdom Ministry of Defense	1
United States Government (USG)	2
United States Securities and Exchange Commission	1
University of California Office of the President	1
University of California-Berkeley	1
University of California-Davis	1

Table 1 (cont). Institutions and the Number of Visits to LANSCE in 2007	
Institution	**Number of Visits**
University of California-Merced	1
University of Florida	1
University of Kentucky	1
University of Massachusetts	1
University of Milano	1
University of New Mexico	5
University of Notre Dame Australia	2
University of Oregon	1
University of Tennessee	1
University of Texas at Austin	1
University of Washington	2
Virginia Tech	1
Westhill University	1
Young Presidents Organization	1

Table 2. Institutions and the Number of Visits to LANSCE in 2008

Institution	Number of Visits
Accelerator for Research in Radiochemistry and Oncology at Nantes Atlantic (ARRONAX)	1
Accenture (Global Management Consulting, Technology and Outsourcing Services)	1
American Association for the Advancement of Science (AAAS)	1
Argonne National Laboratory (ANL)	1
ARM Climate Research Facility	1
ARS International	1
Arthur Morgan School	1
Boston University	1
Brush Wellman Alloy Products	1
Building Technology Associates (BTA)	1
Burns & Roe Engineering, Procurement, Construction, and Maintenance	1
Caltech	2
Cartwright Engineering	1
Case Western Reserve	1
City of Espanola	1
COSMOS	1
Decision Sciences Corporation (DSC)	20
Defense Threat Reduction Agency (DTRA)	5
Demco Inc.	1
Department of Defense (DOD)	1
Department of Energy (DOE)	10
Department of Homeland Security (DHS)	8
Duke Scientific	1
Earth Tech	1
Energy Solutions	1
Environmental Restoration LLC	1
Federal Bureau of Investigation (FBI)	1
Fidelity Investments	1
French Atomic Energy and Alternative Energies Commission (CEA)	1
Girl Scouts of America	1
Honeywell	1

Table 2 (cont). Institutions and the Number of Visits to LANSCE in 2008	
Institution	**Number of Visits**
Indiana University	2
Innovative Technology Solutions Inc. (ITSI)	1
Inserm Institut Thématiques	1
IP Accelerator Works Inc.	1
Jefferson National Accelerator Facility	1
JGMS Inc.	1
KEK High Energy Accelerator Research Organization	3
Kyushu University	1
Lawrence Livermore National Laboratory (LLNL)	3
Lopez Engineering	1
Los Alamos Chamber of Commerce	1
Los Alamos Monitor	1
Los Alamos Public Schools	1
Los Alamos Side Office (LASO)	5
Los Alamos Technical Associates (LATA)	1
Marquette University	2
Military Academy	1
MOTA Corp. (now Siempelkamp Nuclear Services)	1
National Instruments	1
National Nuclear Security Administration (NNSA)	9
National Security Technologies (NSTec)	6
Navy	2
NCC Electric Inc.	1
New Mexico Tech	1
NORESCO Energy Solutions	1
Osaka University	2
Portage Inc.	1
Proctor & Gamble	1
Q Consulting	1
Quiroga Pfeiffer Engineering Corporation (QPEC)	1
Regional Development Corporation	1
Sandia National Laboratories (SNL)	4
Sloan-Kettering Cancer Center	4
Snow College	1

Table 2 (cont.). Institutions and the Number of Visits to LANSCE in 2008	
Institution	**Number of Visits**
Society of Nuclear Medicine	1
Sparks Industrial Services	1
SUBA Technology	1
Texas A&M	1
TSAY Corporation	1
U.K. Atomic Weapons Establishment (AWE)	3
U.S. Congress	1
United States Air Force (USAF)	2
United States Air Force Academy (USAFA)	2
United States Patent & Trademark Office (USPTO)	1
University of California-Davis	1
University of California-Los Angeles	1
University of Illinois	2
University of Michigan	1
University of Nagoya	1
University of New Mexico (UNM)	1
University of Notre Dame	1
University of Sussex	1
Vigil Enterprises	1
Washington University	1

Table 3. Institutions and the Number of Visits to LANSCE in 2009

Institution	Number of Visits
Abilene Christian University (ACU)	1
Air Force Institute of Technology	1
Amplitude Tech	1
Aspen Elementary School	1
Atomic Weapons Establishment (AWE)	4
Bechtel	1
Boeing	1
Caltech	2
Chevron	1
City College of New York	1
City of Santa Fe	1
Clemson University	2
College of William and Mary	1
Colorado School of Mines	1
Colorado State University	1
Columbia University	1
Cornell University	1
COSMOS	1
CVI Melles Griot	1
Defense Board	1
Defense Threat Reduction Agency (DTRA)	3
Department of Energy (DOE)	7
Department of Homeland Security (DHS)	1
Eaton Corp.	2
Espanola Valley High School	1
Francis Marion University	1
French Atomic Energy and Alternative Energies Commission (CEA)	1
Fulbright Association	1
GE Global Research	1
Harvard University	1
Hokkaido University	1
Houghton College	1
Hyroshima University	1
Illinois Institute of Technology (IIT)	1
Institute of Applied Physics	1

Table 3 (cont.). Institutions and the Number of Visits to LANSCE in 2009	
Institution	**Number of Visits**
IP Systems	1
Ithaca College	1
Joint Institute for Nuclear Research-Russia (JINR)	1
Kyushu University	1
Lawrence Berkeley National Laboratory (LBNL)	1
Lawrence Livermore National Laboratory	1
Los Alamos Side Office (LASO)	9
Massachusetts Institute of Technology	1
Max-Planck Institute	1
NASA	1
National High Magnetic Field Laboratory (NHMFL)	1
National Instruments Corp	1
National Nuclear Security Administration (NNSA)	8
National Science Foundation (NSF)	1
National Security Technologies (NSTec)	3
New Mexico Department of Health	1
New Mexico Environmental Department	1
New Mexico State University (NMSU)	2
North American Paper Corp. (NORPAC)	1
North Carolina State University (NCSU)	1
North Dakota State University (NDSU)	1
Northern New Mexico College (NNMC)	1
Pacific Northwest National Laboratory (PNNL)	2
Paul Schemer Institute	1
Princeton University	1
Proctor and Gamble	1
Ray Thorn	1
Renesselaer Polytechnic Institute	1
Rio Physics	1
Rio Rancho Public Schools	1
RTI International	1
Sandia National Laboratories (SNL)	5
Santa Fe Community College (SFCC)	1
Santa Fe Indian School (SFIS)	2
Science and Technology-U.K.	1

Table 3 (cont.). Institutions and the Number of Visits to LANSCE in 2009	
Institution	**Number of Visits**
Science Museum of Virginia (SMV)	1
Sierra Middle School	1
Southern Methodist University	1
St. Michael's High School	1
Stanford University	1
Symmetry Magazine	1
TechSource	1
United States Department of Agriculture Office of the Chief Information Center (OCIO)	1
United States Government	1
United States Government Accounting Office	1
United States Office of Management and Budget	1
United States Senate	1
University of Arizona	1
University of California-Berkeley	1
University of Colorado- Denver	1
University of Colorado-Boulder	1
University of Louisiana	1
University of Maryland	2
University of Nevada-Reno	1
University of New Mexico (UNM)	5
University of Northern Colorado	1
University of Redlands	1
University of Rochester	1
Viad Corp. (VVI)	1
Virginia Tech	1
Wellesley College	1
Western New Mexico University (WNMU)	1
Yale University	1
Youth Development Inc. (YDI)	1

A student tour in 2009. The staff of the Lujan Center regularly host tours of the facility for visiting students and scientists.

News & Conferences

LANSCE-NS hosts NNSA Stockpile Stewardship Academic Alliance Workshop

LANSCE-NS hosted an all-day workshop for the Rutgers University StockpileStewardship Academic Alliance (SSAA) Center of Excellence on October 29. LANLstaff presented an overview of research and programs being conducted in nuclear science and non-proliferation, and the SSAA Center for Excellence members presented results oftheir work. Attendees discussed several potential collaborative efforts.

The SSAA is a NNSA-funded grant program which provides opportunities for university researchers to become involved in defense-related research, providing a conduit for talented students and postdoctoral researchers into the national laboratories, while performing useful measurements for current data needs. Rutgers University professor Jolie Cizewski heads an SSAA Center for Excellence that includes Rutgers, Oak Ridge National Laboratory, Oak Ridge Associated Universities (ORAU), University of Tennessee, Michigan State University, Auburn and other institutions. Center members perform nuclear physics research that has applications to stockpile stewardship issues, such as determining cross sections for neutron-induced reactions on short-lived actinides and unstable fission product nuclei using surrogate reaction techniques.

Research is carried out at facilities around the country, including the Hollifield Heavy-Ion Accelerator at ORNL and the 88-inch cyclotron at Lawrence Berkeley National Laboratory. An element of this workshop was to explore collaborations between the members of the SSAA and the LANL, including conducting nuclear science experiments at the LANSCE Weapons Neutron Research facility.

Jolie Cizewski (Rutgers University) and J. A. Becker (LLNL) discuss student posters at the SSAA workshop hosted by LANSCE-NS. Gus Keksis (LANL C-NR postdoc), and Travis Bray (Auburn University student) are shown at right.

LANL hosts American Conference on Neutron Scattering

The fourth biennial American Conference on Neutron Scattering (ACNS) will be held at the Eldorado Hotel in Santa Fe, May 11–15. The ACNS is sponsored by the Neutron Scattering Society of America and hosted by LANL. The conference is intended to showcase recent scientific results in neutron science across a wide range of fields, including soft and hard condensed matter, liquids, biology, magnetism, engineering materials, chemical spectroscopy, crystal structure, and fundamental physics, as well as highlight developments in neutron instrumentation. Thomas Proffen (LANSCE-LC) and Leilani Conradson (LANSCE-DO) serve as the local organizing committee, and Proffen, Don Brown, and Mike Fitzsimmons (all in LANSCE-LC) are on the program committee. Zoe Fisher (B-8) is an invited speaker.

ACNS conference participants are invited to visit the Lujan Neutron Scattering Center at LANSCE May 15, from 9 a.m. to 1 p.m. Busses will take participants to Los Alamos from the conference hotel and return to Santa Fe and the Albuquerque International Sunport. Additional information: http://lansce.lanl.gov/ACNS2008/.

DOE Basic Energy Sciences (BES) Three-Year Review of the Lujan Center

The Three-Year Review of the Lujan Center occurred February 9-12, 2009, with a panel of eight eminent scientists from the U.S. and Europe. Pedro Montano of DOE BES lauded the scientific presentations by Lujan Center users, remarking that these talks were among the best he has seen. Mike Anastasio (DIR), Terry Wallace (PADSTE), and Susan Seestrom (ADEPS) gave video presentations; and Rich Marquez (DIR), Alan Bishop (ADTSC), Kurt Schoenberg (ADEPS), and Kevin Jones (AOT-DO) gave introductory presentations. Highlighted talks include the following:

- "Magnetic Films" - Steve May (Argonne National Laboratory)
- "Spin Waves" - Rob McQueeney (Ames Laboratory and Iowa State University)
- "Local Structure Investigation of Bulk and Nanophase Materials" - Katharine Page (Lujan Center, recently UCSB)
- "Wrinkling in Physics and Biology" - Ka Yee C. Lee (University of Chicago)
- "Bridge Cable Failures" - Cev Noyan (Columbia University)
- "Pyramid Cement and Concrete" - Michel Barsoum (LANL Wheatley Scholar, Drexel University)

Lujan Center to host Sagamore Conference

Sagamore XVI, sponsored by the Institute of Crystallography, will be hosted by the Lujan Center in Santa Fe, NM. This meeting on spin, charge, and momentum densities in materials brings together 120 of the top x-ray and neutron scattering experts in the world every three years. Sagamore XVI is the first U.S.-based meeting in 40 years. Topics will include charge densities, spin densities and related phenomena: neutron scattering studies of magnetic systems,

momentum densities, the interaction between theory and experiment, time-resolved studies, and the electronic structure of nanoparticles. Joe Thompson (MPA-10) will give an invited presentation in the neutron scattering session. Alan Hurd is on the Program and Advisory Committee, and Thomas Proffen, Hurd, and Leilani Conradson (all in LANSCE-LC) comprise the local organizing committee.

LANSCE hosts NNSA Academic Alliance Workshop

Researchers from the NNSA Academic Alliance Rutgers University Center of Excellence for Stewardship Science visited LANSCE for a workshop. The Center for Excellence is a collaborative effort between Rutgers University, Oak Ridge Associated Universities (ORAU), the University Radioactive Ion Beam (UNIRIB) consortium, Los Alamos National Laboratory, and Livermore National Laboratory. The goal of the Center is to provide nuclear science data with applications to stockpile stewardship, nuclear structure and nuclear astrophysics, and to help train the next generation of scientists for defense-related programs. Jolie Cizewski of Rutgers University leads the Center. Eighteen graduate students and postdoctoral researchers presented talks or posters on their work and attended lectures on defense-related nuclear science at LANL. Two university faculty members also gave talks. Topics presented by the visitors included: the potential use of alternate reactions to deduce nuclear reaction cross sections on unstable nuclides that are difficult to measure directly, development of a neutron detector array for use in radioactive beam research, development of a time projection chamber for neutron measurements, nuclear structure studies, and simulations of new experiment designs. Kurt Schoenberg (ADEPS), Bob Haight, (LANSCE-NS), Shannon Holloway, Patrick Talou, and Takehito Watanabe (T-2); Kevin John (SPO-SC); and Chris Morris (P-25) gave lectures that covered the broad nuclear science program at LANL, including neutron-induced capture, fission, and neutron and charged particle emission reactions, level density studies, nucleosynthesis, isotope production, and proton radiography. A tour of LANSCE facilities capped the visit.

Lujan Center expands its instrumentation suite

Users expecting to use Argonne's Intense Pulsed Neutron Source (IPNS) in 2008 are utilizing expanded neutron scattering capability at the Lujan Center to do their science. Three mainline instruments were transferred from IPNS to Lujan Center. One of these, the Western Hemisphere's only dedicated Single Crystal Diffractometer, took first beam in July 2008.

The front of the Lujan Center at LANSCE.

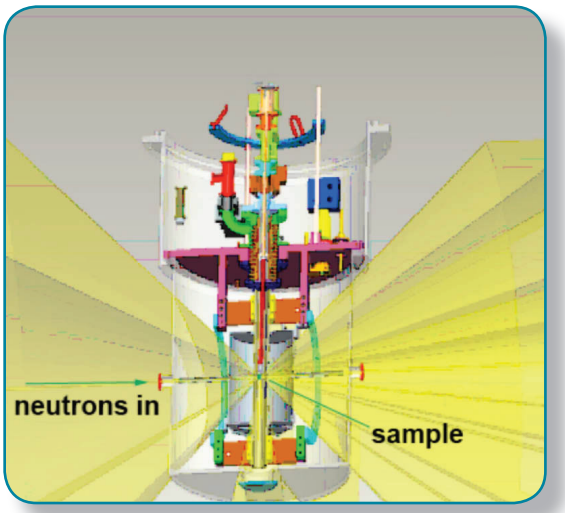

The furnace for in situ neutron diffraction experiments with the capacity to heat samples in excess of 2,200 °C has been developed for the HIPPO instrument at the Lujan Center.

Additional sample environments and ancillary equipment—both new and transferred from IPNS—are available to users, such as the new ultra-high temperature graphite oven custom built for the geomaterials High-Pressure Preferred Orientation Diffractometer (HIPPO) diffractometer. The new oven will serve the geomaterials community and national security studies. Phase diagrams and structure will be accessible for many more materials than before, including past the melt line. Doubled cold neutron flux will be expected from the "Mark III" target currently under design, while the existing "Mark II" has been granted a life extension until the new target is ready. The Mark III Target at Lujan Center will double the cold neutron flux on several instruments that are devoted to soft matter or long-length-scale phenomena. Examples include reflectometry for bioscience and for magnetism, and smallangle scattering for complex fluids.

The 10 instruments now on the floor will be expanded to 14 world-class instruments by 2014 under the major upgrade program, the "Enhanced Lujan Program," for which a call for letters of intent was issued on May 1. The neutron community is engaged in developing ideas for the new instruments, both new scattering instruments and new ancillary equipment. Examples of the ideas proposed include a new inelastic neutron scattering spectrometer for studying correlated electron materials, a new diffractometer for high pressure behavior and equations of state of weapons and geomaterials, upgrades to existing instruments for greater flux and detector coverage, and new environments such as horizontal magnetic fields. These ideas and others will deepen the Lujan Center's ability to investigate materials in extreme environments and for national security applications.

Boy Scouts visit LANSCE and the Isotope Production Facility

On November 30th, a group of 30 Boy Scouts and 15 adults from El Paso, TX were given a tour of LANSCE. Lawrence "Scott" Walker (RP-1) organized the tour at the request of the Scouts. Because of the size of the group, the tour was split into three, with the guides being Walker (RP-1) Matthew Murray (P-25), and Sven Vogel (LANSCE-LC). The Scouts were met at the gate and completed all the security requirements and the site safety orientation. The three tours then each rotated through various locations at LANSCE.

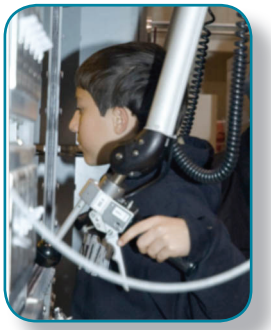

Left, a Scout at the remote manipulators. Right, Scott Walker and Michael Connors explain the heavily leaded glass, three-foot thick shielding walls, and other safety features of the operation to the group.

At the Isotope Production Facility, Kevin John and Michael Connors (both C-IIAC) were on hand to demonstrate target manipulation and share information about the operation. No radiation sources were present in the Isotope Production Facility.

The hot cell manipulators were the highlight of the tour. Kevin John, the program manager for the Isotope Production Facility, said that he feels visits such as this one are very positive for the Laboratory, because outreach to young people is a vital step in steering those who might be interested towards future careers in science.

Girl Scouts tour LANSCE

Members of Girl Scout Troop 306 toured LANSCE experimental areas and the Isotope Production Facility on February 1. The Scouts, eighth- and ninth-grade students from LosAlamos and White Rock, toured to see the variety of LANSCE programs and research.

Steve Greene (P-25) led the tour. The Scouts learned how the beamline is generated and split for different, yet simultaneous experiments. Greene explained the connection between basic research in nuclear physics and applications, such as muon tomography to detect hidden nuclear materials, and irradiation of computer chips and electronics to measure aircraft electronic reliability at high altitudes. Meiring Nortier (C-IIAC) gave the Scouts a demonstration of the Isotope Production Facility hot cell remote manipulators where radioactive materials are processed for medicine and scientific research. The girls had a hands-on opportunity to operate the hot cell arms (photo).

When Keith Stephens (AOT-OPS) showed the LANSCE Control Center to the Scouts, he explained the use of LANSCE by scientists from around the world. Stephens described preparing an elaborate Thanksgiving dinner for the foreign researchers on Thanksgiving Day. "They barely took time to eat it"! Stephens said. "They just wanted to get back to their experiments"! The Scouts' visit to LANSCE was part of their requirement toward earning a Scout science badge, and to explore science and engineering careers.

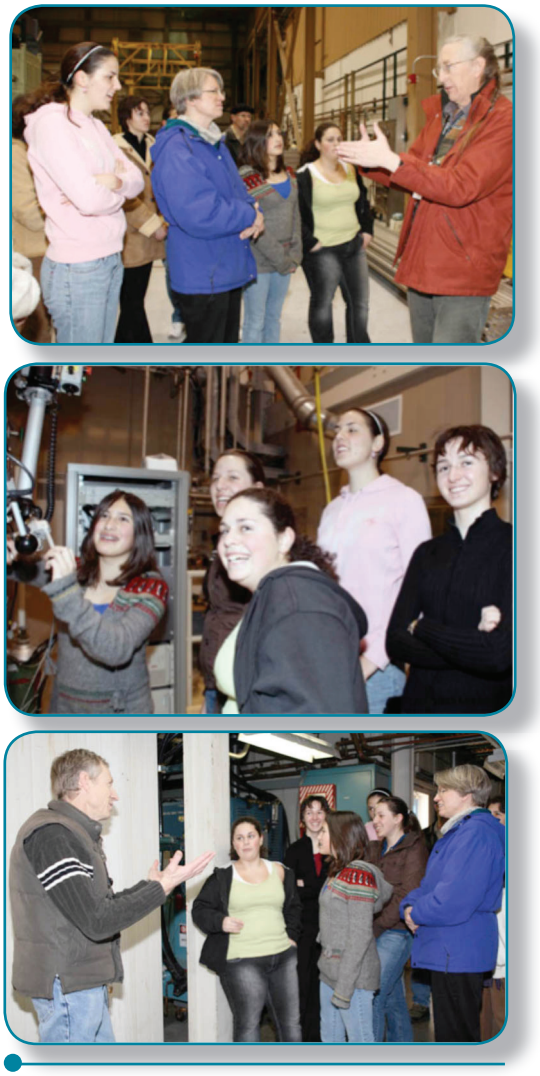

Top: Steve Greene (far right) describes experiments at LANSCE. Middle: Girl Scouts operate the remote manipulators at the Isotope Production Facility hot cell. Bottom: Meiring Nortier (far left) explains isotope production. Photo credit: Sandra Valdez (Records Management, Media Services, and Operations, IRM-RMMSO

New instrument workshops at the International Conference on Neutron Scattering

The neutron scattering community is invited to join discussions for new and upgraded neutron scattering instruments at the Manuel Lujan, Jr. Neutron Scattering Center. As part of the Enhanced Lujan Plan, satellite workshops will be held from May 3-6 during the International Conference on Neutron Scattering (ICNS) 2009 in Knoxville, TN.

For each instrumentation project, the goal is to form an Instrument Advisory Team to develop a letter of intent to realize the instrument. The letter will lead to a white paper pre-proposal, followed by a full proposal for review by DOE Basic Energy Sciences. The science areas under discussion at ICNS are small-angle scattering, powder diffraction and pair distribution functions, reflectometry, and highly radioactive samples. Instrument Advisory Teams were formed for time-of-flight inelastic instrumentation, engineering strain, and texture measurements at prior workshops. Building on three decades of experience with time-of-flight methods and the results of two recent strategic planning workshops addressing some of the community's needs, users will rethink designs for several classes of instruments. The driving factors in considering new designs include:

- Current upgrade plans at Lujan and the second target station at the Oak Ridge National Laboratory Spallation Neutron Source for improved brightness of cold, pulsed neutron sources.
- Need for improved background, optics, data acquisition rates, and instrument flexibility.
- Opportunities to do different types of measurements simultaneously.

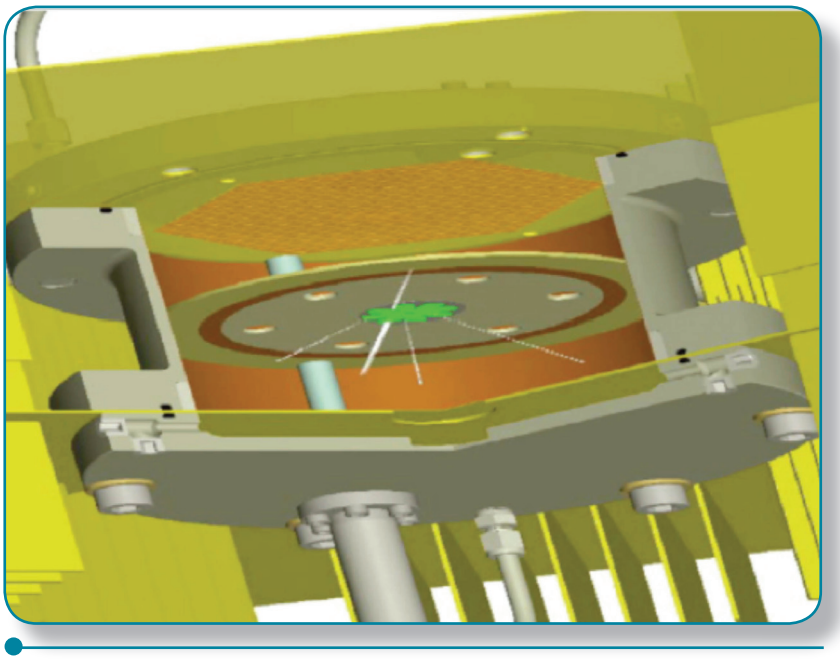

Drawing of the Time Projection Chamber (TPC) that is under construction as a joint LANLLLNL- Universities collaborative project. The fissionable material is at the center; tracks depict the ionization produced by fission fragments. The TPC delivers 3-dimensional images of charge tracks, enabling precise particle identification that minimizes uncertainties.

- Taking full advantage of the wide Q-domain of the broad bandwidth time of flight method.
- Unique opportunities from the time structure of the pulsed neutron source in pulse-probe measurements.
- Polarization and spin-echo techniques to encode ultra low momentum and energy transfers in quantifying nuclear spin incoherence.

Additional workshops will be held at LANL and other venues.

International Workshop on Nuclear Fission held at LANL

LANL held an international workshop on nuclear fission in February. T Division organized the workshop, which brought together scientists working on a fuller understanding of fission and its applications to nuclear energy and defense programs. About 50 staff and postdoctoral researchers from LANL, LLNL, BNL, LBNL, ORNL, NIST, Triangle Universities Nuclear Laboratory, MIT, RPI, IAEA (Austria), and CEA (France) attended the three-and-a-half day workshop. Eric Lynn (INST-OFF), Jerry Wilhelmy (C-NR), and John Becker (X-4-AF2) gave overviews of the status of the field. Presentations on fission work at LANSCE included talks by Bob Haight, Fredrik Tovesson, Alexander Laptev, and Ron Nelson (all of LANSCE-NS); and by Marian Jandel and Dave Vieira (both in C-NR). Tony Hill, project leader for precision fission cross-section measurements in LANSCE-NS, chaired the session on cross-section measurements. Much of the work at LANSCE is centered on precision cross-section measurements using a time projection chamber (Figure 5) and on neutron and gamma ray outputs using FIGARO and DANCE. Stephanie Frankle and Jeff McAninch (both in X-2-IFD), Bob Little (X-1-NAD), Mike MacInnes and Chuck Wilkerson (both in X-2-AT), and John Lestone (X-1-TA) covered issues for Defense Programs. Presentations on developments in fission theory and applications included talks by Patrick Talou, Toshihiko Kawano, Peter Moller, Anna Hayes, and Skip Kahler (all of T-2). Mark Chadwick (T-DO) led discussions and summarized the workshop. There were many illustrations of the importance of creating an enhanced predictive capability for fission and of the impacts of the lack of precise data on fission neutron and gamma-ray multiplicity and energy spectra. Precise cross-section data are necessary to minimize margins and uncertainties in reactors and may have large economic impacts. Knowledge of details of the neutron and gamma ray output from fission has applications ranging from materials identification for security applications to more accurate modeling of reactors and to nuclear forensics. These same types of data are essential for progress in quantifying margins and uncertainties and in enhancing the understanding of nuclear weapons. DOE Defense Programs and Nuclear Energy fund most of the LANL fission work.

Single Crystal Diffractometer takes first beam at the Lujan Center

The Single Crystal Diffractometer, which was transferred from Argonne National Laboratory to LANL, opened its shutter to neutrons on July 15 and recorded a diffraction pattern. With the closure of the Intense Pulsed Neutron Source at Argonne, several world-class instruments were transferred to the Spallation Neutron Source at ORNL and the Lujan Center at LANL. The Diffractometer, which is the only neutron instrument of its kind in the U.S., is one of the best single crystal instruments in the world. The "new" Diffractometer replaces the Lujan Center's old instrument built in the 1980s. It has low temperature capability (to a few Kelvin) and high pressure (to a few kilobars). Art Schultz (LANSCE-LC) built the diffractometer at Argonne and modernized it completely in 2003. The Diffractometer will determine the structure of single-crystal materials such as

superconductors, magnetic materials, metal alloys, and hydrogen-storage materials. With the help of R. Vitt (Argonne) and Schultz, the diffractometer was up and running in the Lujan Center after just three days of installation activities, a remarkable achievement. Professor Heinz Nakotte of New Mexico State University leads the Single Crystal Diffractomer user consortium as the Instrument Scientist. Schultz led a workshop introducing the Diffractometer to the user consortium. During the LANSCE 2008 run cycle, the Diffractometer will operate in commissioning mode.

Single Crystal Workshop participants July 15, at the Lujan Center. Consisting of postdocs, grad students, and staff, the Single Crystal Diffractometer User Consortium will run the diffractometer in 2008. Instrument Scientist Heinz Nakotte is third from the left.

Invited talk at American Physical Society Division of Nuclear Physics Meeting

Tony Hill (LANSCE-NS), Chair of the Nuclear Data Working Group for the Advanced Fuel Cycle Initiative (AFCI)/Global Nuclear Energy Partnership (GNEP), presented an invited talk in a session on "Nuclear Physics Research Needs for Nuclear Energy" at the annual Fall Meeting of the American Physical Society, Division of Nuclear Physics Meeting in Oakland, CA. Hill presented the plans for developing new nuclear energy generation technologies to meet energy and climate change goals using advanced, proliferation resistant nuclear fuel technologies. He described the advances in nuclear data measurement techniques and reductions in uncertainties in nuclear data that drive design margins in costs and in operational parameters for planned and next generation nuclear power plants. Lee Schroeder (Lawrence Berkeley National Laboratory) organized and chaired the session.

Lujan Neutron Scattering Center receives new helium dilution refrigerator

A team from Vericold Corp. in Germany and Oxford Cryogenics in England worked with Lujan scientists to commission the first cryogen-free 3He-4He dilution refrigerator at a U.S. neutron scattering facility. The refrigerator, designed to reach temperatures of 20 mK, performed flawlessly. The Vericold device is a new design, which uses a closed cycle Pulse Tube cooling technique to cool the system to approximately 4K, at which point the dilution heat exchanger can take over and reduce the sample temperature to 20 mK. The Pulse Tube

Frans Trouw (right), leader of the Lujan Center cryogenics team and Alan Shapiro (LANSCE-LC), examine the new dilution refrigerator just commissioned at the Lujan Neutron Scattering Center.

method does not require liquid He as a pre-coolant and thus results in a significant saving in operating costs, compared to conventional He dilution refrigerators. During the commissioning tests the refrigerator exhibited stable long-term operation at 11 mK under no external heat load. The refrigerator was purchased with LANL G&A funds in FY 2006 and is a key initial component in the forthcoming Lujan Enhancement Program to be funded by DOE-BES.

The addition of the dilution refrigerator system to the suite of sample environment resources at the Lujan Center will make ultra-low temperatures available on a number of diffraction, reflectometry, and inelastic instruments available to users. Combined with the existing 11T superconducting magnet, this will enable the Lujan Center to address many of the cutting edge research problems of the condensed matter physics community, especially scattering research in superconducting and other correlated electron systems.

Michel W. Barsoum joins LANSCE as Sixth Wheatley Scholar

Michel Barsoum, Distinguished Professor of Materials Science and Engineering of Drexel University, joined LANSCE's Lujan Center as the sixth John Wheatley Scholar. LANL established the Wheatley Scholar program in 1997, in honor of one of its illustrious researchers, John Wheatley. Barsoum is a Fellow of the American Ceramic Society and an Academician in the World Academy of Ceramics. He has more than 200 papers and 16 issued and pending patents. His textbook, Fundamentals of Ceramics, is in its second printing. Barsoum discovered and characterized the "MAX" phases in ceramics, a new class of machinable ternary carbides and nitrides with remarkable toughness and thermal properties. His inaugural MAX paper in 1996 has been cited more than 500 times. Recently he reported scientific evidence that parts of the Great Pyramids of Giza have an early form of concrete. His surprising discovery established that Egyptian concrete lasts 45 centuries, compared to two centuries for Portland cement. His neutron scattering studies of ancient Egyptian building materials at the Lujan Center established further details of this finding.

During his one-year Wheatley Scholar term, Barsoum will help develop programs in neutron scattering instrumentation, particularly for advanced materials, composites, and ceramics. His studies of archaeoconcrete and MAX phases provide good paradigms for exciting new materials topics for neutron scattering.

American Physical Society's *This Week in Physics* highlights Lujan Center Research

Anna Llobet's (LANSCE-LC) publication with collaborators on intrinsic localized modes in sodium iodide (NaI) was described in the American Physical Society's *This Week in Physics*, which highlights exceptional physics research. A longstanding question in condensed-matter science and nonlinear dynamics is whether intrinsic three-dimensional (3D) localized modes can appear in an atomic lattice in thermal equilibrium. Although the presence of "intrinsic localized modes" was first proposed in the 1980s, there was no experimental evidence. Llobet and collaborators' inelastic neutron scattering measurements at the PHAROS-LANSCE spectrometer show that sodium iodide, a simple three-dimensional ionic crystal, can support a single intrinsic localized mode in thermal equilibrium above 555 K. The mode gains energy with increasing temperature, consistent with molecular dynamic simulations.

The localized mode occurs at a single frequency of 299 meV, which lies near the center of a gap in the phonon spectrum.

This is the first observation of a 3D intrinsic localized mode in a crystalline solid, and it suggests an important role for such modes in the high temperature physical properties of solids. Collaborators include A.J. Sievers, S.A. Kiselev, N.I. Agladze (Cornell University), J.W. Lynn and (National Institute of Standards and Technology), and A. Alatas (Argonne National Laboratory). Reference: "Intrinsic localized modes observed in the high-temperature vibrational spectrum of NaI," Physical Review B 79, 134304 (2009), DOI: 10.1103/PhysRevB.79.1343 04. The work was performed under the auspices of the DOE.

Using accelerator transmutation to address the U.S. nuclear waste issues (from july 2009)
A key roadblock to development of additional nuclear power capacity is a concern over the management of nuclear waste. Nuclear waste is predominantly comprised of used fuel discharged from operating nuclear reactors. The 104 operating U.S. reactors currently produce about 20% of the U.S. electricity and will create about 87,000 tons of such discharged or "spent"' fuel over the course of their lifetimes. Untreated, the long-term radioactivity of the spent fuel drives the need for deep geologic storage that must remain stable for millions of years. If we can safely manage the actinides plutonium and americium, then within a few hundred years the toxic nature of the spent fuel will drop below that of the natural uranium ore that was originally mined for nuclear fuel. LANL researchers are developing a nuclear fuel cycle-based accelerator transmutation of americium and the storage of the plutonium along with the neptunium and uranium as a fuel for the future. The scientists concluded that only two accelerator systems could manage the yearly americium production for the entire U.S. fleet of nuclear power plants. The end result of this nuclear fuel cycle would be: 1% of the initial nuclear plant radiotoxic discharge would be stored in 300-year interim storage facilities, 4% would have a low level of radiotoxicity and would be buried, and approximately 95% of the nuclear waste would be stored as a future fuel reserve. Team members are Gordon Jarvinen (ADSMS), Iain May (C-IIAC), Eric Pitcher (LANSCE-DO), Rich Sheffield (LANSCE-DO), and Holly Trellue (D-5). Program development funding from the Laboratory's Civilian Nuclear Program supports the work.

LANSCE User Group Meeting

The Ninth LANSCE User Group (LUG) Meeting will be held in Santa Fe, NM from September 30 - October 1. The meetings have taken place approximately every 18 months since their founding. This meeting will feature talks on materials science and condensed matter, nuclear science and applications, fundamental physics with neutrons, accelerator physics, and radiation effects. There will be a special tribute to Louis Rosen, the architect of the LANSCE accelerator complex, followed by a presentation from the Rosen Prize winner (Olivier Delaire, California Institute of Technology). The meeting will include plenary talks, a poster session, workshops on new neutron scattering instrument designs, and collaboration meetings. Current and prospective users of this DOE/NNSA/BES facility are encouraged to attend and participate in the science sessions and facility discussions. The Materials Research Society is sponsoring the meeting. Local LANL organizers include Alan Hurd (LANSCE Lujan Center Director), Ron Nelson (LANSCE-NS Deputy Group Leader), and Leilani Conradson (LANSCE User Program Manager). Registration and information are available at http://www.mrs.org/s_mrs/sec.asp?CID=21478&DID=247197. The LANSCE users meeting is organized in coordination with the Center for Integrated Nanotechnology (CINT) Users Conference, which will be held September 29-30 in Santa Fe, NM.

Celebrations

Kim Tait, a graduate student working in LANSCE, received one of the top five scholarships from the Philanthropic Educational Organization (PEO). PEO was founded in 1869 by seven students at Iowa Wesleyan College. PEO has grown from that tiny membership of seven to almost a quarter of a million members in chapters throughout the U.S. and Canada. Tait earned a B.S. and M.S. in geology from the University of Manitoba. She received the International Centre for Diffraction Data Ludo Frevel Scholarship in 2004 and in 2005, was one of five chosen worldwide, and has discovered two new minerals that the International Mineralogical Association have approved. She began her Ph.D. in January 2003 at the University of Arizona and has been at LANL for three years.

Tait conducts her research at LANL on the thesis topic of gas hydrates (clathrates) that have been proposed as a possible energy source for the future. Her mentor is Yusheng Zhao (LANSCE-LC). Nominated by the POE Chapter BB in Tucson, she is the recipient of the Norah L. Wallace Named Scholar Award for 2005–2006.

Shannon McDaniel received honorable mention in the Louis Rosen Prize. Shannon McDaniel (MST-16) was chosen for honorable mention in the Louis Rosen Prize for the outstanding Ph.D. or M.S. thesis based on experimental or theoretical research performed at LANSCE. The LANSCE User Group recognized her thesis, "New Techniques for the Investigation of Deformation Mechanisms in Flow of Fine-Grained Ice," "for its creative and novel use of neutrons." The thesis has added a new dimension to the fields of glaciology and ice mechanics. McDaniel received her Ph.D. from the University of Washington.

Luc Daemen (LANSCE-LC) is the recipient of a Career Development Mentoring award. Eleven people nominated him for the award. He is the instrument scientist at the Lujan Center for the Filter Difference Spectrometer (FDS), used for molecular vibrational spectroscopy by inelastic neutron

scattering. One nominator commented, "Luke is a dedicated scientist who understands the importance of training the next generation to perform the best quality of research possible. This dedication cannot be understated with the daunting challenges facing the next generation of scientists. Luke has extended this opportunity to many young women researchers and thereby helped diversify the next generation of researchers". Another nominator stated, "I have watched students enter the Lujan Center as novices around chemicals and equipment, and leave a few months or years later with extensive experience in conducting experiments, plus hands-on knowledge about maintenance and troubleshooting issues that they have learned under the wonderful mentoring of Luc Daemen".

Sven Vogel receives the 2009 LANSCE Director's Excellence Award Sven Vogel (LANSCE-LC) is one of the world's leading experts on the use of neutron diffraction to study materials microstructure. Kurt Schoenberg (ADEPS) gave Vogel the 2009 LANSCE Director's Excellence Award for his achievements in publishing papers with scientists from around the world on materials transformations, especially geomaterials. H.R. Wenk of the University of California - Berkeley and Lujan Center Director Alan Hurd nominated him. Vogel established a completely new effect in materials science, "texture memory", in studies of phase transitions in quartz with Wenk on the Lujan High-Pressure Preferred Orientation Diffractometer (HIPPO) instrument. This first prominent result from HIPPO was reported in "Neutron Production, Neutron Facilities and Neutron Instrumentation," Reviews in Mineralogy 64, (2006). Roger Pynn established the LANSCE Director's Award in 1999, to recognize the scientific excellence and leadership of a LANL staff member strongly involved with LANSCE, either through their own research program, collaborations with LANSCE users, or programmatic development of the scientific program at LANSCE.

2009 LANL Distinguished Student Awards in Bioscience: Michael Jablin (LANSCE-LC)

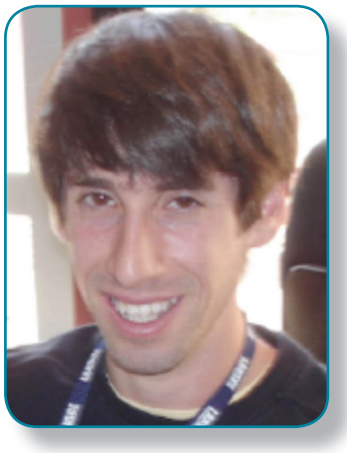

Michael Jablin investigated the interactions of a plant toxin with model biological membranes. Toxin-membrane interactions are important because toxins efficiently breach the membrane, then destroy the membrane or gain entrance into the cell's interior. Jablin created model biological membranes and characterized their structure via neutron reflectometry before and after the introduction of a toxin that plants make to protect themselves from bacteria. His results show marked changes in the membrane structure upon introduction of the toxin and support a rigidified lipid rafts type theory for the disruption of the cell membrane. Through this research, better drug delivery systems might be realized by understanding and eventually mimicking the properties of toxins. Jaroslaw Majewski (LANSCE-LC) mentors Jablin.

Caroline Wurden investigated and developed a systematic approach to the extraction of differential pair correlation functions for binary materials systems. This work is of interest in many areas of science because the relationship between particular chemical species and their neighbors is often critical in determining the functionality of the material. The lack of a data reduction program for handling these data sets had prevented the widespread application of these techniques. Wurden successfully obtained the differential pair correlation functions from experimental neutron and x-ray data of a binary system test case (zinc oxide). Anna Llobet, Katherine Page, and Thomas Proffen (all LANSCE-LC) mentor her.

National Science Foundation awards Hillary Smith a Predoctoral Fellowship

The National Science Foundation selected Hillary Smith (LANSCE-LC) to receive a Predoctoral Fellow award. Smith graduated from Bryn Mawr College in 2006 with a B.S. in physics and chemistry. Currently she works at the LANL Lujan Center as a post-baccalaureate intern with Jaroslaw Majewski (LANSCE-LC) on the surface profile analysis reflectometer (SPEAR). Her main research project, which uses neutron reflectometry to examine the penetration of anthrax toxin into model lipid membranes, is focused on understanding the conditions under which anthrax enters cells. She will enter graduate school, either at Caltech or the University of Pennsylvania, to work towards a Ph.D. in materials science

Thomas Proffen elected officer in the Neutron Scattering Society of America

Thomas Proffen (LANSCE-LC) was elected Communicating Secretary for the Neutron Scattering Society of America, a position on its Executive Committee.

The Society is active in neutron user technical meetings, education and training, and advocacy for user facilities and core research involving neutron scattering. The Neutron Scattering Society of America is an organization of persons who have an interest in neutron scattering research in a wide spectrum of disciplines. Proffen is the NPDF instrument scientist at the Lujan Neutron Scattering Center and received his PhD in crystallography from the University of Munich.

Outstanding Innovation Technology Transfer Awards

Yusheng Zhao (left) and Duncan McBranch

LANL's 2007 Technology Transfer Awards reception took place on May 29 at Fuller Lodge. The event recognizes employees whose technologies have received patents during the past year, employees who have received royalty income from patented and copyrighted work, and employees who have demonstrated an exemplary effort to participate in all facets of technology transfer. TT and the Intellectual Property Office (LC-IP) co-sponsor the event. Manuel Gonzalez, Chevron's manager for the Advance Energy Solutions Alliance with LANL, delivered the keynote address. PADSTE deputy Duncan McBranch presented the awards.

Yusheng Zhao (LANSCE-LC) received the 2007 Distinguished Licensing for his work on "Superhard, Ultratough Nanocomposites," a novel, nanostructured type of composite that consists of diamond particles embedded in a matrix of nanocrystalline silicon carbide. Zhao was recognized for demonstrating outstanding sucbess in the process of transferring his technology to industry through an exclusive license with US Synthetic, a company that leads the industry in the development and production of polycrystalline diamond cutters for oil and gas exploration.

Neutron Science Center and its Founder Celebrate Another Fine Year

Louis Rosen, the founder of the facility, continues to keep regular office hours at LANSCE despite having been retired for decades. LANSCE celebrated Rosen's 90th birthday on June 12 at the auditorium that bears his name, marking another vibrant year of life for Rosen, who spent much of the 1960s paving the political path for the proton accelerator. He received the DOE E. O. Lawrence Award in 1963.

Distinguished Mentor Awards

Jaroslaw Majewski (LANSCE-LC) mentored students who worked on the following projects: Hillary Smith – interactions of lipid membranes with UV light and anthrax toxin association with model lipid membranes, Jessica Saiz, Paulina Zelanay, and Michael Jablin – how nanoparticles penetrate lipid membranes.

LANL Individual Distinguished Performance Awards

Jaroslaw (Jarek) Majewski wants to understand how proteins, biotoxins, and pharmaceuticals cross a cell's outer membrane to reach the cell's interior. Composed of a single lipid bilayer, the cell's plasma membrane is the guardian against assaults by proteins, viruses, and molecular toxins, and is the portal for nutrients and waste products. Understanding the mechanism to traverse the cell's membrane required collecting information from the membrane's lipid layers while they were submerged in liquid—without damaging the delicate layers. Majewski developed new techniques in neutron and x-ray reflectometry and grazing- incidence x-ray scattering to study the mechanism by which the cholera biotoxin breaches the cell membrane. He obtained structural information for the toxin and its effects on the cell's membrane. He is now working to solve the riddle of other biotoxins, including the botulinum neurotoxin and anthrax. His techniques enable researchers to study model biological membranes in realistic aqueous environments.

Alan Hurd receives Employer Support of the Guard and Reserve Patriot Award

Lujan Center Director Alan Hurd has been awarded the Employer Support of the Guard and Reserve (ESGR) Patriot Award for support of Laboratory employee Melvin Borrego's (LANSCE-LC) recent tour of military duty in Iraq. The ESGR is a Department of Defense organization that strives to develop and promote a culture in which all American employers support and value the military service of their employees.

Lujan Center and West Virginia University receive EPSCoR Award

DOE awarded the Lujan Center and West Virginia University an Experimental Program to Stimulate Competitive Research (EPSCoR) Award. The award will help fund research on hydrogen absorption in Pd-based nanostructures. Mike Fitzsimmons (top) (LANSCE-LC) is the project lead and David Lederman (bottom), a student from West Virginia University, is a Lujan Center user. DOE BES also funds the project. EPSCoR is a federal-state partnership program designed to ensure America remains the world leader in scientific research and innovation, and to encourage research that will help meet the nation's energy needs through increased competition in energy-related research and development. The DOE invests up to $5.2 million in 12 basic research projects.

The universities pair with a DOE national laboratory to maximize expertise. The research projects range from advanced solar cells to hydrogen energy systems. Contact: Mike Fitzsimmons.

2009 LANL Career Development Mentoring Awards

Five employees were recognized for exemplary mentoring. Herb Funsten (International

Space and Response Division), Isabel Hodge (Major Subcontract Activities), John Isaacson (Risk Reduction Office), Alex Lacerda (Los Alamos Neutron Science Center), and Heather Volz (Materials Technology: Metallurgy), were selected from 20 nominations to receive a Career Development Mentoring Award from the Women's Employee Resource Group (WERG). The resource group sponsors the awards to promote career development of women at the Laboratory by recognizing and applauding mentors who exhibit exemplary informal or formal mentoring. Mentor nominees may be male or female, but the employee being mentored must be female. LANS regular employee, limited-term employee, or contract workers of the Laboratory are eligible to be nominated. The mentor-mentee relationship may be formal or informal. The Women's Employee Resource Group has sponsored the Career Development Mentoring Awards since 1997 with support from HROEOD and the Work Environment Diversity Work Group. Vivien Zapf nominated Lacerda (LANSCE-DO) because he provided her with the right combination of mentoring and support, equipment, and resources. The opportunities for invited talks, workshops, and recognition enabled her to develop new collaborations and research directions.

Individuals and Teams selected for LANL Distinguished Performance Awards

Individuals or small teams who receive Distinguished Performance Awards have made an outstanding and unique contribution that had a positive impact on the Laboratory's programmatic efforts or status in the scientific community, required unusual creativity or dedication of the individual or team, and resulted from a level of performance substantially beyond what normally would be expected.Individuals: Charles T. Kelsey IV (LANSCE-LC) redefined the LANSCE accelerator design basis accident in an innovative, scientific cost and time savings.

Los Alamos
NATIONAL LABORATORY
EST. 1943

NNSA
National Nuclear Security Administration

LANSCE
Los Alamos Neutron Science Center